INVESTIGATION OF AXIAL PULLOUT BEHAVIOUR OF SMALL DIAMETER MEDIUM-DENSITY POLYETHYLENE PIPES IN SAND

by

© Auchib Reza

A thesis submitted to the

School of Graduate Studies

in partial fulfilment of the requirement for the degree of

Doctor of Philosophy

Faculty of Engineering and Applied Science

Memorial University of Newfoundland

May 2023

St. John's Newfoundland and Labrador

ABSTRACT

Buried polyethylene pipes are increasingly used for gas distribution systems due to various advantages, including low cost, being lightweight, the ease of installation, corrosion resistance, and considerable flexibility. Permanent ground deformations due to ground subsidence, earthquakes, landslides, and slope movements can jeopardize the pipeline's structural integrity. It is often not possible to avoid areas exposed to ground movements for pipeline routing. Although different technologies are currently available to monitor ground movements, such as GPS surveying at discrete points (survey hubs), slope inclinometer, LiDAR image analysis, and satellite image analysis, a reliable tool to correlate the monitored displacements to the condition of the buried pipe is required for assessing the pipeline distress (i.e., wall strains) due to the forces from the moving ground. The objective of this thesis is to develop techniques for predicting pipe performance for pipelines exposed to axial ground movements. Small diameter (i.e., 42.2- and 60.3-mm diameter) medium-density polyethylene (MDPE) pipes, commonly used in gas distribution systems, were considered.

Pipelines are generally laid in the ground with the backfill soil well-compacted to secure ground support. In areas prone to ground movements, the pipelines are sometimes installed in a trench and then backfilled with loose to medium-dense sand to reduce the loads during relative ground movement. The behaviours of MDPE pipes in loose and dense sand were investigated using full-scale axial pullout tests. The tests were conducted under three different loading rates using the test facility developed at Memorial University of Newfoundland. Test results revealed that the load transfer mechanism for MPDE pipe depends on the pipe's extensibility and the loading rate. Three-dimensional (3D) finite-element (FE) analysis is employed to interpret the test results, demonstrating that a rate–dependent interface friction angle could be used to account for the

loading rate effect. Based on the study, simplified methods are proposed to calculate the mobilized frictional lengths and pipe wall strains from the relative ground movement in the pipe's axial direction.

For the pipe buried in loose sands, the maximum pullout resistance could be successfully predicted based on the normal force as the mean overburden pressure at the pipe's springline and a rate–dependent interface friction angle. The conventional FE modelling with Mohr-Coulomb's plasticity successfully simulated the test results. However, the compaction-induced lateral earth pressure and shear-induced soil dilation were found to contribute to the pipe responses for pipes in dense sand that could not be simulated using the conventional methods of FE analysis. Simplified approaches were proposed to account for the effect of soil dilation and calculate the mobilized frictional lengths, pullout resistances, and pipe wall strains for known relative ground displacements in dense sand. The developed method reasonably predicted the pipe responses measured during the tests. For a more rigorous analysis of pipes, 3D FE modelling techniques were developed for the pipes in dense sand. The effect of compaction-induced earth pressure was simulated during analysis using an equivalent temperature load. The method successfully simulated the test results. The study revealed that the effect of shearing-induced soil dilation depends on the magnitude of the earth pressure and could be insignificant for MDPE pipes. The compaction-induced lateral earth pressure was found to be significant for shallowly buried pipes. Based on the results of investigations, a method is proposed to include compaction-induced earth pressure for calculating the maximum spring force for pipeline evaluation using the beam-on-spring type FE modelling techniques recommended in the industry design guidelines.

GENERAL SUMMARY

Pipelines are one of the safest ways of transporting liquids and gases. Most onshore pipelines are buried underground to avoid damage caused by human activities. The buried pipelines are sometimes exposed to ground movements triggered by landslides, earthquake fault rupture, and other natural and human-induced hazards. The response of these pipelines to this type of permanent ground movement is a function of the pipeline orientation with respect to the direction of ground movement. Generally, a pipeline would be exposed to longitudinal, transverse, or some combination of transverse and longitudinal ground loading. The longitudinal ground movement is parallel to the pipeline axis, whereas the transverse movement is across the pipeline axis. Assessment of the effects of these ground movements on the performance of the pipeline is an important consideration for pipeline integrity assessment. This research investigates small-diameter medium-density polyethylene (MDPE) pipes to examine the effects of longitudinal (axial) ground movements. Small-diameter MDPE pipes are widely used in gas distribution systems in Canada and worldwide. However, no design method is currently available for assessing MDPE pipes subjected to ground movements. Existing pipe design guidelines recommend methods of assessment for steel pipes that are not applicable to MDPE pipes. Polyethylene pipes are relatively flexible and possess time−dependent material properties, whereas steel pipes are relatively rigid and do not show time−dependent material properties. As a result, the responses of the pipe due to ground loads are significantly different. The behaviour of buried MDPE pipes under the effects of relative ground movements has not been well investigated in the literature.

In the current research, a series of full-scale laboratory tests was conducted to observe the behaviour of MDPE pipes when subjected to axial movements relative to the soil. Pipes with two different diameters, buried in loose and dense sand, were tested under different loading rates to

capture the time–dependent responses. The test conditions were then simulated using three-dimensional (3D) finite-element (FE) methods to explore the mechanics of pipe–soil interaction. Based on the observed pipe and soil responses during the tests, simplified methods for assessing pipe conditions were developed for pipes in loose and dense sand. It is expected that the findings from this research will be useful for the pipeline industry to assess pipe conditions in unstable ground and ensure the structural integrity of pipelines, minimizing the risk of pipeline failure.

This thesis is dedicated to the soul of my father, Md. Rezaul Haque, who is and always will be my living, breathing superhero. He always believed in me and is there in spirit to enlighten my life's journey. The loss of my father will always sting. But now, everything good that I do is in honour of him and celebrates his life.

ACKNOWLEDGMENTS

All praise to the Almighty, the Most Merciful, and the Kind.

During my last five years at Memorial University of Newfoundland, I have met some incredible people who have helped me both academically and emotionally as I worked on my research. My deepest appreciation goes to Dr. Ashutosh Dhar, my supervisor, for his feedback, research ideas, patience, and help in improving my technical writing skills. He always motivated me to be updated on new research and development and to reflect on it. What stands out to me most is that he always maintained the quality of the research work. In any situation, he was the most helpful. I am truly blessed to be supervised by a person like Dr. Dhar, and I will remember many lessons for the rest of my life. I appreciate his kindness, respect, and ethics.

I would like to express my gratitude to my supervisory committee members, Dr. Bipul Hawlader and Dr. Kamal Hossain, for their contributions to my development as a researcher during this whole process. I would also like to sincerely thank my colleagues, Abu Hena Muntakim, Parththeeban Murugathasan, Riju Chandra Saha, Sudipta Chakraborty, Tanmoy Sinha, Adeniyi Salami, Saifa Anzum, and Darren Anderson, for their invaluable assistance, and time. I am indebted to the lab technicians and undergraduate students who supported me during the laboratory tests.

Finally, I acknowledge the financial and/or in-kind support for this research provided by the Collaborative Research and Development Grant program of the Natural Science and Engineering Research Council of Canada, Innovate NL program of the Government of Newfoundland and Labrador, FortisBC Energy Inc. and WSP Canada Inc.

Last but not least, I would like to remember the sacrifices of my mother, sister, and wife during this journey. My mother is always supportive; words are not enough to show my gratitude for her

sacrifices. Saifa Anzum, my wife, has always trusted me and has tremendous confidence in all my decisions. My sister is the one who has taken care of my mother in my home country. The care of my brothers-in-law, nieces, and parents-in-law has been unforgettable. I am so lucky to have such amazing people in my life.

Table of Contents

List of Figures

List of Tables

List of Symbols

The following symbols are used in this thesis:

A	pipe cross-sectional area
a, b, K	material constant
c	cohesion of soil
D	pipe outer diameter
E	modulus of elasticity of pipe material
E_0	Young's modulus of soil
f	interface friction reduction factor
F_A, P_u	maximum axial soil resistance of pipe
G_0	initial shear modulus of soil
G	secant shear modulus of soil
H	burial depth measured from ground surface to pipe centre
I_D	relative density of soil
I_R	relative density index
K_0	coefficient of lateral earth pressure at rest
K	effective coefficient of lateral earth pressure
L	buried pipe length
l	mobilized frictional length
n	exponent
P	pullout force
p	frictional force per unit length

p_a	atmospheric pressure
p'	mean effective confining pressure at pipe springline level
ΔT	temperature applied to soil layer
T_u	ultimate soil resistance per unit length
u	leading end displacement
u_c	critical shear displacement at maximum shear stress
α	coefficient of expansion for soil
γ	unit weight of soil
δ	pipe–soil interface friction angle
ε	axial strain
$\dot{\varepsilon}$	strain rate
ζ, ξ	normal stress adjustment factor
λ	dilation modulus at peak shear resistance
v	soil Poisson's ratio
$\Delta\sigma_{soil}$	compaction-induced lateral stress in soil
$\sigma_v^{'}$	effective overburden pressure over an inclusion
ϕ_{max}	peak friction angle of backfill soil
ϕ_{cv}	critical state friction angle of backfill soil
ψ_{max}	peak dilation angle of soil
ω	efficiency factor

CHAPTER 1

Introduction

1.1 General

Pipelines are important in the oil and gas industry, transporting crude oil and natural gas from production sites to refineries and distribution areas. More than 119,000 kilometres of pipelines are operated by Canadian transmission pipeline companies, which are about three times the length of Canada's national highway system (CEPA 2016). In Canada, the majority of energy, around 72%, is derived from oil and gas sources, with the vast majority, over 90%, transported through pipelines, according to CEPA (2016). However, failure in a pipeline transporting flammable substances such as oil and gas can result in significant economic and environmental consequences and threaten the safety of individuals. Permanent ground deformations due to ground subsidence, earthquakes, landslides, and slope movements have been identified as major hazards for buried pipelines (EGIG 2020). Although some permanent ground deformations are limited to small areas of the pipeline network, the potential damage due to induced differential movements could be very high (O'Rourke and Nordberg 1992). It's not always possible to avoid areas prone to ground movement when planning pipeline routes. Therefore, assessing pipelines subjected to ground movements is an important consideration for pipeline design and integrity assessment.

Although there is a lack of well-documented data on the failure of distribution pipes due to geohazards, the distribution pipes may also be exposed to ground movements and can undergo distress, resulting in adverse consequences. Figure 1.1 shows the results of an explosion due to a leak in a gas distribution pipe in Regina, Saskatchewan, that occurred in 2014 (CBC 2014). The leak in the pipe was reportedly caused by slow-moving ground in the area. Ground movements

have also been reported for several other communities in Canada, affecting the distribution pipe system (Weerasekara and Rahman 2019). For instance, FortisBC has been currently monitoring several large-scale, slow-moving landslides in different areas of British Columbia, including the West Quesnel, Marble Hill Subdivision, and Hodgson Road slides, which are affecting their gas distribution pipes (Weerasekara and Rahman 2019). The structural integrity of the pipes subjected to ground movements should be assessed for safe operation. However, no design method currently exists, focusing on the assessment of distribution pipes.

Figure 1.1: Explosion in December 2014 in Saskatchewan due to leaking of gas distribution pipe (CBC 2014)

Buried pipeline responses to ground movements significantly depend on the ground deformation patterns. Figure 1.2 shows a pipeline buried in a slope subjected to potential soil slips. Chan and Wong (2004) classified the potential soil movement in a slope as a shallow planar slip or deep-seated slip (planar or circular). In a planar slip (Figure 1.2a), when the direction of the moving soil mass is parallel to the slope's surface, pipelines can be subjected to longitudinal, transverse, or combined soil movement, depending on their orientation with respect to the direction of the ground movement. On the other hand, in deep-seated slips (Figure 1.2), soil movements exert combined longitudinal and transverse loads on the pipeline, particularly at the toe and top of the slip. Note that the longitudinal movement is parallel to the pipeline axis, whereas the transverse movement is across the pipeline axis. The pipelines laid parallel to the general direction of the soil movement in a planar slip situation experience only longitudinal ground loads. This thesis focuses on the pipes subjected to relative ground movement in the longitudinal direction.

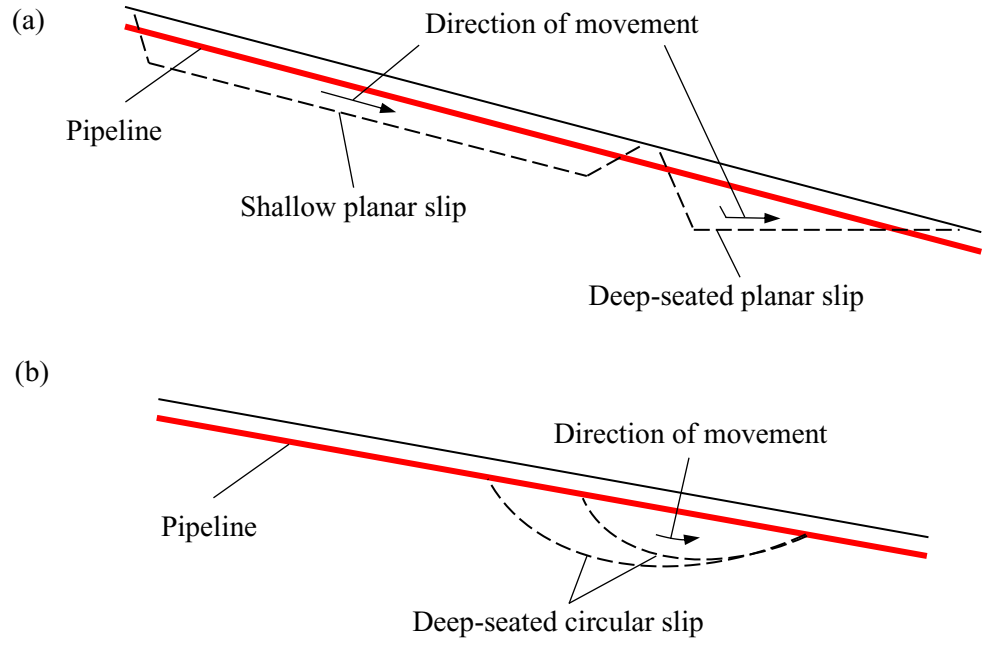

Figure 1.2: Slope sections showing potential slips: (a) Shallow and deep-seated planar; and (b) Deep-seated circular (Chan and Wong 2004)

As the ground moves longitudinally to the pipe axis, a pipeline can be subjected to axial forces due to relative soil–pipe displacement. For a pipe in a slope having downslope movement, shown in Figure 1.3, the upper part of the pipeline embedded in unstable soil mass is subjected to tension, and the lower part of the pipeline is subjected to compression. The pipeline will experience significant strains at the boundaries (i.e., tension strains at the crest and compression strains at the base of a slope). Pipes beyond the boundaries of the moving ground are usually fixed in the stable ground but can experience wall strains, depending on the magnitude of the axial force. With the development of various technologies (e.g., Global Positioning System (GPS) surveys, in-place slope inclinometer (IPSI) string, LiDAR image analysis), ground movements and their variations over time can be detected reasonably precisely in the field. These ground movement data are significantly important for the pipeline industry. This helps pipeline owners and operators take the necessary steps to run the pipelines safely in accordance with their respective integrity management programs for geohazards. However, due to the lack of reliable models to correlate such displacements to the condition of the buried pipe (i.e., axial force and the strain in the pipe wall), the pipe conditions could not be assessed rationally.

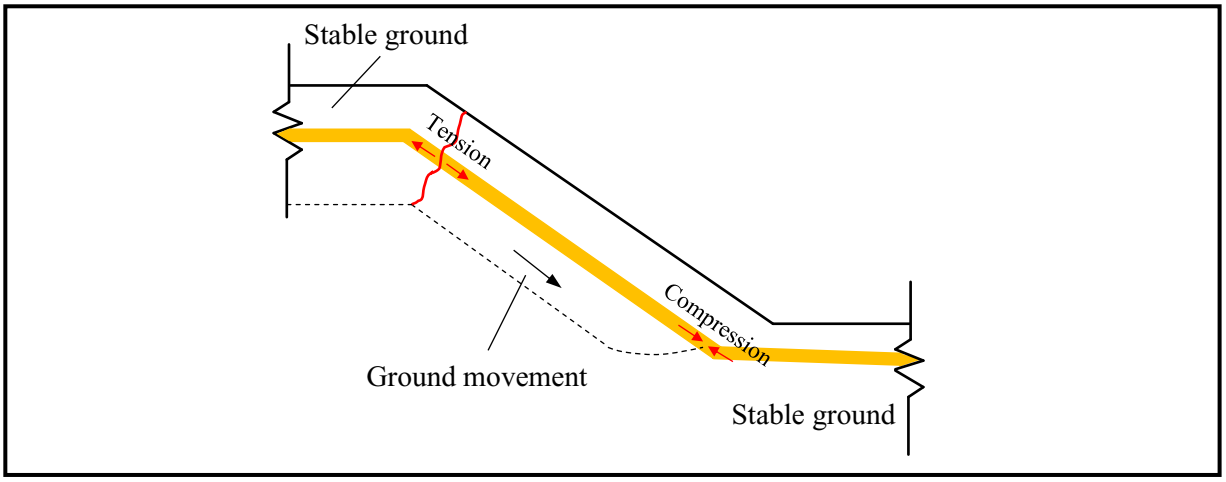

Figure 1.3: Idealized soil movement patterns and pipeline loads

Several experimental and numerical studies have been conducted in the past to understand the mechanics of soil–pipe interaction and develop simplified methods for evaluating pipelines exposed to ground movements (Trautman and O'Rourke 1983; Paulin et al. 1998; Yimsiri et al. 2004; Guo and Stolle 2005; Weerasekara and Wijewickrame 2008; Robert et al. 2015; Roy et al. 2016; Sheil et al. 2018; Sarvanis et al. 2017; Ansari et al. 2018 and many others). Most studies focused on the axial pipeline–soil interaction for rigid pipes (O'Rourke et al. 1995; Bilgin and Stewart 2009a; Wijewickreme et al. 2009; Sheil et al. 2018, 2021; Marino and Osouli 2020; Murugathasan et al. 2021). For rigid pipes subjected to axial ground movements, the relative displacement between the pipe and the soil is uniform over the length. The maximum frictional resistance to the relative displacement depends on the normal stresses acting on the pipe wall and the coefficient of friction of the soil–pipe interface. The current design guidelines (e.g., ALA 2005; PRCI 2017) recommend calculating the normal stresses as the mean value of the overburden stress and the at-rest lateral earth pressure at the pipe springline. However, researchers have demonstrated that the recommended method of calculating normal stress is not applicable, particularly for pipes in dense sand (Wijewickreme et al. 2009). The mechanics of soil–pipe interaction are more complex for flexible pipe (i.e., polyethylene pipe) as the pipe displacement relative to the ground is not uniform along the pipe length, and the pipe diameter is changed. The material properties can also be time−dependent, making the forces on the pipe loading rate dependent. However, studies on the behaviour of flexible pipes exposed to ground movements are very limited.

1.2 Motivation

Polyethylene (PE) pipes have several advantages when used in gas distribution systems, such as

durability, flexibility, low maintenance, being lightweight, and cost-effectiveness. Additionally, they are resistant to corrosion and can be welded together to form a leak-free system. Two types of polyethylene pipes are used for pipeline systems: medium-density polyethylene (MDPE) and high-density polyethylene (HDPE). According to Canadian Gas Association (CGA 2021), approximately 71% of the gas distribution system in Canada is composed of MDPE and HDPE. Among the PE pipes, MDPE pipes account for two-thirds of the gas distribution network (Weerasekara and Wijewickreme 2008). MDPE pipes have the added advantage of higher ductility and fracture toughness, as well as long-term strength and stiffness comparable to those of HDPE. However, no design method currently exists for evaluating MDPE pipes considering the soil–pipe interaction rationally. Studies on the understanding of the soil–pipe interaction for MDPE pipes are also very limited. Anderson (2004), Weerasekara and Wijewickreme (2008), and Wijewickreme and Weerasekara (2015) experimentally investigated the axial pullout behaviour of 60- and 114-mm diameter MDPE pipes under certain burial conditions. They reported axial elongation and reduction in cross-sectional dimensions for pipes during axial pullout. It was argued that the soil shear strength mobilizes gradually along the pipe length due to nonuniform elongation. However, the mechanism was not extensively investigated for pipes with various diameters, burial conditions, and under different loading rates.

Small-diameter (i.e., 42-mm diameter) MDPE pipes are widely used in gas distribution systems. The performance of the small-diameter pipes buried in areas prone to ground movement has not been evaluated to date. Pipelines are generally laid in the ground with the backfill soil well-compacted to secure ground support. In areas prone to ground movements, the pipelines are sometimes installed with the backfill material purposely left loose to reduce the loads during

relative ground movement (PRCI 2017). However, during the lifetime of a buried pipeline, environmental loading might compact the backfill material into a dense condition (Vanden Berghe et al. 2005). Consequently, backfill soil density often varies from site to site for the gas distribution system. Behaviours of pipes under various backfill soil conditions are expected to be different. Particularly, soil compaction can significantly increase lateral earth pressures on buried pipes during installation (Elshimi and Moore 2013; Dezfooli et al. 2014ab; Wang et al. 2017). As a result, the stresses due to compaction of the soil during backfilling can increase the interface frictional resistance, resulting in a higher pullout resistance of the pipe. However, no method is currently available in the existing design guidelines to properly account for the effect of compaction during backfilling.

Various rates of landslide movement have been reported in the literature ranging from imperceptibly slow (millimetres per year) to extremely rapid (many meters per second) (Keefer et al. 1983; Cruden and Varnes 1996; Kalaugher et al. 2000; Petley 2004; Picarelli et al. 2004). Pipe behaviour under different loading rates can be different. Existing design guidelines do not recommend any method to account for the loading rates in the assessment of pipelines.

In summary, no design tool is currently available for the assessment of MDPE pipes exposed to ground movement. Designers often follow the existing design guidelines, developed focusing on steel pipelines, for assessing polyethylene pipes. In these methods, the pipe is idealized as a beam, and the interaction of the pipe with the soil is represented as elastic-perfectly plastic (bilinear) springs. One of the challenges in the analysis is to determine the spring parameters, representing the soil–pipe interaction expected in the field. However, numerical modelling and

analytical methods are too complex for use in regular design. A simplified design tool would be suitable for assessing pipe conditions quickly. All these limitations motivate the candidate to develop improved design tools for the assessment of MDPE gas distribution pipes subjected to ground movement.

1.3 Objectives

The main objective of the present study is to develop an improved method for assessing MDPE pipelines subjected to axial ground movements. Considering that the behaviour of flexible MDPE pipelines depends extensively on the pipe–soil interaction, a better understanding of soil–pipe interaction will be developed using experimental and numerical methods. The following are the specific objectives of the research.

1. Develop a comprehensive experimental database on the behaviour of MDPE pipelines subjected to axial ground movements for pipes with various diameters commonly used in gas distribution systems.
2. Review and evaluate the applicability of existing methods for MDPE pipes using the measured responses.
3. Develop numerical modelling techniques (continuum-based three-dimensional FE analyses) to interpret the measured responses and investigate the details of pipe–soil interaction for MDPE pipe in loose and dense sand.
4. Develop simplified methods of wall strain assessment for MDPE pipes buried in loose and dense sands.
5. Propose improvement/modification to the existing beam-on-spring modelling by simulating the test results.

1.4 Scope of the Thesis

The following steps are taken in this research project to accomplish the research objectives.

Step 1: Review available literature on analytical, experimental, and numerical methods applied to investigate pipe–soil interaction of buried pipelines subjected to axial ground movements. This study identifies the research gaps.

Step 2 (objective 1): Conduct full-scale tests to develop an experimental database on the behaviour of MDPE gas distribution pipes buried in loose and dense sand under axial ground movements. The experiments were designed to apply relative ground movement along the pipe axial using a soil box. A database on the responses of pipes under different burial conditions, pipe sizes, and loading rates has been developed.

Step 3 (objectives 2 and 3): Conduct continuum-based three-dimensional (3D) finite-element (FE) analysis of a buried pipe in the sand under axial loading to capture the features that could not be measured during the tests, including the soil, pipe and interface parameters contributing to the pipe's behaviour.

Step 4 (objective 4): Apply simplified idealizations to develop design tools for pipe wall strain assessment of MDPE pipes buried in loose and dense sand.

Step 5 (objective 5): Examine the conventional Winkler spring-based numerical model along with 3D FE analyses to identify model parameters for simulating the pipe responses.

1.5 Outline of Thesis

This thesis is prepared in manuscript format. The outcome of the study is presented in seven chapters and seven appendices (A–G).

Chapter 1: Introduction

This first chapter introduces the problem, discusses the motivation for the study, and states the objectives and contributions of this research.

Chapter 2: Literature Review

This chapter presents a general literature review. As the thesis is prepared in manuscript format, the problem-specific literature reviews are provided in Chapters 3–6 and in Appendices A–E.

Chapter 3: Axial Pullout Behavior of Buried Medium-Density Polyethylene Gas Distribution Pipes

This chapter presents full-scale laboratory tests, finite element modelling and a simplified strain calculation method for 60.3-mm diameter MDPE pipes in loose to medium-dense sands. The details of the test program conducted under three different loading rates are discussed in this chapter along with finite element modelling, achieving objectives 1 to 3 for the specific pipe (i.e., 60.3 mm pipe in loose to medium-dense sand). Based on the analysis of results, a method is developed for calculating pipe wall strains for the pipes (objective 4). A version of this chapter has been published as a technical paper in the International Journal of Geomechanics, ASCE. Parts of this study have been published as two conference papers: one in the 7th International Conference on Engineering Mechanics and Materials, CSCE, June 12–15, Laval (Greater Montreal), QC, Canada (Appendix A), and the other in the 100th Transportation Research Board Meeting, January 2021, Washington D.C. (Appendix B).

Chapter 4: Effects of Axial Relative Ground Movement on Small Diameter Polyethylene Piping in Loose Sand

This paper presents a similar study as in Chapter 3 but focuses on 42.2-mm diameter pipes (in loose sand). The FE modelling technique developed in Chapter 3 was employed to simulate the

test results. The strain calculation method developed in Chapter 3 is applied to simulate the pipe strains measured for small-diameter (42.2 mm diameter) pipes. A version of this chapter has been published as a technical paper in Infrastructures, MDPI. A part of this study has been published in the 72nd Canadian Geotechnical Conference, GeoSt.John's 2019, Sept. 29–Oct. 2, St. John's, NL, Canada (Appendix C).

Chapter 5: Strain assessment of polyethylene pipes in dense sand subjected to axial displacements

This chapter presents the tests conducted with pipes in dense soil, an analysis of test results, and the developments of strain calculation methods for pipes in dense sand, meeting objectives 1, 2, and 4. Finite-element modelling (objective 3) of pipes in dense backfill involved more complex mechanisms, presented in the following chapter. A version of this chapter has been published for publication as a technical paper in Geosynthetics International, ICE publishing. A part of this study has been published in the 74th Canadian Geotechnical Conference, GeoNiagara 2021, September 26–29, Niagara Falls, ON, Canada (Appendix D).

Chapter 6: Finite-Element Modeling of Axial Movements of Polyethylene Pipes in Dense Sand

The 3D FE modelling of MDPE pipe–soil interactions in dense sand is presented in this chapter. Compaction-induced lateral earth pressure was found to contribute significantly to the behaviour of pipes in dense sand. A method is proposed to account for the compaction-induced lateral earth pressure during 3D FE modelling. The spring parameter for beam-on-spring analysis was then modified, including the compaction-induced lateral earth pressure. The beam-on-spring analysis technique with modified spring force is presented, evaluating test results. This chapter has been submitted to a journal as a technical paper for review. A part of this study has been published in

the 75th Canadian Geotechnical Conference, GeoCalgary 2022, October 2–5, Calgary, AB, Canada (Appendix E).

Chapter 7: Conclusions and Recommendations for Future Research

This chapter presents the general conclusions of the thesis and recommendations for future studies. However, problem-specific conclusions are provided at the end of each chapter (Chapters 3–6) and appendices (Appendices A–G).

The response of pipes in 3D FE modelling with internal pressure is presented in Appendix F. The details of an additional pullout test to investigate the effect of stress relaxation in MDPE pipes are described in Appendix G.

As the thesis is prepared in manuscript format, the references cited in Chapters 3–6 and Appendices A–E are listed at the end of each chapter and appendix. The references cited in Chapters 1, 2 and Appendices F and G are listed in the "References" section at the end of the thesis.

1.6 Significant Contributions

The following technical papers have been produced from the research presented in this thesis.

Journal Articles

1. **Reza, A.** and Dhar, A. S. (2021a). Axial Pullout Behaviour of Buried Medium Density Polyethylene Gas Distribution Pipes, *International Journal of Geomechanics*, ASCE, 21(7):04021120.
2. **Reza, A.** and Dhar, A. S. (2021b). Effects of Axial Relative Ground Movement on Small Diameter Polyethylene Piping in Loose Sand, *Infrastructures*, MDPI, 6(12): 168.
3. **Reza, A.,** Dhar, A. S. and Rahman, M. (2023). Strain assessment of polyethylene pipes in

dense sand subjected to axial displacements. *Geosynthetics International*, ICE Publishing, (Accpeted, ahead of print)

4. **Reza, A.** and Dhar, A. S. (2023). Finite-Element Modeling of Axial Movements of Polyethylene Pipes in Dense Sand. (Under review).

Conference Papers

1. **Reza, A.**, Dhar, A. S. and Muntakim, A. H. (2019). Full-Scale Laboratory Pullout Testing of a 60 mm Diameter Buried MDPE Pipes, *7th International Conference on Engineering Mechanics and Materials*, CSCE, June 12–15, Laval (Greater Montreal), QC, Canada.
2. **Reza, A.**, Dhar, A. S., Rahman, M. and Weerasekara, L. (2019). Pulling rate effects on the pullout force of buried small diameter MDPE pipe in loose sand, *72nd Canadian Geotechnical Conference, GeoSt.John's 2019*, Sept. 29–Oct. 2, St. John's, NL.
3. **Reza, A.** and Dhar, A. S. (2021). Numerical Evaluation of Buried Medium Density Polyethylene Pipelines Subjected to Axial Ground Movement, *In Proceedings of 100th Transportation Research Board Meeting*, Washington D.C., January 2021.
4. **Reza, A.** and Dhar, A. S. (2021). Finite element modeling of pipe–soil interaction under axial loading in dense sand, *74th Canadian Geotechnical Conference, GeoNiagara 2021*, Niagara Falls, ON, Canada, September 26–29.
5. **Reza, A.** and Dhar, A. S. (2022). Axial ground movement analysis for buried polyethylene pipelines using nonlinear pipe–soil interaction model, *75th Canadian Geotechnical Conference, GeoCalgary 2022*, Calgary, AB, Canada, October 2–5.

Co-Authorship: Most of the research presented in journal articles 1–4 and conference papers 1–5 has been performed by the author of this thesis, Mr. Auchib Reza, under the supervision of Dr. Ashutosh Dhar. Mr. Reza also prepared the draft manuscripts. The other authors mainly supervised the research and reviewed the manuscripts.

CHAPTER 2

Literature Review

2.1 Introduction

Ground movements resulting from various causes, including landslides, earthquakes, and ground subsidence, can pose severe threats to the performance and integrity of pipelines. The pipes may experience unacceptable levels of strain due to the loads from the moving ground. A detailed investigation of these pipelines subjected to relative movement is an essential step to ensure the safe design of the pipe network and to improve the knowledge of pipe–soil interaction during the events. Over the last few decades, several studies have been undertaken to determine buried pipelines' response to ground movement. These investigations include laboratory tests ranging from full-scale pipe pullout tests to centrifuge tests, field pipe testing, and monitoring of the piping system. Based on these experimental results, several numerical and analytical models have been developed to determine the response of buried pipes subject to ground movements.

Depending on the pipeline's orientation with respect to the direction of ground movement, pipelines might be subjected to various loadings, as shown in Figure 2.1. This chapter presents a review of existing pipe design guidelines and previous studies on the physical and numerical modelling of pipelines subjected to axial ground movements.

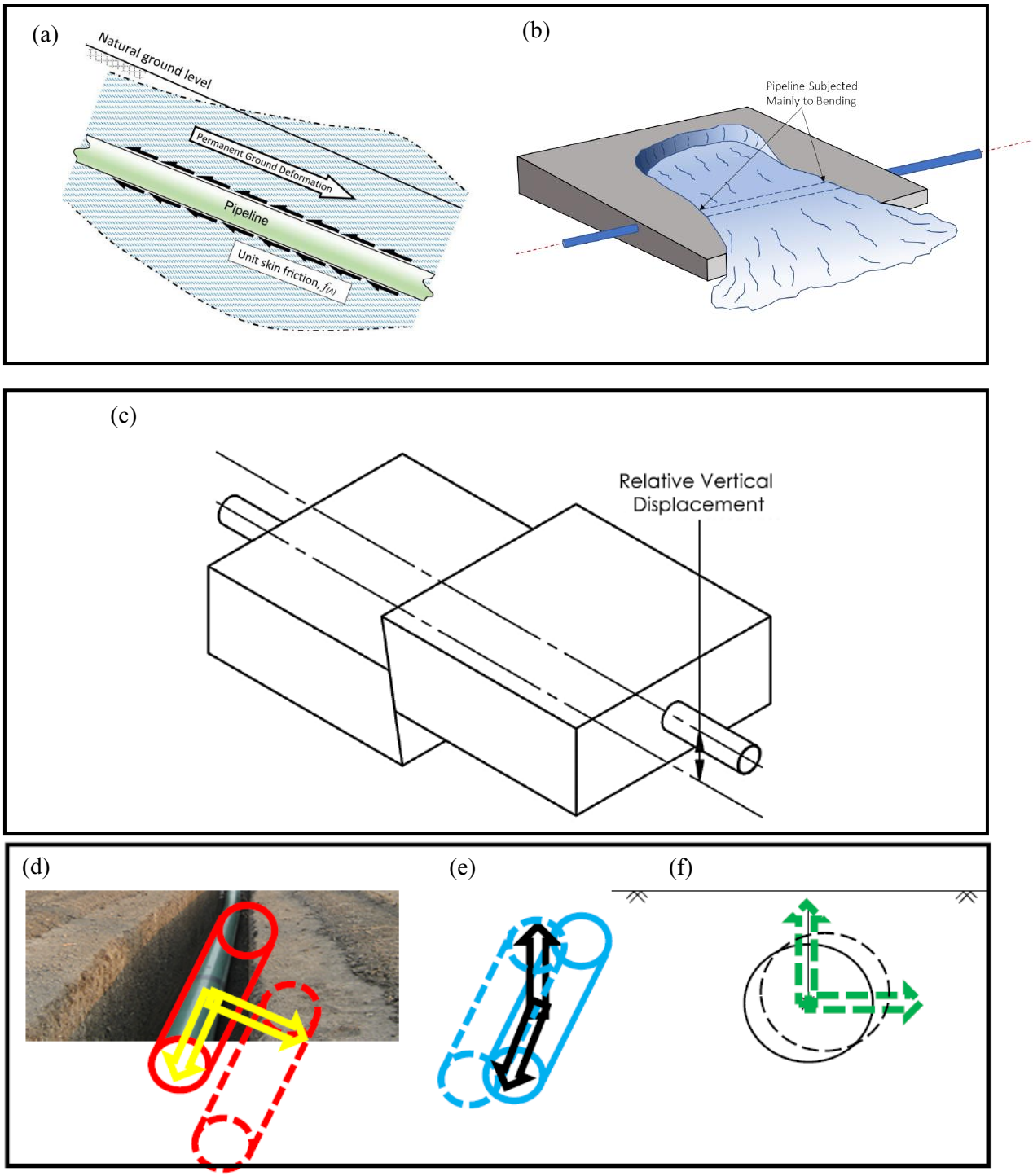

Figure 2.1: Ground movement loading on the pipe: (a) Axial loading (Al-Khazaali and Vanapalli 2019a); (b) Lateral loading (Esmaeilzadeh 2019); (c) Upward vertical loading (Cugnetto et al. 2021); (d) lateral–axial; (e) axial–vertical; and (f) lateral–vertical oblique loadings (Morshed 2019)

2.2 Current Design Guidelines

To evaluate the structural response of a pipeline, the current design guidelines recommend modelling the pipeline as a beam and the soil reactions to the pipelines as a series of independent bilinear elastoplastic springs (ALA 2005; PRCI 2017). The springs are defined in the axial, lateral, upward, and downward directions to account for the corresponding direction of relative displacements, as shown in Figure 2.2. The response of the soil springs in the three orthogonal directions is independent, which means that any loading in one direction does not translate to loading in the other two directions. The general form of the load–displacement relations for these springs can be expressed as:

$$T = f(x);\ P = f(y);\ Q = f(z) \tag{2.1}$$

where T, P and Q are the soil loads applied to a unit length of the pipeline, and x, y and z are the relative displacements between the pipe and surrounding soil in the longitudinal, lateral, and vertical directions, respectively.

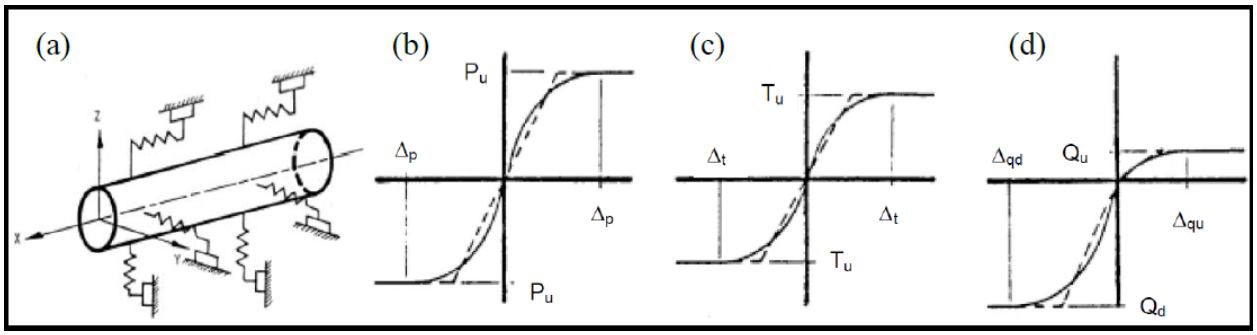

Figure 2.2: Current design guidelines: (a) Idealized pipe–soil interaction with discrete springs; (b) Lateral loading; (c) Axial loading; and (d) Vertical loading (ALA 2005)

The design guidelines (e.g., ALA 2005) recommend Eq. (2.2) to estimate the maximum axial soil force acting per unit length of the pipes buried in cohesionless soils.

$$T_u = \pi D \gamma H \left(\frac{1+K_0}{2} \right) \tan(\delta) \qquad (2.2)$$

where T_u = ultimate soil resistance on the pipe per unit length; γ = unit weight of soil; H = burial depth measured from the ground surface to pipe springline; D = pipe outer diameter; K_0 = at-rest lateral earth pressure coefficient for the soil; and δ = interface friction angle between the pipe and surrounding soil. Eq. (2.2) is proposed based on the estimation of the normal stresses acting on the pipe and the frictional characteristics of the soil–pipe interface. The normal stresses are estimated as the mean value of the overburden stress and the at-rest lateral earth pressure at the pipe springline. The value of the interface friction angle, δ, depends on the interface behaviour between the soil and the pipe, including the roughness and hardness of the pipe surface. The ALA (2005) guideline suggests that δ can be estimated as $\delta = f\phi$, where ϕ is the internal friction angle of the backfill material, and f is the coating-dependent factor relating the internal friction angle of the soil to the friction angle at the soil–pipe interface. Representative values of f for various types of external pipe coatings are recommended in Table 2.1.

Table 2.1. Friction factors for different pipe coatings (ALA 2005)

Pipe Coating	***f***
Concrete	1.0
Coal Tar	0.9
Rough Steel	0.8
Smooth Steel	0.7
Fusion Bonded Epoxy	0.6
Polyethylene	0.6

The yield displacement (the peak displacement required to obtain the ultimate axial soil force per unit length of the pipe) of the axial soil springs depends on the type of surrounding soil (i.e., Δ_t = 3 mm for dense sand, Δ_t = 5 mm for loose sand, Δ_t = 8 mm for stiff clay, and Δ_t = 10 mm for soft clay, according to ALA 2005).

Various approaches can be used to calculate the coefficient of earth pressure at rest (K_0). According to the continuum mechanics theory, K_0 solely depends on the Poisson's ratio (v) of soil and is given by Eq. (2.3).

$$K_0 = \frac{v}{1 - v} \tag{2.3}$$

However, the coefficient of earth pressure at rest proposed by Jaky (1944) is accepted as the horizontal-to-vertical stress ratio in loose deposits and normally consolidated clays, as given in Eq. (2.4).

$$K_0 = 1 - \sin\phi' \tag{2.4}$$

where ϕ' stands for the effective internal friction angle of the soil. Sherif (1984) reported that Eq. (2.4) might grossly underestimate the lateral earth pressure at rest for a dense, compacted sand backfill. This underestimation results because of the process of compaction of backfill. For this reason, he recommended the relationship for compacted sand as follows.

$$K_0 = (1 - \sin\phi) + 5.5\left[\frac{\gamma_d}{\gamma_{d(min)}} - 1\right] \tag{2.5}$$

where γ_d is the actual compacted dry unit weight of the sand and $\gamma_{d(min)}$ is the dry unit weight of the sand in the loosest state.

However, Eq. (2.2) was found the underestimate the maximum pullout force measured in

Karimian (2006). To predict the measured peak pullout, Wijewickreme et al. (2009) suggested using a much larger K value in place of K_0 for pipes buried in dense sands. PRCI (2017) adopted the experimental findings reported in Karimian (2006) and introduced a new parameter, K, instead of K_0, in the design equation to calculate the peak interface frictional resistance for axially loaded pipes. As stated in PRCI (2017), the value of K (termed as an effective coefficient of horizontal earth pressure) may vary from the at-rest conditions for loose soil to values as high as 2 in dense dilative soils.

2.3 Studies on the Axial Pipe–Soil Interaction

2.3.1 *Review of Experimental Studies*

Several experimental studies were conducted to understand the axial pullout resistance of pipes buried in sands (e.g., Paulin et al. 1998; Anderson 2004; Bilgin and Stewart 2009ab; Weerasekara and Wijewickreme 2008; Wijewickreme et al. 2009; Alam and Allouche 2013; Wijewickreme and Weerasekara 2015; Sarvanis et al. 2017; Sheil et al. 2018; Marino and Osouli 2020; Murugathasan et al. 2021). A summary of various tests conducted for the axial pullout of pipes in sands is presented in Table 2.2.

Wijewickreme et al. (2009) investigated the performance of buried steel pipes subjected to relative soil movements in the axial direction using a full-scale testing facility. The pipes were backfilled with dry sand. The tests were conducted under displacement-controlled loading conditions, where a hydraulic actuator pulled one end of the pipe, and the other end was free to move. The pipes were buried in two different soil conditions: loose sand with a relative density (D_r) of ~20% and dense sand with a D_r of ~75%. It was reported that the measured axial soil loads

on pipes buried in loose dry sand were comparable to those predicted using the equation recommended in the design guidelines [Eq. (2.2)]. However, the peak axial pullout resistance observed for pipes in dense sand was several-fold (more than two times) higher than those predicted using Eq. (2.2). In addition, during the tests, the normal soil stress on the pipe was measured using total-pressure transducers mounted at selected circumferential locations on the pipes. The soil pressure measurements undertaken during pullout tests in dense sand indicated that the overall normal soil stresses on the pipe during pullout increased substantially compared to the initial values. This increase in normal stress is associated with the constrained dilation of sand in the shear zone during interface shear deformations. To account for the increased normal stress, they suggested using a higher lateral earth pressure coefficient, K, than the at-rest lateral earth pressure coefficient (K_0) in Eq. (2.2).

Sarvanis et al. (2017) conducted three large-scale experimental tests on coated and noncoated steel pipes (219.6-mm diameter) buried in dense sand. Tests were performed on two different types of sand with similar compaction efforts (soil mass density was measured at approximately 1600 kg/m^3). For sand type 1, the peak friction angle (ϕ_{peak}) was measured as 45°, and the residual value of the internal angle of friction (ϕ_{res}) was measured as 37° using the direct shear tests. For sand type 2, the value of ϕ_{peak} and ϕ_{res} were measured as 48.2° and 41.7°, respectively. The peak dilation angle of the soil (ψ_{peak}) was calculated as 8° and 6.5° for sand type 1 and type 2, respectively. In all tests, the maximum axial resistance was consistently higher than the resistance predicted by the ALA guidelines. The maximum axial soil resistance was significantly higher for sand type 1 than sand type 2 due to the higher ψ_{peak} of sand type 1.

Sheil et al. (2018) investigated the cyclic axial soil resistance and the distribution of contact stresses around a trenched steel pipeline buried in sand backfill. In some of the tests, a pressure bag system was used to simulate backfill depths exceeding the height of the testing tank. Similar to the observations reported in Wijewickreme et al. (2009) and Sarvanis et al. (2017), the maximum forces calculated using the existing guidelines were significantly less than those observed in laboratory tests for dense sand. They identified the potential for a compacted damp sand backfill to 'arch' completely over the pipe because of differential settlement of the pipe relative to the backfill during the first few cycles of axial displacement. However, no arching occurred for loose, damp sand, leading to higher axial soil resistance. The measured initial normal stress at the pipe crown was greater than the nominal overburden pressure. They postulated that the high normal stress results from the rigid inclusion of the steel pipe. This effect is also not considered in the current design guidelines. They also proposed including pipe self-weight and redistribution of normal stresses around the pipe circumference in calculating the pullout resistance. Later, Sheil et al. (2021) measured the contact stresses around buried steel pipes, applying and subsequently reducing surcharge pressures, and found 'locked in' normal stresses on the pipe after reducing the surcharge pressure. The locked-in normal stress cannot be estimated based on the overburden pressure recommended in the existing design guidelines.

Al-Khazaali and Vanapalli (2019b) investigated the axial force–displacement responses of a steel pipeline in sand under saturated and unsaturated conditions. The soil-matrix suction in unsaturated soils was measured using four soil moisture probe tensiometers installed at different depths in the testing box. The test results under the unsaturated condition showed a significantly higher axial force on the pipeline than those in the saturated condition, which is attributed to the

contribution of matrix suction. The soil dilatancy effects on the mobilized axial force were found for both saturated and unsaturated soil conditions. However, the effect was more pronounced under an unsaturated condition up to the residual zone of unsaturation.

Murugathasan et al. (2021) conducted five axial pullout tests of a ductile iron pipe using a laboratory facility to examine the pullout resistance under various conditions, including different pipe burial depths, relative densities of soil, and pulling rates. The maximum pullout resistance was successfully calculated with the ALA (2005) equation using the at-rest lateral earth pressure coefficient (K_0 = 0.42) for the pipe in loose sand. However, a higher value for the coefficient of lateral earth pressure (i.e., K_1 = 1.6) was back-calculated using the equation designed for dense sand. In addition, they reported that the pulling rate has an insignificant effect on ductile iron pipes embedded in sand material.

A few experimental studies are also available in the literature with polyethylene pipes. Bilgin and Stewart (2009b) investigated the interface shearing resistance of buried 168.3-mm diameter high-density polyethylene (HDPE) pipes at different temperatures (21 °C, 10 °C, 7 °C, 6 °C, and 2 °C). They observed that pipe pullout resistance decreases linearly with an increasing temperature drop. The longitudinal pullout resistance was reduced by 60% when the soil temperature dropped from 21 to 2 °C, due to the pipe's diameter reduction. The reduction in pipe diameter results in a decrease in the particle contact stresses and normal stresses around the pipe. They also carried out cyclic tests to evaluate pullout resistance under repeated loads, simulating thermal contraction and expansion of pipes caused by seasonal temperature fluctuations. The soil resistance was found to degrade considerably in each cycle. For example, in only ten cycles, the shearing resistance

degraded by 75% of the resistance in the first cycle. The effect of the loading cycle governed the interface shearing resistance for pipes with a diameter of 150 mm or smaller, while the pipe's diameter decrease due to the temperature drop governed the interface shearing resistance for pipes having a diameter of 200 mm or larger. The findings suggest that the mechanics of soil–pipe interaction can be different for pipes with different diameters.

Anderson (2004) performed five axial pullout tests in loose Fraser river sand and three axial pullout tests in dense sand with medium-density polyethylene (MDPE) pipes of two different pipe sizes (i.e., 60- and 114-mm). The experimental results for MDPE pipes showed that maximum pullout resistance occurred at a much greater displacement than was recommended for steel pipelines (2 to 3 mm). Similar behaviour was observed by Weerasekara and Wijewickreme (2008) and Wijewickreme and Weerasekara (2015) for MDPE pipes in dense sand. The pipes were buried in a backfill compacted to a unit weight of 15.8 kN/m^3, corresponding to a relative density of ~75% in Weerasekara and Wijewickreme (2008). The pipes were pulled at the specific displacement rate of 0.6 mm/min. The maximum pulling forces measured in the tests were significantly higher than those calculated using the methods recommended in the design guidelines. They used the coefficient of lateral earth pressures (K) of 2.4 and 1.4 for 60-mm and 114-mm diameter MDPE pipes, respectively, in the design equation, instead of the at-rest earth pressure coefficient, to match the maximum axial soil resistance observed during the tests. It was reported that the frictional resistance at the MDPE pipe's surface is not uniformly mobilized over its entire length at the same time, unlike the behaviour of steel pipes. The length of shear strength mobilization was found to increase with the increase of relative ground movement. Wall strains were developed only over the length of shear strength mobilization during axial pullout, which was confirmed by the

measurements of strains.

Wijewickreme and Weerasekara (2015) conducted field axial pullout tests of 60-mm diameter MDPE pipes at various pulling rates. The backfill soil was compacted to unit weights ranging from 15.7 kN/m^3 to 16.1 kN/m^3, corresponding to the relative densities of 82% to 92%. They found that the pulling rate has significant effects on the pullout resistance. The effects of pulling rate on the progression of mobilized friction length could not be assessed in that study. Wijewickreme and Weerasekara (2015) considered a nonlinear, strain rate–dependent stress–strain response of the PE pipe material to analyze the pipe responses under axial soil loading to account for the pulling rate effects. The cavity expansion theory was applied to estimate the normal stress increase on the pipe surface due to shearing-induced soil dilation. The applicability of this approach of analysis under various burial conditions of pipelines was not investigated.

2.3.2 *Review of Numerical Studies*

Numerical methods provide a rational basis for conducting pipe–soil interaction studies. Two approaches of FE modelling are commonly employed in the analysis of buried pipes. The first approach is a structural-type FE model where the pipe is idealized as a structural beam, while the soil–pipe interaction is modelled using independent springs. This approach is relatively simple and suitable for analyzing pipe lengths in the order of kilometres. The major challenge in this method is to identify the spring parameters that represent the soil–pipe interaction appropriately. The other method is the continuum-based FE model, where both pipe and the soil are modelled as an elastic or elasto-plastic continuum. This method is robust and provides opportunities to model the pipe and soil appropriately. However, identifying a material model that appropriately represents the

ground conditions is often challenging. Furthermore, 3D continuum-based models require extensive calculations and data-storage capability, making them difficult to apply to large-scale problems. To this end, researchers employ 2D continuum-based idealization (i.e., plane strain), targetting the investigation of specified mechanisms.

A few numerical studies on axial pipe–soil interaction are available in the literature (e.g., Wijewickreme et al. 2009; Meideni et al. 2017, 2018; Al-Khazaali and Vanapalli 2019a; Murugathasan et al. 2021; Muntakim and Dhar 2021). A summary of those studies for pipes in the sand is presented in Table 2.3.

Wijewickreme et al. (2009) employed a 2D continuum-based finite difference method, using FLAC 2D, to study the effect of soil dilation on the normal stress increase on the pipe. The soil dilation of the shear zone was mimicked by radially expanding the pipe (0.7 to 1 mm) instead of simulating the pullout directly. The soil was modelled using hyperbolic stress–strain relations with a Mohr-Coulomb (MC) failure criterion, as described by Duncan and Chang (1970). Unbonded interface elements with the Coulomb shear strength criterion were used to model the interface between the pipe and soil during radial expansion of the pipe.

Meideni et al. (2017) used the discrete-element method (DEM) to study the axial pipe–soil response of a steel pipeline buried in granular material. The experimental results reported by Wijewickreme et al. (2009) were used to validate the numerical model. The pipe was modelled using triangular facet elements (flat discrete elements) with a material modulus comparable to the steel pipe. The soil was modelled using spherical discrete elements. An increase in normal stresses

was noticed around the pipe during the pullout, confirming the effects of soil dilation on the pipe buried in dense sand. They noticed that most of the soil movement occurred in the close vicinity of the pipe (approximately 1.5 times the pipe diameter, 1.5*D*).

Al-Khazaali and Vanapalli (2019a) carried out a plane strain finite-element analysis using commercial FE software, SIGMA/W, to investigate the force–displacement behaviour of a buried pipeline in saturated and unsaturated conditions. The soil was modelled using the MC criteria for both the soil conditions, where apparent cohesion value was used to model the unsaturated sand (derived using the Vanapalli et al. 1996 model). For saturated soil conditions, the soil's modulus of elasticity was considered constant with depth, while the variation of the unsaturated modulus of elasticity with depth was estimated using the Vanapalli and Oh-model (Vanapalli and Oh 2013).

Saberi et al. (2022) introduced the 'Hybrid-Winkler-Interface' (HWI) modelling approach to simulate axial soil–pipe interaction. In the hybrid formulation, the pipe was modelled by beam elements. The surrounding soil mass was represented by Winkler springs at the pipe top (crown), two sides (springlines) and bottom (invert). A solid thin layer of interface elements represented the soil-pipe interface. The interface element was based on the bounding surface plasticity constitutive model described by Saberi et al. (2016, 2017). The Winkler soil springs were defined using the bilinear elastic-perfectly plastic spring models recommended in ALA (2005). This model was implemented in Abaqus by developing a user subroutine UMAT. The HWI model was validated using the full-scale laboratory pullout tests of steel pipes (Sheil et al. 2018) and HDPE pipes (Weidlich and Achmus 2008; Bilgin and Stewart 2009b) in sands of different relative densities. The efficiency of the proposed HWI model depended on the initial distribution of the

normal stress around the pipe circumference, which was applied to the interface element in the model.

Meidani et al. (2018) employed a finite-discrete element approach to examine the test results of an MDPE pipe reported in Weerasekara and Wijewickreme (2008). The pipe was modelled using finite elements, and the soil was modelled using discrete elements. The study confirmed the elongation of the pipe and reduction in the cross-section during pullout of a flexible MDPE pipe.

Muntakim and Dhar (2021) developed a three-dimensional (3D) FE model to investigate the load transfer mechanisms of flexible MDPE pipes during axial pullout loading. The conventional MC model was used to characterize the stress–strain behaviour and shear failure of the sand. The MDPE pipe was idealized as a linear elastic material. The FE model was first validated with experimental data available in the literature for MDPE pipes (Weerasekara and Wijewickreme 2008). A parametric study was conducted for the modulus of elasticity of the soil and the soil friction angle. Based on FE modelling, they demonstrated that the relative rigidity of the pipe with respect to the surrounding soil could influence the normal stress on the pipe. The normal stress was reduced due to the pipe's diameter reduction, causing positive arching of soil. A normal stress factor was introduced in the design equation for rationally calculating the normal stress and hence the pullout force for MDPE pipes.

Table 2.2. Summary of previous experimental studies on axial pipe–soil interaction

Reference	Pipe material	Pipe diameter, (mm)	Burial depth, (m)	Pipe length, (m)	Backfill material	Relative density, D_R (%)	Loading rate, (mm/min)
Paulin et al. (1998)	Steel	324	0.75	6	Well-graded sand	~0 & ~100	0.1667
Anderson (2004)	MDPE	60 & 114	0.72–0.75	5	Fraser River sand	43–70	0.1667
			0.48–0.52			91–102	
Weerasekara and Wijewickreme (2008)	MDPE	60.3 & 114.3	0.6	3.8	Uniformly graded Fraser River sand	~75	0.6
Bilgin and Stewart (2009a)	Cast iron	176.5	0.76	3.66	Loose and dense sand	–	–
Bilgin and Stewart (2009b)	HDPE	168.3	0.76	1.22	Poorly graded sand (USCS classification=SP)	–	24
Wijewickreme et al. (2009)	Sand-blasted steel	457	1.24	3.8	Uniformly graded Fraser River sand	~20	120–3000
			1.14	3.8 & 5		~75	
Alam and Allouche (2013)	Coated steel	203.2	1.2–4.88	3.65	Pea gravel, sand, silty clay	–	–
Wijewickreme and Weerasekara (2015)	MDPE	60.3	0.56, 0.57 & 0.98	8.5	Uniformly graded Fraser River sand	88, 92 & 82	0.601, 2.145 & 2.185
Sarvanis et al. (2017)	Steel	219.6	2	3	Two different types of sand	–	–
Sheil et al. (2018)	Steel	350	0.35–1.2	1.31	Dry Hostun sand and damp, silty sand	35± 2	4 & 14

Reference	Pipe material	Pipe diameter, (mm)	Burial depth, (m)	Pipe length, (m)	Backfill material	Relative density, D_R (%)	Loading rate, (mm/min)
Al-Khazaali and Vanapalli (2019b)	Steel	114.3	0.25	1.5	Poorly graded silica sand (saturated and unsaturated conditions)	69	2
Marino and Osouli (2020)	Coal tar–coated steel	203	1.2 & 1.8	6.4	Silty clay with trace to little sand and trace gravel	–	0.15–0.6
					Clayey medium to fine sand with no to little coarse- to fine-grained gravel		0.3–0.48
Murugathasan et al. (2021)	Ductile iron	178	0.69 & 0.825	2.7	Well-graded sand (USCS classification=SW)	0 & 75%–80%	1, 30 & 60

Table 2.3. Summary of previous numerical studies on axial pipe–soil interaction

Reference	Numerical Method	Software	Pipe material	Pipe diameter, (mm)	Burial depth, (m)	Relative density, D_R (%)	Remarks
Wijewickreme et al. (2009)	Explicit finite difference	FLAC 2D	Steel	457	1.14	75	MC model (ϕ'=45°, ψ=15°); Hyperbolic model
Meideni et al. (2017)	Discrete element	YADE (open soure code)	Steel	460	1.15	75	Contact law to model interaction between particles
Meideni et al. (2018)	Finite-discrete element	YADE (open soure code)	MDPE	114	0.6	75	Contact law to model interaction between particles
Al-Khazaali and Vanapalli (2019a)	Implicit finite element	SIGMA/W	Steel	114.3	0.25	69	MC model (ϕ'=35.3°, ψ=6.75°)
Muntakim and Dhar (2021)	Implicit finite element	Abaqus/Standard	MDPE	114	0.6	75	MC model (ϕ'=33°, ψ=0.1°)
Murugathasan et al. (2021)	Implicit finite element	Abaqus/Standard	Ductile iron	178	0.825	0	MC model (ϕ'=30°, ψ=8°)
						75–80	MC model (ϕ'=38°, ψ=0.1°)
Saberi et al. (2022)	Hybrid beam-spring-interface element	Abaqus/Standard	Steel	350	0.35–1.2	35	Bounding surface plasticity constitutive model
			HDPE	140, 168.3	0.21–0.76	40,50,70	

2.4 Shear Mechanisms

As discussed in previous sections, the axial resistance of buried pipelines significantly depends on the pipe–soil interface frictional behaviour. In this regard, the shear mechanism of the interface with microscopic observation in experimental sand–polymer interface tests is discussed below.

Various studies revealed that the interface behaviour between sand and polymer depends on the polymer's surface roughness (or smoothness), hardness, topography, tensile strength, modulus and the sand's composition, grain size, water content, density, and applied normal stress at the interface (Williams and Houlihan 1987; O'Rourke et al. 1990; Dove and Frost 1999; Dove and Jarrett 2002; Scarpelli et al. 2003; DeJong and Westgate 2005). O'Rourke et al. (1990) studied the interface behaviour of HDPE, MDPE, and polyvinyl chloride (PVC) geomembrane in contact with Ottawa sand. They reported that the primary shear mechanism for the HDPE/MDPE–sand interface was the sliding of the sand grains, while particle rolling occurred at a relatively softer PVC–sand interface, as shown in Figure 2.3. Several parallel scratches on the HDPE surface after the shear test confirmed the sliding of the sand particles along the polymer surface (Figure 2.3a). In comparison, no surface deformations were observed on PVC geomembrane interfaces. Shear force on the sand grains adjacent to the interface causes a rolling and recoverable indentation of the relatively soft polymer (Figure 2.3b). Dove and Frost (1999) found a similar shearing mechanism on smooth HDPE geomembrane/sand interfaces. A study on sand–HDPE polymer performed by DeJong and Westgate (2005) summarized that sand particle sliding during shearing dominates at low stress, transitioning to particle rolling at high normal stresses.

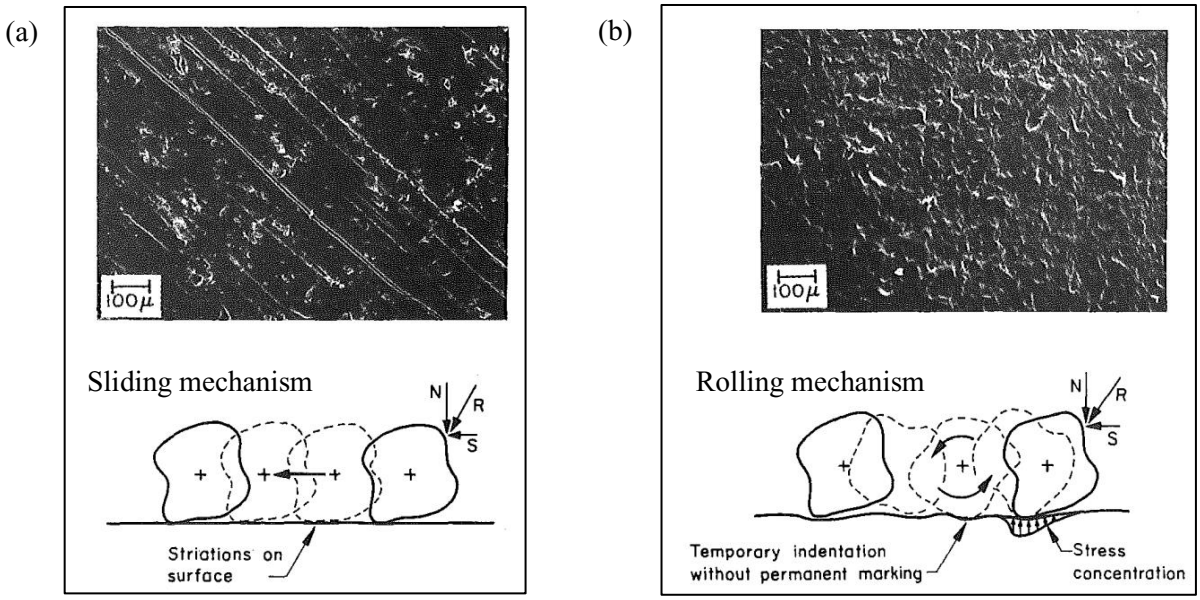

Figure 2.3: Scanning Electron Microscope (SEM) photograph after shearing with Ottawa sand (under 20.7 kPa normal stress): (a) HDPE surface; and (b) PVC surface (O'Rourke et al. 1990)

Volume change of soil due to dilatancy is one of the key properties of the soil–structure interface. As discussed in section 2.3, the shearing-induced dilation at the pipe–soil interface can increase the normal stresses, resulting in a higher axial soil resistance in dense sand (Wijewickreme et al. 2009). Researchers (e.g., Wijewickreme and Weerasekara 2015) applied the cavity expansion theory to estimate the maximum normal stress increase on the pipe surface due to shearing-induced soil dilation. However, the normal stress increase at the interface (hence, soil dilatancy) has yet to be comprehensively examined during axial pullout tests of pipes, particularly for PE pipes. The dilatancy of the interface has been investigated by using direct shear type and simple shear type devices (e.g., O'Rourke et al. 1990; Reddy et al. 2000; Dove and Jarrett 2002). Many tests were also conducted to identify the main factors that influence the dilatancy behaviour of the interface. The surface roughness of a structure (e.g., pipeline) is now known to be a major influential factor (e.g., Nakamura et al. 1999; Dove and Jarrett 2002; Zhang et al. 2011).

Results of direct shear tests on an HDPE geomembrane/sand interface by O'Rourke et al. (1990) observed no volume change or dilatancy above the smooth HDPE interface, even in dense sand. This behaviour is in contrast with the conventional belief of interface soil dilation for buried pipe. Later, Dove and Jarrett (2002) investigated the influence of polymer surfaces' topography (smooth or rough) on the interface shear strength. They concluded that when the size of sand grains is large with respect to the asperities of the interfacing material (i.e., smooth interface), the soil volume changes are small above the interface. These interface systems were referred to as "nondilative" (Figure 2.4a). In "dilative" interface systems (Figure 2.4b), on the other hand, the sand particle sizes are small with respect to the surface asperities of the opposing material. In this case of sand grains against a "rough" surface, significant volume change can occur during shearing, resulting in higher interface strengths. Schlosser (1982) suggested earlier that the dilation behaviour of the soil essentially governs the interface frictional resistance between rough inclusion (i.e., soil nails) and soil. During pullout of the inclusion, shear stresses on the interface cause soil particles to slide and roll around the inclusion, resulting in the dilation of the soils in the vicinity of the inclusion.

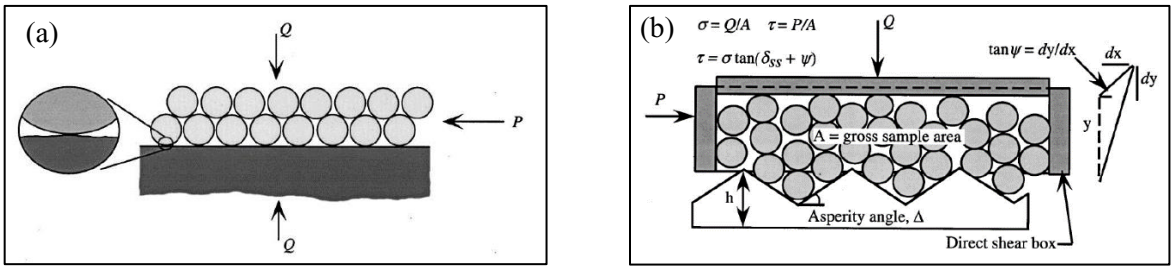

Figure 2.4: (a) Schematic illustration of nondilative interface system; and (b) Idealized dilative interface system (Dove and Jarrett 2002)

2.5 Summary

Axial soil load on a pipe is one of the main concerns for pipeline design engineers for pipes subject to relative axial displacement. Current design guidelines adopt a design equation to calculate the maximum axial force in cohesionless soil based on soil–pipe interface parameters and an assumed failure mechanism of the soil. Over the past few decades, researchers have performed experimental studies and evaluated the recommendations in the design guidelines for correctly calculating the axial soil resistance for steel pipes. Based on the experimental results, it was argued that the shearing-induced dilation at the pipe–soil interface increases the normal stresses, leading to a higher axial soil resistance than the one calculated using the method recommended in the design guidelines. However, the measured axial soil loads on pipes buried in loose, dry sand were comparable to those predicted using the equation recommended in the design guidelines. The present literature review shows that studies on the soil–pipe interaction for flexible pipes (e.g., PE pipes) under axial ground movements are limited.

The design methods developed for steel pipes are often used in the design of PE pipes. PE pipe can experience significant axial elongation and reduction in cross-sectional dimensions when subjected to axial force due to ground movements. The reduction in pipe diameter resulted in a decrease in particle contact stresses and, therefore, normal stresses around the pipe. The behaviour of the PE pipe was found to be more complex and showed nonlinear time–dependent stress–strain responses. Researchers considered the nonlinear, strain rate–dependent stress–strain response of the PE pipe material to analyze the pipe responses under axial soil loading to account for the pulling rate effects. The cavity expansion theory was applied to estimate the normal stress increase on the pipe surface due to shearing-induced soil dilation. The applicability of this approach of

analysis under various burial conditions of pipelines was not investigated. In addition, the normal stress increase at the interface (hence, soil dilatancy) of smooth PE pipes has not been examined during the axial pullout tests of pipes.

Finally, although the studies on steel pipes have been used to develop the current design guidelines for buried pipeline design, the literature review shows discrepancies between the responses of steel and PE pipes. Further studies will provide a better understanding of the PE pipe–soil interaction behaviour for different burial conditions, pipe sizes, and pulling rates.

CHAPTER 3

Axial Pullout Behavior of Buried Medium-Density Polyethylene Gas Distribution Pipes

Co-Authorship: A version of this chapter has been published in the International Journal of Geomechanics as: Reza, A. and Dhar, A. S. (2021). 'Axial Pullout Behavior of Buried Medium-Density Polyethylene Gas Distribution Pipes.' Most of the research presented in this chapter has been conducted by the first author. He also prepared the draft manuscript. The other author mainly supervised the research and reviewed the manuscript.

3.1 Abstract

This paper presents an experimental investigation into the axial pullout behaviour of buried 60-mm diameter medium-density polyethylene (MDPE) pipes under various pulling rates. Tests were conducted in a facility developed at Memorial University of Newfoundland. During the tests, pipe elongations and axial strains were measured to examine the mobilization of axial force with leading end displacement, and circumferential strains were measured to capture the effects of pipe diameter change. Finite-element (FE) modeling of the tests was used to evaluate the interface friction angle and the effect of diameter changes on the normal stresses on the pipe surface, which influence the pullout resistance of the soil. The results indicated that the pipes' elongation, diameter decrease, and pulling rate significantly influence the pullout forces for buried MDPE pipes subjected to axial ground movement. FE analysis with interface friction angles of 0.75ϕ, 0.86ϕ, and 0.9ϕ was found to successfully simulate the test conditions under pulling rates of 0.5, 1, and 2 mm/min, respectively. Based on the study, simplified methods were proposed to calculate the mobilized frictional length and pipe wall strain from the leading end displacement.

3.2 Introduction

Pipelines are used extensively worldwide for the transportation and distribution of liquids and gases. Canada's transmission pipeline companies operate more than 119,000 kilometres of pipeline within Canada, which is almost three times the length of Canada's national highway system (CEPA 2016). In Canada, 72% of the energy is provided by oil and gas, of which more than 90% is delivered in pipelines (CEPA 2016). However, the failure of a pipeline conveying flammable material such as oil and gas poses economic, environmental, and safety concerns. Pipe failure can lead to severe damage, death, service disruption, and environmental pollution. Ground movements have been identified as one of the major causes of pipeline failure (CEPA 2017). Assessment of pipelines subjected to ground movement is, therefore, an important consideration for pipeline integrity assessment.

Pipelines are subjected to axial force when the direction of the ground movement is parallel to the pipe axis. With the recent advancement of sensor technologies, ground movement can be monitored with reasonable accuracy. However, rational design tools are required to assess pipe wall stresses/ strains related to the amounts of ground movements. For the assessment of pipelines subjected to axial ground movement, ASCE (1984) and ALA (2001) adopted a design equation to calculate the maximum axial force in cohesionless soil, as expressed in Eq. (3.1):

$$F_A = \pi D \gamma H L \left(\frac{1+K_0}{2}\right) \tan(\delta) \qquad (3.1)$$

where F_A = the maximum axial force, which is equal to the maximum soil resistance to pipe movement; γ = unit weight of soil; H = depth from the ground surface to pipe springline; L = pipe length; D = pipe outer diameter; K_0 = coefficient of lateral earth pressure at rest, and δ = interface friction angle between the pipe and the surrounding soil. Eq. (3.1) is based on the interface

frictional resistance on the pipe surface, calculated assuming the normal stress as the arithmetic means of the vertical overburden pressure and the estimated at-rest lateral earth pressure at the springline level of the pipe. Over the years, numerous studies have been conducted to validate the equation through proper understanding of the soil–pipe interaction mechanisms for pipes subjected to axial ground movements (Wijewickreme et al. 2009; Meidani et al. 2017; Bilgin et al. 2009ab; Liu et al. 2011; Gerlach and Achmus 2018; Sheil et al. 2018). Most of these studies have focused on steel pipes, and the pipes are assumed to be rigid. For steel pipes, Eq. (3.1) was found to underpredict the maximum pullout force for a pipe buried in dense sand.

Flexible polyethylene pipes are also used extensively for oil and gas transportation, particularly in the gas distribution system. Studies on the performance of flexible polyethylene pipe subjected to ground movement are very limited. For flexible pipes, axial force causes the pipe to elongate, reducing the diameter (Weerasekara and Wijewickreme 2008; Meidani et al. 2017; Muntakim and Dhar 2017). As a result, the unit frictional resistance on the pipe wall is not uniform, affecting the pullout forces. For HDPE pipe, Bilgin and Stewart (2009b) showed that the pullout force is reduced due to diameter decrease. Furthermore, polyethylene pipe materials show nonlinear time–dependent stress–strain behaviour. Thus, the force incurred by polyethylene pipes may depend on the rate of ground movements. Ground movements of various rates ranging from imperceptibly slow (millimetres per year) to extremely rapid (many meters per second) have been observed in the field (Cruden and Varnes 1996). The forces experienced by the polyethylene pipes subjected to these various rates of ground movements are not well understood. The current study focuses on an investigation of the axial pullout force on a medium-density polyethylene (MDPE) pipe under various rates of relative ground movements. The MDPE pipes are CSA B137.4 certified and are

mostly used for gas utilities across Canada.

Weerasekara and Wijewickreme (2008) and Wijewickreme and Weerasekara (2015) conducted axial pullout tests of MDPE gas distribution pipes buried in Fraser river sands to investigate the behaviour of the pipes subjected to axial ground movements. The pipes were buried in a backfill compacted to a unit weight of ~16 kN/m^3 (ranged from 15.8 to 16.1 kN/m^3), corresponding to a relative density of ~75%. Weerasekara and Wijewickreme (2008) presented the laboratory axial pullout tests of 60- and 114-mm diameter MDPE pipes where the pipes were pulled at the specific rate of displacement of 36 mm/hour. Unlike for steel pipes, it has been reported that the frictional resistance at the pipe's surface is not uniformly mobilized over its entire length at the same time, due to elastic-plastic elongation of the pipe. The length of shear strength mobilization was found to increase with the increase of relative ground movement. To understand the progression of the mobilized load, they measured pipe wall strains on two pipes at several locations along the length. However, test results were found to be affected by the presence of the strain gauges and, therefore, could be used for evaluation of the mobilized friction lengths against the pullout forces. Wijewickreme and Weerasekara (2015) presented field tests of 60-mm-diameter MDPE pipes conducted at various pulling rates. They found that the pulling rate has significant effects on the pullout resistance. The effects of pulling rate on the progression of mobilized friction length could not be assessed in that study, as the wall strains within the buried segment of the pipe were not measured. Wijewickreme and Weerasekara (2015) considered a rate–dependent modulus of elasticity of the pipe material to determine the pipe response under axial soil loading, in an attempt to account for the pulling rate effects. However, the interaction of the pipe surface with the surrounding soil is also expected to be rate–dependent, which was not examined. Moreover,

backfill soil density often varies from site to site for the gas distribution system. The effects of the backfill soil density on the behaviour of the pipe were not investigated.

The objective of the current study is to address the research gaps discussed above for MDPE pipes and examine the effect of loading rate on the behaviour of the pipes, including the mobilized friction length. Full-scale tests were conducted with pipe wall strains measurements to capture the mechanics of soil–pipe interaction experimentally. FE analysis was then employed to capture the features that could not be measured during the tests, including the soil, pipe, and interface parameter's contributions to the pipe behaviour. One of the challenges in identifying the rate–dependent interaction during experiments is measuring the effect. This challenge could be overcome through finite-element (FE) modeling, with validation of the model using the responses that could be measured during the tests. Since the loading rate effect is found more significant on the interface behaviour, the finite-element analysis did not consider the effects of loading rate on the pipe materials elasticity (which depends on the strain rate; not on the axial pullout rate). Details relating to these loading rate effects are discussed in the FE modeling section. Using the tests and finite-element analysis results, a simplified method for calculating mobilized frictional length and pipe wall strain for MDPE pipe is proposed.

Pipes buried in a backfill soil compacted to a density of ~14.5±0.5 kN/m^3 were considered in this study that would enrich the database in the body of knowledge with the behaviour of pipes buried in a different soil condition (different from the one in Weerasekara and Wijewickreme 2008). Understanding the behaviour under various backfill conditions would also be helpful in future design and construction of pipes in the areas of slow-moving ground, properly knowing

their behaviour. Note that PRCI (2009) recommends burying pipelines in loose to moderately dense granular backfill as a practical means of reducing soil restraint. Soil density considered in this study is consistent with the PRCI (2009) recommendation.

3.3 Test Facility

A full-scale pipe testing facility has been developed at Memorial University of Newfoundland to investigate pipes subjected to relative ground movements. The facility is designed to simulate the movement of pipes with respect to surrounding soil; the soil is fixed in a box, and a buried pipe is pulled through the soil (Murugathasan et al. 2021). It is a steel box with inside dimensions of 4 m in length, 2 m in width, and 1.5 m in height, as shown in Figure 3.1. The rigidity of the boundary walls is increased by adding longitudinal and transverse stiffeners outside the cell to control lateral soil movement and thus obtain the lateral earth pressure expected in the field (Figure 3.1a) (Murugathasan et al. 2018). Two circular openings of adjustable size on two opposite walls in the long direction of the box allow pulling of pipes of different diameters. The opening size is adjusted using a separate steel plate fitted with a replaceable hard-rubber gasket with the opening (hole) at the center (Figure 3.1b), bolted to the test box. The rubber gasket with the right opening size is fitted with the steel plate to change the opening size. The hole in the rubber gasket is somewhat larger than the pipe diameter. For example, a 62-mm diameter hole is used for the axial pulling of a 60-mm diameter pipe. The gaskets allow the pipe's movement at both ends of the box while preventing the sand from escaping from the box. The face of the rubber gasket openings is lubricated using grease to minimize the friction between the pipe and the wall of the openings. The records of several independent pullout tests demonstrated that the frictional resistance at the gasket is around 0.2 kN, which is considered negligible in comparison to the total pullout resistance measured during the tests.

No sidewall treatment is applied to reduce wall friction between the cell wall and the soil. Friction between the soil and the test facility's interior walls is particularly important under a vertical load to reduce the arching effect (Alam and Allouche 2010; Tognon et al. 1999; Dhar and Moore 2004). For the horizontal load (axial pulling), the soil and the test cell walls are fixed. No sliding of soil with respect to the cell walls is expected. Wijewickreme et al. (2009) reported that the effect of sidewall friction on axial pullout tests is insignificant.

A hydraulic ram is used to pull the pipe from one end while the other end of the pipe is free to move. With a maximum displacement capacity of 150 mm, the hydraulic ram is connected to a hydraulic actuator system and a data acquisition system. To measure the pulling force, a load cell is attached to the hydraulic actuator system and connected to the buried pipe by a solid steel coupling. The pipe is tightly gripped at the leading end with the solid steel coupling, using two steel hose clamps. A linear variable displacement transducer (LVDT) is used at the other end of the pipe, herein called the trailing end, during the tests to obtain trailing end movements of the pipe. The load cell capacity is 22.25 kN with a system accuracy of ±4.45 N. The LVDT has a total travel capacity of 110 mm with an accuracy of about 0.5 mm. The test configuration is shown in Figure 3.2.

The test pipe is protruded out of the test box at both ends through two circular openings to facilitate pulling at the leading end and to ensure that the trailing end does not get into the test box during axial pulling. Thus, the length of the pipe in contact with the soil remains the same, which is the length of the test box.

3.4 Test Program

The test program is planned to investigate the axial pullout behaviour of MDPE pipes in the sand under various rates of ground movements. Segments of a 60-mm diameter MDPE pipe are tested. This type of pipe is commonly used for the gas distribution system in Canada (Anderson et al. 2004). The Standard Dimension Ratio (SDR) (ratio of the pipes outside diameter to wall thickness) of the pipes is 11. The pipe segments (herein called 'pipe') are placed over 0.6 m of bedding layer in the test box, simulating trench installation. The pipes are buried at a depth of 0.48 m, which is around eight times the pipe diameter. The soil width on each side of the pipes in the 2 m wide test cell is about 16 times the pipe diameter, which is sufficiently far to minimize the boundary effects during axial pullout tests. The pipes are pulled at three different pulling rates: 0.5 mm/min (Test 1), 1 mm/min (Test 2), and 2 mm/min (Test 3) at the leading end. The pulling rates were selected based on feasibility under the laboratory condition. Note that the pulling rates fall in the velocity Class 5 (>0.3 and <30 mm/min) corresponding to moderate landslide velocity, according to Cruden and Varnes (1996). The test results would be useful for developing a model to estimate the pipe behaviour for ground movement scenarios expected in the field (through interpolation or extrapolation).

The pipes were instrumented with electrical resistivity strain gauges to capture the mobilization of axial force along the pipe's length and the effects of changes in pipe diameter during the test. Note that, due to the small size of the pipe, pipe diameter changes could not be measured. Three uniaxial strain gauges are installed at the distances of one-fourth, half, and three-fourths of the pipe length within the box from the leading end, respectively, to measure the responses due to mobilized axial pullout force. The uniaxial strain gauges are placed at the pipe crown. One biaxial strain

gauge is attached at the middle of the pipes (half-length within the test box) at the springline to monitor longitudinal and circumferential strains. The circumferential strains are used as the measures of the effect of pipe diameter change. However, installing the strain gauges involving gauges, wires, and protecting wraps, as shown in Figure 3.3, is found to affect the interface property, resulting in a higher pulling force (Weerasekara and Wijewickreme 2008). To examine the effects, a set of companion pipes is tested without any strain gauges. Tests conducted without the strain gauges on the pipes are herein termed Test 1, Test 2, and Test 3 for tests conducted at the pulling rates of 0.5, 1, and 2 mm/min, respectively. The corresponding tests with strain gauges are termed Test 4, Test 5, and Test 6, respectively. All instruments are connected to a data acquisition system equipped with a personal computer to record data simultaneously. The pipe backfill materials and installation procedures used are discussed in the following.

3.4.1 *Backfill Material*

A locally available well-graded sand (SW, according to USCS) is used as the backfill material for the pipe. The material contains approximately 1.30% of fines and 98.70% of sand. The maximum dry density is estimated as 18.8 kN/m^3, using Standard Proctor Compaction tests (ASTM D698 2003; Saha et al. 2019). After completing the axial pullout, density measurements are taken at three different locations inside the testing tank, which yielded an average unit weight of 14.5±0.5 kN/m^3 from the top surface to the pipes springline level. Thus, the average relative compaction of the backfill material is roughly 80% of the Standard Proctor Maximum dry density. An air-dried condition of sand with a water content of around 0.8%–1.50% is confirmed for all the tests conducted. The mechanical properties of the sand were determined using direct shear tests at various normal stresses (Saha et al. 2019). It was found that the peak friction angle is high at a lower normal stress level and decreases with the increase of stress level. At the stress level

expected for the pipe (i.e., ~10 kPa), the peak friction angle can be estimated as 40°, based on the test results (Saha et al. 2019). Saha et al. (2019) also reported that the stress–strain behaviour of the sand depends on the presence of moisture in the soil. At the density level expected in the tests, the sand shows post-peak degradation of shear strength in a dry condition. However, post-degradation was not observed in the moist sand. Thus, the dilation angle of the moist soil (used in the test) can be assumed to be zero.

3.4.2 *Pipe Installation*

To simulate trench installation, backfill material is first placed in the facility up to the top surface of the ground. The sand is dumped from bags directly into the tank from an overhead crane, maintaining a height of approximately 1 m and spread using hoes and rakes in 150-mm-thick lifts. The soil is partially compacted by kneading and levelling the soil surface at each lift. Then, a trench with sloped sides is excavated over the entire length (i.e., 4 m) of the cell to place the 60-mm-diameter MDPE pipe. An illustration of the trench preparation and cross-section are provided in Figure 3.4. The width and depth of the trench are five times the outer pipe diameter (5D), measured from the center to the trench bottom. It is assumed that sand further than 5D distances has minimal effects during the axial pullout.

The backfill material is then placed in the trench to the required density (medium dense condition), and then the pipe is laid parallel to the longer direction of the test cell. A large spirit level of 1000 mm basic length is used to ensure the straightness of the pipe during backfilling. Note that the flexible MDPE pipe may not always be straight, particularly on uneven ground, which may affect the pullout force. Phillips et al. (2004) reported that slight axial misalignment could cause a significant increase in the mobilized axial resistance. The effect of out-of-

straightness on the pullout force has not been investigated here.

The test pipe and sand were removed from the tank after each test, and the pipe installation procedure was repeated consistently for the following tests. Note that the pipe, once used in the test, was not reused in the subsequent tests to avoid the effects of any possible residual stresses.

3.5 FE Modeling of the Tests

FE analysis is performed to simulate the test conditions for pipes, to explore the mechanics of soil interaction and the parameters contributing to the axial pullout forces under various pullout displacement rates. The modeling is performed using the commercially available FE software, Abaqus (version 6.14) (Dassault Systems 2014). Dynamic analysis is performed using the Abaqus/ Standard module that uses implicit time integration to calculate a system's response. Three-dimensional (3D) analyses are performed to model the soil–pipe interaction in the pullout tests of 60-mm diameter MDPE pipes. The pipe and soil domains are modelled using C3D8R solid elements, available in Abaqus. A finer mesh is used in the pipe's close vicinity over a radial distance of 2.0 times the pipe diameter (2*D*). A mesh sensitivity study was conducted, which showed that a minimum element size of 3.5 mm was suitable, which was selected for the analysis. The coarser mesh is used beyond 2*D* to reduce the computational time. Figure 3.5 shows a typical FE mesh used in the analysis. The contact between soil and pipeline is modelled using the general contact algorithm to model all possible contacts between the bodies. A penalty algorithm is used to model tangential contact behaviour with a friction coefficient. For the general contact interaction, the pipe surface is modelled as a pure master, and the soil surface is modelled as a slave. It is common practice to model the stiffer surface as a pure master and the relatively low stiff surface as a slave (Dassault Systems 2014). This technique allows slip and/or separation

between different elements in the contact. The pipe is extended beyond the test cell boundary at the front and rear ends so that the total length of contact of the soil with the pipe remains unchanged during axial pullout (similar to the laboratory tests).

Murugathasan et al. (2018) demonstrated that the test cell's boundary walls could reasonably be considered rigid under axial pullout loading. Therefore, a zero-displacement boundary condition is used for each side of the test box, except for the pipe's axial movement. Axial movement of the pipe is allowed to apply pullout force. The load is applied using the following steps: (i) gravitational load is applied in layers to simulate the initial condition, (ii) axial displacements is applied from one end of the pipe (herein termed the 'leading end') and the other end (termed as the 'trailing end') is free to move.

3.5.1 *Material Parameters*

The MDPE pipe is idealized as a linear elastic material. However, the stress–strain relation for polymer material is nonlinear and known to be strain rate and temperature–dependent. Suleiman and Coree (2004) proposed a modified hyperbolic model to account for the strain rate–dependent modulus of elasticity of polyethylene pipe material, as expressed in Eq. (3.2):

$$E_{\text{ini}} = a(\dot{\varepsilon})^b \tag{3.2}$$

where E_{ini} = initial Young's modulus of the material, $\dot{\varepsilon}$ = strain rate; and a and b = constants obtained from uniaxial tension or compression tests. Wijewickreme and Weerasekara (2015) reported the constant a and b as 2020 and 0.109, respectively.

During the laboratory pullout tests, the measured average strain rate on the pipe wall was found

to vary from 2.85×10^{-6}/s to 5.85×10^{-6}/s. Using the measured average strain rates and the hyperbolic stress–strain relation (Eq. 3.2) with a = 2020 and b = 0.109, Young's modulus was calculated that ranges from 500 to 550 MPa. Thus, the modulus of elasticity of pipe material, E_p, is expected to vary between 500 to 550 MPa (around 10% variation) during the tests with the pulling rates of 0.5–2 mm/min.

For the soil, the built-in elastic-perfectly plastic model with Mohr–Coulomb (MC) plasticity, available in Abaqus, is employed to model the stress–strain behaviour and shear failure of the sand. In this model, the soil is assumed to deform elastically until the stress state reaches the MC failure criteria (yield surface). When the stress state reaches the yield surface, plastic deformation occurs, and the soil dilates at a constant dilation angle. Although the soil in the field may experience plastic strains before it reaches the yield surface and may have a non-constant dilation angle, the conventional MC model successfully simulated the ultimate soil resistance during the axial pullout (Muntakim and Dhar 2017; Yimsiri et al. 2004).

Young's modulus for the soil is estimated using Eq. (3.3) (Hardin and Black 1966; Janbu 1963):

$$E = Kp_a\left(\frac{p'}{p_a}\right)^n \tag{3.3}$$

where K is a material constant; p_a is the atmospheric pressure (100 kPa); p' is mean effective confining pressure, and n is an exponent. This power function is widely used in the numerical modeling of pipe–soil interaction problems (Yimsiri et al. 2004; Guo and Stolle 2005; Daiyan et al. 2011; Jung et al. 2013). The value of E is estimated based on the mean effective stress (p') at the springline level of the pipe with K = 150 and n = 0.5 (Roy et al. 2015) as E = 5 MPa for the

sand used in the tests. A constant Poisson's ratio of 0.3 is assumed for the medium dense condition of the sand. The angle of internal friction is selected based on Saha et al.'s (2019) test results. Saha et al. (2019) determined that the angle of internal friction of the sand is high at a low-stress level, decreases with the increase of stress level, and eventually reaches a constant value. The dilation angle was negligible for the moist condition of the sand. Therefore, a constant angle of internal friction of 40° is used, which corresponds to the average stress level (~10 kPa) expected in the tests. A small dilation angle of 0.1° and a small cohesion of 0.1 kPa is applied for numerical stability during analysis. The minimum values of dilation angle and cohesion are required to avoid ill-conditioning during numerical calculations. Table 3.1 shows the soil parameters used in the analysis.

To examine the effect of the changes in the modulus of elasticity of the pipe material due to the strain rate–dependent effects, FE analysis was performed to calculate the pullout forces with E_p = 500 MPa and E_p = 550 MPa, respectively. The calculated pullout force was not significantly different (<4% variation) for the change in the modulus of elasticity. Thus, a constant modulus of elasticity can be used to reasonably approximate the pipe conditions in the tests. E_p = 550 MPa is used in finite-element analysis to simulate the test conditions.

From an extensive parametric study using FE analysis, the pulling rate was found to affect the pipe–soil interface most significantly. Therefore, the interface friction parameter is identified to account for the pulling rate effect during FE analysis, as discussed below.

3.5.2 *Interface Parameter*

In a general contact algorithm, the sliding occurs when the shear stress at the contact interface reaches the critical shear stress (i.e., interface shear strength), the friction coefficient (i.e., $\mu = \tan\delta$) times the normal stress. The interface shear strength is limited to the shear strength of the surrounding soil. The value of the angle of interface shearing resistance, δ, depends on the interface behaviour between the soil and the pipe, including the roughness and hardness of the pipe surface. ALA (2001) guideline suggests that δ can be estimated as $\delta = f\phi$, where 'ϕ' is the internal friction angle of the backfill material, and 'f' is the interface friction reduction factor, relating the internal friction angle of the soil to the friction angle at the soil–pipe interface. Scarpelli et al. (2003) conducted measurements of the friction coefficient, $\tan\delta$, for various materials and showed that soil grains could penetrate some materials (Figure 3.6), increasing the friction coefficient. Grain penetration can also occur on the MDPE pipe surface, causing a higher value of the interface friction angle. Also, interface behaviour for the MDPE pipe is expected to be pulling rate–dependent due to the time–dependent behaviour of the material. A pulling rate–dependent angle of interface friction can account for the time–dependent effects. Thus, FE analysis was performed with various angles of interface friction to simulate the test results for various rates of pulling. Table 3.2 summarizes the parameters for the interface friction for various test conditions.

3.6 Analysis of Results

3.6.1 *Force–Displacement Responses from Tests*

During the axial pullout of pipes in the tests, the surrounding soil offers resistance to pipe movements. The soil's resisting force is equal to the pullout forces applied to the pipe. The measured pullout responses obtained during the tests are presented in Figure 3.7, which shows a

nonlinear relationship between the soil resistances with the pulling displacements at the leading end of the pipe. The force–displacement responses from all tests match each other at lower leading end displacements in Figure 3.7, indicating consistent burial conditions (including straightness) of the test pipes. The effects of the pulling rates become significant at higher displacements when the plastic deformations are predominant, resulting in differences in the responses. As seen in the figure (Figure 3.7), nonlinearity in the load–displacement response starts almost immediately (at the leading end displacement of ~0.5 mm), indicating minimal elastic displacements. Beyond 0.5 mm of leading end displacement, the interface friction capacity starts to mobilize at the leading end of the pipe that progresses gradually toward the trailing end. The nonlinearity in the force–displacement response in Figure 3.7 is associated with the gradual mobilization of the interface shear strength. The figure also reveals that the rate of increase in the shearing resistance is higher for the higher pulling rates, confirming the effect of pulling rate on the interface behaviour (as mentioned earlier). The nonlinear increase of pullout resistance continues until the interface shear strength is mobilized over the entire length of the box (i.e., 4 m), beyond which the pullout resistance reduces due to the release of the trailing end. The mechanism is further examined with pipe elongations, as discussed below.

The flexible MDPE pipe elongates during pulling due to the development of axial forces. The elongations of the pipes obtained during Tests 1 to 3 are presented in Figure 3.8. Figure 3.8 plots pipe elongations, calculated from the difference between the leading end displacements and trailing end displacements, against the leading end displacements. In the figure, the pipes elongation increases almost linearly with the leading end displacement up to a peak value, after which the pipes elongation decreases. The trailing end movements against the leading end

movements are also plotted in Figure 3.8. Note that the trailing end movement is initially zero and starts increasing when the elongation of the pipe reaches the maximum. Thus, the leading end displacement is initially due to the elongation of the pipes only, not due to the movement of the entire pipe. With the movement of the trailing end, the axial force is gradually released, and therefore, the pipe elongation continues to decrease. The trailing end starts to move at the leading end displacements of 9 mm to 12 mm in the tests, where the pullout forces (Figure 3.7) (and pipe elongations in Figure 3.8) are maximal. Thus, at the maximum pullout force, the interface shear strength is mobilized over the entire length of the pipes at these displacements, beyond which the axial force decreases due to the release of the trailing end. It is worth mentioning that the post-peak degradation seen in Figure 3.7 is associated with the release of the load from the pipe to the surrounding soil when the trailing end of the pipe started to move. A similar mechanism was observed earlier in the work of Weerasekara and Wijewickreme (2008). Since the trailing end release is usually not the case for real pipe, the post-peak behaviour has not been discussed further in this paper.

In Figure 3.7, the soil resistance is higher for the tests with higher displacement rates. Note that the pullout resistances for the tests with strain gauges on the pipes are consistently higher than the corresponding pullout resistances from the tests without strain gauges by about 10%. The higher resistances for the pipes with strain gauges are due to the increase of surface roughness caused by the strain gauges, wires, and wraps. Weerasekara and Wijewikreme (2008) also reported a higher pulling resistance for the pipe with strain gauges. Since the results of the pipes with the strain gauges are influenced by the strain gauge installation, pullout forces from the tests without strain gauges are examined in more detail. For the tests without strain gauges (Tests 1 to 3), the peak

resistances of approximately 1.78, 2.5, and 2.84 kN are obtained at the pipes leading end displacements of 9–12 mm for the corresponding displacement rates of 0.5 mm/min (Test 1), 1 mm/min (Test 2), and 2 mm/min (Test 3), respectively. The peak values are increased by 40% and 59.5% in order to increase the pulling rates two times and four times, respectively, from the lowest pulling rate. Wijewickreme and Weerasekara (2015) performed a large-scale field test of 60-mm diameter pipe applying different constant rates of displacement at the leading end of the pipe. The peak pullout resistance was found to increase by 57.7% for a pulling rate changing from 0.6 to 2.15 mm/min. The experimental results on MDPE pipes show that maximum pullout resistances occur at a much greater displacement (9–12 mm) than those recommended for steel pipelines (0.25 mm) (Anderson et al., 2004). This is due to a progressive failure response of the interface soil with the flexible MDPE pipes; a uniform pipe–soil interface response would be expected for steel pipe.

Figure 3.9 plots the non-dimensional peak pullout forces against the pulling rate. The pulling force is normalized by the overburden pressure at the springline level and the contact surface area of the pipe with the surrounding soil (i.e., $P_u/\pi DL\gamma H$). This figure shows that the pullout force increase is high initially, increasing with the pulling rate and then stabilizing. Thus, the pullout force is expected to be less when the ground movement rate is less. The corresponding strains on the pipe are also expected to be less if the relative ground movement is slow. The non-dimensional maximum pullout forces from the Weerasekara and Wijewickreme (2008) and Wijewickreme and Weerasekara (2015) are included in Figure 3.9 for comparison.

3.6.2 *Comparison with FE Analysis*

FE analysis is performed to explore the soil–pipe interaction mechanism that could not be measured during the tests. Particularly, the interface behaviour and the effect in pipe diameter

change on pulling resistance could not be measured during the tests. The FE model is first validated through comparison with measured responses. Then the mechanics of soil–pipe interaction is examined to develop an improved design method for assessing the MDPE pipes subjected to axial pulling.

The measured axial pullout forces from Tests 1 to 3 are compared with those calculated using FE analysis in Figure 3.10. FE analysis with various interface friction coefficients is conducted to simulate the measured load–displacement responses. As seen in the figure, the maximum pullout forces are successfully simulated using the FE analysis with the '*f*' (interface friction reduction factor) of 0.75, 0.86, and 0.90 for Test 1 (0.5 mm/min), Test 2 (1 mm/min), and Test 3 (2 mm/min), respectively. Thus, interface friction reduction factors of 0.75, 0.86, and 0.9 correspond to the loading rates of 0.5, 1, and 2 mm/min, respectively. However, the pipe's initial responses were not successfully simulated for Test 2 and Test 3 in Figure 3.10, which resulted in the differences between the laboratory test results and the FE calculation for the required displacements to reach the peak pullout resistance. This might be due to the use of a linear elastoplastic model for the soil and a linear elastic model for the pipe material. An investigation of the maximum pullout force is the interest of the current study, as it is a concern for pipeline design.

Based on the results of FE analysis, the friction reduction factors (*f*) are obtained for various rates of relative ground movement, as shown in Figure 3.11. Figure 3.11 illustrates that the factor can be less at the slower ground movement and increases nonlinearly with the increase of the rate of relative ground movement. It stabilizes to a value close to 0.9 (i.e., $\delta = 0.9\phi$) at the highest ground movement rate. This rate–dependant friction factor can be used for calculating the pullout

force using a simplified design equation.

3.6.3 *Pipe Elongations and Wall Strains*

The FE analysis results are also compared with measured pipe elongations and wall strains. Figure 3.12 compares the elongation of pipe and trailing end displacements to leading end displacements. Pipe elongation and the leading displacement are reasonably simulated using the FE analysis. Although the pullout force was somewhat underestimated by FE analysis before the peak value, the effects appear to be insignificant on the deformation, which may be due to lower magnitudes of the pulling force discrepancies (<1 kN).

Figure 3.13 compares the measured longitudinal strains with those calculated using FE analysis. Strains were measured at the pipe crown at distances of one-fourth ($L/4$), half ($L/2$), and three-fourths ($3L/4$) from the leading end in Tests 4–6, which are plotted in the figure. The adhesive used to attach strain gauges was reported to increase the polymer pipe's wall stiffness at the locations of the strain gauges (Brachman 1999; Dhar and Moore 2001). Due to the increased stiffness, the measured strain was lessened by a factor of 0.7 for high-density polyethylene pipe (Brachman 1999). Assuming a similar reduction for the MDPE pipes for this comparison presented here, the measured strains are corrected by dividing by 0.7 before plotting. In Figure 3.13, FE results match the test results with reasonable accuracy, implying that the employed FE modeling approach can reasonably simulate the test conditions.

Note that the strain at the distance of $L/4$ starts increasing with a very small leading end displacement that increases with leading end displacement (Figure 3.13). The strains at $L/2$ and $3L/4$ do not start immediately but begin at certain levels of leading end displacements. For

example, in Test 4, the strains at $L/4$, $L/2$, and $3L/4$ start at the leading end displacements of u_1 = 0.65 mm, u_2 = 2.3 mm, and u_3 = 4.47 mm, respectively. These imply that the axial force or the interface shearing resistance is mobilized up to the distances of 1 m, 2 m, and 3 m (i.e., $L/4$, $L/2$, and $3L/4$) at these pulling end displacements, respectively. This observation confirms again that the axial force of flexible MDPE pipe is not mobilized over the entire pipe length simultaneously (unlike for steel pipe, based on which the existing design guidelines were developed).

The strain distributions along the pipe length for these leading end displacements (u_1 = 0.65 mm, u_2 = 2.3 mm, and u_3 = 4.47 mm) in Test 4 are plotted in Figure 3.14. Measurements and FE calculations match each other in the figure. However, corresponding relative displacements from FE analysis were u_1 = 0.65 mm, u_2 = 1.88 mm, and u_3 = 4 mm, respectively. The figure shows that at u_1 = 0.65 mm, the strain is zero at all other points beyond the distance of $L/4$ = 1 m. Similarly, at u_2 = 2.3 mm and u_3 = 4.47 mm, the strains at points beyond $L/2$ = 2 m and $3L/4$ = 3m, respectively, are zero. The strains corresponding to the maximum pullout force (u_4 = 8.86 mm) are also plotted in the figure when the strain/axial force is mobilized over the entire pipe length. Figure 3.14 illustrates that the strain distribution is almost linear over the lengths of the interface friction mobilization and also the axial force. Consequently, the axial force can be assumed to be linearly distributed over the friction mobilization length, with the maximum value at the leading end and zero value at a distance equal to the mobilized friction length. Thus, the axial force distribution can be assumed to be linear along the pipe length at full mobilization. As a result, if the pulling force and the mobilized length are known (which would depend on the relative ground movement, u), the maximum strain on the pipe could be evaluated for the assessment of the pipe, assuming a linear distribution, as discussed in a forthcoming section.

3.6.4 *Mobilized Frictional Length*

As discussed above, the frictional resistance on the pipe surface is mobilized over a certain length of the flexible MDPE pipe, herein called 'mobilized frictional length', which depends on the leading end displacement. The leading end displacement is equal to the elongation of the pipe over the mobilized frictional length until the trailing end starts to move or the friction is mobilized over the entire pipe length. Therefore, it is important to understand the mobilized frictional length to calculate the pipe wall strain on MDPE pipes subjected to the axial ground movement (Weerasekara and Rahman 2019). The mobilized frictional length is experimentally examined during the tests presented here through measurements of axial strains at various points along the pipe's length. The friction is mobilized to a point when the strain gauge located at this point starts to give a reading.

Assuming a linear distribution of the axial force (p) over the length of the mobilized friction length (l), l can be related to the leading end displacement (u), as below:

$$\frac{1}{2}\frac{pl}{AE} = u \tag{3.4}$$

or

$$l = \frac{2AE}{p}u \tag{3.5}$$

where A is the cross-sectional area of the pipe, and E is the modulus of elasticity of the pipe material.

Weerasekara and Rahman (2019) presented an equation based on the work of Weerasekara (2011) to calculate the mobilized frictional length by considering a constant material stiffness, as

in Eq. (3.6):

$$l = \left(\frac{1}{\sqrt{\lambda}}\right) \cos^{-1}\left(1 - \frac{u\lambda}{\kappa}\right) \tag{3.6}$$

where $\lambda = \frac{T_1 - T_2}{EA\overline{u_2}}$, $\kappa = \frac{T_1}{EA}$, T_1 is the peak frictional resistance force considering the effect of dilation of interface soil, T_2 is the frictional resistance force without considering the effect of soil dilation and $\overline{u_2}$ is the displacement at which the interface soil dilation is negligible. Eq. (3.6) was developed based on the assumption of the linear distribution of the axial force from T_1 to T_2 along the pipe's length. Based on the linear distribution of axial strain observed during the tests in this study (Figure 3.14), a linear distribution of the axial force along the pipe length can be assumed. However, the strains were measured to be zero at the end of the mobilized length (not corresponding to a non-zero T_2).

The mobilized frictional lengths calculated using various methods are compared with those estimated from the tests, shown in Figure 3.15. The measured axial force (p) and leading end displacement (u) corresponding to the known mobilized lengths (strain initiation during the tests) are used in the calculation. For using Eq. (3.6), $T_1 = p/l$, $T_2 = 0$ and $u_2 = u$ are used. The figure shows that the FE calculation matches well with the measurements, while Eq. (3.5) and Eq. (3.6) provide reasonable estimations of the mobilized friction lengths. Thus, if the axial force (p) and relative ground movement (u) are known, the mobilized friction length can be estimated using either of the equations. Eq. (3.5) would be easy to use and therefore, is recommended for pipeline assessment.

3.6.5 *Effects of Diameter Decrease*

During axial pullout, pipe's diameter is reduced, which may affect the normal force on the pipe.

Since frictional resistance primarily depends on the normal force, the pipe diameter change during axial pullout is examined to identify the effects. A biaxial strain gauge is used at the springline of the pipe at mid-length to examine the effect of diameter change during the tests. Figure 3.16 shows the measured springline strains from Tests 4, 5, and 6. The figure shows that the longitudinal strain is tensile and that the circumferential strain is compressive, both of which increase as a function of increasing leading end displacement. The compressive circumferential strain is associated with a decrease in pipe diameter. Although diameter decrease could not be measured during the tests, the FE analysis results show that both vertical and horizontal diameter decrease with increasing leading end displacement (Figure 3.17). Figure 3.17 shows that the change in horizontal and vertical diameters is almost identical, indicating uniform circumferential shortening of the pipe, which occurs due to hoop compression.

The normal stresses on the pipe, not measurable during the tests, are examined from the results of FE analysis that account for the effects of pipe diameter change. Figure 3.18 plots the variation of the circumferential average of the normal stresses and the pipe diameter changes along the pipe length at the peak pullout force. In the figure, the pipe diameter decrease is the highest at the leading end and the lowest at the trailing end. However, the average normal stress is the lowest at the leading end and highest at the trailing end. At the leading end, the lower normal stress is due to the higher decreasing in pipe diameter and a higher arching effect. The average normal stresses are also calculated using a conventional design equation (ALA 2001) as: $\frac{1}{2}(1+K_0)\,\gamma H$. Figure 3.18 shows that although the parameters such as K_0, γ, and H are the same as those used in FE analysis, the average normal stress calculated using the conventional design equation is higher than the average normal stress calculated from FE analysis. This is because the conventional design

equation does not account for the arching effect associated with the pipe diameter change. Thus, if the effect of arching is significant, it should be taken into account to calculate the normal stress on the pipe correctly.

3.7 Proposed Method of MDPE Pipe Evaluation

For the evaluation of MDPE pipelines subjected to axial ground movement, the mobilized friction length and the pulling force corresponding to relative ground movement need to be estimated to assess pipe wall strains. Both the mobilized friction length and the pulling force depend on the frictional resistance of pipe–soil interface. Since the frictional resistance is mobilized over the mobilized friction length, the frictional resistance can be calculated as the normal stress times the coefficient of interface friction. The integration of the frictional resistance over the mobilized length would provide the pulling force at the leading end. Thus, the pulling force (p) at the leading end is given by Eq. (3.7).

$$p = \zeta \left(\frac{1+K_0}{2}\right) \gamma H \, (\pi D l) \tan\delta \tag{3.7}$$

In Eq. (3.7), a normal stress adjustment factor, ζ is proposed to account for the reduction of normal stress due to the reduction in pipe diameter.

Placing Eq. (3.7) to Eq. (3.5), the expression for mobilized friction length can be obtained as a function of the relative ground movement (u), as shown in Eq. (3.8).

$$l = \sqrt{\frac{4AE}{\zeta (1+K_0) \gamma H \pi D \tan\delta}\, u} \tag{3.8}$$

In Eq. (3.7), $\tan\delta$ ('f' used in FE analysis) and ζ depend on the rate of loading for viscoelastic pipe material, the modulus of elasticity of the pipe material, and the diameter of the pipe. Extensive

testing and FE can be performed to determine the parameters for various pipes and the rates of ground movements. As discussed earlier, the interface friction reduction factors are 0.75, 0.86, and 0.9 for Tests 1, 2, and 3, respectively (Figure 3.11). Corresponding normal stress adjustment factors are 0.91, 0.85, and 0.90, respectively.

Once the pulling force and the mobilized friction length are estimated, the longitudinal strain, ε, on the pipe wall can be calculated, assuming a linear distribution of the strain over the mobilized friction length, as in Eq. (3.9).

$$\varepsilon = \frac{p}{AEl}(l - x) \tag{3.9}$$

where x is the distance from the leading end. Strains calculated using Eq. (3.9) at a distance (x) of $L/4$, $L/2$ and $3L/4$ in the tests are compared with the measurements in Figure 3.19. In Figure 3.19, the strains calculated using the proposed method are found to reasonably estimate the strains measured during the tests.

3.8 Conclusions

Six axial pullout tests of 60-mm diameter MDPE pipes are conducted using the test facility at Memorial University of Newfoundland to investigate the effect of pulling rate on the pipe's behaviour. Axial pullout resistance, pipe movements, and axial pipe strain are measured to understand the mechanics of soil–pipe interaction during the tests. Finite-element analysis of the tests is performed to interpret the observed behaviour and determine the soil–pipe interaction parameters. A simplified method is proposed to calculate the pipe wall strains due to axial ground movements. Some key findings from the study are summarized below based on the study.

- The pullout force on MDPE pipes depends on the rates of relative ground movement. The peak pullout force is higher with higher rates of ground movements. However, current design guidelines (ASCE 1984; ALA 2001) do not account for the rate of ground movements.
- MDPE pipe significantly elongates under axial loading, while pipe elongation is negligible for steel pipes. Due to elongation, interface shear strength is not immediately mobilized over the entire pipe length. The pipe elongation occurs over the length of interface shear strength mobilization, which increases with increasing leading end displacement. Pipe diameter also decreases under the axial pullout force. The decrease in pipe diameter influences normal stresses on the pipe.
- Three-dimensional FE analysis successfully simulated the responses observed during the tests. Analysis with various interface friction angles was conducted, which demonstrates that friction angles of 0.75ϕ, 0.86ϕ, and 0.9ϕ reasonably correspond to the test conditions with pulling rates of 0.5, 1, and 2 mm/min, respectively.
- The distribution of the pipe's axial strain is almost linear over the length of mobilized interface friction. Thus, the distribution of the axial force along the pipe length can be assumed to be linear.
- Based on the assumption of the linear distribution of axial strain, a simplified equation is proposed to estimate the mobilized frictional length from the leading end displacement. The equation is found to reasonably estimate the mobilized frictional length observed during the tests and calculations using the FE analysis.
- A simplified method is proposed to calculate pipe wall strains from the known relative ground movement. In this method, a normal stress adjustment factor is introduced to

account for the effect of diameter change on normal stress. Different interface friction coefficients are proposed to account for the rate of loading. The method successfully simulated the pipe wall strains measured during the tests.

Finally, based on the findings from the test and finite-element analysis, it is reasonable to be cautious when applying the existing design guidelines for estimating the axial pullout resistance to assess buried MDPE pipelines subjected to axial ground movements. The investigation of the pulling rate effects presented in this study is a step towards representing the complex pipe–soil interaction for extensible MDPE pipe. Further studies are recommended to examine the behaviour for different burial conditions, pipe sizes, and pulling rates.

3.9 Acknowledgments

The Collaborative Research and Development Grant program of the Natural Science and Engineering Research Council of Canada, Innovate NL program of the Government of Newfoundland and Labrador, FortisBC Energy Inc. and WSP Canada Inc., are gratefully acknowledged for providing the financial and/or in-kind support for this research. The authors are thankful for the technical assistance of Jason Murphy, Shawn Organ and Matt Curtis in the Faculty of Engineering and Applied Science at Memorial University of Newfoundland. Undergraduate students Alex David McNeil and Shadi Soliman helped with instrumentation and pipe installation and de-installation during the tests.

3.10 References

ALA (American Lifelines Alliance). 2001. *Guidelines for the design of buried steel pipe*. Available from https://www.americanlifelinesalliance.com/pdf/Update061305.pdf (accessed 14 January

2020).

Alam, S. & Alloche, E. N. (2010). Experimental investigation of pipe soil friction coefficients for direct buried PVC pipes. *Proceedings of the Pipeline Division Specialty Conf. 2010*, American Society of Civil Engineers, Keystone, Colorado, USA, 2: 1160–1169.

Anderson, C., Wijewickreme, D., Ventura, C. & Mitchell, A. (2004). Full-scale laboratory testing of buried polyethylene gas distribution pipelines subject to lateral ground displacements. *Proceedings of the 13th World Conf. on Earthquake Engineering*, Aug. 1–6, Vancouver, B.C. Canadian Association of Earthquake Engineering. Paper 1543.

ASCE (American Society of Civil Engineers). (1984). *Guidelines for the seismic design of oil and gas pipeline systems*. Committee on Gas and Liquid Fuel Lifelines, Technical Council on Lifeline Earthquake Engineering, New York, pp. 573.

ASTM (American Society for Testing and Materials). D698. (2003). *Standard test method for laboratory compaction characteristics of soil using standard effort*. 2003 annual book standards, West Conshohocken, Pa, Vol. 04.08.

Bilgin, Ö. & Stewart, H. E. (2009a). Pullout Resistance Characteristics of Cast Iron Pipe. *Journal of Transportation Engineering*, **135**, No. 10, 730–735.

Bilgin, Ö. & Stewart, H. E. (2009b). Design Guidelines for Polyethylene Pipe Interface Shear Resistance. *Journal of Geotechnical and Geoenvironmental Engineering*, **135**, No. 6, 809–818.

Brachman, R. W. I. (1999). Structural Performance of Leachete Collection Pipes. *Ph.D. thesis*, Department of Civil and Environmental Engineering, The University of Western Ontario, London, Canada.

CEPA (Canadian Energy Pipeline Association). (2016). Available from www.aboutpipelines.com/en/pipeline-101/pipeline-history/ (accessed 14 January 2020).

CEPA (Canadian Energy Pipeline Association). (2017). Available from www.pr17.cepa.com (accessed 14 January 2020).

Cruden, D. M. & Varnes, D. J. (1996). *Landslide types and processes. Landslides—Investigations and mitigation*, pp. 36–75, edited by Turner, A. K. and Schuster, R. L. Special Report, 247. Washington, DC: Transportation Research Board.

Dassault Systems. (2014). ABAQUS/CAE user's guide, Providence, RI: Dassault Systemes Simulia.

Daiyan, N., Kenny, S., Phillips, R. & Popescu, R. (2011). Investigating pipeline-soil interaction under axial–lateral relative movements in sand. *Canadian Geotechnical Journal*, **48**, No. 11, 1683–1695.

Dhar, A. S. & Moore, I. D. (2001). Liner Buckling in Profiled Polyethylene Pipes. *Geosynthetics International*, **8**, No. 4, 303–326.

Dhar, A. S. & Moore, I. D. (2004). Laboratory Investigation of Local Bending in Profiled Thermoplastic Pipes. *Advances in Structural Engineering*, **7**(3): 201–215.

Gerlach, T. & Achmus, M. (2018). Numerical Investigations on District Heating Pipelines Under Combined Axial and Lateral Loading. *Proceedings of the 16th International Symposium on District Heating and Cooling*, Sept. 9–12, Hamburg, Germany.

Guo, P. J. & Stolle, D. F. E. (2005). Lateral PipeSoil Interaction in Sand with Reference to Scale Effect. *Journal of Geotechnical and Geoenvironmental Engineering*, **131**, No. 3, 338–349.

Hardin, B. O. & Black, W. L. (1966). Sand stiffness under various triaxial stresses. *Journal of the Soil Mechanics and Foundations Division*, ASCE, **92**, No. 2, 27–42.

Janbu, N. (1963). Soil compressibility as determined by oedometer and triaxial tests. *Proceedings of the European Conference on Soil Mechanics and Foundation Engineering*, vol. 1, pp. 19–

25. Essen, Germany: German Society for Earthworks and Foundations.

Jung, J., O'Rourke, T. & Olson, N. (2013). Uplift soil–pipe interaction in granular soil. *Canadian Geotechnical Journal*, **50**, No. 7, 744−753.

Liu, R., Guo, L., Yan, S. & Xu, Y. (2011). Studies on Soil Resistance to Pipelines Buried in Sand. *Advanced Materials Research*, **243–249**, 3151–3156.

Meidani, M., Meguid, M. A. & Chouinard, L. E. (2017). Evaluation of Soil–Pipe Interaction under Relative Axial Ground Movement. *Journal of Pipeline Systems Engineering and Practice*, **8**, No. 4, 1–10.

Muntakim, A. H., Dhar, A. S. & Rahman, M. (2017). Pipeline behaviour subjected to large ground movement. *Proceedings of the Canadian Geotechnical Conf., Geo*Ottawa 2017, Oct. 1–4, Ottawa, Ontario, Canada: Canadian Geotechnical Society.

Murugathasan, P., Dhar, A. S. & Hawlader, B. C. (2021). An experimental and numerical investigation of pullout behaviour of ductile iron water pipes buried in sand. *Canadian Journal of Civil Engineering*, **48**, No. 2, 134–143.

Murugathasan, P., Dhar, A. S. & Hawlader, B. C. (2018). A laboratory facility for studying pullout behaviour of buried pipelines. *Proceedings of the 71st Canadian Geotechnical Conf., GeoEdmonton 2018*, Sept. 23-26, Edmonton, Alberta, Canada: Canadian Geotechnical Society.

Phillips, P., Nobahar, A. & Zhou, J. (2004). Combined axial and lateral pipe–soil interaction relationship. *Proceedings of the international pipeline conference, ASME. IPC2004,* Calgary, Alberta, Canada, pp. 299–303.

PRCI (Pipeline Research Council International). (2009). *Guidelines for constructing natural gas and liquid hydrocarbon pipelines through areas prone to landslide and subsidence hazards*. Report prepared for the Design, Material, and Construction committee, Chantilly, VA, USA:

Pipeline Research Council International, Inc.

Roy, K., Hawlader, B., Kenny, S. & Moore, I. D. (2016). Finite element modeling of lateral pipeline–soil interactions in dense sand. *Canadian Geotechnical Journal*, **53**, No. 3, 490–504.

Saha, R. C., Dhar, A. S. & Hawlader, B. C. (2019). Shear strength assessment of a well-graded clean sand. *Proceedings of the 72nd Canadian Geotechnical Conf., GeoSt.John's 2019*, St. John's, Newfoundland and Labrador, Canada: Canadian Geotechnical Society.

Scarpelli, G., Sakellariadi, E. & Furlani, G. (2003). Evaluation of soil–pipeline longitudinal interaction forces. *Rivista Italiana di Geotecnica*, **4**, No. 3, 24–41.

Sheil, B. B. Ã., Martin, C. M. Ã., Byrne, B. W. Ã., Plant, M., Williams, K. & Coyne, D. (2018). Full-scale laboratory testing of a buried pipeline in sand subjected to cyclic axial displacements. *Géotechnique*, **68**, No. 8, 684–694.

Suleiman, M. T. & Coree, B. J. (2004). Constitutive model for high density polyethylene material: Systematic approach. *Journal of Materials in Civil Engineering*, **16**, No. 6, 511–515.

Tognon, A. R., Rowe, R. K. & Brachman, R. W. I. (1999). Evaluation of sidewall friction for a buried pipe testing facility. *Geotextiles and Geomembranes*, **17**, 193–212.

Weerasekara, L. (2011). Pipe–soil interaction aspects in buried extensible pipes. *Ph.D. thesis*, Department of Civil Engineering, The University of British Columbia, Vancouver, BC, Canada.

Weerasekara, L. & Wijewickreme, D. (2008). Mobilization of soil loads on buried polyethylene natural gas pipelines subject to relative axial displacements. *Canadian Geotechnical Journal*, **45**, No. 9, 1237–1249.

Weerasekara, L. & M. Rahman. (2019). Framework for assessing the integrity of natural gas distribution pipes in landslide areas. *Proceedings of the 72nd Canadian Geotechnical Conf., GeoSt.John's 2019*, St. John's, Newfoundland and Labrador, Canada: Canadian Geotechnical

Society.

Wijewickreme, D. & Weerasekara, L. (2015). Analytical Modeling of Field Axial Pullout Tests Performed on Buried Extensible Pipes. *International Journal of Geomechanics*, **15**, No. 2, 04014441-12.

Wijewickreme, D., Karimian, H. & Honegger, D. (2009). Response of buried steel pipelines subjected to relative axial soil movement. *Canadian Geotechnical Journal*, **46**, No. 7, 735–752.

Yimsiri, S., Soga, K., Yoshizaki, K., Dasari, G. R. & O'Rourke, T. D. (2004). Lateral and upward soil–pipeline interactions in sand for deep embedment conditions. *Journal of Geotechnical and Geoenvironmental Engineering*, **130**, No. 8, 830–842.

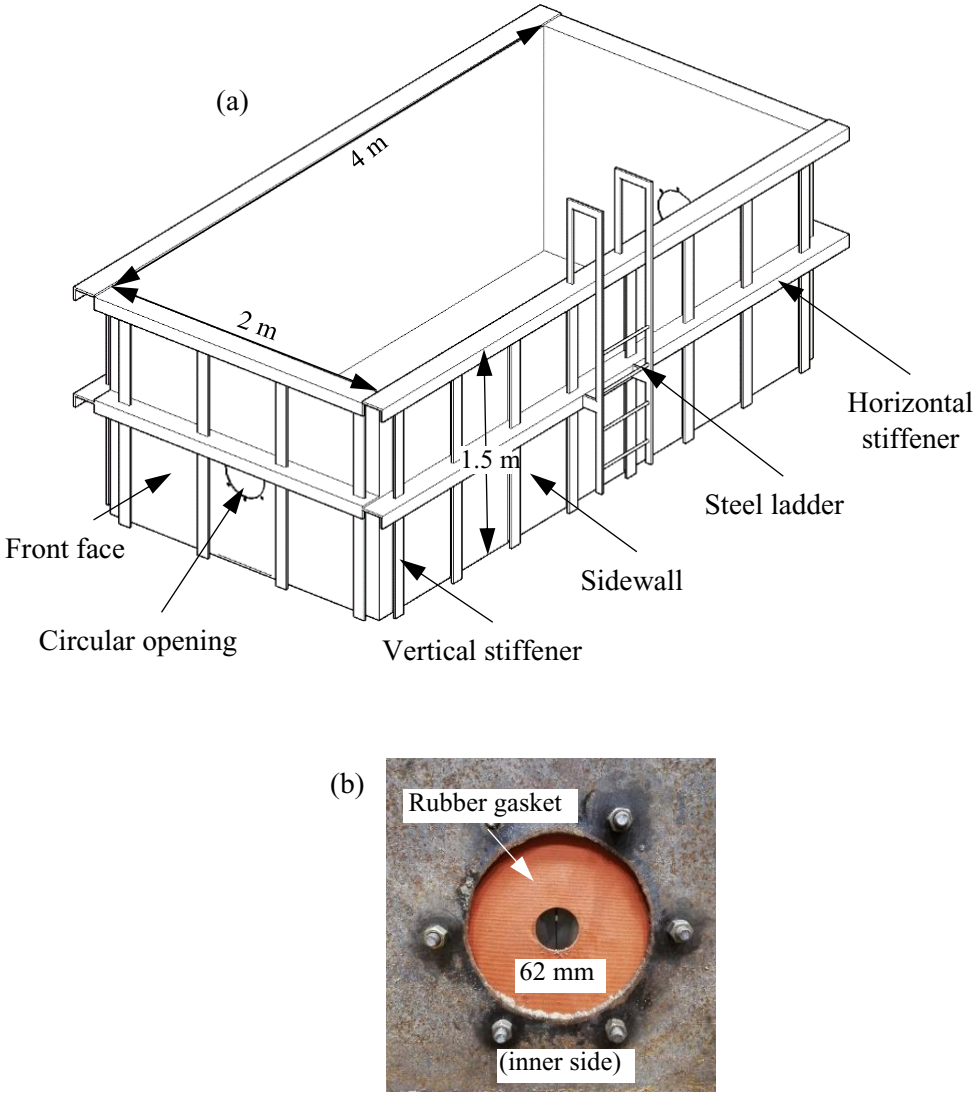

Figure 3.1: Test facility: (a) isometric view of test cell; and (b) adjustable circular opening

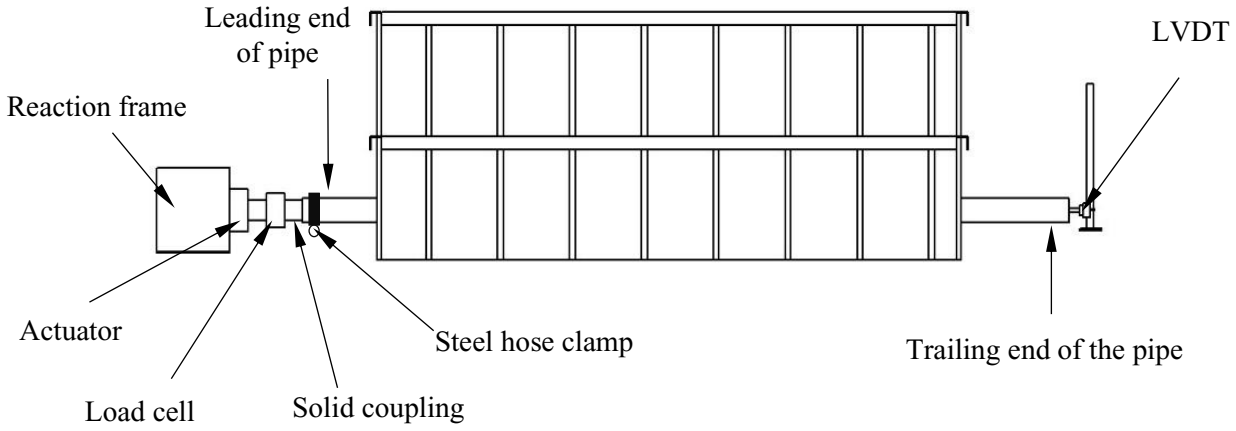

Figure 3.2: Test cell configuration

(a)

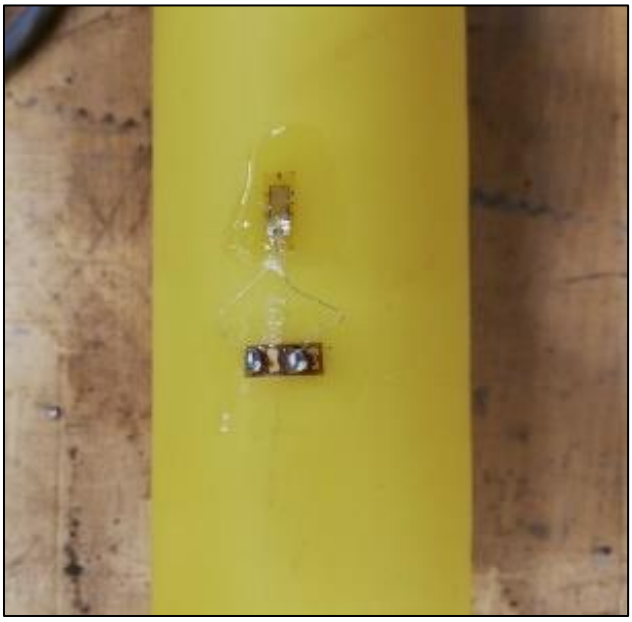

(b)

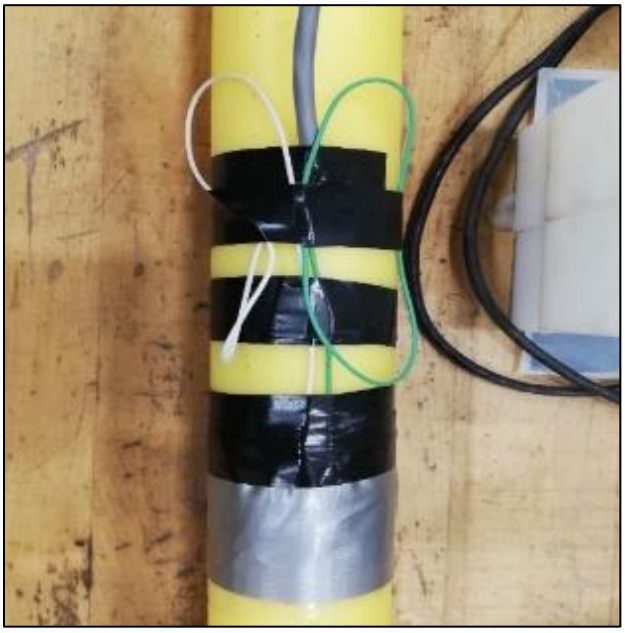

Figure 3.3: Strain gauge installation: (a) before wrapping; and (b) after wrapping

(a)

(b)

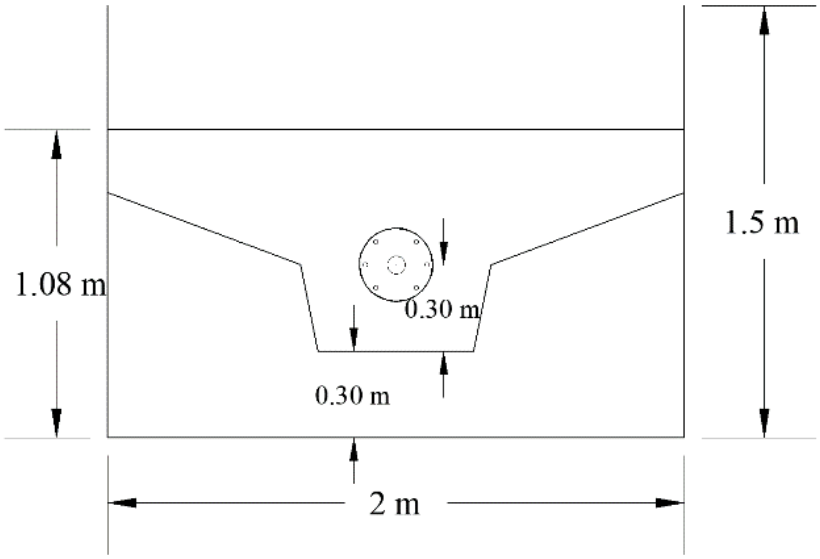

Figure 3.4: Trench installation simulation: (a) pipe trench; and (b) cross-sectional view

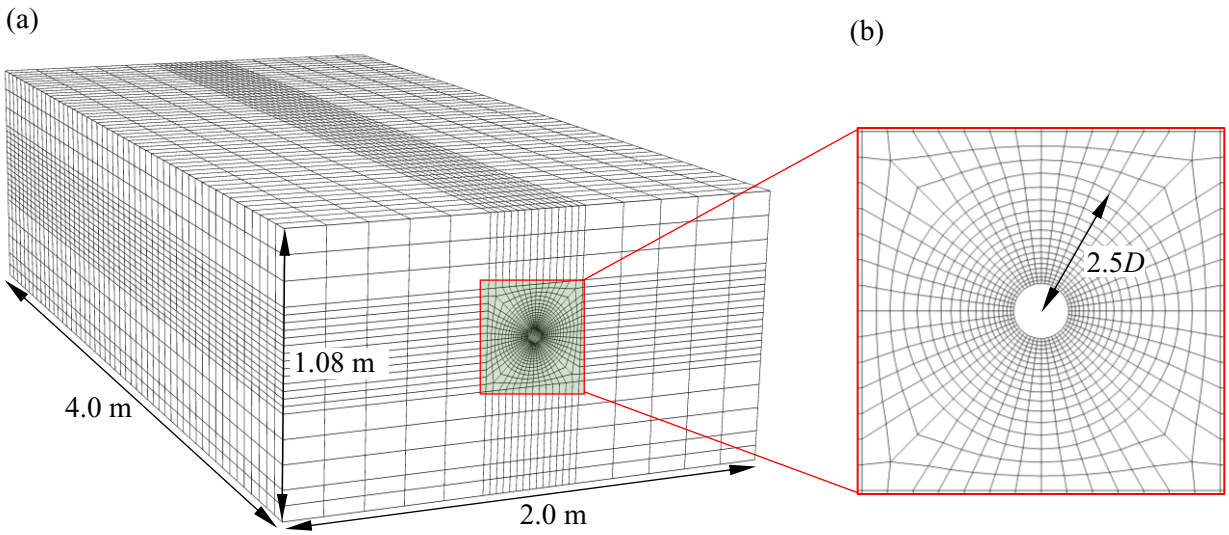

Figure 3.5: FE model: (a) 3D FE mesh; and (b) cross-section near the pipe

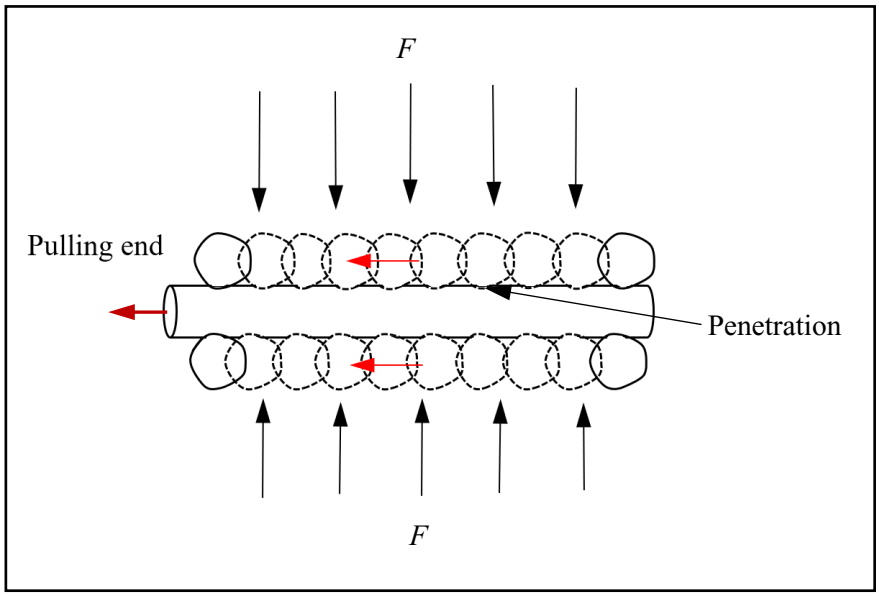

Figure 3.6: Grain penetration on the MDPE pipe surface

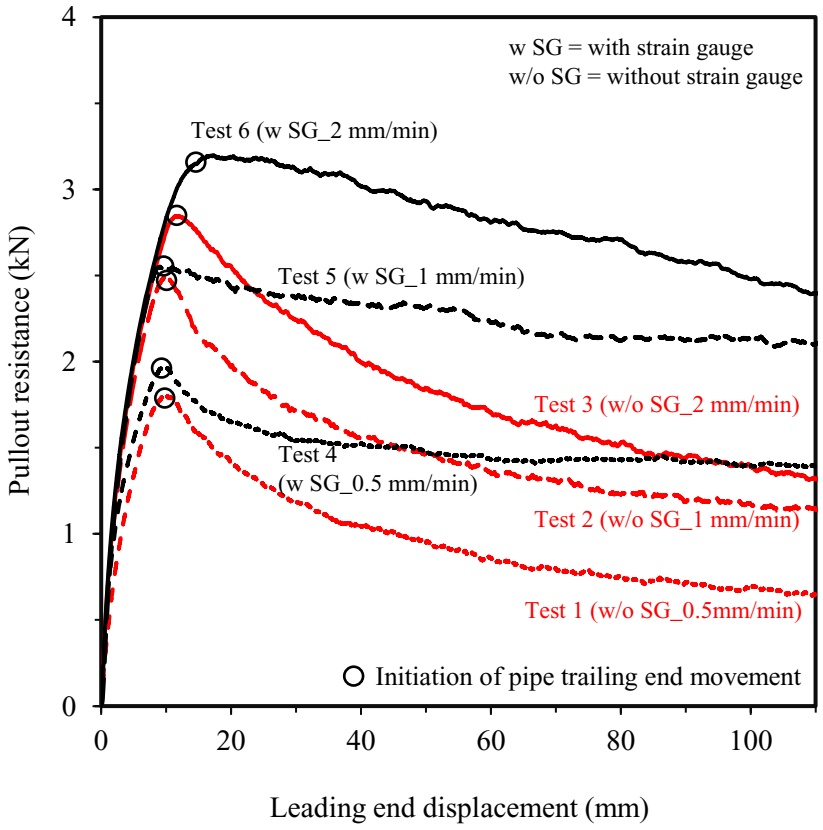

Figure 3.7: Axial pullout resistance with leading end displacement

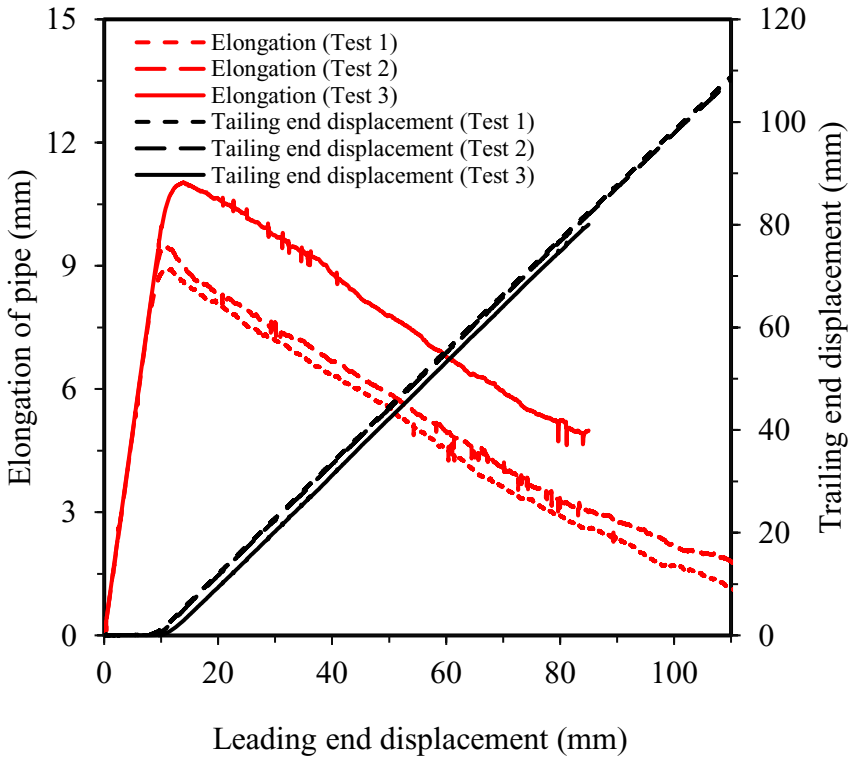

Figure 3.8: Pipe elongation and trailing end displacement with leading end displacement

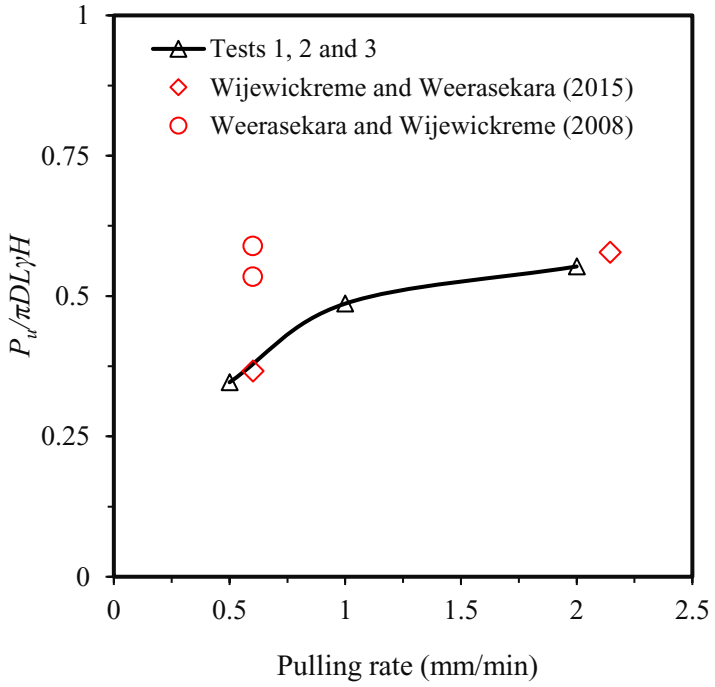

Figure 3.9: Normalized peak pullout forces with pulling rates

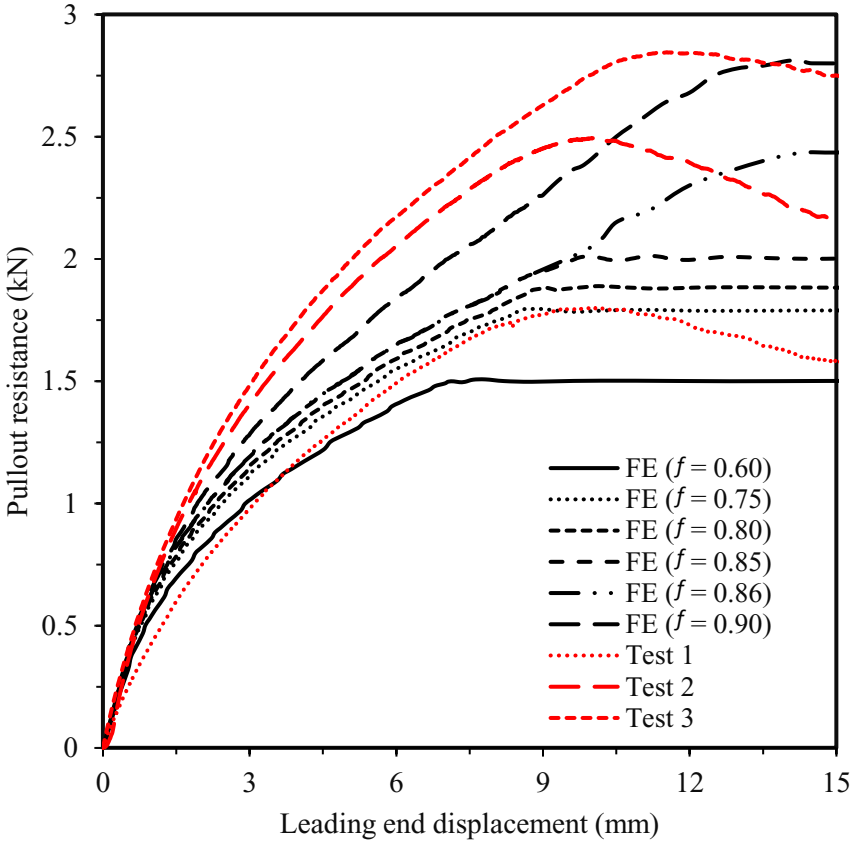

Figure 3.10: Comparison of FE calculation of pullout resistance with measurements

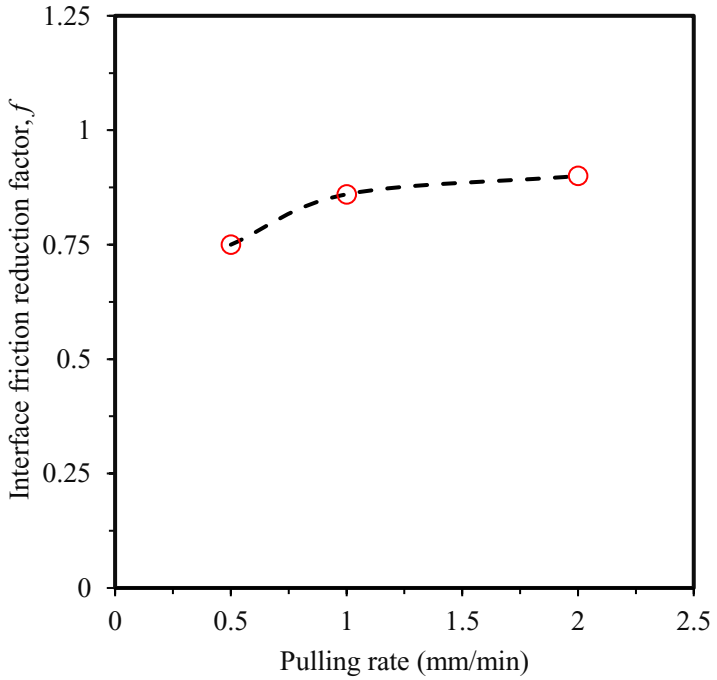

Figure 3.11: Interface friction reduction factor with pulling rates

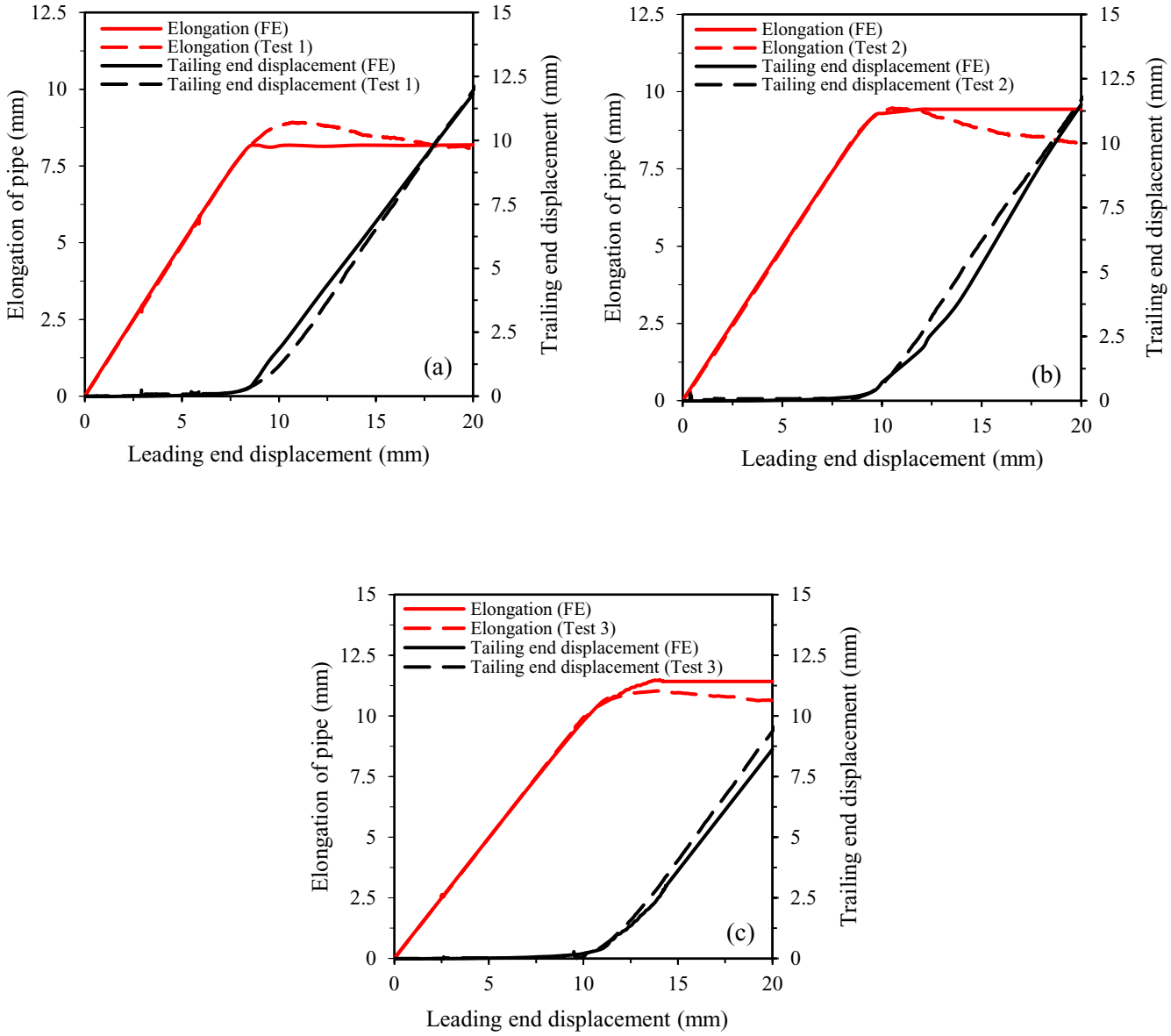

Figure 3.12: Comparison of pipe elongations and trailing end displacements: (a) Test 1; (b) Test 2; and (c) Test 3

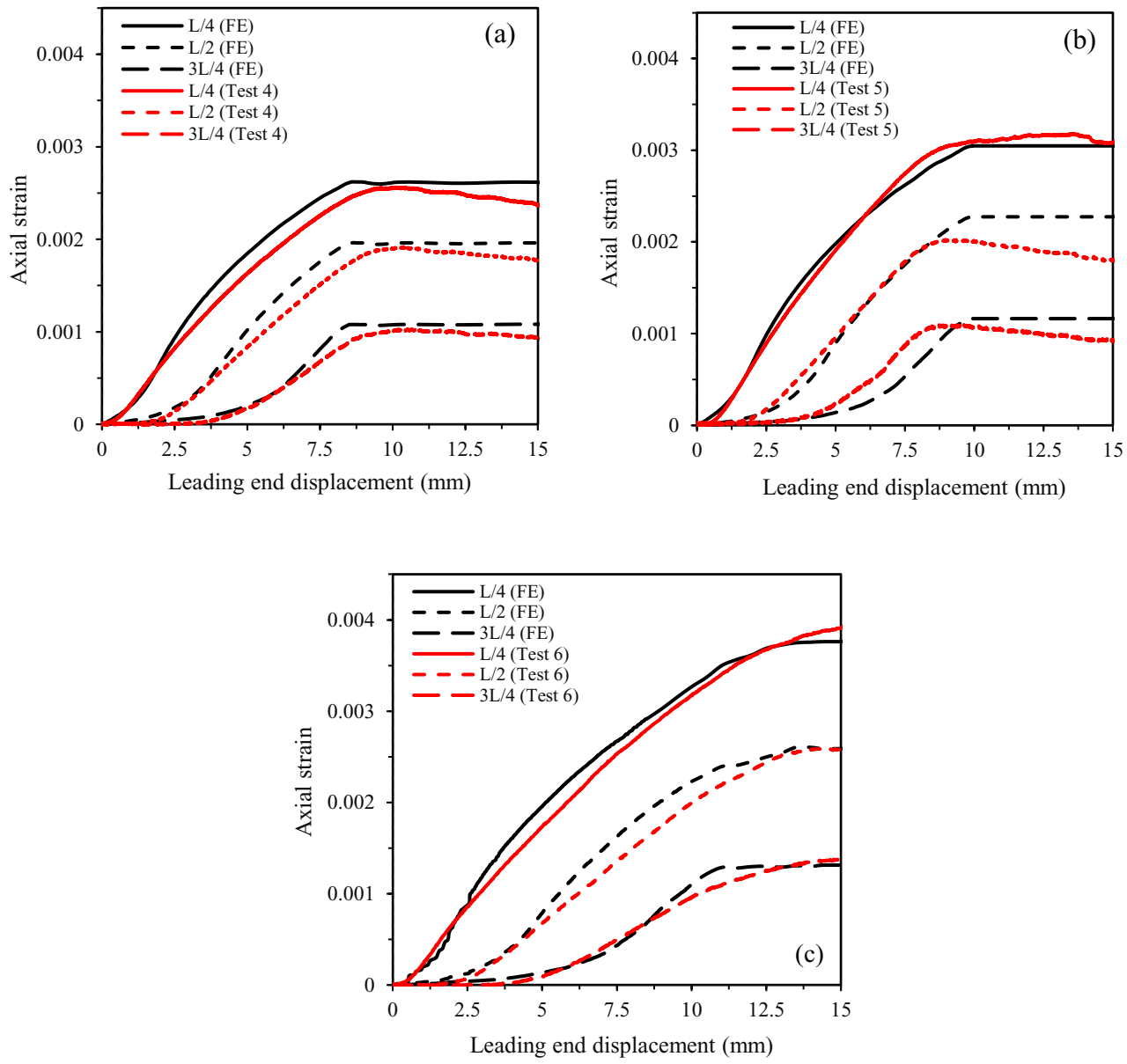

Figure 3.13: Comparison of axial strains at various locations: (a) Test 4; (b) Test 5; and (c) Test 6

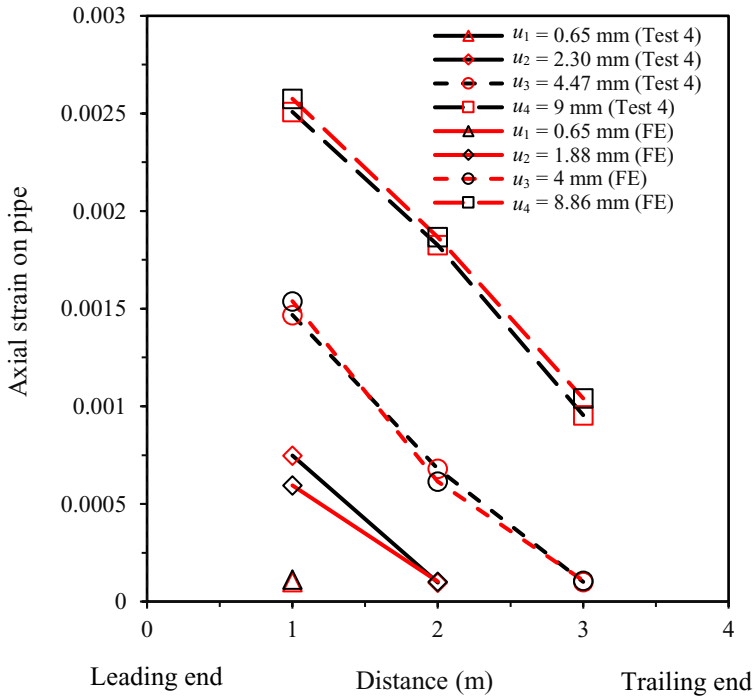

Figure 3.14: Strain distribution along the length of the pipe at various leading end displacements. u_1, u_2, u_3, and u_4 are the leading end displacements when the axial force is mobilized to the distance of 1, 2, 3, and 4 m, respectively, from the leading end.

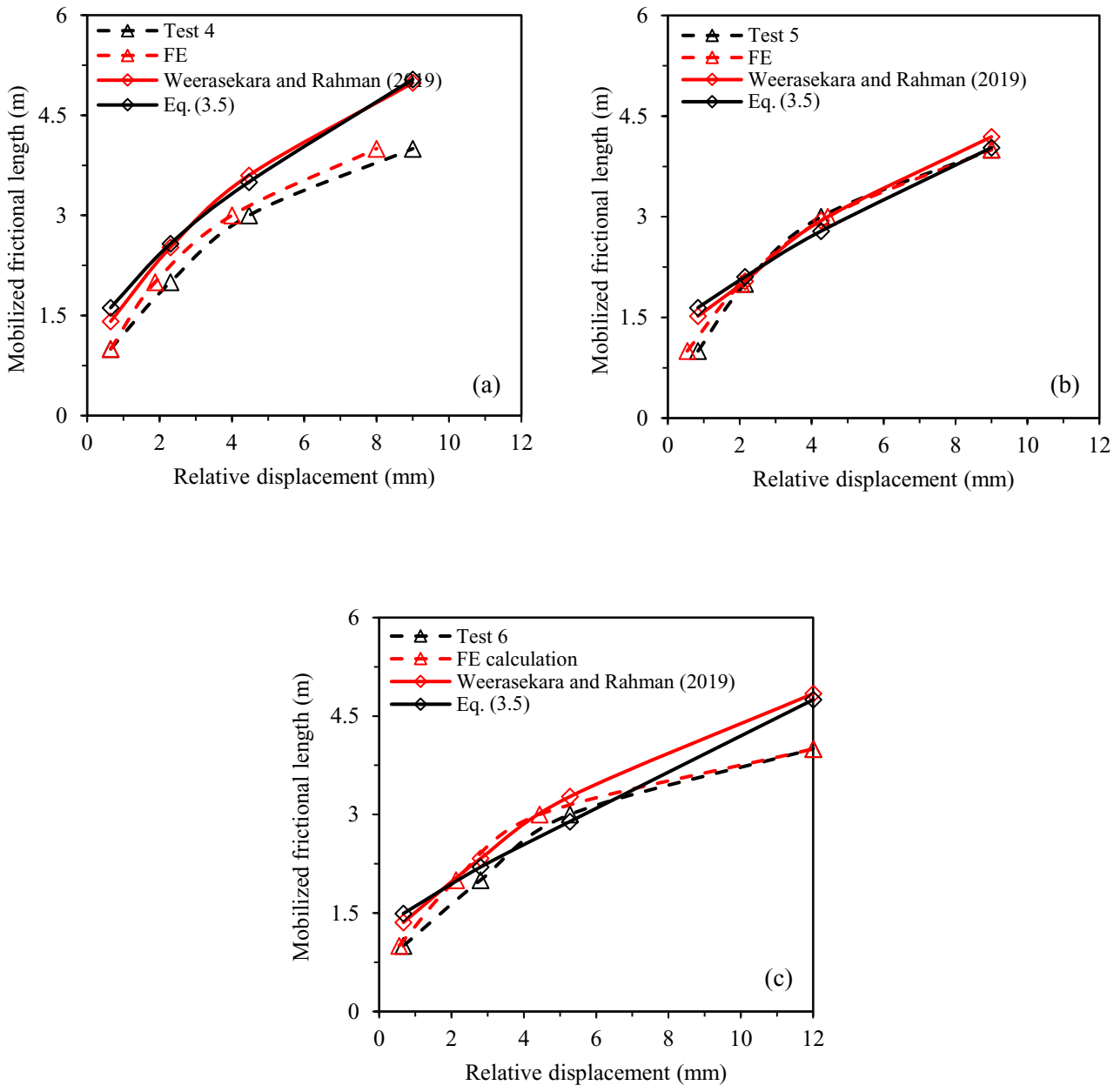

Figure 3.15: Comparison of mobilized friction lengths versus relative displacement: (a) Test 4; (b) Test 5; and (c) Test 6

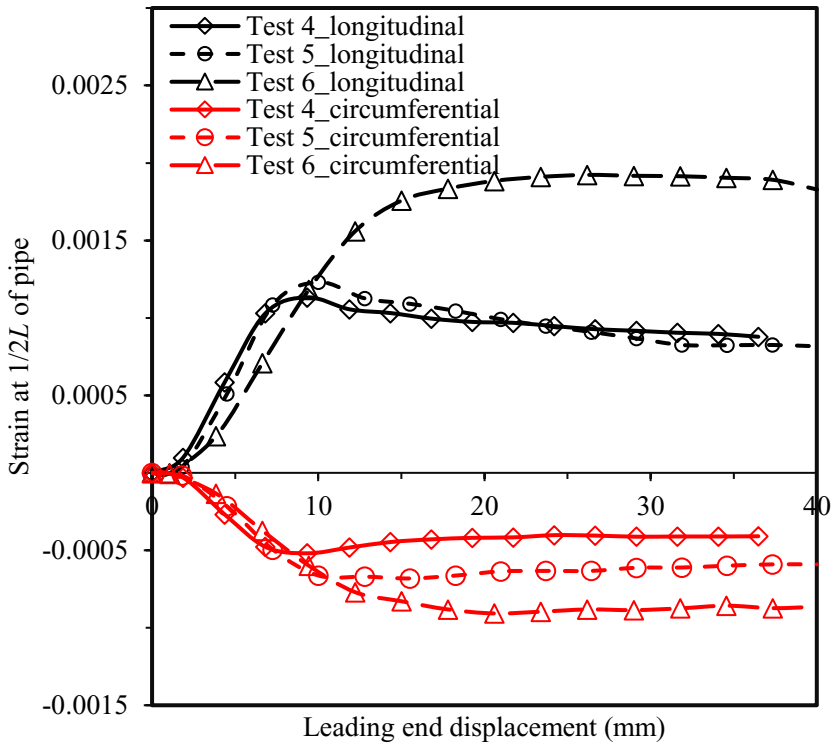

Figure 3.16: Longitudinal and circumferential strains at pipe springline

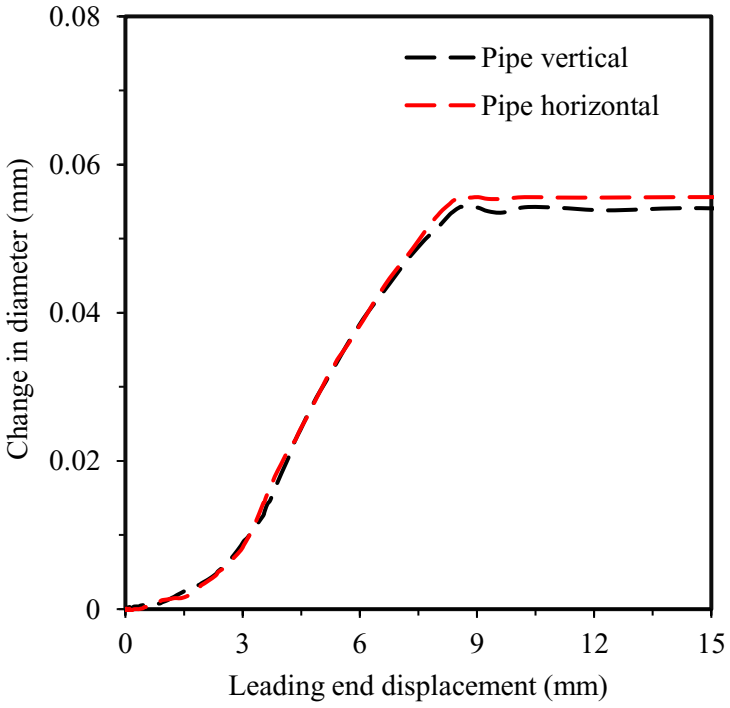

Figure 3.17: Diameter decrease at *L*/2 (FE calculation) in Test 1

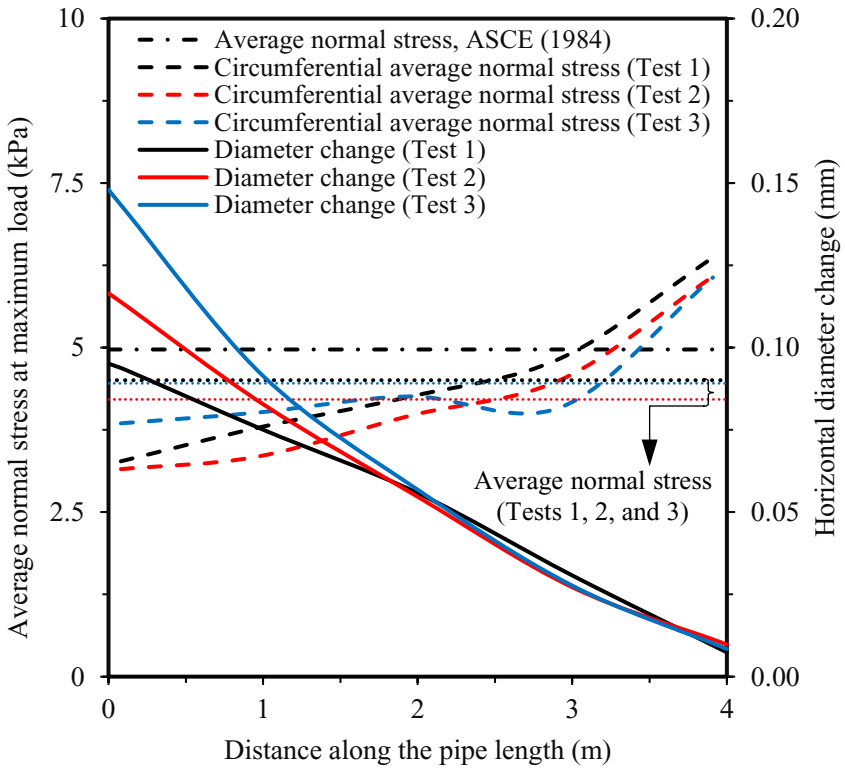

Figure 3.18: Normal stress distribution and horizontal diameter decrease along the pipe length from the FE calculation

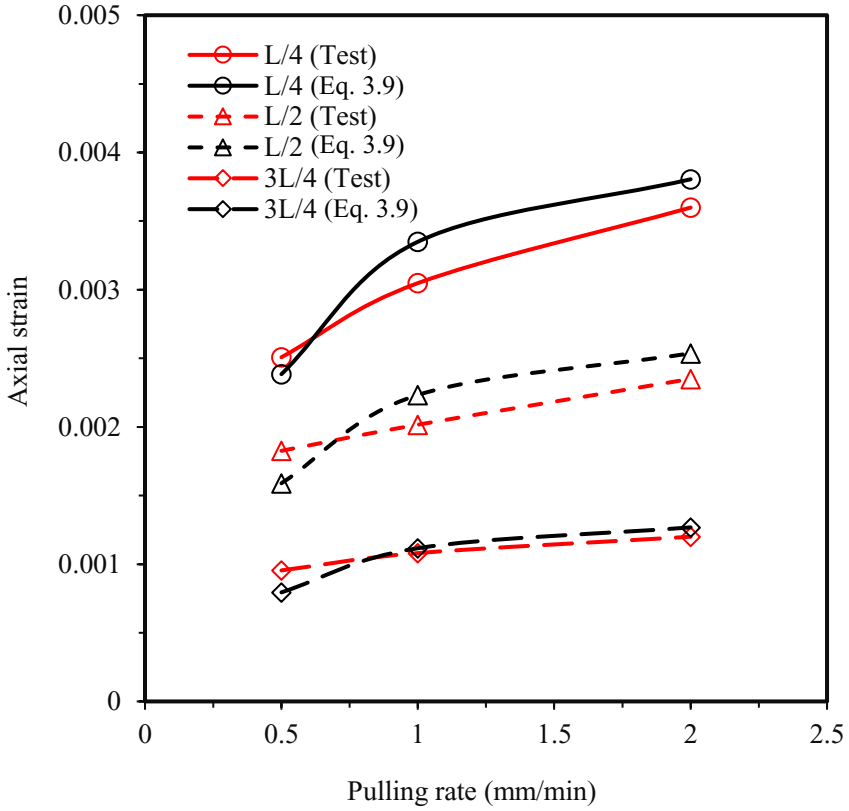

Figure 3.19: Comparison of experimental strains with calculations using the proposed method

Table 3.1. Soil parameters for the FE analysis

Parameters	Value
Young's Modulus, E_s (MPa)	5
Poisson's ratio, ν	0.3
Unit Weight (kN/m^3)	14.5
Friction angle, ϕ	40°
Dilation angle, ψ	0.1°
Cohesion, c (kPa)	0.1

Table 3.2. Friction coefficients corresponding to the test conditions

Loading rate (mm/min)	Interface friction reduction factor, f	Friction angle, ϕ	Interface angle of shear resistance, $\delta = f\phi$	Tangential friction coefficient, tanδ
0.5	0.75	40°	30°	0.577
1	0.86		34.4°	0.684
2	0.90		36°	0.726

CHAPTER 4

Effects of Axial Relative Ground Movement on Small Diameter Polyethylene Piping in Loose Sand

Co-Authorship: A version of this chapter has been published in Infrastructures as: Reza, A. and Dhar, A. S. (2021). 'Effects of Axial Relative Ground Movement on Small Diameter Polyethylene Piping in Loose Sand.' Most of the research presented in this chapter has been conducted by the first author. He also prepared the draft manuscript. The other author mainly supervised the research and reviewed the manuscript.

4.1 Abstract

Small diameter (42-mm) medium-density polyethylene (MDPE) pipes are widely used in the gas distribution system in Canada and other countries. They are sometimes exposed to ground movements resulting from landslides or earthquakes. The current design guidelines for evaluating the pipes subjected to ground movement were developed for steel pipes of larger diameters and may not apply to flexible MDPE pipes. This paper evaluates 42-mm diameter MDPE pipes buried in loose sand under axial relative ground movement for developing a design method for the pipes. MDPE is a viscoelastic material; therefore, the behaviour of MDPE pipes exposed to landslides would depend on the rate of ground movements. In this research, full-scale laboratory tests were conducted to investigate the responses of buried pipes under various rates of relative axial displacement. Finite-element modelling of the tests was used to interpret the observed behaviour using the continuum mechanics framework. The study revealed that the pulling force on the pipe depends on the rate of relative ground displacement (pulling rate). The nondimensional pulling force possessed a nonlinear relationship with the pulling rate. A rate–dependent interface friction

angle could be used to calculate the maximum pulling forces using the conventional design guidelines for the pipes in loose sand. Based on the pulling force, the pipe wall strains can be estimated using the methods available for larger diameter pipes (Chapter 3).

4.2 Introduction

Pipelines are a safe, reliable, and environmentally friendly way of transporting liquids and gas. However, ground movements resulting from various causes, including landslides, earthquakes, and ground subsidence, can pose severe threats to the performance and integrity of pipelines. The pipes may experience unacceptable levels of strain due to the loads from the moving ground (Kunert et al. 2016). When the direction of ground movement is parallel to the pipe axis (axial ground movement), the pipelines are subjected to longitudinal forces resulting from the friction between the pipe and the moving ground, causing axial strains in the pipe wall. The longitudinal force along the pipeline depends on the relative axial displacement between the soil and pipe, which is evaluated in the current design practices (i.e., ASCE 1984; ALA 2005; PRCI 2009) based on an evaluation of the normal stresses acting on the pipe wall and the frictional characteristics of the soil–pipe interface. However, evaluating the normal stresses and the frictional characteristic is very complex, as these depend on the soil–pipe interaction. The mechanics of soil–pipe interaction depend extensively on pipe material and diameter, burial depth, ground conditions, and the ground movement rate.

Over the past few decades, many experimental and numerical studies were carried out to develop simplified design methods for assessing pipelines subjected to ground movements. Some of the studies focused on the axial pipeline–soil interaction of metal pipes in sand (Paulin et al. 1998; Bilgin and Stewart 2009a; Wijewickreme at al. 2009; Meidani et al. 2017; Sarvanis et al.

2017; Murugathasan et al. 2021). These studies identified the effects of interface soil dilation for pipes in dense sand that are not accounted for in the current design guidelines. Sheil et al. (2018) measured initial normal stress at the pipe crown, where the stress was greater than the nominal overburden pressure. They postulated that the high normal stress is the result of the rigid inclusion of the steel pipe. This effect is also not considered in the current design guidelines. Marino and Osouli (2020) employed pipe jacking tests to examine the interface friction coefficient for coal tarcoated steel pipes buried at various depths. The interface friction angles for clayey and sandy backfill materials were about 0.9 and 0.8 times that of the soil internal friction angles, respectively.

However, studies on the soil–pipe interaction for flexible pipes under axial ground movements are limited. Weerasekara and Wijewickreme (2008) and Wijewickreme and Weerasekara (2015) experimentally investigated the axial pullout behaviour of 60- and 114-mm diameter MDPE pipes. They reported that the interface frictional resistance for MDPE pipes is influenced by pipe elongation and diameter decrease during axial pullout. As a result, the length of shear strength mobilization along the pipe length is nonuniform and increases with the increase of relative ground movement. Meidani et al. (2018) employed a finite-discrete element approach to examine the test results of a pipe reported in Weerasekara and Wijewickreme (2008). The pipe was modelled using finite elements, and the soil was modelled using discrete elements. The study confirmed that interface soil dilation contributes to the pullout resistance of a pipe buried in dense sand. The finite-discrete element approach was also found to successfully simulate the behaviour of MDPE pipe subjected to lateral movement induced by two symmetrically applied loads (Meidani et al. 2020). Bilgin and Stewart (2009b) investigated the effect of pipe diameter change due to temperature variations on the pullout resistance of buried high-density polyethylene (HDPE) pipes. The effect

of pipe diameter changes was different for the pipes of different diameters investigated (i.e., 150, 200, and 250 mm). Alam and Allouche (2010) performed full-scale axial pullout tests of PVC (polyvinylchloride) pipes and recommended the pipe–soil friction coefficient for the pipes buried in different soil conditions. A similar study was conducted in Alam et al. (2013), where the pipe–soil friction coefficients were evaluated for cement mortar, polyurethane, and prefabricated polyethylene tape coating systems on steel pipes. The effects of earth pressure, friction mobilization through the pipes, and pulling rate were not examined in those studies. For polyethylene-coated pipes, Scarpelli et al. (2003) observed parallel scratches on the coating due to soil grain penetration that increased the friction coefficient. Reza and Dhar (2021) examined 60-mm diameter MDPE pipes further, monitoring the length of shear strength mobilization during axial pullout and investigating the pulling rate effect on the pullout resistance. Finite-element analysis was employed to capture the features that could not be measured during the tests, including the contributions of the soil, pipe, and interface parameters to the pipe behaviour. It revealed that the interface friction angle depends on the pulling rate due to the time–dependent property of the pipe material. Based on the study, a simplified method for calculating the mobilized frictional length and pipe wall strain was proposed for MDPE pipes in loose to medium dense sand. The applicability of the method for small diameter pipes (i.e., 42-mm diameter MDPE pipe) was not investigated.

The 42-mm diameter MDPE pipelines are CSA B137.4 certified and widely used in the local gas distribution system in Canada. These pipes are highly susceptible to ground movement impacts due to their operations inside the local community. Therefore, the performance assessment of the pipes buried in areas prone to ground movement needs considerable attention. Pipelines are often

installed with the backfill material purposely left loose to reduce the loads during relative ground movement. The Pipeline Research Council International (PRCI 2009) suggests burying pipelines in loose to moderately dense granular backfill as a practical method of reducing soil restraint. The current study focuses on the assessment of 42-mm diameter MDPE pipes in loose sand subjected to axial relative ground movement.

The objective of the current study is to develop a database and an improved understanding of the behaviour of small diameter MDPE pipelines subjected to axial ground movements. Full-scale axial pullout tests were conducted with 42-mm diameter MDPE pipes buried in loose sand. The pipes were pulled at three different rates to examine the effect of the pulling rate on the pipe behaviour. Force–displacement responses, pipe wall strains, and elongations were monitored during the tests. Three-dimensional (3D) finite-element (FE) analyses were used to investigate the loading rate–dependent interaction factor under various pulling rates. Finally, the applicability of the method was examined for the 42-mm diameter pipes.

4.3 Test Facility

A full-scale pipe testing facility developed at Memorial University of Newfoundland, St. John's, NL, was used to investigate MDPE pipes subjected to axial ground movements. The details of the test cell, pulling mechanisms, and data acquisition system are described in Murugathasan et al. (2021) and Reza and Dhar (2021). The facility idealizes the movement of a prismatic soil mass along failure planes parallel to the pipe axis (Murugathasan et al. 2021). However, a relative ground movement was applied by fixing the soil in a box and pulling a buried pipe through the soil. In a real field situation, the pipe is restrained in the stable ground, and the soil moves relative to the pipe. Similar test facilities were used by others for studying the axial ground movement

effects on buried pipes (Paulin et al. 1998; Bilgin and Stewart 2009a; Wijewickreme et al. 2009; Sheil et al. 2018).

The test cell was a steel box with inside dimensions of 4.0 m × 2.0 m × 1.5 m. Two circular openings on opposite walls in the box's longer direction allowed the pipes to pass in and out of the box during axial pullout tests. For the axial pullout tests, the test pipe was passed through the openings extending beyond the boundaries of the test box at both ends when the portion of the pipe within the box was buried in the sand. Thus, the length of the pipe within the test box remained constant when the pipe was axially pulled. The buried pipe was pulled from one end (herein called the leading end) using a single-acting hydraulic actuator in a displacement-controlled manner, while the other end of the pipe was free to move. The axial pipe displacement at the other end of the pipe (referred to as the trailing end) was measured using a linear variable displacement transducer (LVDT). An overall arrangement of the test setup is shown in Figure 4.1.

4.3.1 *Pipe Installation and Test Program*

The test pipe was buried in loose well-graded sand in the test cell for the test. Index properties of the sand are shown in Table 4.1 (after Saha et al. 2019). As it was intended to have the sand in a loose condition around and above the pipe, the test cell was first backfilled up to a depth of five times the pipe diameter below the pipe centre (or the centre of the opening in the test cell) to represent native soil (Figure 4.2a). The sand was then poured into the box, dropping from a height of approximately 150 mm, using sandbags with the help of an overhead crane. The sand was spread uniformly using a wooden spreader carefully to maintain the loose condition. Once the pipe invert level was reached, the soil surface was uniformly levelled, and the pipe was placed straight, parallel to the longer direction of the test cell (Figure 4.2b). A 1000 mm long spirit level was used to ensure

the pipe's straightness. The soil backfilling then continued until the desired burial depth for the pipe was reached (Figure 4.2c). In the present study, maintaining consistency in the soil condition (e.g., in situ density) of the test cell is an important consideration for the quality control of the constructions. In this regard, soil density was measured using in situ density pots at different locations inside the test box. The average value of soil unit weight ranged from 12–13 kN/m^3. Thus, the average relative compaction of the backfill material was around 65%± 3% of the standard Proctor maximum dry density. The backfill material used in each test was in air-dry condition (moisture content less than 1.5%).

The test pipe and sand were removed from the tank after each test, and the pipe installation procedure was repeated for the subsequent tests. Once used in the test, the pipe was not reused in the next tests to avoid the effect of residual stresses, if any. Although the pipelines under operation may experience residual stresses, the influence of residual stress on the test results was avoided for ease of interpretation without estimation of the contribution of the residual stress on the observed behaviour.

The test program was designed to monitor shear strength mobilization along the pipe length for 42-mm diameter piping subjected to axial pullout at various rates. Five tests (Test T1–T5) were conducted by pulling the pipes at three different pulling rates. Pipe segments of 4.6 m in length were installed in the test box as discussed above; 4.0 m was inside the box, and 300 mm extended beyond the box on each side. The pipe had a standard dimension ratio (SDR) of 10.

The pipes were generally buried at a depth of 340 mm, resulting in the ratio of soil cover (measured from springline) to pipe diameter (H/D) of 8. A test with a higher burial depth (test T5)

and a soil cover depth of 560 mm (H/D = 13.2) was also conducted to examine the effect. These burial depths fall within the range of standard practice for installation of gas distribution pipes at shallow depth from 0.3 to 1.5 m (Groves and Wijewickreme 2013). The soil width on each side of the pipes was 1.0 m, about 24 times the pipe diameter, which is sufficiently far to minimize the boundary effects during the axial pullout tests. During the tests, the pipes were axially pulled to a displacement of 120 mm. The pulling rates were 0.5, 1, and 2 mm/min at the leading end in tests T1 and T5, T2 and T4, and T3, respectively. Test T4 was a repetition of test T2, as the result from test T2 appeared as an outlier (discussed later in the paper). The pulling rates were selected based on feasibility under the laboratory conditions. Note that the pulling rates fall in the velocity Class 5 (>0.3 and <30 mm/min), corresponding to moderate landslide velocity, according to Cruden and Varnes (1996).

An array of electrical resistivity strain gauges was placed at selected locations on the pipe's outer surface. Three uniaxial strain gauges (gauge length 5 mm, strain range ±15%, gauge resistance 119.8±0.2 ohms) were installed at the distances of one-fourth, half, and three-fourths of the pipe length within the box from the leading end. These gauges, mounted at the pipe crown, provided an opportunity to capture the mobilization of axial force along the pipe's length and served as a useful check on the strain rate variations throughout the pullout tests. The analog data from all instruments (such as the load cell, LVDT, and strain gauges) were translated into a digital signal by a data acquisition system (DAQS) and recorded on a personal computer at a rate of 2 Hz.

4.4 Experimental Force–Displacement Responses

Figure 4.3 presents the force–displacement responses observed during axial pullout of the pipes in

tests T1–T5. The pulling force is shown as the pullout resistance in the figure, as the pulling force is essentially equal to the resistance offered by the surrounding soil. As seen in Figure 4.3, the pullout resistance increases nonlinearly with the pulling displacements at the leading end of the pipe. The increase of pullout resistance is continued until the soil's shear strength at the pipe–soil interface is fully mobilized over the entire pipe length inside the soil box (i.e., 4.0 m). After full mobilization, the pullout forces are stabilized or slightly reduced upon further axial displacement of the pipe. This reduction in pullout forces is due to the release of the load from the pipe to the surrounding soil when the trailing end of the pipe started to move. Similar responses were measured for 60-mm diameter pipes presented in Reza and Dhar (2021). Then, nonlinear force–displacement responses are due to progressive mobilization of interface shearing resistance, starting from the leading end towards the trailing end. The pullout forces are maximal when the trailing end of the pipe starts to move. Thus, the leading end displacement up to the maximum pullout force is due to the elongation of the pipe. This elongation of the flexible pipe during axial pulling causes a reduction in the cross-sectional area (Meidani et al. 2018; Reza and Dhar 2021). As a result, the frictional resistance (i.e., soil resistance) along the pipe's length is nonuniform.

Figure 4.3 also illustrates the effect of the loading rate on the pipe–soil interaction force for 42-mm diameter pipes buried in sand. Reza and Dhar (2021) earlier investigated the pulling rate effect on the axial soil resistance of 60-mm diameter pipes and revealed that the pullout resistance is higher for a higher rate of pulling. Similar responses are observed in Figure 4.3, except that the maximum pullout force is less in test T2 than in test T1 (conducted at a slower pulling rate). Therefore, an additional test with a pulling rate of 1 mm/min (test T4) was conducted that showed a higher maximum pullout force than in test T2.

Thus, the maximum pullout force in test T2 is considered an outlier, which can result from local voids around the pipe in the soil placed without compaction. The results from tests T1, T3, and T4 reveal that the peak pullout resistances can be 14% and 60% higher for the pulling rates of 1 mm/min and 2 mm/min, respectively, than for the pulling rate of 0.5 mm/min. Figure 4.3 also shows the effect of H/D on pullout resistance obtained by increasing the burial depth (H) in test T5. The peak pullout resistance increased by approximately 49% for changing H/D from 8 to 13.2.

The peak pulling forces, normalized for soil density, burial depth, pipe diameter, and test pipe length (i.e., $P_u/\pi DL\gamma H$), are compared in Figure 4.4 for various pulling rates. The normalized peak pullout resistances from test results presented in Anderson (2004) and Reza and Dhar (2021) are also included in Figure 4.4 for comparison. The figure shows that the nondimensional maximum pullout forces follow a general trend of increasing nonlinearly with the increase of pulling rate. The nondimensional forces obtained from the current study for 42-mm diameter pipes match well with the trend of results from previous studies with 60-mm diameter pipes (Anderson 2004; Reza and Dhar 2021) and 115-mm diameter pipes (Anderson 2004). Thus, for pipes buried in loose and medium dense sands, a common relationship between the pulling force (nondimensional) and the pulling rate can be used, regardless of pipe diameters. Through curve fitting of the data, the following regression equation for the maximum pulling force is developed for MDPE pipelines buried in loose/medium sand.

$$\frac{P_u}{\pi DL\gamma H} = 0.183 \ln(\text{pulling rate in mm/min}) + 0.46 \quad (4.1)$$

4.5 Finite-Element Analysis

Finite-element (FE) analysis was performed to investigate the interface shearing behaviour that

could not be measured during the experiment. Conventionally, the interface friction factor is expressed using a friction angle, δ, which is the internal friction angle of soil times a friction reduction factor, f (i.e., $\delta = f\phi$). The American Lifelines Alliance (ALA 2005) recommends the friction reduction factor of $f = 0.6$ for polyethylene-coated steel pipe. Reza and Dhar (2021) employed FE analyses to evaluate the interface friction factors for 60-mm diameter pipes subjected to different rates of axial pulling. They reported that interface friction angles for MDPE pipes could vary from 75% to 90% of the peak friction angle of the surrounding soil, depending on the rate of pulling. A similar study was conducted in the current research to evaluate the friction reduction factor for 42-mm diameter pipes. Three-dimensional (3D) FE analysis was performed using the Abaqus/Standard (version 2019) software package. The model dimensions were the same as those in the physical model (i.e., 4.0 m in length, 2.0 m in width, and 0.94 m in height, where the pipe was buried at a depth of 0.34 m). The soil and pipe were represented by reduced integration eight-noded linear (lower order) hexahedral elements (C3D8R). Since the 'lower order' elements might have been overly stiff, very fine meshes were used for a mesh sensitivity study. Finer mesh with a minimum element size of 3.0 mm was used in the close vicinity of the pipe over a radial distance of 2.5 times the pipe diameter (2.5D), and coarser mesh was used beyond 2.5D to reduce the computational time. The sides of the soil block were constrained in the horizontal direction. The bottom was constrained in all translational directions. Figure 4.5 shows the FE model used in the analysis.

For MDPE pipe material, the isotropic elastic-plastic model was implemented in the FE analysis. The stress–strain responses of MDPE pipe material are highly nonlinear and strain rate–dependent. The strain rate–dependent stress–strain relationship for the MDPE pipe material was

represented using the hyperbolic model of Suleiman and Coree (2004), as shown in Eq. (4.2).

$$\sigma = E_{\text{ini}} \left(\frac{\varepsilon}{1 + \eta\varepsilon} \right) \tag{4.2}$$

where E_{ini} is the initial Young's modulus, and η is a hyperbolic constant. These strain rate–dependent parameters can be obtained using the following equations (Suleiman and Coree 2004):

$$E_{\text{ini}} = a(\dot{\varepsilon})^b \tag{4.3}$$

$$\eta = \frac{a(\dot{\varepsilon})^b}{c + d\ln(\dot{\varepsilon})} \tag{4.4}$$

where $\dot{\varepsilon}$ is the strain rate, and a, b, c, and d are model parameters. The model parameters were adopted from Wijewickreme and Weerasekara (2015). The average strain rates measured during the tests were used to obtain the stress–strain relations. The true nonlinear stress–strain responses corresponding to the strain rates were then used as the input for the FE analysis. The average strain rate during the tests ranged from 2.48×10^{-6} s^{-1} to 1.0×10^{-5} s^{-1}. The Poisson's ratio and density of MDPE were assumed as 0.46 and 940 kg/m^3, respectively, at the laboratory temperature (23 °C), after Bilgin et al. (Bilgin et al. 2007).

Young's modulus (E_s) of soil was estimated based on the nonlinear model of Janbu (1963) for a stress–dependent modulus of elasticity. Janbu (1963) showed that the initial tangent modulus of elasticity, E_{s_ini}, varies as a power function of the confining pressure, p', as shown in Eq. (4.5).

$$E_{s\_ini} = Kp_a \left(\frac{p'}{p_a} \right)^n \tag{4.5}$$

where K is the material constant; p_a is the atmospheric pressure (i.e., 101.3 kPa); p' is the mean effective confining pressure; and η is a power exponent determining the rate of variation of E_{s_ini}

with p'. For the sand used in the experiments, E_{s_ini} = 2 MPa is estimated based on p' at the springline level of the pipe with K = 100 and η = 0.5 (Fellenius 2009). A Poisson's ratio of 0.25 was considered, which is within the typical values for loose sand (Budhu 2011). Soil plasticity was modelled using the conventional Mohr–Coulomb (MC) criteria. The conventional MC model was found to successfully simulate the ultimate soil resistance during the axial pullout (Muntakim and Dhar 2021). For the loose condition of the sand, the typical peak friction angle for the soil is 34.5° at high stress levels (Saha et al. 2019). However, at low stress levels, the peak friction angle can be much higher than the typical value. Saha et al. (2019) found a ratio of the peak shear stress to the normal stress of around 0.8, corresponding to a friction angle of 39°, from direct shear tests at the normal stress of 12.5 kPa. Similar results were reported in Ansari et al. (2018). Based on this information, the friction angle ϕ of 38° was selected for the FE analysis of the stress levels expected in the soil around the pipes. Minimum value cohesion, c = 0.1 kPa, and the dilation angle, ψ = 0.1°, were chosen for numerical stability.

The interaction between the pipeline and the surrounding soil was modelled using the contact surface approach available in Abaqus/Standard that allows sliding and separation at the interface between the pipe and soil. Tangential and normal behaviour were defined between the contact surfaces. For the tangential contact behaviour, the friction coefficient, μ, between the soil and the pipe was introduced using a penalty friction formulation, while for the normal interaction behaviour, a non-penetrating condition was defined (referred to as 'hard' contact in Abaqus). The Coulomb friction model was used for the frictional interaction between the pipe and soil. In this method, the maximum allowable frictional shear stress (τ_{crit}) across the interface is related to the contact pressure ($\sigma_n^{'}$) between the pipe and the soil. The allowable frictional shear stress, τ_{crit}, is a

fraction of the contact pressure, $\sigma_n^{'}$, between the contacting surfaces ($\tau_{crit} = \mu\sigma_n^{'}$). The fraction, μ (= tanδ), is known as the coefficient of friction, and δ is the interface friction angle (as mentioned previously). The contacting surfaces stick together and behave elastically when the shear stress, τ, at the contact interface, is less than τ_{crit}. The sliding along the interface between the buried pipe and surrounding soil takes place when $\tau = \tau_{crit}$ (i.e., interface shear strength), and the separation between the soil and pipe occurs when $\sigma_n^{'} < 0$.

As the magnitude of the interface friction angle is unknown, analyses with various interface friction angles were performed to simulate the measured load–displacement responses. The FE analyses with an interface friction angle of 77%, 88%, and 95% of the peak friction angle of the soil were found to match the maximum pulling force reasonably for test T1 (pulling rate: 0.5 mm/min), test T4 (pulling rate: 1 mm/min), and test T3 (pulling rate: 2 mm/min), respectively. As mentioned earlier, the maximum pulling force in test T2 was considered an outlier and, therefore, was not simulated using the FE method.

4.6 Comparison of Results

Figure 4.6 compares the load–displacement responses from the FE analysis and the experiments. The FE method reasonably simulated the load–displacement responses with the interface friction reduction factors (f) of 0.77, 0.88, and 0.95, corresponding to the loading rates of 0.5, 1, and 2 mm/min, respectively. Similar comparisons were reported in Reza and Dhar (2021) for 60-mm diameter MDPE pipes. The FE analysis slightly underestimates the peak pullout force for test T3, which might be due to uncertainty in the soil condition around the pipe. Although the backfill soil was carefully placed, it was difficult to maintain uniformity during backfilling with the loose

condition of the sand. Note that the maximum pullout force for test T5 (with a deeper burial depth, $H = 0.56$ m) was also successfully simulated using the friction reduction factor (i.e., $f = 0.77$) used for test T1 conducted at the same pulling rate (0.5 mm/min). Thus, the factor f can be considered independent of the burial depth. The friction reduction factors for the 42-mm diameter pipes from the current study are compared with those from Reza and Dhar (2021) in Figure 4.7. They show that the pulling rate–dependent friction reduction factors for 42-mm diameter pipes match those for 60-mm diameter pipes. Thus, the same friction reduction factors can be used for calculating the pulling forces for 42-mm and 60-mm diameter pipes.

The FE analysis results were also compared with the measured pipe wall strains (Figure 4.8). In Figure 4.8, the calculated longitudinal strains at the pipe crown at distances of one-fourth ($L/4$), half ($L/2$), and three-fourths ($3L/4$) from the leading end are plotted with the measured strains in test T1. The results from the FE analysis match reasonably well with the test results in Figure 4.8, implying that the developed FE modelling approach can reasonably simulate the test conditions.

4.7 Strain Calculations

During axial pullout of flexible MDPE pipes, the axial force and the interface shearing resistance are gradually mobilized from the leading end toward the trailing end. The friction mobilization length, l (called herein the 'mobilized frictional length'), depends on the leading end displacement (or the relative ground movement in the field). The mobilized frictional length is required for estimating the pipe wall strains under axial ground movement. Reza and Dhar (2021) proposed a simplified equation for predicting the mobilized frictional length, assuming a linear distribution of axial strains over the mobilized frictional length observed during the tests for 60-mm diameter

pipe. The simplified equation for estimating the mobilized frictional length, l, as a function of known relative ground movement (u) is as follows:

$$l = \sqrt{\frac{4AE}{\zeta(1+K_0)\gamma H\pi D\tan\delta}}\, u \tag{4.6}$$

where ζ is the normal stress adjustment factor, associated with reducing normal stress on the pipe wall (due to the pipe's diametric reduction); A is the cross-sectional area of the pipe; and E is the elastic modulus of the pipe material. The factor ζ was calculated from the test results using the framework of the existing design equation (ALA 2005) for calculating the maximum pullout force as follows in Eq. (4.7).

$$\zeta = \frac{\textit{Peak pullout resistance from test results}}{\pi DL(\frac{1+K_0}{2})\gamma H\tan\delta} \tag{4.7}$$

In Eq. (4.7), $\tan\delta$ is the coefficient of friction that can be calculated using the friction reduction factor, f, discussed earlier. The coefficient of lateral earth pressure was calculated using $K_0 = \nu/1-\nu$. Using this method, the normal stress adjustment factors (ζ) were calculated as 0.95, 0.92, and 1.10 for tests T1, T4, and T3, respectively, which are close to 1. Thus, the reduction in normal stress due to the elongation of the pipe would be insignificant for 42-mm diameter pipes in loose sand.

Note that Eq. (4.6) was developed based on a linear distribution of the axial strain over the mobilized frictional length of the pipe. Linear distributions of the axial strains were also observed for the 42-mm diameter pipes presented in this study, as shown in Figure 4.9. Figure 4.9 plots the distribution of axial strains along the pipe length at the leading end displacements, corresponding to the mobilization of frictional resistance to the distances from the leading end of 1, 2, 3, and 4 m

(trailing end), termed herein as u_1, u_2, u_3, and u_4, respectively. The distances of frictional resistance mobilization were estimated using the measurements of axial strain. For example, when the axial strain starts increasing at a point (e.g., 1 m from the leading end), the frictional resistance (and hence the axial force) is mobilized to that point. In test T1, the distances were: u_1 = 0.24 mm, u_2 = 1.35 mm, u_3 = 4.0 mm, and u_4 = 8.1 mm. In test T4, these were: u_1 = 0.23 mm, u_2 = 1.24 mm, u_3 = 3.92 mm, and u_4 = 10.5 mm. In test T3, these were: u_1 = 0.19 mm, u_2 = 0.83 mm, u_3 = 3.8 mm, and u_4 = 12.16 mm. As seen in Figure 4.9, the distributions of the axial strains are essentially linear. Thus, the equation proposed for 60-mm diameter pipes (Eq. 4.6) is applicable for 42-mm diameter pipe to calculate the mobilized friction length. Using the mobilized friction length, the pipe wall strains can be estimated using Eq. (4.8).

$$\varepsilon = \frac{p}{AEl}\,(l - x) \tag{4.8}$$

where l = mobilized frictional length corresponding to known relative ground movement; x = distance from the leading end of the pipe; and p = pulling force at the leading end. Pipe wall strains calculated using Eq. (4.8) are compared with measured strains in Figure 4.10 for different leading end displacements (u_1, u_2, u_3, and u_4, discussed earlier). The calculated strains compare very well with the measured strains in the figure. Thus, the equations proposed for 60-mm diameter pipes in Reza and Dhar (2021) are applicable for the 42-mm diameter pipes presented in this study.

4.8 Conclusions

This paper presents the behaviour of 42-mm diameter MDPE pipes buried in loose sand subjected to relative axial ground movement. Axial pullout tests were conducted at various pulling rates to investigate the effects. FE analyses of the tests were conducted to evaluate the pipe–soil interaction parameters. Measured responses were then compared with the simplified models previously

proposed by the authors. The following presents the major findings from this study.

- The pullout resistance increases nonlinearly with the pulling displacements at the leading end of the pipe. The nonlinear force–displacement responses are due to progressive mobilization of interface shearing resistance, starting from the leading end towards the trailing end. The pullout forces are maximal when the trailing end of the pipe begins to move. Thus, the leading end displacement up to the maximum pullout force is due to the elongation of the pipe only. This confirms the nonuniform nature of the frictional resistance mobilized on the pipe surface.
- The pullout force of the pipe increases with the rate of relative ground movement, regardless of pipe diameter. The nondimensional maximum pullout force follows a general trend of increasing nonlinearly with the increase of pulling rate and can be presented using Eq. (4.1).
- Rate–dependent friction reduction factors can be used for the calculation of the maximum pullout resistance. The friction reduction factor increases nonlinearly with the pulling rate, which is the same for 60- and 42-mm diameter pipes.
- The effect of pipe diameter decrease is negligible for the small diameter pipes. The normal stress adjustment factor (ζ) is close to 1. Thus, the conventional design equation (i.e., ALA 2005) may reasonably calculate the maximum pullout force for pipes buried in loose sand with the application of a pulling rate–dependent friction coefficient.
- Linear distributions of the axial strains were observed for the pipes presented in this study, implying that the unit shear resistance at the pipe–soil interface can be assumed to be constant over the pipe length.

- The pipe wall strains calculation method proposed by Reza and Dhar (2021) for 60-mm diameter pipe can be used for 42-mm diameter pipes.

4.9 Acknowledgments

The Collaborative Research and Development Grant program of the Natural Science and Engineering Research Council of Canada, Innovate NL program of the Government of Newfoundland and Labrador, FortisBC Energy Inc. and WSP Canada Inc., are gratefully acknowledged for providing the financial and/or in-kind support for this research. The authors are thankful for the technical assistance by Jason Murphy, Shawn Organ, and Matt Curtis in the Faculty of Engineering and Applied Science at Memorial University of Newfoundland. Undergraduate student Thabiso Mthethwa helped with instrumentation and pipe installation and deinstallation during the tests.

4.10 References

Alam, S. & Alloche, E. N. (2010). Experimental investigation of pipe soil friction coefficients for direct buried PVC pipes. *Proceedings of the Pipeline Division Specialty Conf. 2010*, American Society of Civil Engineers, Keystone, Colorado, USA, 2: 1160–1169.

Alam, S., Allouche, E. N., Bartlett, C., Sherpa, A. & Keil, B. (2013). Experimental evaluation of soil–pipe friction coefficients for coated steel pipes. *Proceedings of the Pipelines 2013: Pipelines and Trenchless Construction and Renewals—A Global Perspective*, Fort Worth, TX, USA, 23–26 June 2013, pp. 360–371.

Anderson, C. (2004). *Soil–pipeline interaction of polyethylene natural gas pipelines in sand*. M.Sc. thesis, Department of Civil Engineering, The University of British Columbia, Vancouver, BC, Canada.

Ansari, Y., Kouretzis, G. & Sloan, S. W. (2018). Development of a prototype for modelling soil–pipe interaction and its application for predicting uplift resistance to buried pipe movements in sand. *Canadian Geotechnical Journal*, **55**, No. 10, 1451–1474.

ASCE (American Society of Civil Engineers). (1984). *Guidelines for the seismic design of oil and gas pipeline systems*. Committee on Gas and Liquid Fuel Lifelines, Technical Council on Lifeline Earthquake Engineering, New York, pp. 573.

ALA (American Lifelines Alliance) (2005). *Guidelines for the design of buried steel pipe*. Washington, DC and Reston, VA, USA: Federal Emergency Management Agency (FEMA) and American Society of Civil Engineers (ASCE).

Bilgin, Ö., Stewart, H. E. & O'Rourke, T. D. (2007). Thermal and mechanical properties of polyethylene pipes. *Journal of Materials in Civil Engineering*, **19**, No. 12, 1043–1052.

Bilgin, Ö. & Stewart, H. E. (2009a). Pullout Resistance Characteristics of Cast Iron Pipe. *Journal of Transportation Engineering*, **135**, No. 10, 730–735.

Bilgin, Ö. & Stewart, H. E. (2009b). Design Guidelines for Polyethylene Pipe Interface Shear Resistance. *Journal of Geotechnical and Geoenvironmental Engineering*, **135**, No. 6, 809–818.

Budhu, M. (2011). *Soil mechanics and foundations*. 3rd edition. John Wiley & Sons, Inc., United States of America.

Cruden, D. M. & Varnes, D. J. (1996). *Landslide types and processes. Landslides—Investigations and mitigation*, pp. 36–75, edited by Turner, A. K. and Schuster, R. L. Special Report, 247. Washington, DC: Transportation Research Board.

Fellenius, B. H. (2009). *Basics of Foundation Design*. Electronic: Calgary, AB, Canada. Available online: www.fellenius.net (accessed on 2 August 2022).

Groves, A. & Wijewickreme, D. (2013). Field monitoring of buried polyethylene natural gas

pipelines subjected to ground movement. *Proceedings of the 66th Canadian Geotechnical Conference, GeoMontreal 2013*, Montreal, QC, Canada, 29 Sept.–3 Oct. 2013.

Janbu, N. (1963). Soil compressibility as determined by oedometer and triaxial tests. *Proceedings of the European Conference on Soil Mechanics and Foundation Engineering*, vol. 1, pp. 19–25. Essen, Germany: German Society for Earthworks and Foundations.

Kunert, H. G., Marquez, A. A., Fazzini, P. & Otegui, J. L. (2016). *Failures and integrity of pipelines subjected to soil movements*. Handbook of Materials Failure Analysis with Case Studies from the Oil and Gas Industry, 105–122.

Paulin, M. J., Phillips, R., Clark, J. I., Trigg, A. & Konuk, I. (1998). A full-scale investigation into pipeline–soil interaction. *Proceedings of the ASME. IPC1998*, June 7–11, Calgary, Alberta. pp. 779–788.

PRCI (Pipeline Research Council International) (2009). *Guidelines for Constructing Natural Gas and Liquid Hydrocarbon Pipelines through Areas Prone to Landslide and Subsidence Hazards*. Report Prepared for the Design, Material, and Construction committee. Chantilly, VA, USA.

Marino, G. & Osouli, A. (2020). Slip Resistance Behavior of Coal Tar–Coated Steel Pipelines Buried in Clayey and Sandy Backfills from Ground Movement. *Journal of Pipeline Systems Engineering and Practice*, **11**, No. 3, 05020001.

Meidani, M., Meguid, M. A. & Chouinard, L. E. (2017). Evaluation of Soil–Pipe Interaction under Relative Axial Ground Movement. *Journal of Pipeline Systems Engineering and Practice*, **8**, No. 4, 1–10.

Meidani, M., Meguid, M. A. & Chouinard, L. E. (2018). A finite-discrete element approach for modeling polyethylene pipes subjected to axial ground movement. *International Journal of Geotechnical Engineering*, **14**, No. 7, 717–729.

Meidani, M., Meguid, M. A. & Chouinard, L. E. (2020). On the response of polyethylene pipes to lateral ground movements: insights from finite-discrete element analysis. *International Journal of Geosynthetics and Ground Engineering*, **6**, 15.

Muntakim, A. H. & Dhar, A. S. (2021). Assessment of Axial Pullout Force for Buried Medium-Density Polyethylene Pipelines. *Journal of Pipeline Systems Engineering and Practice*, **12**, No. 2, 04020074.

Murugathasan, P., Dhar, A. S. & Hawlader, B. C. (2021). An experimental and numerical investigation of pullout behaviour of ductile iron water pipes buried in sand. *Canadian Journal of Civil Engineering*, **48**, No. 2, 134–143.

Reza, A. & Dhar, A. S. (2021a). Axial Pullout behavior of Buried Medium Density Polyethylene Gas Distribution Pipes. *International Journal of Geomechanics*, **21**, No. 7, 04021120.

Saha, R. C., Dhar, A. S. & Hawlader, B. C. (2019). Shear strength assessment of a well-graded clean sand. *Proceedings of the 72nd Canadian Geotechnical Conf., GeoSt.John's 2019*, St. John's, Newfoundland and Labrador, Canada: Canadian Geotechnical Society.

Sarvanis, G. C., Karamanos, S. A., Vazouras, P., Mecozzi, E., Lucci, A. & Dakoulas, P. (2017). Permanent earthquake-induced actions in buried pipelines: Numerical modeling and experimental verification. *Earthquake Engineering Structural Dynamics*, **47**, No. 4, 966–987.

Scarpelli, G., Sakellariadi, E. & Furlani, G. (2003). Evaluation of soil–pipeline longitudinal interaction forces. *Rivista Italiana di Geotecnica*, **4**, No. 3, 24–41.

Sheil, B. B. Ã., Martin, C. M. Ã., Byrne, B. W. Ã., Plant, M., Williams, K. & Coyne, D. (2018). Full-scale laboratory testing of a buried pipeline in sand subjected to cyclic axial displacements. *Géotechnique*, **68**, No. 8, 684–694.

Suleiman, M. T. & Coree, B. J. (2004). Constitutive model for high density polyethylene material:

Systematic approach. *Journal of Materials in Civil Engineering*, **16**, No. 6, 511–515.

Weerasekara, L. & Wijewickreme, D. (2008). Mobilization of soil loads on buried polyethylene natural gas pipelines subject to relative axial displacements. *Canadian Geotechnical Journal*, **45**, No. 9, 1237–1249.

Wijewickreme, D., Karimian, H. & Honegger, D. (2009). Response of buried steel pipelines subjected to relative axial soil movement. *Canadian Geotechnical Journal*, **46**, No. 7, 735–752.

Wijewickreme, D. & Weerasekara, L. (2015). Analytical Modeling of Field Axial Pullout Tests Performed on Buried Extensible Pipes. *International Journal of Geomechanics*, **15**, No. 2, 04014441-12.

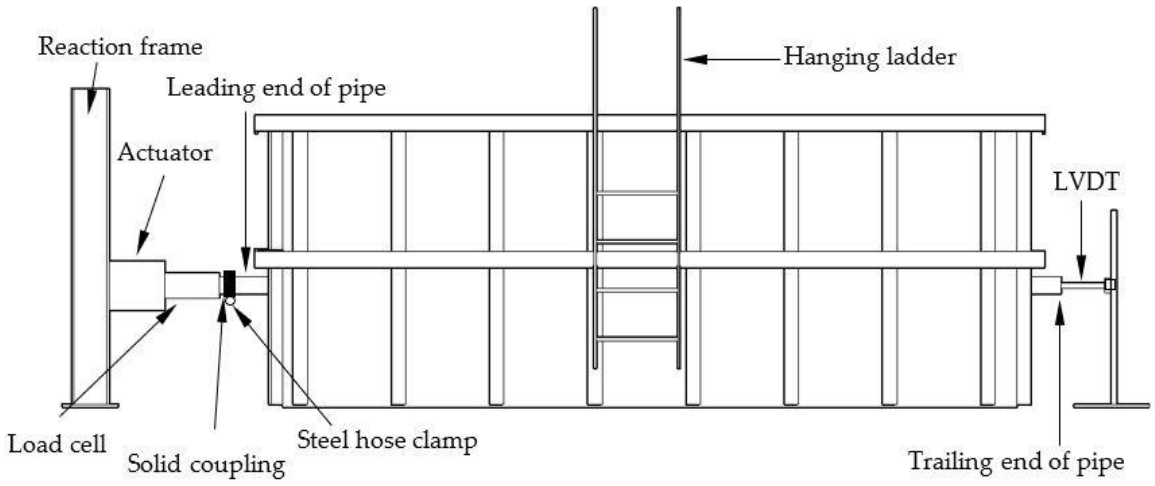

Figure 4.1: Test cell configuration

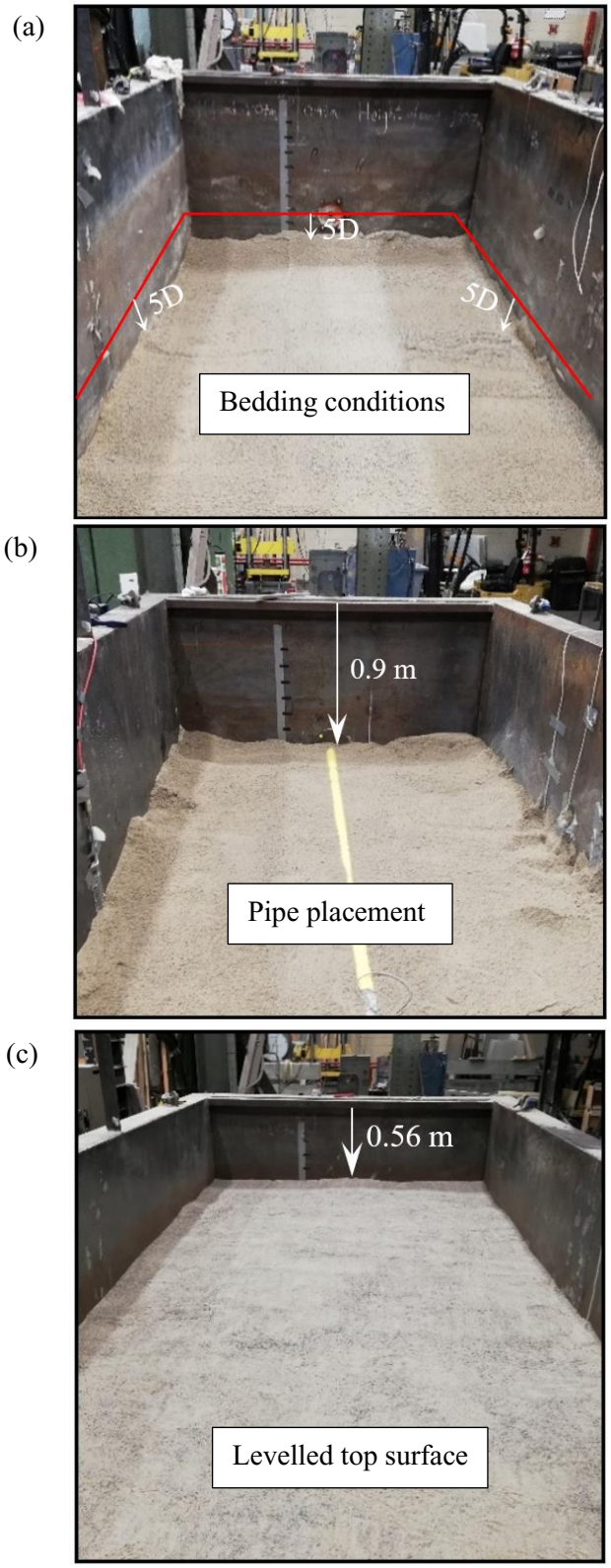

Figure 4.2: Test preparation

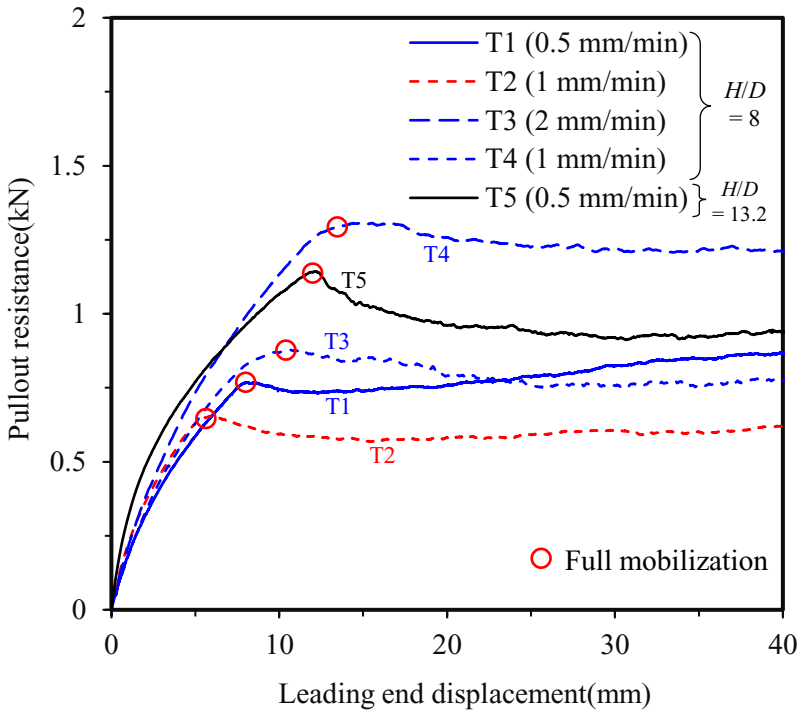

Figure 4.3: Axial pullout resistance with leading end displacement

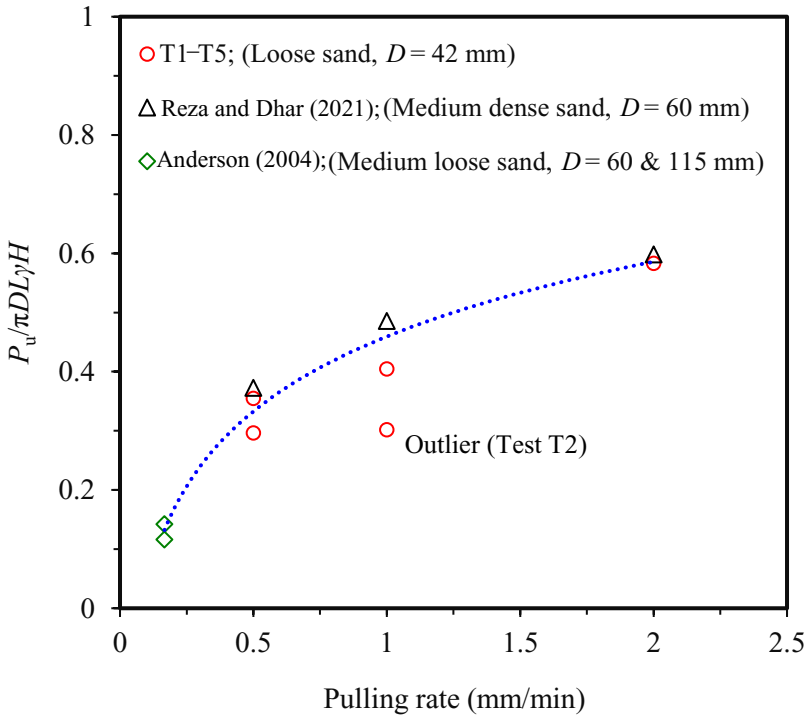

Figure 4.4: Normalized peak pullout forces with pulling rates in loose/medium sand

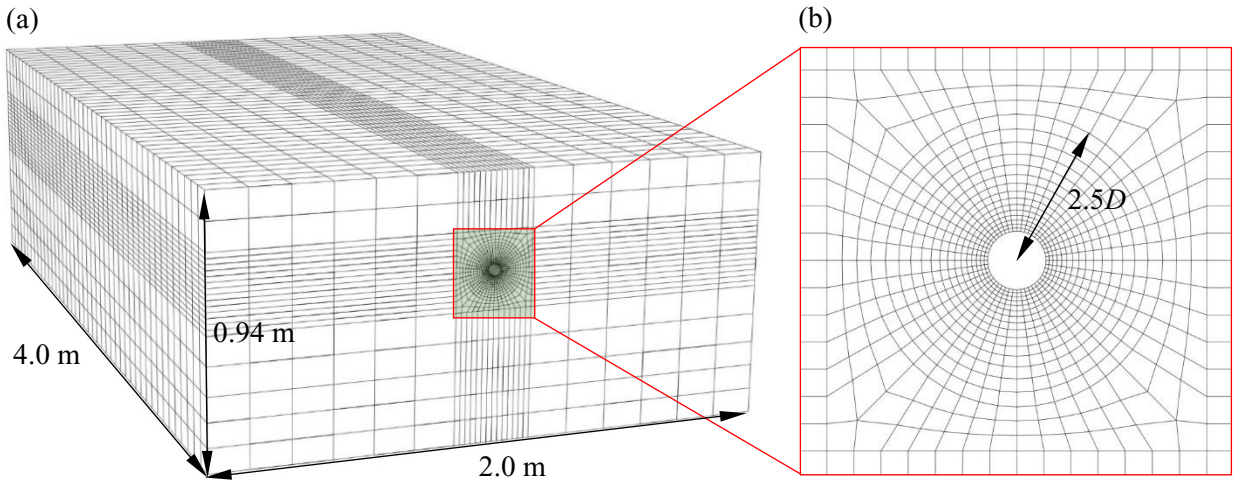

Figure 4.5: FE mesh of the pipe–soil system. (a) 3D FE mesh; and (b) cross-section near the pipe

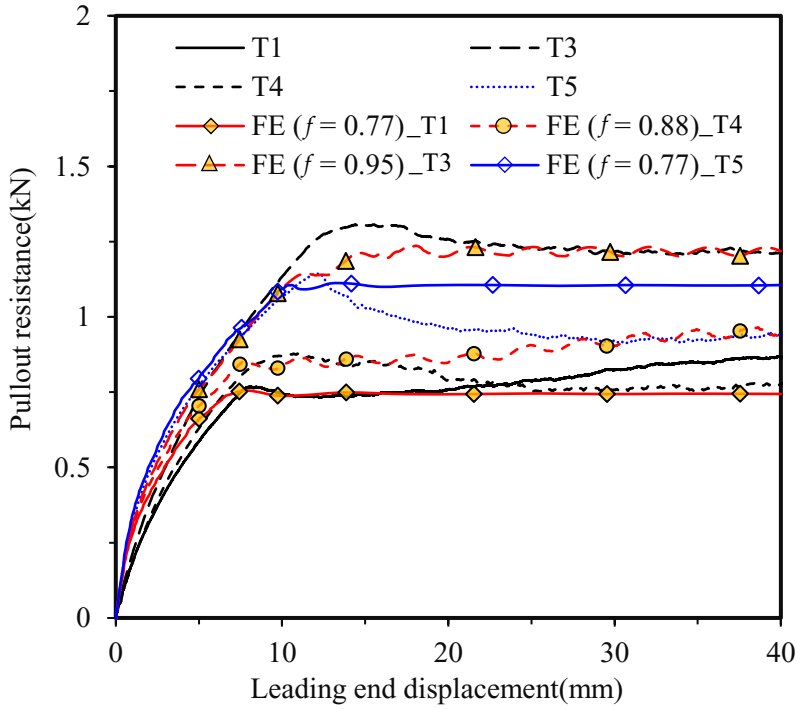

Figure 4.6: Simulation of load–displacement response

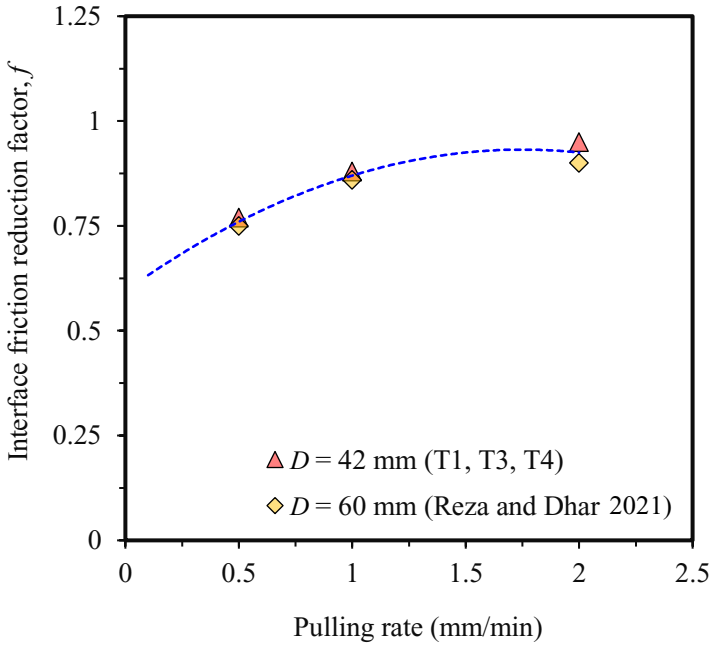

Figure 4.7: Interface friction reduction factor with pulling rates

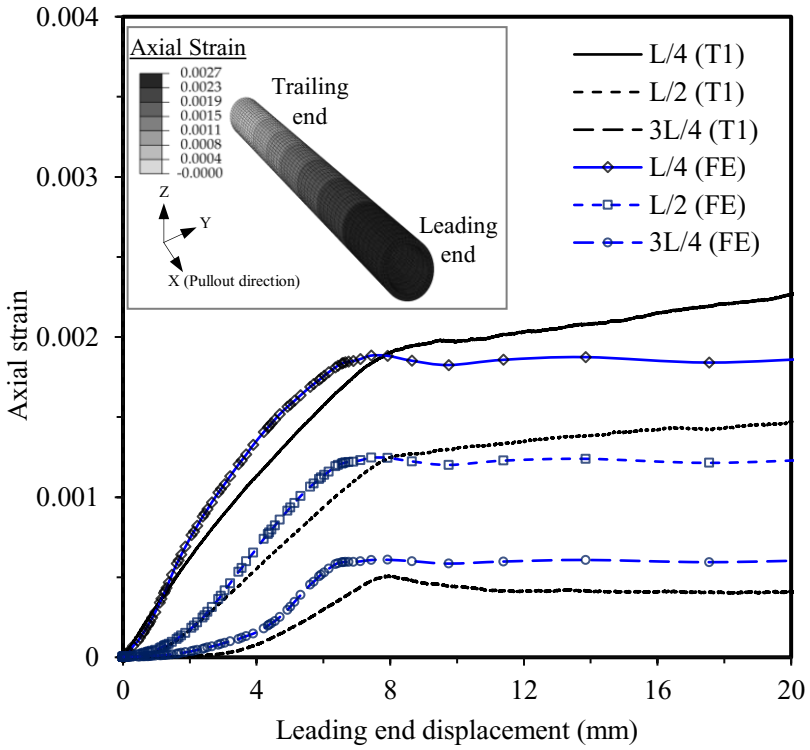

Figure 4.8: Comparison of axial strains at different locations of the pipes in test T1 (the inserted figure shows pipe axial strain from FE calculation at peak pullout load)

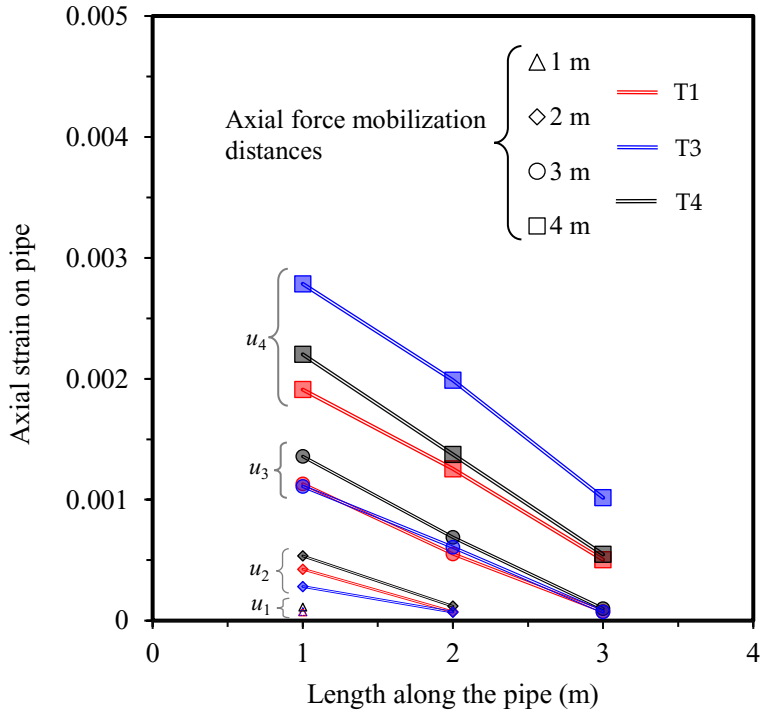

Figure 4.9: Strain distribution along the length of the pipe

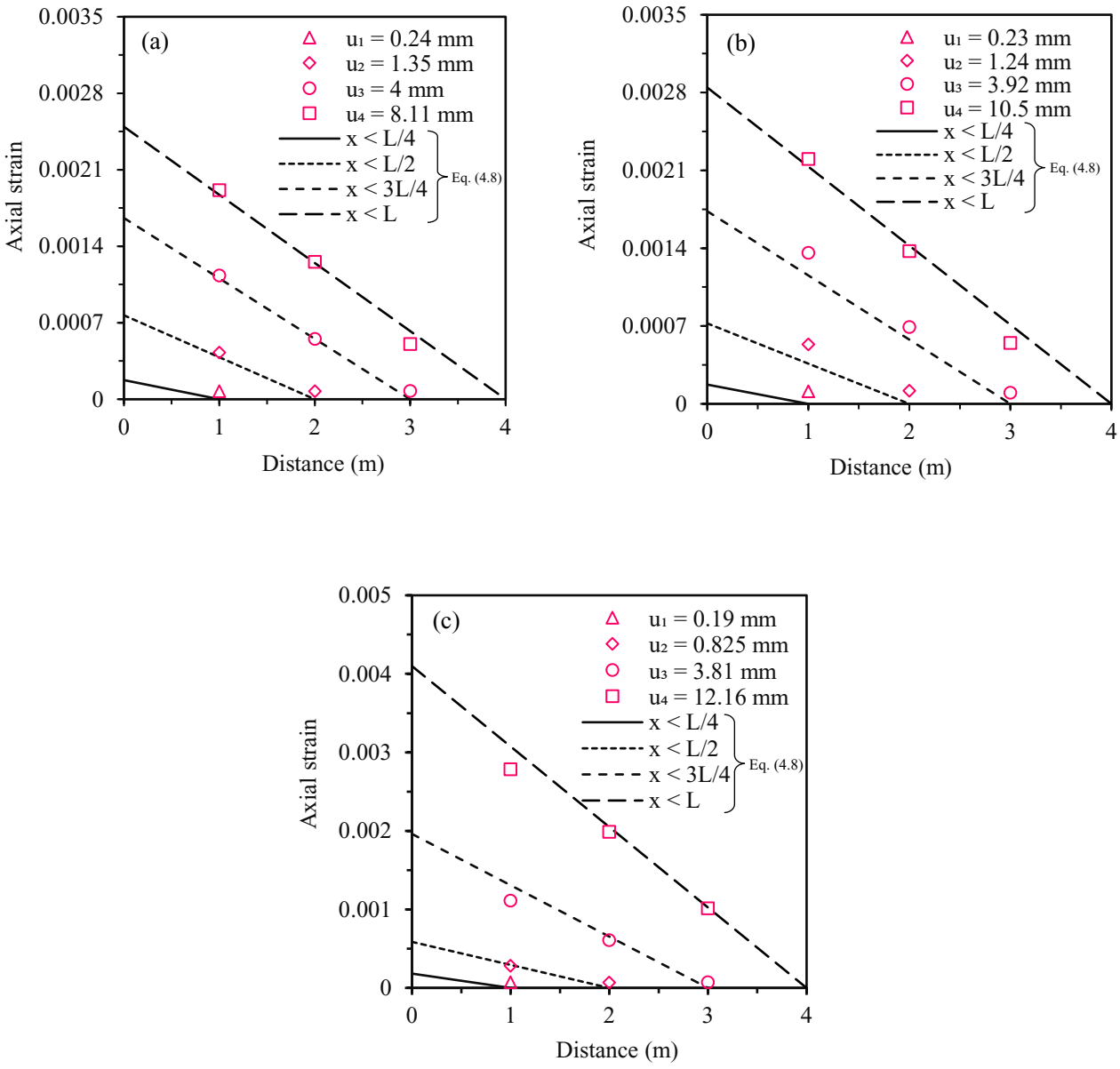

Figure 4.10: Comparison of experimental strains with calculations using the simplified method for (a) T1; (b) T4; and (c) T3. u_1, u_2, u_3, and u_4 are the leading end displacements when the axial force is mobilized to the distance of 1, 2, 3, and 4 m (trailing end), respectively, from the leading end.

Table 4.1. Sand properties.

Property	Value
Median particle size, D_{50} (mm)	0.742
Coefficient of uniformity, C_u	5.81
Coefficient of curvature, C_c	2.04
Fines content (%)	1.3
Gravel content (%)	0.87
Specific gravity of particles, G_s	2.62
Minimum void ratio, e_{min}	0.33
Maximum void ratio, e_{max}	0.65
Maximum dry density (Standard Proctor compaction), $\gamma_{d(max)}$(kN/m^3)	18.8

CHAPTER 5

Strain Assessment of Polyethylene Pipes in Dense Sand Subjected to Axial Displacements

Co-Authorship: A version of this chapter has been published in Geosynthetics International as: Reza, A., Dhar, A. S. and Rahman, M. (2023). 'Strain Assessment of Polyethylene Pipes in Dense Sand Subjected to Axial Displacements.' Most of the research presented in this chapter has been conducted by the first author. He also prepared the draft manuscript. The other authors mainly supervised the research and reviewed the manuscript.

5.1 Abstract

Buried polyethylene pipes used in gas distribution systems can experience excessive wall strains when exposed to ground movements that can affect the performance of the pipes in service. This paper presents full-scale laboratory tests performed to investigate the responses of medium-density polyethylene (MDPE) gas-distribution pipes in dense sand when subjected to axial ground movements. Pipes buried in sand in a large test box were pulled at rates of 0.5, 1, and 2 mm/min to simulate the relative ground movements in the longitudinal direction. The test facility was instrumented to measure pulling force, pipe wall strains, and soil stresses. The measured pullout force was significantly higher than predicted using the equations recommended in current design guidelines, which is attributed to the increase of normal stress on the pipe wall by shear-induced dilation of interface soil. The cavity expansion theory was successfully applied to calculate the normal stress increase. The distribution of measured strains was nonlinear along the pipe length. Assuming a parabolic distribution of the strains, simplified equations were developed to calculate pullout resistances and pipe wall strains from the relative ground displacement. The developed method reasonably predicted the pipe strains measured during the tests.

5.2 Introduction

Polyethylene (PE) pipes are widely used in natural gas distribution systems due to their various advantages, including low cost, lightweight, ease of installation, corrosion resistance, and high flexibility. According to the Plastics Industry Pipe Association (PIPA), 90% of natural gas distribution systems in North America use plastic pipes, of which 99% are PE (PIPA 2001). Permanent ground deformations (PGDs) due to ground subsidence, earthquakes, landslides, and slope movements have been identified as major hazards for buried pipelines (EGIG 2020). The PGDs can induce large strain in the pipe wall, leading to leaks, local buckling, and subsequent raptures (O'Rourke and Nordberg 1992; Sarvanis et al. 2017). The strains on the pipe wall should be predicted reasonably to compare with the allowable strain limits for the integrity assessment of pipelines subjected to the PGDs (Weerasekara and Rahman 2019). Although the ground movements can be measured with reasonable accuracy using different advanced technologies, including monitoring hubs and satellite images, relating the ground movements to pipe wall strains has been challenging. The problem is more complex for gas distribution pipes due to their smaller sizes, intricate configuration and components, and complex material characteristics of PE (Weerasekara and Rahman 2019). Figure 5.1 shows a segment of a ground movement scenario recorded for a natural gas distribution system in Canada using a monitoring program led by the third author. A slow-moving ground was monitored using GPS (Global Positioning System) hubs located at discrete locations, shown in Figure 5.1. It reveals that the pipe segments, running parallel to the roads, can be subjected to longitudinal, transverse, or combined ground movements depending on their locations. Stress concentrations are also expected at the connections of a pipe segment with other(s). The situations in each pipe segment need to be examined to develop strain prediction models for integrity assessment. The current study focuses on examining the effects of

ground movement in the longitudinal direction of the pipes. It corresponds to a scenario similar to the pipe segment along Purmal Ave subjected to ground movements measured by GPS 11-47 and GPS 11- 48 (encircled in blue in Figure 5.1) but idealized for simplification in the investigation.

Current design guidelines (e.g., ALA 2005; PRCI 2017) recommend using beam-on-spring analysis to assess pipelines subjected to ground movements for steel pipes. Elastic, perfectly plastic-type bilinear models are recommended in the guidelines for the spring constants, developed based on observations of steel pipes. The maximum values of the spring force are obtained as the longitudinal frictional force per unit length along the pipe length, calculated based on the estimation of the normal stresses acting on the pipe and the frictional characteristics of the soil–pipe interface. Normal stresses are estimated as the mean value of the overburden stress and at-rest lateral earth pressure at the pipe springline. However, the maximum forces calculated using this method were found to be significantly less than those observed in laboratory tests for dense sand (Weerasekara and Wijewickreme 2008; Wijewickreme et al. 2009; Sheil et al. 2018). For dense sand, the shearing-induced dilation at the pipe–soil interface can increase the normal stresses, resulting in a higher axial soil resistance (Wijewickreme et al. 2009), which is not accounted for in the design equation. Researchers performed extensive experimental and numerical studies to identify the key parameters contributing to the soil–pipe interaction for accurately calculating the axial soil resistance for steel pipes (Paulin et al. 1997; Wijewickreme et al. 2009; Sarvanis et al. 2017; Meidani et al. 2017; Sheil et al. 2018). They proposed different approaches to account for the normal stress increase due to the interface soil dilation, using either a higher coefficient of lateral earth pressure (e.g., Wijewickreme et al. 2009; Meidani et al. 2017) or an empirical equation (Sarvanis et al. 2017). Sheil et al. (2021) measured the contact stresses

around buried steel pipes, applying and subsequently reducing surcharge pressures, and found 'locked in' normal stresses on the pipe after reducing the surcharge pressure. The locked-in normal stress cannot be estimated based on the overburden pressure recommended in the existing design guidelines. In addition, Muntakim and Dhar (2021) demonstrated, based on finite element modelling, that the relative rigidity of the pipe with respect to the surrounding soil can influence the normal stress on the pipe. The finding is consistent with the observations of Bilgin and Stewart (2009), where normal stress (hence the pullout resistance) was found to reduce, due to the reduction of pipe diameter, for buried high-density polyethylene (HDPE) pipes. Thus, the spring parameters recommended for steel pipes in the design guidelines require further improvement with a proper understanding of various contributing factors. The behaviour of PE pipe is more complex, as it can experience significant axial elongation and reduction in cross-sectional dimensions when subjected to axial force due to the ground movements (Weerasekara and Wijewickreme 2008; Reza and Dhar 2021a). Due to the axial elongation, the mobilization of maximum frictional resistance at the interface is nonuniform over the pipe length. No recommendation is available in the existing design guidelines for assessing PE pipes. While beam-on-spring analysis can provide a relatively rigorous solution, a simplified design tool would be suitable for quickly assessing the pipe conditions. A simplified tool for pipe condition assessment is currently not available in the design guidelines.

Weerasekara and Wijewickreme (2008) and Wijewickreme and Weerasekara (2015) conducted laboratory and field tests to investigate the axial pullout behaviour of medium-density polyethylene (MDPE) pipes buried in specific conditions of Fraser River sand in Canada. The backfill soil was compacted to unit weights ranging from 15.7 to 16.1 kN/m^3, corresponding to

relative densities of 82% to 92%. The test results highlighted the need to consider soil dilation effects in estimating the MDPE pipe's behaviour. The maximum pulling forces measured in the tests were significantly higher than those calculated using the methods recommended in the design guidelines. Weerasekara and Wijewickreme (2008) used the coefficient of lateral earth pressures of 2.4 and 1.4 for 60-mm and 114-mm diameter MDPE pipes, respectively, in the design equation, instead of the at-rest earth pressure coefficient, to match the maximum axial soil resistance observed during the tests. Wijewickreme and Weerasekara (2015) applied the cavity expansion theory to estimate the maximum normal stress increase on the pipe surface due to shearing-induced soil dilation. They also developed an analytical method to estimate the elongation of the pipe and its effect on the interface shear stress mobilization and the pipe wall strains. For extensible MDPE pipe, the interface shear stress was progressively mobilized along the pipe length (called herein 'mobilized friction length') with the increase of displacement of the pipe at the pulling end. Similar behaviour was observed by Reza and Dhar (2021ab) for small diameter MDPE pipes in loose to medium dense sand, where the interface shear stress mobilization was monitored through measuring pipe wall strains at different locations during axial pullout testing. Reza and Dhar (2021a) extended the study to develop a simplified method for calculating the mobilized frictional length and the pipe wall strains for MDPE pipes in loose to medium-dense sands.

Reza and Dhar (2021ab) showed that for the pipes in loose to medium-dense sand, the effect of dilation on the axial pullout resistance is negligible. However, due to the time–dependent property of MDPE pipe material, interface friction angles were pulling rate–dependent. Pulling rate–dependent friction reduction factors were proposed to account for the rate–dependent effects. Additionally, linear distribution of the interface shearing stress was assumed over the mobilized

friction length that reasonably simulated the observed responses for pipes in loose to medium-dense sand. However, although pipelines are often installed with the backfill material purposefully left loose to minimise loads during relative ground movements, environmental loading might compact the backfill material into a dense condition (Vanden Berghe et al. 2005). As a result, dense backfills for buried pipes are very common in the field. Roy et al. (2016, 2018ab) investigated the lateral forces on pipes under plane-strain loading conditions. However, a simplified method of strain assessment for MDPE pipes in dense sand backfill is currently unavailable.

The present study focuses on developing a simplified method for assessing the MDPE gas distribution pipes buried in dense sand subjected to relative ground movement in the axial direction. The commonly used MDPE pipings for gas distribution systems in Canada (i.e., 42-mm and 60-mm diameter pipes) were considered for developing the design method. A series of full-scale axial pullout tests was conducted, measuring the pipe and soil responses to understand the pipe–soil interaction. Based on the analysis of test results, a simplified method is proposed, which accounts for the effect of soil dilation, pipe elongation, and the pulling rate–dependent soil–pipe interaction.

5.3 Test Methods

5.3.1 *Apparatus*

A test facility designed to simulate the effects of axial ground movement on a buried pipe was used in the test program. Murugathasan et al. (2021) provided the details of the idealization used in the test cell design (Figure 5.2). In general, a buried pipe is pulled through a static soil mass

(Figure 5.2a) to simulate the relative movement of the soil with respect to the pipe shown in Figures 5.2b and 5.2c. Figure 5.2b shows an idealized prismatic soil mass moving along a failure plane parallel to the pipe axis where the upslope soil is stable. The pipe is restrained in the stable upslope soil. Figure 5.2c shows a pipe restrained at one end to another pipe or an anchor when the prismatic soil mass is moving toward the other end. Other researchers also used a similar test facility to study axial ground movements' effects on steel, cast iron, and polyethylene pipes (Bilgin and Steward 2009; Wijewickreme et al. 2009; Daiyan et al. 2011; Sheil et al. 2018).

The test facility comprised a steel test box with inside dimensions of 4.0 m in length, 2.0 m in width, and 1.5 m in height, an actuator with hydraulic controls to pull a pipe, a data acquisition system, and instruments for measuring pipe and soil responses. The test box sidewalls were rigid to simulate lateral earth pressure at rest conditions (K_0). The strains on the sidewall during placement of the soil and pullout testing were negligible, confirming the K_0 conditions (Murugathasan et al. 2021). No sidewall treatment was required to reduce the interface friction between the soil and vertical sidewalls of the test cell, as no sliding of soil with respect to the cell walls was expected during axial pulling. Friction between the soil and interior walls of the test facility is particularly important under vertical load (e.g., Dhar et al. 2004). Chakraborty et al. (2020) revealed through measurement of vertical stresses at limited locations during soil placement in the test facility that the sidewall friction did not reduce the vertical stress in the soil.

A schematic of the test facility is shown in Figure 5.3. Two circular openings on opposite walls in the box's longer direction allowed the pipes to pass in and out of the box during axial pulling. A circular steel plate with a hole at the center bolted to the testing tank was used for adjusting the

opening size. The plate included a replaceable hard-rubber gasket with a hole in the centre (Figure 5.3b and 5.3c). The hole in the rubber gasket was smaller than the hole in the steel plate and was slightly larger than the pipe diameter (e.g., 45- and 62-mm diameter holes for 42- and 60-mm diameter test pipes, respectively) to minimise friction between the pipe and the openings. Several independent pullout tests were performed that showed negligible frictional resistance at the gasket (i.e., 0.1 kN to 0.2 kN for different pipe sizes).

For axial pullout, the test pipe was extended beyond the test box at both ends through the holes to ensure a constant pipe–soil interaction length within the box during the test (Figure 5.3a). A single-acting hydraulic actuator pulled the buried pipe from one end (herein called the leading end) in a displacement-controlled manner, while the other end was free to move. The leading end displacement was measured by the movement of the actuator. The axial pipe displacement at the other end of the pipe (referred to as the trailing end) was measured using a linear variable displacement transducer (LVDT). The axial pulling forces were measured using a load cell connected to the actuator.

5.3.2 *Backfill Material*

The backfill material used for the pipe was locally manufactured sand having the grain size distribution curve shown in Figure 5.4. The sand is classified as well-graded sand (SW), according to the Unified Soil Classification System (USCS). Table 5.1 lists the key physical properties of the sand. Saha et al. (2019, 2020) conducted an extensive laboratory investigation to determine the strength and deformation parameters of the sand for a wide range of stress conditions. It was found that the peak friction angle of the soil is high at the low-stress levels and decreases with the increase

of the stress level, reaching a constant value at very high stresses. The peak friction angles (ϕ_{max}) at the normal stresses ranging from 12.5 kPa to 400 kPa in direct shear tests ranged from 50° to 38°. The critical state friction angle (ϕ_{cv}) for the sand was 35°. The peak friction angles from triaxial tests were approximately 5° lower than those from the direct shear tests (Saha 2021).

5.3.3 *Pipe Installation*

The backfill soil and the pipe were placed in the test box in a few steps shown in Figure 5.5. First, the soil was placed and compacted up to a depth of five times the pipe diameter below the pipe centre to represent native soil (Figure 5.5a). The sand was then placed in a more controlled manner, maintaining a drop height of approximately 1 m, using sandbags with the help of an overhead crane. The sand was spread uniformly using a wooden spreader, providing 150 mm thick lifts. It was compacted using a custom-made tamper (steel plate attached to the end of a metal handle) with six passes in alternating patterns. Once the level of sand reached the inverted elevation of the pipe, the instrumented (or bare) pipe was placed straight, parallel to the longer direction of the test cell passing through the holes in the box (Figure 5.5b). Additional care was given to ensure the straightness of the pipe, since a small pipe misalignment in the vertical or horizontal plane could significantly increase the mobilized axial resistance (Phillips et al. 2004). A 1000 mm long spirit level was used to check the pipe's straightness. One end of the pipe was connected to the load cell through a solid steel coupling. Then, the backfilling and compaction continued in the same way until the required cover depth was achieved (Figure 5.5c). The densities of the compacted soil were measured using the sand cone method (ASTM D1556 (ASTM 2015)) at the top surface and the pipe springline level. The average value of soil unit weight ranged from 18.0 to 19.2 kN/m^3 for all the tests conducted for the current study. The densities corresponded to 100% of the standard

Proctor maximum dry density (i.e., 18.8 kN/m^3 after Saha et al. 2019). It is acknowledged that obtaining a prescribed density is challenging for backfill material during installation of pipes, which can affect the test results to some extent.

Vertical and horizontal earth pressures were measured at the springline level of the pipe during backfilling and pulling process using null pressure sensors (Talesnick et al. 2014). Using the null pressure sensors, the earth pressure is measured by applying a controlled internal air pressure in the sensors to keep the diaphragm of the sensors undeflected in the soil mass. Thus, the applied internal air pressure is equivalent to the pressure in the soil mass, which is measured. The locations of the pressure sensors are shown in Figure 5.6. The sand was air-dried with less than 1% moisture content in all the tests. Therefore, no suction stress was expected (Saha 2021). After each test, the sand was transferred to bulk bags for storage and later use, while the test pipe was removed from the tank and not reused in the next tests to avoid the effects of any possible residual stresses.

5.3.4 *Test Program*

The test program was designed to investigate the load transfer mechanism of buried MDPE pipe in dense sand during axial pullout. Pipe strains were measured at three locations using 5-mm long electrical strain gauges to monitor the mobilization of the axial force along the length. The strain gauges were placed at the pipe crown. However, the strain gauges along with electrical wires and protecting wraps, as shown in Figure 5.7, were reported to increase the frictional resistance of the soil by about 10% for pipes in medium-dense/loose sand (Reza and Dhar 2021ab). To understand the frictional resistance increase for the pipes in dense sand, tests were also conducted with pipes without any strain gauges (i.e., bare pipe). As mentioned earlier, 42.2-mm and 60.3-mm diameter pipes, commonly used in Canadian gas distribution systems, were tested. Tests were conducted at

three different pulling rates (i.e., 0.5, 1, and 2 mm/min) to investigate the rate–dependent effect. The pulling rate effect was evident for the pipes in medium-dense/loose sand (Reza and Dhar 2021ab). The top of the soil surface was visually observed before, during, and after the tests. However, no changes on the soil surface were noticed, indicating no propagation of ground deformation to the top surface.

Table 5.2 summarises the test program undertaken. A total of 11 tests was conducted, six with strain gauges and five without strain gauges. The first series of tests (Tests 1–6) was conducted on pipes instrumented with strain gauges, and the second series of tests (Tests 7–11) on bare pipes. Tests 1–3 and 7–9 used 42.2-mm diameter pipe segments, with and without strain gauges, respectively. Tests 4–6 and 10–11 were with 60.3-mm diameter pipes, with and without strain gauges, respectively. The burial depths were selected based on the typical depths used in the field for gas distribution pipes. The gas distribution pipes are typically buried at depths of 0.3 m to 1.5 m in western Canada (Groves and Wijewickreme 2013). For the minimum depth of 0.3 m, the burial depth ratio (H/D) (ratio of soil cover measured from pipe springline to pipe diameter) for the smaller diameter pipe is ~8. Therefore, the burial depth ratio (H/D) of 8 was used in all the tests. However, the failure surface (slip surface) during axial pullout mainly develops along the pipe–soil interface (Weerasekara and Wijewickreme 2008; Meidani et al. 2017). Meidani et al. (2017) observed through discrete element analysis that most of the soil movements (representing slip surface) occurred within the close vicinity of the pipe surface. Although the soil failure mechanism at the soil–pipe interface could not be monitored during the tests, the slip surface did not propagate to the soil surface during the tests (confirmed through observing the soil surface). Thus, it assumed that the choice of the H/D ratio would not significantly affect the soil failure

mechanism during the axial pullout of pipes. The assumption is consistent with the recommendations in the current design guidelines, where the axial pullout forces were reported to depend on the burial depth and not on the H/D ratio (ALA 2005). More detailed studies on the effect of H/D on the axial pullout resistance are not available in published literature.

The total length of each pipe segment was 4.6 m, with 4 m inside the cell (called herein 'buried pipe length') and 0.3 m extended beyond the test box on each side. During the tests, the leading end of the pipes was pulled at a constant pulling rate of 0.5 mm/min (in Tests 1, 4, 7, and 10), 1 mm/min (in Tests 2, 5, 8, and 11), and 2 mm/min (in Tests 3, 6, and 9). Note that according to Cruden and Varnes (1996), these pulling rates are in velocity Class 5 (>0.3 and <30 mm/min), which corresponds to moderate landslide velocity. All the tests were performed at room temperature (~23°C).

5.4 Test Results

5.4.1 *Soil Pressures*

The earth pressures were measured to monitor the load transfer mechanism within the soil and estimate the soil parameters. Figure 5.8 plots the earth pressure measured at the springline level during backfilling. The backfilling process included dumping soil, spreading it to level, and compacting. Therefore, the measured pressure varied with time until stabilization at the end of the backfilling. Figure 5.8a shows that at the end of backfilling, the measured earth pressures matched well with the geostatic stress (~9 kPa) calculated using the measured unit weight (i.e., γ = 19 kN/m^3) and the final soil cover depth (i.e., H = 0.48 m). This implies that even though no treatment was applied to reduce the sidewall friction, the vertical soil stress was not reduced by the wall

friction. The presence of the pipe also did not influence the soil stress at a distance of 600 mm from the pipe (location of the sensors). Figure 5.8b shows the measured horizontal stress at the springline level during backfilling. After the completion of backfilling, the horizontal stresses were around 50% of the vertical stresses, indicating the lateral earth pressure coefficient at rest, K_0, of ~0.5. The earth pressure did not change significantly during axial pullout (Figure 5.9), confirming that interface soil movement did not influence the stress field at 600 mm from the pipe axis.

5.4.2 *Load–Displacement Responses*

The force–displacement responses observed during the axial pullout tests of the pipes are shown in Figure 5.10. The pulling force applied to the pipes essentially equals the shearing resistance offered by the interface soil, i.e., the pullout resistance, as shown in the figure. The axial pullout load–displacement behaviour of a 60-mm diameter MDPE pipe, from Weerasekara and Wijewickreme (2008), (with γ = 15.8 kN/m^3, H = 0.6 m, L = 3.8 m, and pulling rate 0.6 mm/min) is included in Figure 5.10b (bare pipe test results). The overall load–displacement response from that study is similar to those observed in the current study.

With the application of a pulling force, the flexible MDPE pipes start elongating from the pulling end (leading end). If the pipe wall displacement due to elongation relative to the soil is large enough at any point, the interface frictional resistance at that point is fully mobilized. With the increase of axial force, the pipe length with mobilization of friction resistance (i.e., mobilized friction length) increases and extends toward the trailing end. Thus, the interface frictional resistance is nonuniform over the pipe length and continues increasing with the increase of the pulling force until the frictional resistance over the full length of the pipe is mobilized. This

mechanism was observed earlier in Weerasekara and Wijewickreme (2008) and Reza and Dhar (2021ab). As seen in Figure 5.10, the pullout resistances initially increase nonlinearly with the pulling displacements (hence the pulling load) and reach the peak values at certain leading end displacements. The peak values are dependent on the material properties, cross-sectional dimensions, and length of the pipe samples, which cannot provide the frictional force per unit length as in rigid pipes, where the frictional force is almost uniform over the pipe length. For the flexible pipe tests, the mobilized friction length and the corresponding pulling force not affected by the length of the test pipes are of fundamental importance for the interpretation of the results. Once the interface shear strength is mobilized over the entire pipe length, the trailing end of the pipe starts moving, which was monitored using LVDT during the tests. During the tests, the trailing end of the pipe started to move when the leading end displacements were 45 to 55 mm and 16 to 40 mm for 42- and 60-mm diameter pipes, respectively. Pulling forces and the leading end displacements corresponding to the initiation of the trailing end movement are shown using the circles in Figure 5.10. All data beyond that point are influenced by the length of the test box and, therefore, not considered further.

Figures 5.10a and 5.10b show the load–displacement responses for the pipes with and without strain gauges, revealing the effects of strain gauges on the increase of interface shearing resistance. The strain gauges on the pipe wall increase the roughness of the surface, increasing the pullout resistance. For the tests conducted in the current study (pipes in dense sand), the pullout resistances were increased significantly (up to 35%) for tests using the strain gauges. For the same pipes, the pullout resistances were found to increase by about 10% for pipes in loose to medium dense sands (Reza and Dhar 2021a). Thus, the effects of strain gauges for pipes in dense sand are significantly

higher than those for pipes in loose to medium dense sand. Therefore, while strain measurements are required to understand the progression of the frictional resistance along the pipe length, the effects should be considered during the analysis of results. Figure 5.10 also reveals that the load–displacement responses of the pipes are pulling-rate dependent. The pullout resistances are higher for higher pulling rates. Similar observations were reported for the same pipes buried in loose to medium dense sand (Reza and Dhar 2021ab).

Figure 5.11 plots the normalized pullout resistance against the pulling rates under various conditions. The pullout force is normalized by soil unit weight (γ), burial depth (H), pipe perimeter (πD), and mobilized friction length (L, which is the same as the pipe length for the force at the initiation of the trailing end movements obtained from the tests) into a dimensionless term to assist in comparing the results for pipes of different diameters and burial depths. It shows that the normalized pullout resistance increases with the increase of pulling rate. The rate of increase is high, up to a pulling rate of 1 mm/min; after that, the effect is less significant. The normalized pullout resistance from Weerasekara and Wijewickreme (2008), pulled at 0.6 mm/min, is in between the normalized pullout resistances from the current study for 0.5 mm/min and 1 mm/min pulling rates, and thus consistent with the results from this study. As the stress–strain responses of sand are independent of the rate of loading (Holtz et al. 2011; Saha et al. 2019), the time–dependent property of the pipe material is considered responsible for the rate–dependent responses. Reza and Dhar (2021a) argued that the pulling-rate–dependent responses of the pipe are due to the time–dependent behaviour of the pipe–soil interface. During sliding, the sand particles slightly penetrate the pipe surface and interact with the pipe material with time–dependent behaviour, leading to rate–dependent responses. The penetration of sand particles was confirmed from the scratches on

the pipe surface after the test (Figure 5.12). They proposed a rate–dependent friction factor to account for the rate–dependent pullout resistance for pipes in loose to medium-dense sand. The applicability of this approach for pipes in dense sand will be examined in the current study.

Figure 5.11 also shows that the non-dimensional pullout forces are significantly higher for pipes in dense sand than those in loose sand. For the pipe in dense sand, the compaction of the soil during backfilling can cause locked-in normal stress around the sides of the pipe (after Sheil et al. 2021), in addition to the overburden stress. Shearing-induced dilation can also increase the normal stress, resulting in a higher pullout resistance of the pipes. Note that normalized pullout resistance is higher for the 42-mm diameter pipes than for 60-mm diameter pipes in dense sand. However, no noticeable effect of the pipe size was observed in normalized load for pipes in medium/loose sand (i.e., non-dilative sand), Reza and Dhar (2021ab). The higher resistance for the 42-mm pipes in dense sand is attributed to the higher soil dilation around the pipe at a relatively shallower depth (keeping H/D constant) with a lower stress level. According to the elastic cavity expansion theory, the increase of normal stresses on the pipe due to soil dilation is expected to be less for large diameter pipes (Johnston et al. 1987).

5.4.3 *Pipe Wall Strains*

Strains were measured at the pipe crown at distances of one-fourth ($L/4$), half ($L/2$), and three-fourths ($3L/4$) from the leading end in Tests 1 to 6. The measured strains from Tests 1 and 2 are shown in Figure 5.13. As shown in the figure, the strain at the distance of $L/4$ starts increasing (responded) with a very small leading end displacement. The strains at $L/2$ and $3L/4$ do not start immediately but begin at certain levels of leading end displacements. For example, in Test 1

(Figure 5.13a), the strains at $L/4$, $L/2$, and $3L/4$ start increasing at the leading end displacements of u_1 = 1.0 mm, u_2 = 6.2 mm, u_3 = 19.7 mm, respectively. These imply that the axial force or the interface shearing resistance is mobilized up to the distances of 1 m, 2 m, and 3 m (i.e., $L/4$, $L/2$, and $3L/4$) at these pulling end displacements, respectively. The friction is mobilized up to a point once the strain gauge there starts responding. The frictional resistance was mobilized over the entire pipe length when the trailing end started to move. The leading end displacement corresponding to the mobilization of frictional resistance over the entire pipe length (i.e., 4 m) is u_4 = 50.5 mm in Test 1. The leading end displacements for different mobilized friction lengths with corresponding pulling forces from Tests 1 to 6 are provided in Table 5.3.

The strain distributions along the pipe length for different leading end displacements (u_1, u_2, u_3 and u_4) during Tests 1 and 2 are shown in Figure 5.14. A nonlinear distribution over the mobilized friction length was found to represent better the measured strain (further discussed later). The nonlinearity is attributed to the nonlinear stress–strain relations of pipe material, particularly at high strains experienced by the pipes in dense sand. The strain distribution was linear for the pipe in loose to medium dense sand where the pipe strains were relatively less (Reza and Dhar 2021ab). The nonlinear strain distribution for the pipes in dense sand is idealized as a parabola to develop a simplified equation for pipe wall strain calculation, discussed later in the paper. The axial strain (ε) at any point within the mobilized friction length can be calculated using an equation of a parabola (Eq. 5.1).

$$\varepsilon = \frac{P}{AE\,l^2}(l - x)^2 \tag{5.1}$$

where x is the distance from the leading end of the pipe, P is the pullout force corresponding to the mobilization of friction length l, A is the pipe's cross-sectional area, and E is the modulus of

elasticity of pipe material. Axial stains calculated using Eq. (5.1) with observed pullout forces and mobilized friction lengths are plotted in Figure 5.14. Note that strains at three discrete locations were only measured to minimise disturbance on the pipe surface during the tests, while strain measurements at more points could provide a better representation of the strain distribution. Nonetheless, the strains calculated based on the assumption of parabolic distribution reasonably represent the measured values in Figure 5.14. Thus, Eq. (5.1) can be used to calculate pipe wall strains if the pullout force and the mobilized friction length corresponding to any relative ground movement can be determined. Simplified approaches are proposed below to estimate the pullout force and the mobilized friction length due to relative ground movement.

Note that the time–dependent material properties influence the behavior of MDPE pipe material. However, the current research did not deliberately investigate the effect of time–dependent responses such as relaxation and creep. For the analysis of the test results, a strain-rate–dependent constant modulus was used to account for the time–dependent effect for the duration of the tests. Researchers successfully applied a time–dependent constant modulus to analyze test results with time–dependent polyethylene pipes (Dhar et al. 2004). The model of Das and Dhar (2021) was used to obtain the strain and strain-rate dependent modulus of elasticity of the MDPE pipe material. Strain rates and the strain levels measured during the tests were used to obtain the modulus of elasticity for strain calculations using Eq. (5.1). The average strain rates during the tests ranged from 10^{-6}/s to 10^{-5}/s with pulling rates of 0.5 to 2 mm/min. The strain rates and the magnitude of strains also varied between the points over the mobilized friction length, depending on the magnitudes of leading end displacements. The strain and strain-dependent modulus of elasticity was calculated at various points over the mobilized friction length for different leading

end displacements, and the average modulus was obtained. Figure 5.15 shows the average modulus of elasticity with leading end displacement for the tests conducted in this study.

5.5 Pullout Force Calculation

5.5.1 *Proposed Model*

Current design guidelines (e.g., ALA 2005 and PRCI 2017) recommend the following design equation (Eq. 5.2) to estimate the maximum axial resistance of pipes buried in cohesionless soils.

$$P_u = \gamma H\left(\frac{1+K_0}{2}\right)\tan(\delta)\,(\pi DL) \tag{5.2}$$

where P_u = maximum axial soil resistance on the pipe or pullout force; γ = unit weight of soil; H = burial depth measured from the ground surface to pipe springline; L = pipe length; D = pipe outer diameter; K_0 = at-rest lateral earth pressure coefficient for the soil; and δ = interface friction angle between the pipe and surrounding soil. The equation is based on the assumption of an interface shearing resistance that is mobilized over the entire pipe length, which is constant over the pipe length. As discussed earlier, the interface shearing resistance is gradually mobilized for PE pipes. Therefore, it is proposed to use the mobilized friction length, l (instead of total pipe length), to calculate the pulling force at any instant of relative ground movement for the PE pipes. For the pipes in dense sand, the shearing-induced dilation and pipe diameter change can influence the normal stress on the pipe (not considered in Eq. 5.2). As a result, the mobilized shearing stress may be nonuniform over the mobilized pipe length. For simplicity, Eq. (5.3) is proposed to calculate the mean value of the frictional force per unit length, p (lower case letter use to represent force per unit length), for the PE pipes in dense sand.

$$p = \xi\,\gamma H\left(\frac{1+K_0}{2}\right)\tan(\delta)\,(\pi D) \tag{5.3}$$

A normal stress adjustment factor, ξ, is proposed to account for the normal stress change. The total

axial force, P_l, can be obtained multiplying the force per unit length by the mobilized length. The normal stress adjustment factor ξ from the test results can be obtained using the pullout force required to mobilize the interface shearing resistance over the entire pipe length, L (i.e., initiation of trailing end movement) and Eq. (5.4).

$$\xi = \frac{P_{\mathrm{L}}}{\pi DL(\frac{1+K_0}{2})\gamma H\tan\delta} \tag{5.4}$$

where, P_{L} is the pullout force for the initiation of trailing end movement.

5.5.2 *Shear-Induced Soil Dilation*

Shear-induced dilation can increase the normal stress on the pipe wall during the axial pullout. Extensive laboratory studies have shown that soil dilation substantially affects the pullout resistance of soil inclusions (e.g., soil reinforcements, piles, pipes) in dilative soils (Schlosser and Elias 1978; Ingold 1983; Luo et al. 2000; Wijewickreme et al. 2009). Schlosser (1982) suggested that the dilation behaviour of the soil essentially governs the interface frictional resistance between inclusion and soil. During pullout of the inclusion, shear stresses on the interface cause soil particles to slide and roll around the inclusion (i.e., soil nails), resulting in dilation of the soils in the vicinity of the inclusion. However, the dilation (radial/outward soil expansion) is constrained by the surrounding soil mass (soil outside the shear zone), which leads to an increase of normal stress on the surface of the inclusion. The increase in normal stress due to the soil dilation is directly proportional to the increase in pullout resistance. However, if the normal confining pressure is very high around the inclusion, soil particles may be crushed in the shearing process before rolling and overriding their neighbours. In this case, soil volume will contract rather than dilate, and the potential dilation effect on the interface shear resistance during pullout may completely vanish (Luo et al. 2000).

Johnston et al. (1987) suggested the elastic cavity expansion theory to estimate the increase of normal stress on cylindrical objects due to soil dilation. Luo et al. (2000) developed a method to account for soil dilation using a sawtooth-type model (a slightly different method from traditional elastic cavity expansion theory). They proposed a theoretical factor, ω (also known as efficiency factor), to calculate the normal stress increase for pullout resistance due to interface soil dilation, as expressed in the following equation (Eq. 5.5).

$$\omega = \frac{\lambda}{\sigma_v'} \tan\psi_{max} + 1 \tag{5.5}$$

where λ (dilation modulus at peak shear resistance) = $\frac{2Gu_c}{D}$; G = shear modulus of the soil; u_c = critical shear displacement at which the maximum shear stress is mobilized; D = diameter of the inclusion; ψ_{max} = the dilation angle at peak shear resistance.

The peak dilation angle, ψ_{max}, is a measure of the dilatancy of sand during shear failure. It is well established that the sands dilate when shear stress leads to failure, depending on the relative density and stress levels. Researchers employed different approaches to relate the dilatancy to soil state parameters representing the relative density and stress level (Rowe 1963; Been and Jefferies 1985; Bolton 1986 and many others). Bolton (1986) defined a parameter called relative dilatancy index, I_R, and related it to the peak dilation angle (ψ_{max}) for triaxial and plane-strain conditions. For triaxial stress conditions, a mechanism expected for buried pipe, the relations are as below.

$$I_R = I_D\,(10 - \ln p') - 1 \tag{5.6}$$

$$\psi_{max} = 3I_R \tag{5.7}$$

Here, p' = mean confining pressure expressed in kN/m^2; and I_D = relative density of soil. Luo et al. (2000) expressed the mean confining pressure in terms of effective overburden pressure over

an inclusion, σ_v', assuming the lateral earth pressure at rest as $K_0 = \nu/(1-\nu)$, where ν is the Poisson's ratio of soil. Then, Eqs. (5.6) and (5.7) were combined to develop an expression of the peak dilation angle, ψ_{max}, as in Eq. (5.8).

$$\psi_{max} = 3I_D\,[11.1 - \ln(\tfrac{1+\nu}{1-\nu}\,\sigma_v')] - 3 \tag{5.8}$$

Combining Eqs. (5.5) and (5.8) gives:

$$\omega = \frac{\lambda}{\sigma_v'} \tan\{3I_D\,[11.1 - \ln(\tfrac{1+\nu}{1-\nu}\,\sigma_v')] - 3\} + 1 \tag{5.9}$$

Luo et al. (2000) stated the validity condition of Eq. (5.9) as below.

$$\frac{3\,(1-\nu)}{(1+\nu)} \exp\left(10 - \frac{5}{I_D}\right) < \sigma_v' < \frac{3\,(1-\nu)}{(1+\nu)} \exp\left(10 - \frac{1}{I_D}\right) \tag{5.10}$$

The factor, ω, is equivalent to the normal stress adjustment factor ξ in Eq. (5.3). The applicability of Eq. (5.9) for calculating the normal stress factor is, therefore, examined through comparison with test results. The input parameters of the equations for the test conditions were determined as discussed below.

5.5.2.1 *Shear modulus of soil*

The shear modulus (G) of soil decreases with the increase of shear strain (γ), which can be represented by the hyperbolic relationship proposed in Hardin and Drnevich (1972), Eq. (5.11):

$$\frac{G}{G_0} = \frac{1}{(a\gamma + b)} \tag{5.11}$$

where G is secant shear modulus, G_0 is initial shear modulus, and 'a' and 'b' are material constants controlling the shape of the normalized degradation curve. Seed et al. (1986) determined the values of a and b as 15.0 and 1.0, respectively, from the hyperbolic fit with the experimentally obtained shear modulus degradation curves. The initial shear modulus of soils at strain levels below 0.001%

is usually constant. It can be determined using different experimental techniques (such as bender element, resonant column, and torsional shear tests) and/or empirical relationships (Hardin and Drnevich 1972; Altun and Goktepe 2006). However, in typical geotechnical applications, there are uncertainties in the direct measurements of the initial shear modulus. Therefore, it is of interest to relate the shear modulus of the soil to the elastic modulus (i.e., Young's modulus, E_0) and Poisson's ratio (v) as follows (Eq. 5.12).

$$G_0 = \frac{E_0}{2(1+v)} \tag{5.12}$$

The initial elastic modulus, E_0 is stress-dependent and can be obtained using Janbu's (1963) model (Eq. 5.13).

$$E_0 = Kp_a \left(\frac{p'}{p_a}\right)^n \tag{5.13}$$

where K is a material constant; p_a is the atmospheric pressure (i.e., 101.3 kPa); p' is mean effective confining pressure, and n is an exponent determining the rate of variation of E_0 with p'. The value of E_0 is estimated here based on the mean effective stress (p') at the springline level of the pipe, with $K = 150$ and $n = 0.5$ (Roy et al. 2016) and as $E_0 = 5$ MPa for the sand used in the tests. Typical values of Poisson's ratio (v) for dense sand could vary from 0.25 to 0.35 (Budhu 2011). The Poisson's ratio back-calculated from the relation: $K_0 = v/(1-v)$ with $K_0 = 0.5$, obtained from the soil stress measurement (as mentioned previously), is 0.33. Thus, a Poisson's ratio of 0.33 was considered for the sand in the test conditions. An initial shear modulus G_0 of 1.88 MPa was calculated using the parameters.

The shear modulus of sand decreases rapidly with increasing strain amplitude (Eq. 5.11) and could be less than 60% of G_0 at a shear strain of 0.1%. Hardin and Drnevich (1972) also reported

lower values for the shear modulus of sand, as low as $G_0/3$, at a shear strain amplitude of 0.001 (0.1%). Assuming the shear strain levels of 0.05%–0.2% during the tests to calculate the mean value of ω in Eq. (5.5), G of 0.5 MPa – 1.0 MPa were estimated for the test conditions. Similar values of G (i.e., 0.6 MPa – 0.9 MPa) were reported in Wijewickreme and Weerasekara (2015) for the test conditions using Fraser River sand backfill.

5.5.2.2 *Critical shear displacement*

Several studies are available on investigating the critical shear displacements. Billam (1972) reported that confining pressure does not significantly influence the critical shear displacement. Dove (1996) found that the sliding of dense Ottawa sand on the smooth high-density polyethylene (HDPE) geomembrane occurred at the relative displacement of approximately 0.3 mm. O'Rourke et al. (1990) performed direct shear tests on an MDPE–sand interface and found that the maximum frictional resistance mobilizes in dense sand at a shear displacement (critical shear displacement, u_c) of 0.5 mm. The critical shear displacement, u_c = 0.5 mm, is chosen for the test conditions presented in this study (after O'Rourke et al. 1990). Note that for the soil–pipe interface, shear displacement is the relative displacement of the pipe with respect to the soil, which is essentially the displacement of the pipe at any given point (since the soil is static).

5.5.2.3 *Interface friction angle*

The value of the interface friction angle, δ, depends on a number of different parameters, including the roughness of the pipe surface, the hardness of the pipe wall, and the degree of relative movement between pipe and soil. Generally, the value of δ lies between 50% to 100% of the peak friction angle (ϕ_{max}) of the surrounding soil (Yimsiri et al. 2004). According to ALA (2005), δ is

related to the internal friction angle of the soil (ϕ) by a factor, f, (termed herein as interface friction reduction factor) as $\delta = f\phi$, where $f = 0.6$ is recommended for pipes with polyethylene coating. However, for the MDPE pipe surface considered in this study, the interface friction angle would be pulling rate–dependent due to the time–dependent behaviour of the pipe material (as discussed earlier). Reza and Dhar (2021a) demonstrated the values of f as 0.75, 0.86, and 0.9, corresponding to the pulling rates of 0.5, 1, and 2 mm/min, respectively, in pullout tests. These values of loading rate–dependent f were used in the current study for the tests conducted with the pulling rates of 0.5, 1, and 2 mm/min, respectively.

5.5.3 *Comparison of Results*

The normal stress adjustment factors (ξ) obtained from the experiments (Eq. 5.4) are compared with the theoretical factors, ω (Eq. 5.9) in Figure 5.16. The input parameters used to calculate the factors are listed in Table 5.4 for the laboratory test conditions. As seen in Figure 5.16a, for the 42-mm diameter pipes, the magnitudes of ω are 1.80 and 1.54 for Tests 1–3 and 7–9, respectively. The calculated values of ξ are between 1.78 to 1.88 (in Tests 1–3) and 1.47 to 1.62 (in Tests 7–9), showing good agreement (<5% differences) with those obtained from the tests. Similarly, in Figure 5.16b, for 60-mm diameter pipes, ξ = 1.32 to 1.44 (in Tests 4–6) and 1.10 to 1.13 (in Tests 10–11), corresponding ω of 1.38 and 1.18, respectively, show reasonable agreement. Thus, Eq. (5.9), after Luo et al. (2000), can be used to account for the effects of soil dilation for calculating the axial pullout resistance for pipes in dense sand. Further studies can be conducted to recommend typical values of the factor, ξ, for commonly expected situations in the field for design convenience.

5.6 Pipe Strain Calculation

5.6.1 *Mobilized Friction Length*

As mentioned earlier, the interface shearing resistance is gradually mobilized from the leading end toward the trailing end during the axial pullout of flexible MDPE pipes. The leading end displacement of the pipe (i.e., the relative ground movement) during the test is associated with elongation due to axial strains over the mobilized frictional length (l). The leading end displacement can be obtained by integrating the strains over the mobilized frictional length. The method is similar to calculating settlements of axially loaded piles under axial loads, except that axial compression is applied instead of the tension (pulling force) in the current case. Crispin et al. (2018) developed closed-form solutions for load–displacement relations for the axially loaded piles, modelling the pile–soil interaction as elastic-perfectly plastic springs. They divided the pile length into a plastic region over the distance of L_p (called the "plastic length") from the pile head (the ground surface) and an elastic region beyond that distance. The springs have a linear elastic response over the elastic region and a perfectly plastic response with an ultimate shaft resistance over the plastic region. A power-law variation in the ultimate shaft resistance was considered to develop equations to calculate the pile load and displacement. While the variation of the shaft resistance with depth is commonly observed for piles, the interface frictional resistance for the horizontally laid pipe is constant along the pipe length. Thus, neglecting the terms for the variation shaft resistance with depth, the following equation for the displacement, u (i.e., the leading end displacement), can be obtained.

$$u = u(L_p) + \frac{P(L_p)}{EA} L_p + \frac{p_u}{2EA} L_p^2 \tag{5.14}$$

where $P(L_p)$, p_u, $u(L_p)$ are the axial force/load at a depth of L_p, ultimate shaft resistance per unit length, and axial displacement at depth L_p, respectively. In the above equations, L_p corresponds to

the mobilized friction length for the pipe. As discussed earlier, the frictional force is mobilized at a very small displacement; thus, $P(L_p)$ and $u(L_p)$ are assumed to be zero. Therefore, the equation for leading end displacement, u, is reduced to Eq. (5.15).

$$u = \frac{p_u}{2EA} L_p^2 \tag{5.15}$$

The equation corresponds to the displacement of the pipe segment over the pipe length of L_p subjected to a linear distribution of strain as $\varepsilon(x) = p_u x/(AE)$, where $x \in [0, L_p]$ is the distance from the restrained end.

However, as discussed earlier, the strain distribution over the mobilized friction length is nonlinear (assumed parabolic) for pipes in dense sand. Considering the parabolic distribution of the strain, the leading end displacement (u) can be related to the mobilized frictional length (l) and the corresponding pullout force as in Eq. (5.16).

$$u = \frac{Pl}{3AE} \tag{5.16}$$

where A is the pipe's cross-sectional area; E is the modulus of elasticity of the pipe material. The pulling force (P) can be calculated using Eq. (5.3) for pipes in dense sand, where $\xi = \omega$ (i.e., Eq. 5.9). Putting P from Eq. (5.3) into Eq. (5.16) and rearranging, an expression for the mobilized frictional length (l) as a function of relative ground movement (u) is obtained (Eq. 5.17).

$$l = \sqrt{\frac{6AE}{\omega(1+K_0)\gamma H \pi D \tan\delta}\, u} \tag{5.17}$$

For validation, the mobilized frictional length calculated using Eq. (5.17) is compared with those observed during the tests (using strain measurements). The modulus of elasticity of the pipe material shown in Figure 5.15 was used in the calculation. Figure 5.17 compares the predicted

mobilized frictional length with those measured from Tests 1–6. As shown in the figure, the predicted mobilized lengths agree well with the experimental results for all the tests.

5.6.2 *Proposed Strain Calculation Method*

Based on the findings presented above, a method for assessing pipelines subjected to an axial ground movement of u is proposed. Figure 5.18 presents a flow chart for estimating the pipe wall strains for a known relative axial ground movement. First, the pipe and soil parameters are determined, including burial depth, outer pipe diameter, pipe wall thickness, pipe elastic modulus, and sand unit weight. The interface friction angle is estimated based on the best information about the pipe material and ground movement scenario, following the method discussed in Section 5.5.2.3. For the pipes in dense sand, the normal stress adjustment factor ($\xi = \omega$) due to interface soil dilation is calculated using Eq. (5.9). Next, the mobilized frictional length is calculated using Eq. (5.17) and the corresponding pulling force at the leading end using Eq. (5.3). Finally, the longitudinal strain on the pipe wall is calculated using Eq. (5.1). The strains calculated using these methods are compared with the measured strains in Figure 5.19 for Tests 1–2. The calculated strains match well with the measurements in the figure. Figure 5.19 compares the strains to the leading end displacement of 50 mm, as the trailing end started moving beyond this displacement in all tests (Figure 5.10). The test cell boundary (limited length) affects the measured strains beyond that displacement.

Note that the test data of strains can be affected by the presence of the gauge itself (Beatty and Chewning 1979; Brachman et al. 2000). Brachman et al. (2000) reported strain readings consistently smaller because of a reinforcing effect provided by the gauge (metal foil, polymer

backing, and adhesive), resulting in a local reduction in the measured strains on the pipe's wall. They employed a correction factor of 1.4 to the measured strains to obtain the corrected strain. Assuming similar effects in the measured strains, the measured strains were corrected, multiplying by 1.4. Therefore, some level of uncertainty might be expected in the measured strains. Nonetheless, the comparison in Figure 5.19 reveals that the proposed method effectively calculated the pipe wall strains unless the pipe length influences the strains. The discrepancies between the measurements and predictions observed in the figure can be attributed to the assumptions used in the derivation of the equations, the modulus of elasticity chosen for the pipe material, and the uncertainties in the measured strains. For the derivation of the equations, the nonlinear distribution of the strains was assumed as parabolic, which may not be truly parabolic. Besides, the modulus of elasticity of the pipe material is strain and strain-rate–dependent. While strains and strain rates vary along the pipe length, an equivalent constant value was used in the strain calculation. However, the calculated strains are generally greater than the measured strains, providing a conservative and safer estimation of the strains.

5.7 Conclusions

This research uses full-scale tests to investigate the behaviours of 42- and 60-mm diameter MDPE pipes buried in dense sand subjected to relative axial movement. During the tests, pipe wall strains were measured at different locations along the length of the pipe. Tests were conducted at three different loading rates. The key findings from the research are summarised below.

- Axial strains and elongation develop in the flexible MDPE pipes during the axial pullout. The strain and elongation first develop toward the pulling end (leading end), propagating gradually toward the trailing end as the frictional resistance of the soil mobilizes. Until

the trailing end started to move, the displacement of the pulling end resulted from the elongation over the length of frictional resistance mobilization (i.e., mobilized friction length).

- The load–displacement responses for the pipes are pulling rate–dependent. A rate–dependent friction factor can reasonably account for the rate–dependent pullout resistance for pipes in both loose sand and dense sand.
- The normal stress on the pipe in dense sand is increased due to shearing-induced dilation of interface soil, increasing the pullout resistance. As a result, the equation available in the current design guidelines underestimates the pullout resistance for pipes in dense sand. The dilation effect was higher for the 42-mm diameter pipes than the 60-mm diameter pipes. A normal stress adjustment factor based on a sawtooth-type model for cavity expansion theory (after Luo et al. 2000) can be used to account for the dilation-induced increase of normal stress on the pipes for calculating the pullout resistance.
- The strain gauges on the pipe wall affect the frictional resistance more significantly for pipes in dense sand than pipes in loose sand. While strain measurements are required to understand the behaviour of the pipes during tests, the effects should be carefully considered during the analysis of results.
- The strain distribution over the pipe length is nonlinear and can be assumed parabolic for the pipes in dense sand.
- Simplified equations are proposed to calculate pullout resistance, mobilized frictional length, and pipe wall strains for the MDPE pipes in dense sand. Strains measured during the tests were reasonably predicted using the proposed method. The developed simplified method avoids the complexity of rigorous numerical and analytical solutions.

- The modulus of elasticity of the pipe materials depends on the strain rate and strain that varies between the points within the mobilized friction length. An average value was successfully used to calculate the pipe wall strains using the proposed simplified method.

In this study, the pipe responses to an idealized ground movement scenario expected in the field were investigated. The pipe responses to any other loading conditions, such as temperature loading, were not examined. Further studies can be conducted for other loading scenarios and to recommend parameters for the strain calculation equations for the conditions expected in the field.

5.8 Acknowledgments

The authors acknowledge the financial and/or in-kind support for this research provided by the Collaborative Research and Development Grant program of the Natural Science and Engineering Research Council of Canada, Innovate NL program of the Government of Newfoundland and Labrador, FortisBC Energy Inc. and WSP Canada Inc.

5.9 References

ALA (American Lifelines Alliance) (2005). *Guidelines for the design of buried steel pipe*. Washington, DC and Reston, VA, USA: Federal Emergency Management Agency (FEMA) and American Society of Civil Engineers (ASCE).

Altun, A. & Goktepe, S. (2006). Dependence of dynamic shear modulus of uniform sands on stress level and density. *Civil Engineering and Environmental Systems*, **23**, No. 2, 101–116.

Anderson, C. (2004). *Soil–pipeline interaction of polyethylene natural gas pipelines in sand*. M.Sc. thesis, Department of Civil Engineering, The University of British Columbia, Vancouver, BC, Canada.

ASTM (American Society for Testing and Materials) D1556. (2015). *Standard test method for density and unit weight of soil in place by the sand-cone method*. ASTM International, West Conshohocken, PA, USA.

Beatty, M. F. & Chewning, S. W. (1979). Numerical analysis of the reinforcement effect of a strain gauge applied to a soft material. *International Journal of Engineering Science*, **17**, No. 7, 907–915.

Been, K. & Jefferies, M. G. (1985). A state parameter for sands. *Géotechnique*, **35**, No. 2, 99–112.

Billam, J. (1972). Some aspects of the behaviour of granular materials at high pressures. *Proceedings of the Roscoe Memorial Symposium,* Parry R.H.G., Foulis G. T., editors. Whitefriars Press Ltd., Henley-on-Thames, Oxfordshire, England, pp. 69–80.

Bilgin, Ö. & Stewart, H. E. (2009). Design guidelines for polyethylene pipe interface shear resistance. *Journal of Geotechnical and Geoenvironmental Engineering*, *ASCE* **135**, No. 6, 809–818.

Bolton, M. D. (1986). The strength and dilatancy of sands. *Géotechnique*, **36**, No. 1, 65–78.

Brachman, R. W. I., Moore, I. D. & Rowe, R. K. (2000). Local strain on a leachate collection pipe. *Canadian Journal of Civil Engineering*, **27**, No. 6, 1273–1285.

Budhu, M. (2011). *Soil mechanics and foundations*. 3rd edition. John Wiley & Sons, Inc., New York, United States of America.

Chakraborty, S., Dhar, A. S., Talesnick, M. & Muntakim, A. H. (2020). Behaviour of a branched buried MDPE gas distribution pipe under axial ground movement. *Proceedings of the 73rd Canadian Geotechnical Conf., GeoVirtual 2020*, Virtual (Online), Canada: Canadian Geotechnical Society.

City of Quesnel. (2020). *West Quesnel Land Stability Program*, Quesnel, BC. Project No.

KX0439755. Prepared for City of Quesnel, 410 Kinchant Street Quesnel, BC V2J 7J5.

Cruden, D. M. & Varnes, D. J. (1996). *Landslide types and processes. Landslides—Investigations and mitigation*, pp. 36–75, edited by Turner, A. K. and Schuster, R. L. Special Report, 247. Washington, DC: Transportation Research Board.

Crispin, J. J., Leahy, C. P. & Mylonakis, G. (2018). Winkler model for axially loaded piles in inhomogeneous soil. *Géotechnique Letters*, **8**, No. 4, 290–297.

Daiyan, N., Kenny, S., Phillips, R. & Popescu, R. (2011). Investigating pipeline-soil interaction under axial–lateral relative movements in sand. *Canadian Geotechnical Journal*, **48**, No. 11, 1683–1695.

Das, S. & Dhar, A. S. (2021). Nonlinear Time-dependent Mechanical behaviour of a Medium Density Polyethylene Pipe Material. *Journal of Materials in Civil Engineering*, **33**, No. 5, 04021068.

Dhar, A. S., Moore, I. D. & McGrath, T. J. (2004). Two-Dimensional Analysis of Thermoplastic Culvert Deformations and Strains. *Journal of Geotechnical and Geoenvironmental Engineering*, *ASCE* **130**, No. 2, 199–208.

Dove, J. E. (1996). *Particle-geomembrane interface strength behaviour as influenced by surface topography*. PhD Thesis, School of Civil and Environmental Engineering, Georgia Institute of Technology, Atlanta, USA.

EGIG (European Gas Pipeline Incident Data Group) (2020). *Gas Pipeline Incidents: 11th Report of the European Gas Pipeline Incident Data Group (period 1970 – 2019)*, EGIG VA 20.0432, Groningen, Netherlands.

Groves, A. & Wijewickreme, D. (2013). Field monitoring of buried polyethylene natural gas pipelines subjected to ground movement. *Proceedings of the 66th Canadian Geotechnical*

Conference, GeoMontreal 2013, Montreal, QC, Canada, 29 September–3 October 2013.

Hardin, B. O. & Drnevich, V. P. (1972). Shear modulus and damping in soils. *Journal of the Soil Mechanics and Foundations Division*, **98**, No. 7, 667–692.

Holtz, R. D., Kovacs, W. D. & Sheahan, T. C. (2011). *An introduction to geotechnical engineering*. 2nd edition. Pearson Education, Inc., Upper Saddle River, New Jersey, USA.

Ingold, T. S. (1983). Laboratory pullout testing of grid reinforcements in sand. *Geotechnical Testing Journal*, **6**, No. 3, 101–111.

Janbu, N. (1963). Soil compressibility as determined by oedometer and triaxial tests. *Proceedings of the European Conference on Soil Mechanics and Foundation Engineering*, Wiesbaden, Germany, Vol. 1, pp. 19–25. German Society for Earthworks and Foundations, Essen, Germany.

Johnston, I. W., Lam, T. S. K. & Williams, A. F. (1987). Constant normal stiffness direct shear testing for socketed pile design in weak rock. *Géotechnique*, **37**, No. 1, 83–89.

Luo, S. Q., Tan, S. A. & Yong, K. Y. (2000). Pullout resistance mechanism of a soil nail reinforcement in dilative soils. *Soils and Foundations*, **40**, No. 1, 47–56.

Meidani, M., Meguid, M. A. & Chouinard, L. E. (2017). Evaluation of soil–pipe interaction under relative axial ground movement. *Journal of Pipeline Systems Engineering and Practice*, **8**, No. 4, 04017009.

Muntakim, A. H. & Dhar, A. S. (2021). Assessment of Axial Pullout Force for Buried Medium-Density Polyethylene Pipelines. *Journal of Pipeline Systems Engineering and Practice*, **12**, No. 2, 04020074.

Murugathasan, P., Dhar, A. S. & Hawlader, B. C. (2021). An experimental and numerical investigation of pullout behaviour of ductile iron water pipes buried in sand. *Canadian Journal*

of Civil Engineering, **48**, No. 2, 134–143.

O'Rourke, T. D., Druschel, S. J. & Netravali, A. N. (1990). Shear strength characteristics of sand-polymer interfaces. *Journal of Geotechnical Engineering*, **116**, No. 3, 451–469.

O'Rourke, M. J. & Nordberg, C. (1992). *Longitudinal permanent ground deformation effects on buried continuous pipelines*. Taipei, Taiwan: National Center for Earthquake Engineering Research, Project Number 90-3003.

Paulin, M. J., Phillips, R., Clark, J. I., Hurley, S. & Trigg, A. (1997). Establishment of a full-scale pipeline/soil interaction test facility and results from lateral and axial investigations in sand. *Proceedings of the 16th International Conference of Offshore Mechanics and Arctic Engineering*. Yokohama, Japan: Ocean, Offshore and Arctic Engineering (OOAE) Division, American Society of Mechanical Engineers, vol. 5, pp. 139–146.

PIPA (Plastics Industry Pipe Association of Australia Limited) (2001). *Polyolefins technical information*, Chatswood, NSW, Australia. Accessed November 30, 2021. Available from www.pipa.com.au.

Phillips, P., Nobahar, A. & Zhou, J. (2004). Combined axial and lateral pipe–soil interaction relationship. *Proceedings of the international pipeline conference, ASME. IPC2004,* Calgary, Alberta, Canada, pp. 299–303.

PRCI (Pipeline Research Council International) (2017). *Pipeline seismic design and assessment guideline*, Catalogue No: PR-268-134501-R01. Chantilly, VA, USA: PRCI.

Reza, A. & Dhar, A. S. (2021a). Axial Pullout behaviour of Buried Medium Density Polyethylene Gas Distribution Pipes. *International Journal of Geomechanics*, **21**, No. 7, 04021120.

Reza, A. & Dhar, A. S. (2021b). Effects of Axial Relative Ground Movement on Small Diameter Polyethylene Piping in Loose Sand. *Infrastructures* **6**, No. 12, 168.

Rowe, P. W. (1963). Stress-dilatancy, earth pressures, and slopes. *Journal of the Soil Mechanics and Foundations Division*, **89**, No. 3, 37–61.

Roy, K., Hawlader, B., Kenny, S. & Moore, I. (2016). Finite element modeling of lateral pipeline–soil interactions in dense sand. *Canadian Geotechnical Journal*, **53**, No. 3, 490–504.

Roy, K., Hawlader, B., Kenny, S. & Moore, I. (2018a). Upward pipe–soil interaction for shallowly buried pipelines in dense sand. *Journal of Geotechnical and Geoenvironmental Engineering*, **144**, No. 11, 04018078.

Roy, K., Hawlader, B., Kenny, S. & Moore, I. (2018b). Uplift failure mechanisms of pipes buried in dense sand. *International Journal of Geomechanics*, **18**, No. 8, 04018087."

Saha, R. C., Dhar, A. S. & Hawlader, B. C. (2019). Shear strength assessment of a well-graded clean sand. *Proceedings of the 72nd Canadian Geotechnical Conf., GeoSt.John's 2019*, St. John's, Newfoundland and Labrador, Canada: Canadian Geotechnical Society.

Saha, R. C., Dhar, A. S. & Hawlader, B. C. (2020). Assessment of shear strength parameters of moist sands using conventional triaxial tests. *Proceedings of the 73rd Canadian Geotechnical Conf., GeoVirtual 2020*, Virtual (Online), Canada: Canadian Geotechnical Society.

Saha, R.C. (2021). *Shear strength assessment of a manufactured well-graded sand*. M.Eng. thesis, Department of Civil Engineering, Memorial University of Newfoundland, St. John's, NL, Canada.

Sarvanis, G. C., Karamanos, S. A., Vazouras, P., Mecozzi, E., Lucci, A. & Dakoulas, P. (2017). Permanent earthquake-induced actions in buried pipelines: Numerical modeling and experimental verification. *Earthquake Engineering Structural Dynamics*, **47**, No. 4, 966–987.

Schlosser, F. & Elias, V. (1978). Friction in reinforced earth. *Proceedings of the symposium on earth reinforcement*, Pittsburgh, Pennsylvania, ASCE, New York, USA. Pp: 735–763.

Schlosser, F. (1982). Behaviour and design of soil nailing. *Proceedings of the symposium,* Bangkok, Thailand, Asia Institute of Technology, pp. 399–419.

Seed, H. B., Wong, R. T., Idriss, I. M. & Tokimatsu, K. (1986). Moduli and damping factors for dynamic analyses of cohesionless soils. *Journal of Geotechnical Engineering*, **112**, No. 11, 1016–1032.

Sheil, B. B., Martin, C. M., Byrne, B. W., Plant, M., Williams, K. & Coyne, D. (2018). Full-scale laboratory testing of a buried pipeline in sand subjected to cyclic axial displacements. *Géotechnique*, **68**, No. 8, 684–698.

Sheil, B. B., Martin, C. M. & Byrne, B. W. (2021). Simulation of overburden pressure during laboratory investigations of axial pipe–soil interaction. *Géotechnique*, **71**, No. 3, 272–278.

Talesnick, M. L., Ringel, M. & Avraham, R. (2014). Measurement of Contact Soil Pressure in Physical Modelling of Soil-structure Interaction. *International Journal of Physical Modelling in Geotechnics*, **14**, No. 1, 3–12.

Vanden Berghe, J. F., Cathie, D. & Ballard, J. C. (2005). Pipeline uplift mechanisms using finite element analysis. *Proceedings of the 16th International Conference on Soil Mechanics and Geotechnical Engineering*, Osaka, Japan. pp. 1801–1804. Millpress Science Publishers, Amsterdam, Netherlands: IOS Press.

Weerasekara, L. & Wijewickreme, D. (2008). Mobilisation of soil loads on buried polyethylene natural gas pipelines subject to relative axial displacements. *Canadian Geotechnical Journal*, **45**, No. 9, 1237–1249.

Weerasekara, L. & M. Rahman. (2019). Framework for assessing the integrity of natural gas distribution pipes in landslide areas. *Proceedings of the 72nd Canadian Geotechnical Conf., GeoSt.John's 2019*, St. John's, Newfoundland and Labrador, Canada: Canadian Geotechnical

Society.

Wijewickreme, D., Karimian, H. & Honegger, D. (2009). Response of buried steel pipelines subjected to relative axial soil movement. *Canadian Geotechnical Journal*, **46**, No. 7, 735–752.

Wijewickreme, D. & Weerasekara, L. (2015). Analytical modelling of field axial pullout tests performed on buried extensible pipes. *International Journal of Geomechanics*, **15**, No. 2, 04014044.

Yimsiri, S., Soga, K., Yoshizaki, K., Dasari, G. & O'Rourke, T. D. (2004). Lateral and upward soil–pipeline interactions in sand for deep embedment conditions. *Journal of Geotechnical and Geoenvironmental Engineering*, **130**, No. 8, 830–842.

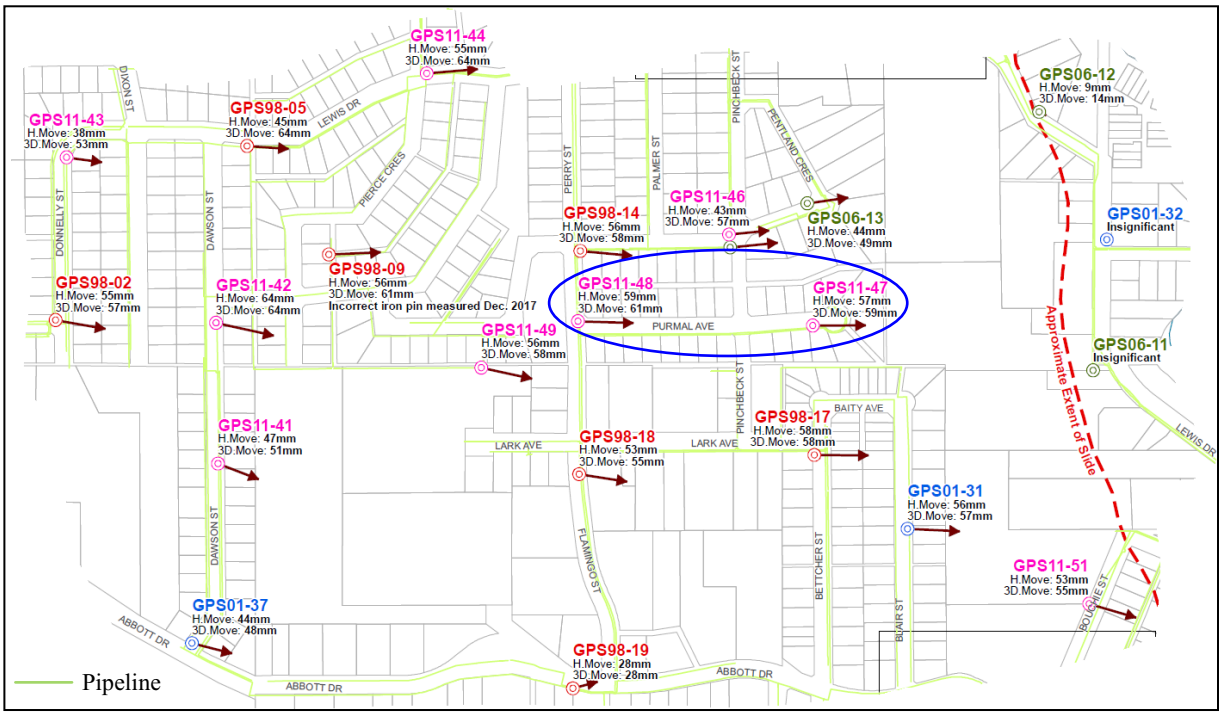

Figure 5.1: Ground movement scenario at a FortisBC project site (City of Quesnel 2020, West Quesnel Land Stability Program)

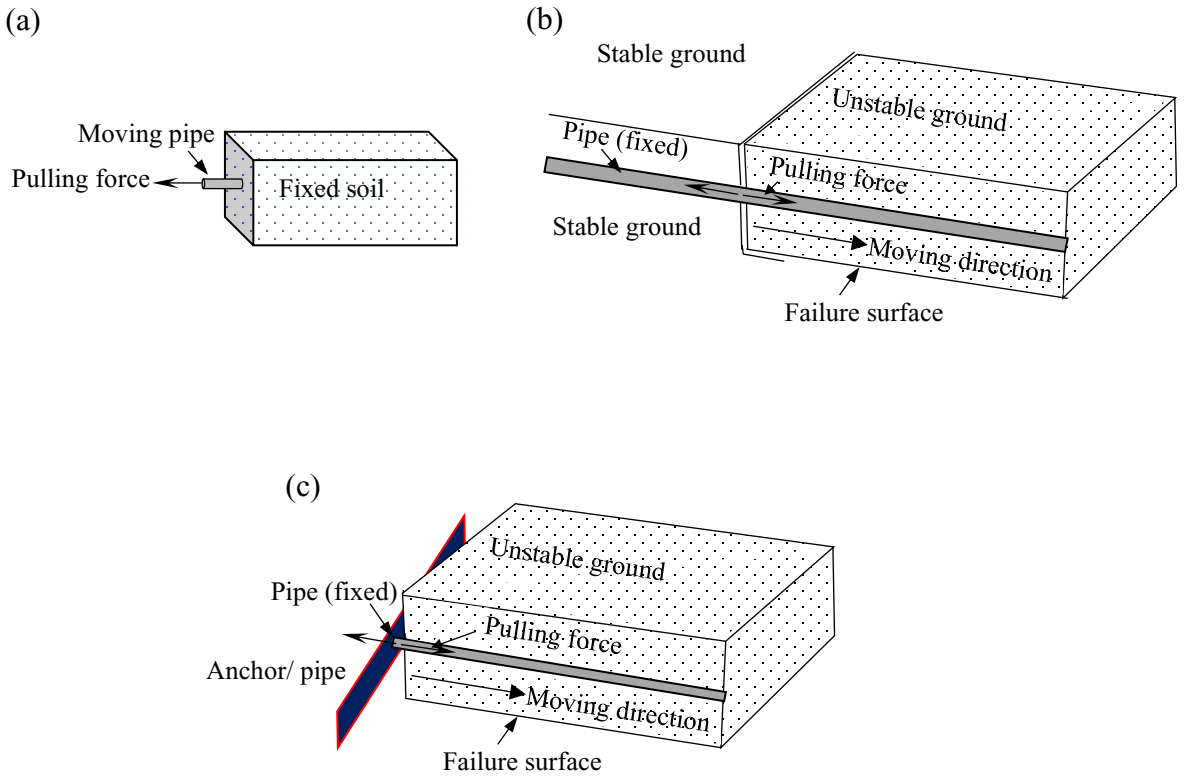

Figure 5.2: Laboratory idealization of a pipe subjected to axial ground movements (after Murugathasan et al. 2021): (a) Laboratory idealization; b) Idealized field condition 1; and c) Idealized field condition 2

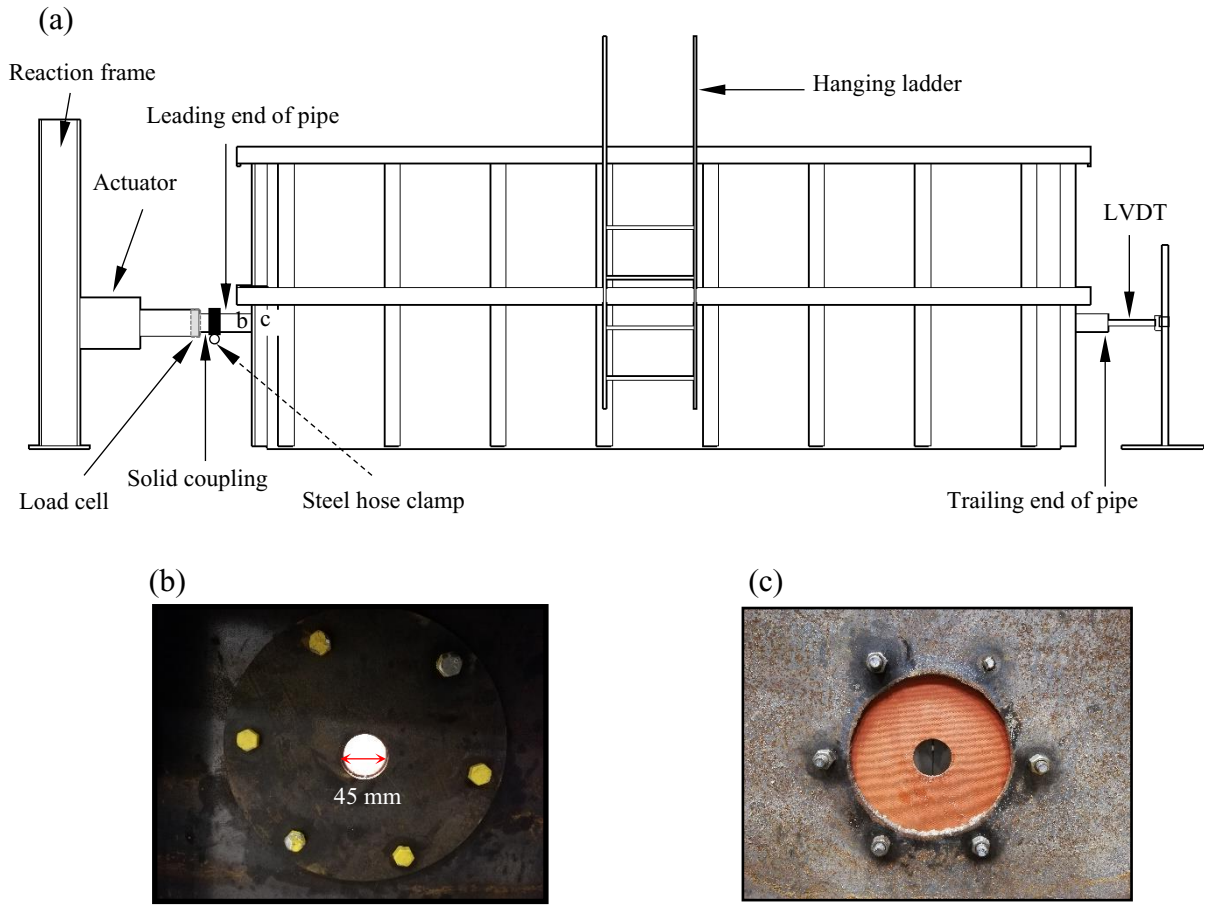

Figure 5.3: Test cell configuration: (a) test cell; b) adjustable circular opening (outer side); and c) adjustable circular opening (inner side)

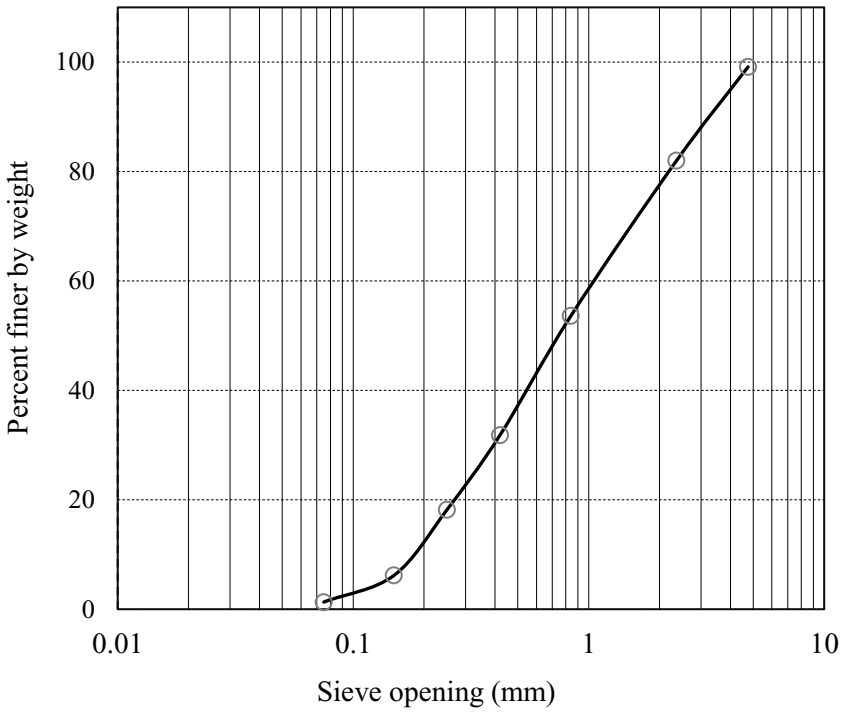

Figure 5.4: Grain size distribution of backfill sand (after Saha et al. 2019)

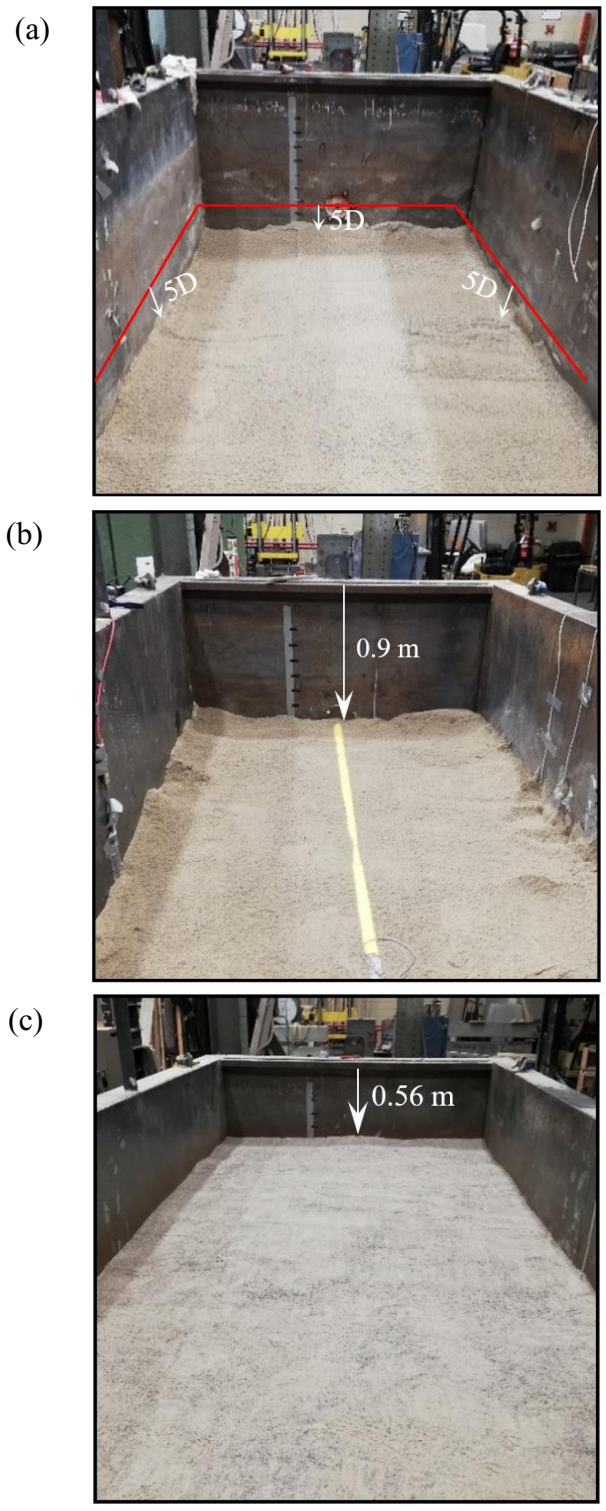

Figure 5.5: Backfilling and pipe installation (shown for 42-mm diameter pipes): (a) bedding conditions; (b) pipe placement; and (c) levelled top surface

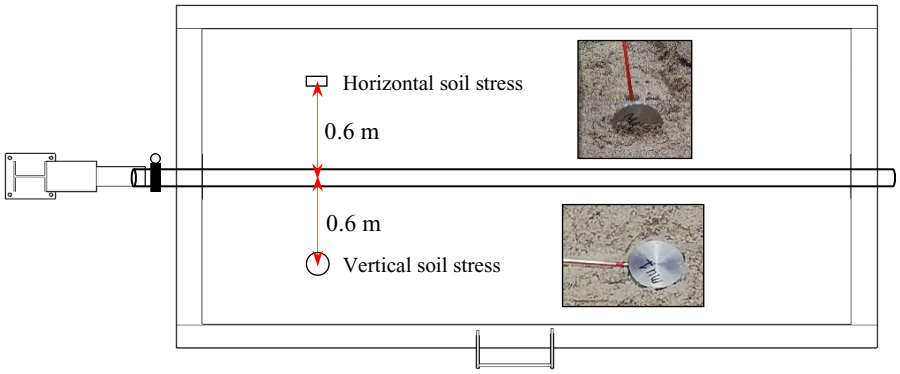

Figure 5.6: Schematic locations of earth pressure sensors at the pipe springline level

Figure 5.7: Strain gauge installation including electrical wires and protecting wraps

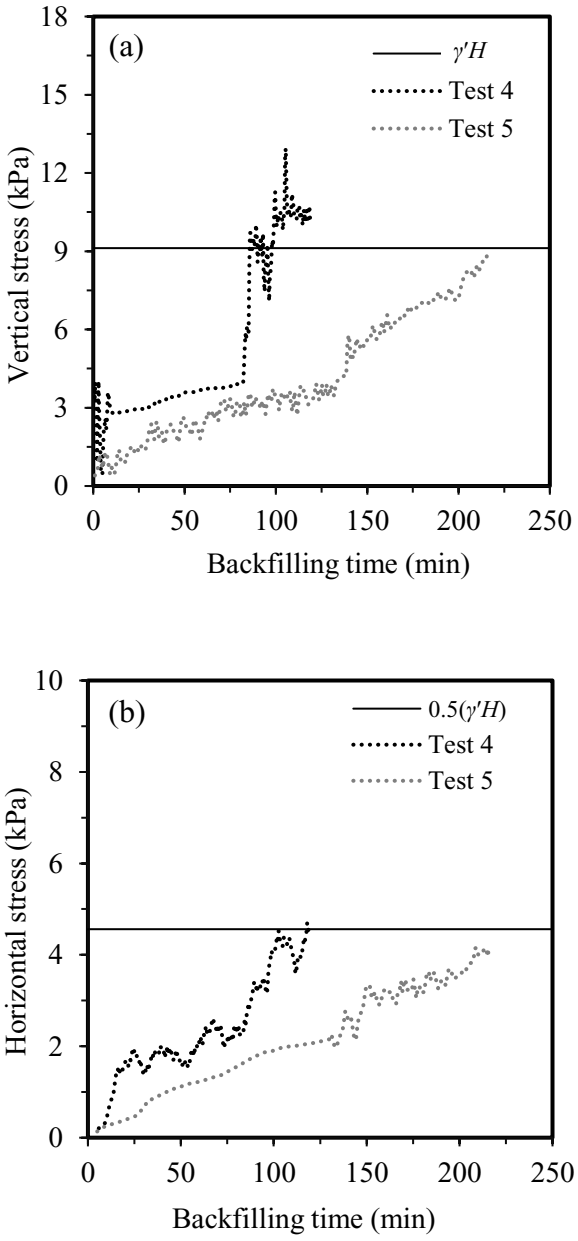

Figure 5.8: Earth pressure measurements during backfilling: (a) vertical stress; and (b) horizontal stress

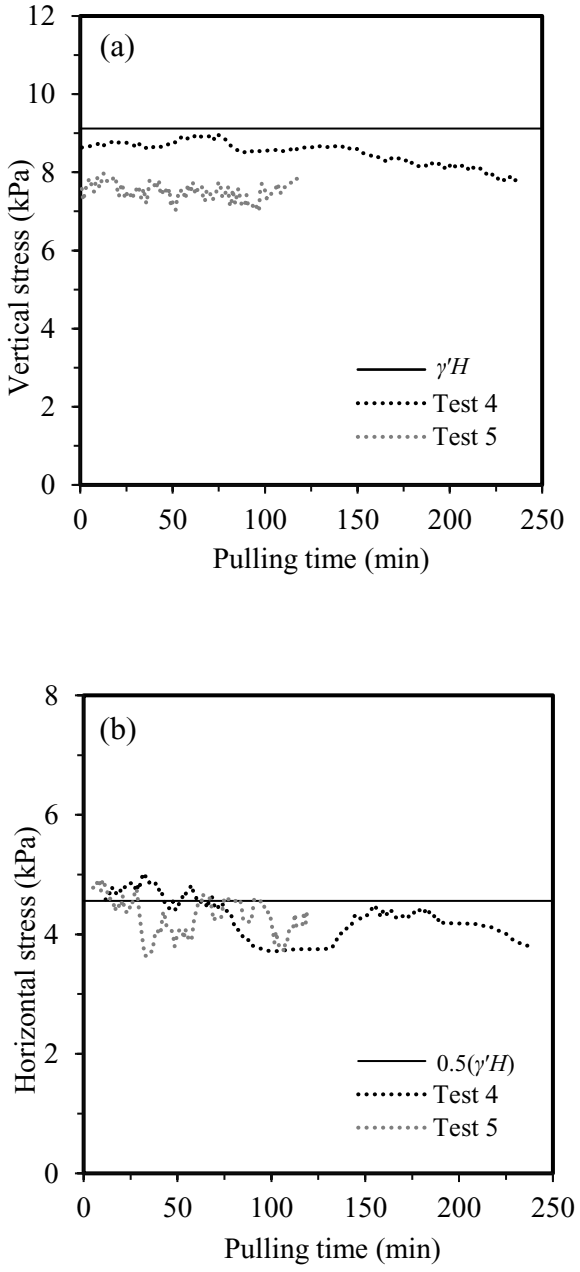

Figure 5.9: Earth pressure measurements during axial pulling: (a) vertical stress; and (b) horizontal stress

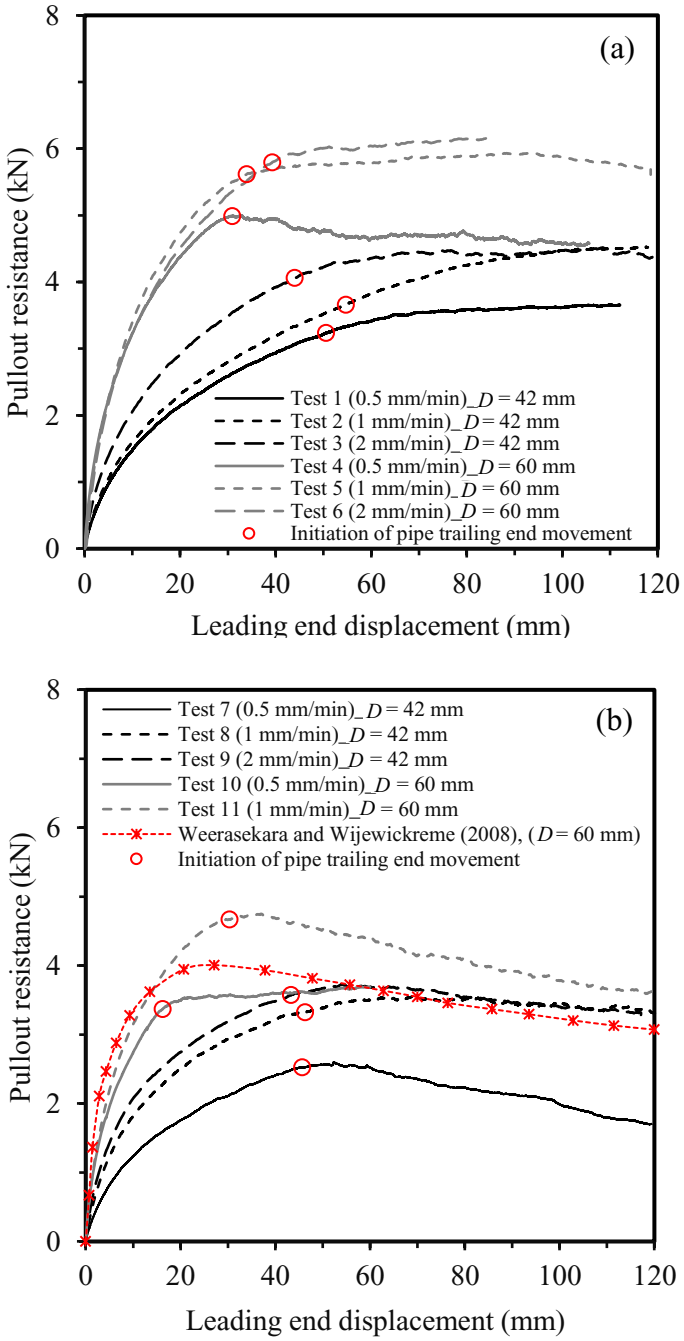

Figure 5.10: Axial pullout resistance with leading end displacement for: (a) with strain gauges; and (b) without strain gauges

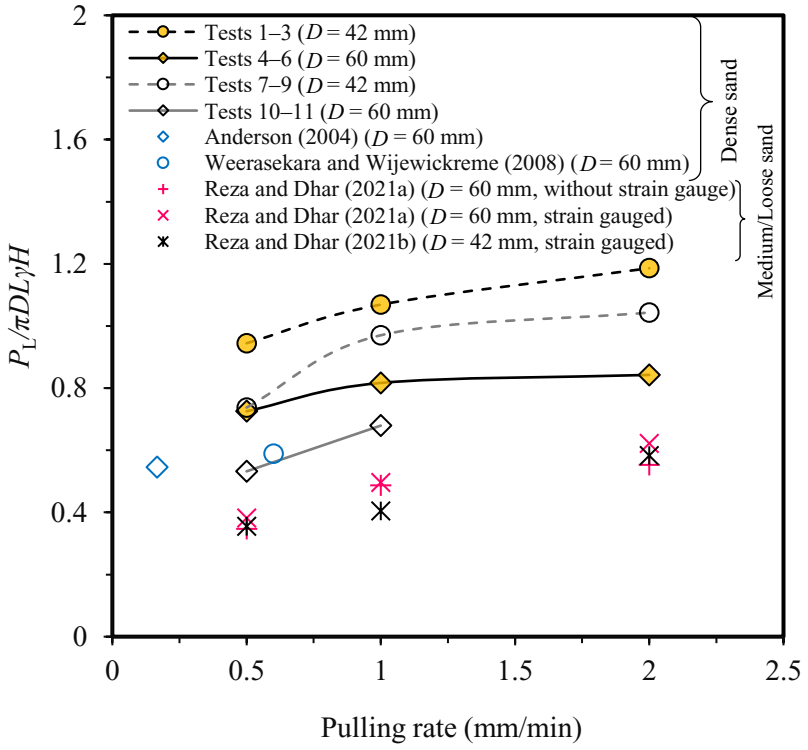

Figure 5.11: Normalized pullout forces with pulling rates

(a)

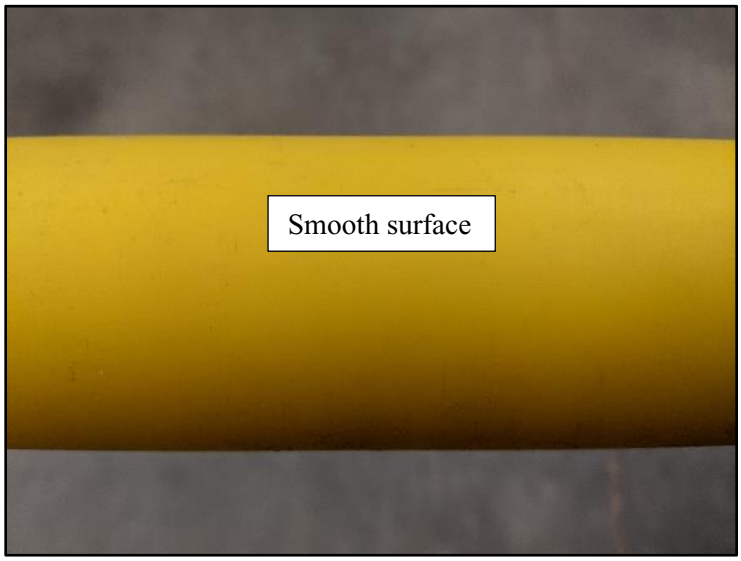

(b)

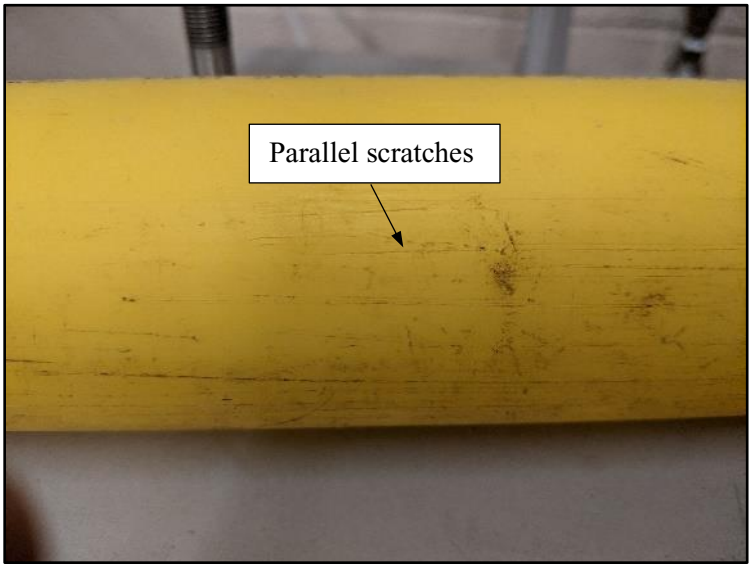

Figure 5.12: Pipe surface condition: (a) before pullout; and (b) after pullout tests

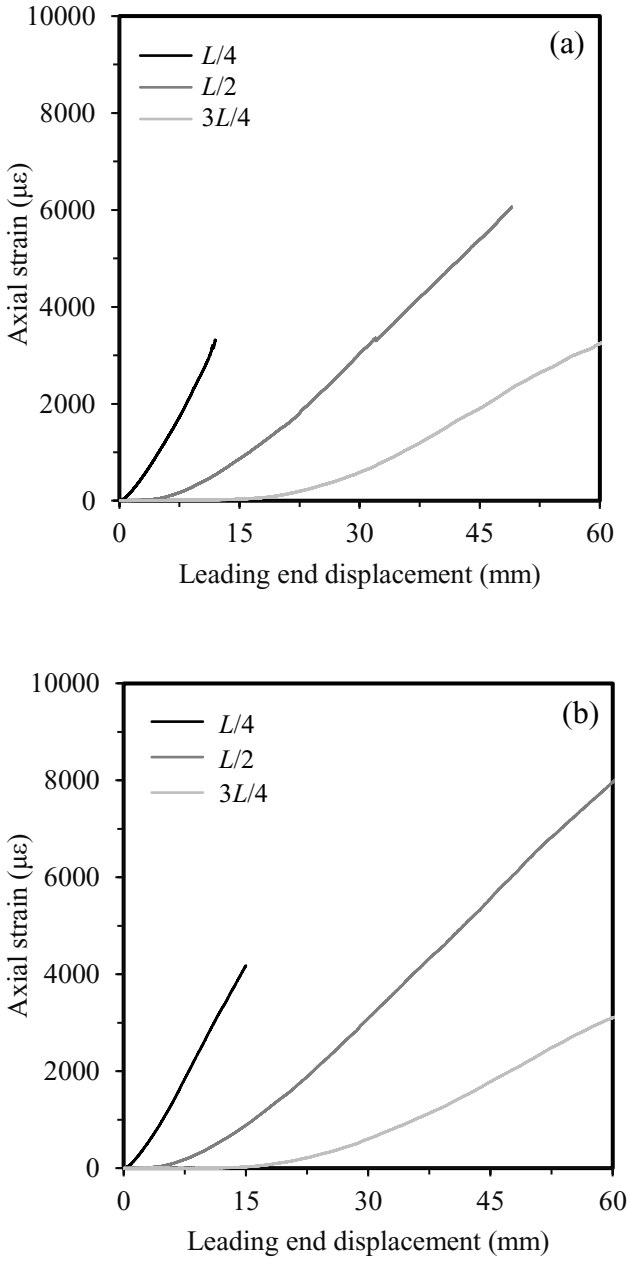

Figure 5.13: Pipe wall strains: (a) Test 1; and (b) Test 2

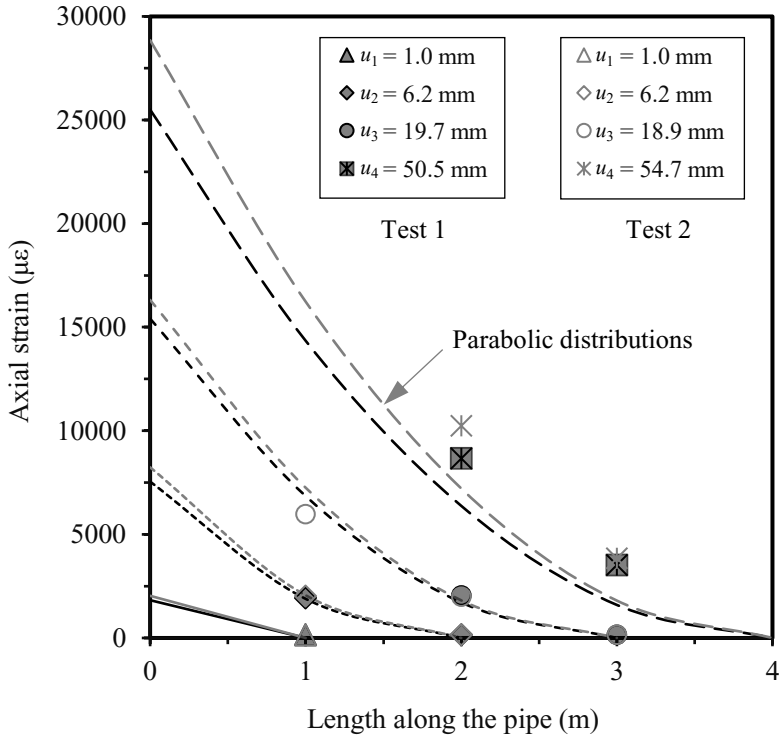

Figure 5.14: Distribution of axial strains along the pipe length in Tests 1–2

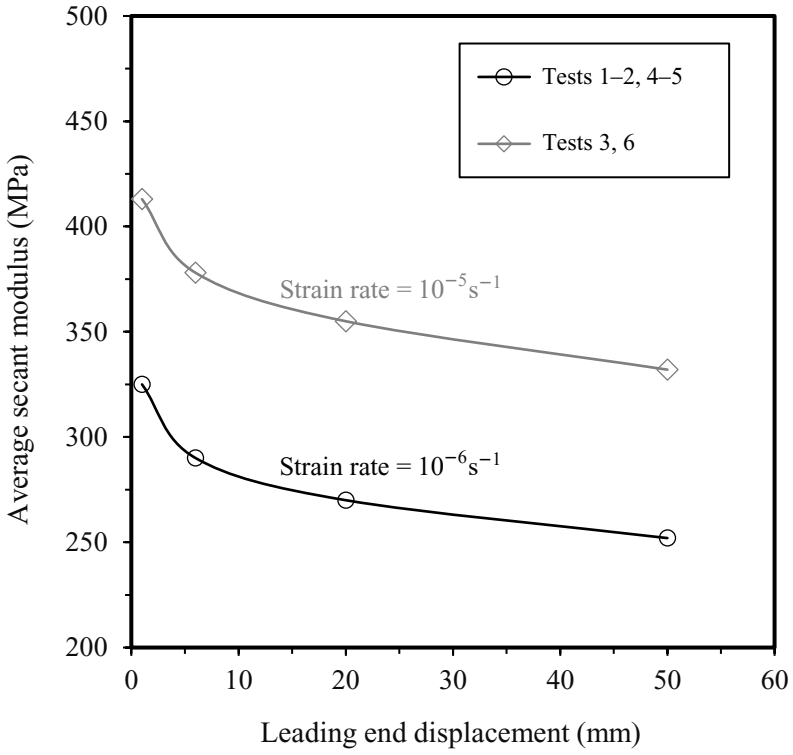

Figure 5.15: Variation of average modulus with leading end displacement

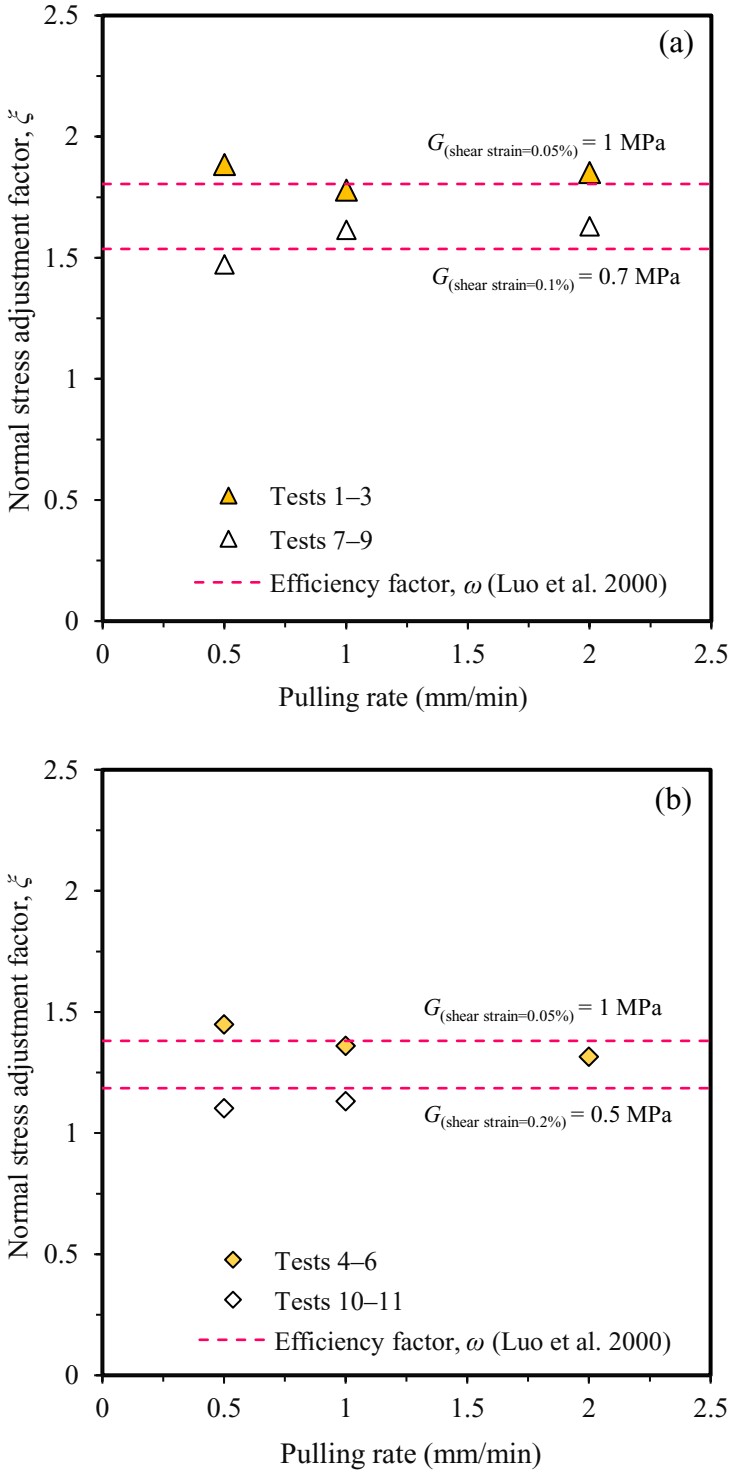

Figure 5.16: Normal stress adjustment factor with pulling rates for: (a) 42-mm; (b) 60-mm diameter pipes

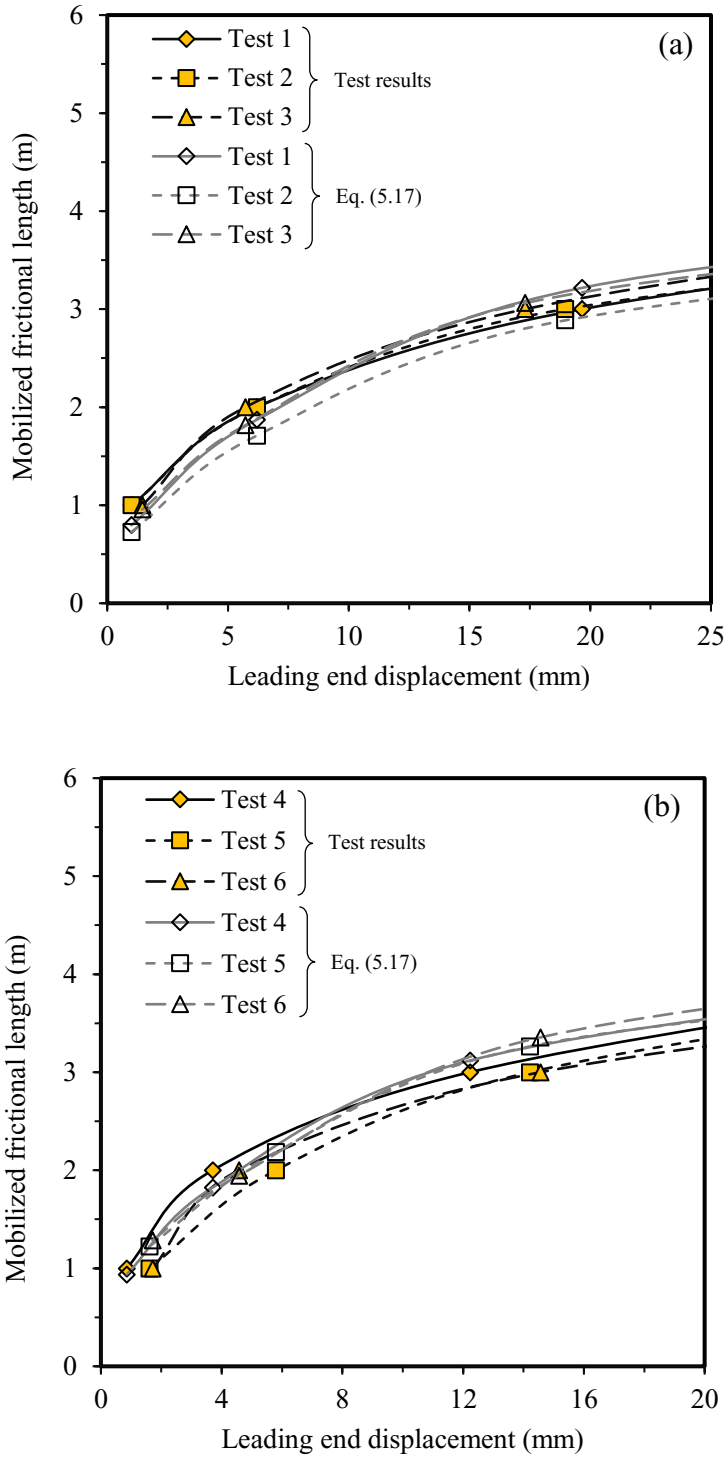

Figure 5.17: Comparison of mobilized friction lengths for: (a) 42-mm; and (b) 60-mm diameter pipes

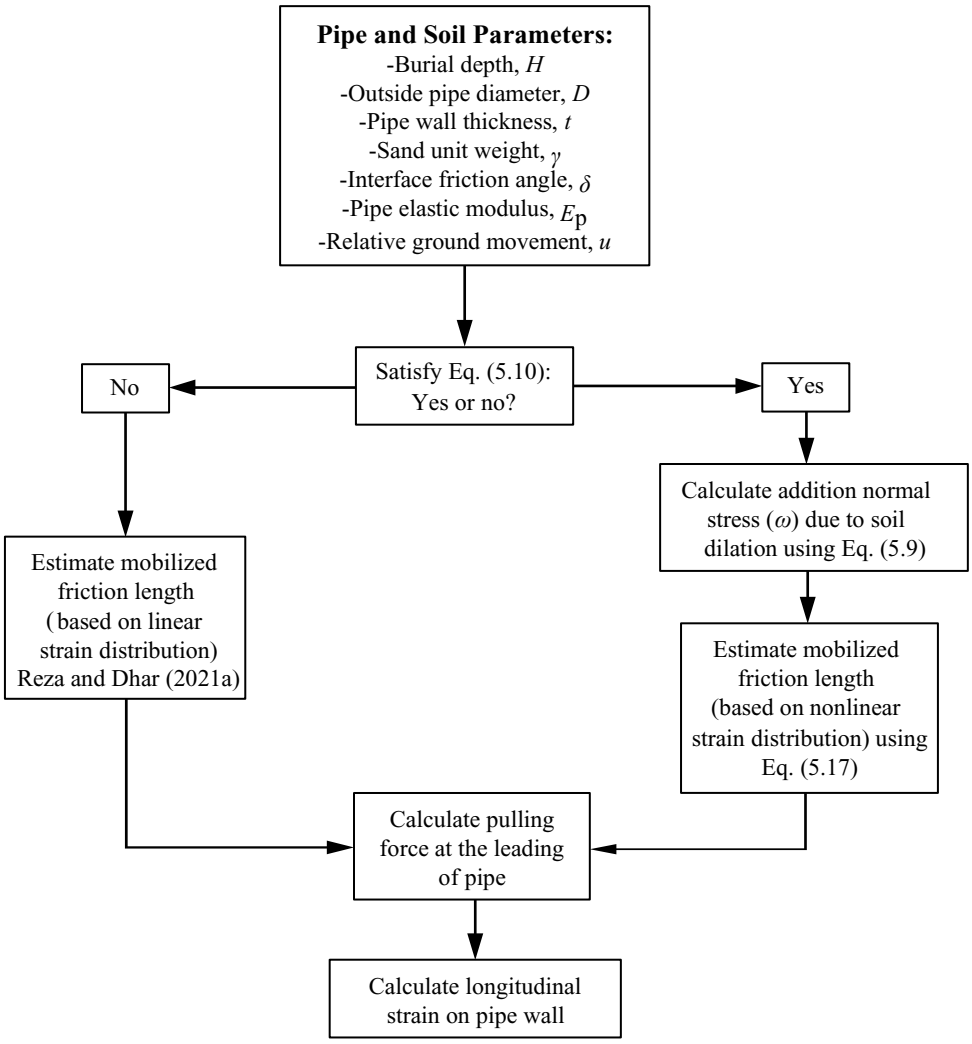

Figure 5.18: Flowchart for calculation of pipe wall axial strain

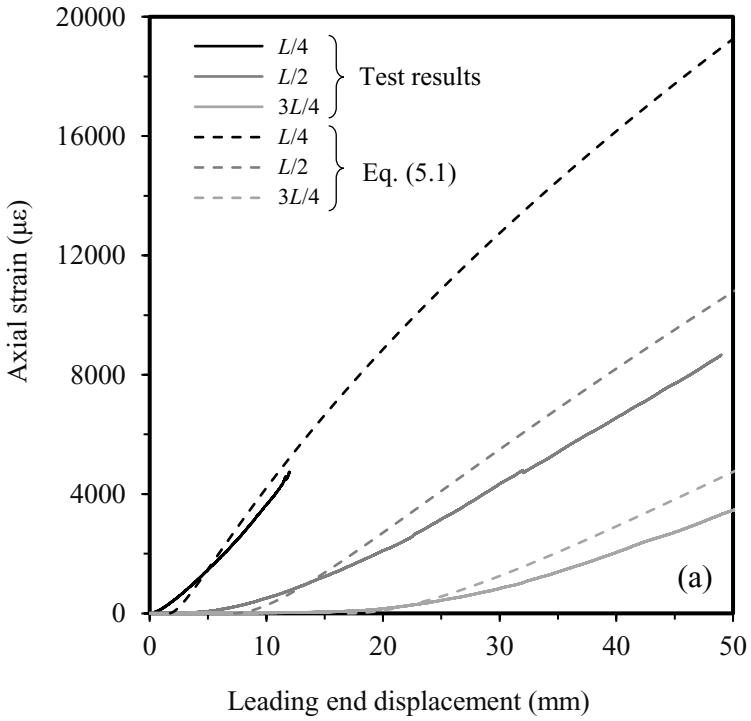

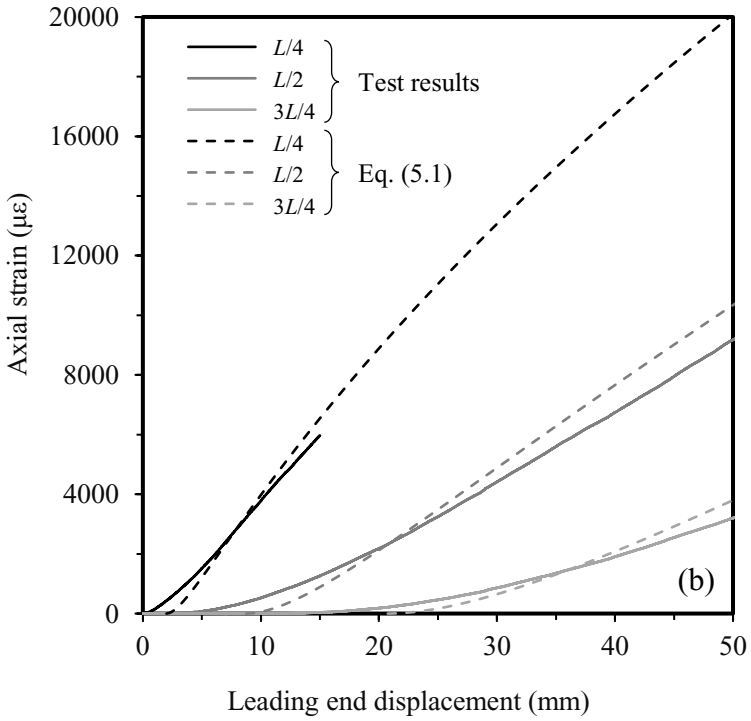

Figure 5.19: Comparison of pipe wall strains for: (a) Test 1; and (b) Test 2

Table 5.1. Backfill sand properties

Property	Values
Median particle size, D_{50} (mm)	0.742
D_{10} (mm)	0.18
D_{30} (mm)	0.40
D_{60} (mm)	1.18
Coefficient of uniformity, C_u	5.81
Coefficient of curvature, C_c	2.04
Fines content (%)	1.3
Gravel content (%)	0.87
Specific gravity, G_s	2.62
Minimum void ratio, e_{min}	0.33
Maximum void ratio, e_{max}	0.65

Note: D_{10}, D_{30}, D_{60}, soil particle diameter at which 10%, 30%, and 60% of the mass of a soil specimen are finer, respectively.

Table 5.2. Summary of the test program

Description of physical parameters	Tests 1–3	Tests 4–6	Tests 7–9	Tests 10–11
Average unit weight, $\overline{\gamma}$ (kN/m^3)	19			
Relative compaction of backfill soil (%)	~100%			
Burial depth, H (m)	0.34	0.48	0.34	0.48
Pulling rate (mm/min)	0.5, 1, 2	0.5, 1, 2	0.5, 1, 2	0.5, 1
Buried pipe length, L (m)	4			
Pipe outside diameter, D (mm)	42.2	60.3	42.2	60.3
Pipe wall thickness, t (mm)	4.22	5.48	4.22	5.48
Standard dimension ratio (SDR)	10	11	10	11
H/D	8			
Strain gauged or not	Yes		No	

Table 5.3. Leading end displacements and pulling forces with mobilized lengths

Test number	Mobilized friction length (m)	Leading end displacement (mm)	Pulling force (kN)
1	1	1.0	0.30
	2	6.2	1.11
	3	19.7	2.12
	4	50.5	3.24
2	1	1.0	0.33
	2	6.2	1.21
	3	18.9	2.25
	4	54.7	3.66
3	1	1.45	0.62
	2	5.7	1.51
	3	17.3	2.74
	4	43.9	4.06
4	1	0.85	0.70
	2	3.7	1.89
	3	12.22	3.56
	4	30.87	4.99
5	1	1.6	1.02
	2	5.8	2.46
	3	14.2	4.09
	4	33.9	5.62
6	1	1.7	0.96
	2	4.57	2.06
	3	14.56	3.89
	4	39.25	5.79

Table 5.4. Parameters used for the calculation of efficiency factor, ω (Eq. 5.9)

Property	Tests 1–3	Tests 4–6	Tests 7–9	Tests 10–11
Effective overburden pressure at pipe springline, $\sigma_v^{'}$ (kPa)	6.46	9.12	6.46	8.65
Pipe diameter, D (mm)	42.2	60.3	42.2	60.3
Initial shear modulus, G_0 (MPa)	1.88			
$G_{(\text{shear strain}=0.05\% - 0.2\%)}$ (MPa)	1.0		0.7	0.5
Relative density, I_D (%)	60			
Lateral earth pressure coefficient at rest, K_0	0.5			
Poisson's ratio, v	0.33			
Critical shear displacement, u_c (mm)	0.5			

CHAPTER 6

Finite-Element Modelling of Axial Movements of Polyethylene Pipes in Dense Sand

Co-Authorship: A version of this chapter has been submitted to a journal as a technical paper for review as: Reza, A. and Dhar, A. S. (2023). 'Finite-Element Modelling of Axial Movements of Polyethylene Pipes in Dense Sand.' Most of the research presented in this chapter has been conducted by the first author. He also prepared the draft manuscript. The other author mainly supervised the research and reviewed the manuscript.

6.1 Abstract

The current design guidelines have been reported to underpredict the axial pullout resistance measured in laboratory and field tests for pipes buried in dense sand. The higher pullout resistances in the tests were believed to be due to the shearing-induced soil dilation at the pipe–soil interface. However, the mechanism of soil dilation could not be measured during the tests. In the current study, three-dimensional finite-element (FE) analysis was employed to examine the mechanism, which revealed that the effect of shearing-induced dilation could be insignificant for medium-density polyethylene pipes, depending on the magnitude of the earth pressures. For pipes buried at shallow depths, the compaction-induced lateral earth pressures significantly contributed to higher interface normal stresses and the increase of normal stress due to shear-induced dilation, resulting in relatively higher pullout resistances. The stiffness of the pipe and soil also influenced the normal interface stress. The compaction-induced lateral earth pressure increase was modelled using equivalent temperature loads in the FE analysis that successfully simulated the measured pipe responses. Based on the findings, a modification to the current design equation to calculate the

maximum axial spring force was proposed, incorporating the compaction-induced lateral earth pressure and a normal stress adjustment factor. The conventional beam-on-spring analysis with the modified spring force successfully simulated the pipe responses observed during the tests. The compaction effect was insignificant for deeply buried pipes.

6.2 Introduction

Buried pipes are widely used worldwide for transporting liquids and gases. The use of polyethylene (PE) pipes has been increasing for oil and gas transportation and distribution since the late 1950s (PHMSA 2015). About 71% of the gas distribution system in Canada uses medium-density polyethylene (MDPE) and high-density polyethylene (HDPE) (CGA 2021). Permanent ground deformation often threatens the structural integrity of buried pipelines in service. Permanent ground deformation refers to nonrecoverable soil movement due to ground subsidence, earthquakes, landslides, or slope movements that can cause leakage or rupture in the pipelines, leading to environmental and financial consequences. The maintenance and operational decisions of the pipelines exposed to ground movements require evaluation of pipeline distress (i.e., wall strains) due to the forces from the moving ground. Different technologies are currently available to monitor ground movements, such as GPS surveying at discrete points (survey hubs), LiDAR image analysis, and satellite image analysis. To this end, a reliable tool for assessing the pipe wall strain due to ground movement is required for evaluating pipe conditions. Current design guidelines, such as ALA (2005) and PRCI (2017), recommend using beam-on-spring analysis to calculate pipe wall strains for pipelines subjected to ground movements. Elastic-perfectly plastic parameters were proposed in the design guidelines for axial, lateral, and vertical springs. The maximum force (per unit length) for the axial spring is estimated as the maximum frictional

resistance of the pipe–soil interface based on a normal stress on the pipe wall and an interface friction angle (δ). The normal stress is taken as the arithmetic mean of the vertical overburden pressure and the at-rest lateral earth pressure (i.e., geostatic stresses) at the springline level of the pipe. However, the method for calculating the maximum spring force was unable to simulate the stress field observed during laboratory tests, particularly for pipes in dense sand (Weerasekara and Wijewickreme 2008; Wijewickreme et al. 2009; Sheil et al. 2018; Reza et al. 2023).

Researchers performed experimental studies and evaluated the recommendations in the design guidelines for correctly calculating the axial soil resistance for steel pipes (Paulin et al. 1997; Wijewickreme et al. 2009; Sarvanis et al. 2017; Sheil et al. 2018). Based on the experimental results, it was argued that the shearing-induced dilation at the pipe–soil interface increases the normal stresses, resulting in a higher axial soil resistance than the one calculated using the method recommended in the design guidelines. Wijewickreme et al. (2009) proposed using a higher coefficient of lateral earth pressure, while Sarvanis et al. (2017) proposed an empirical equation to account for the higher normal stress for pipes in dense sand. Sheil et al. (2021) measured the contact stresses around buried steel pipes, applying and subsequently reducing surcharge pressures, and found 'locked-in' normal stresses on the pipe after reducing the surcharge pressure. The effect of locked-in normal stress is not considered in the existing design guidelines. Wijewickreme and Weerasekara (2015) applied the cavity expansion theory to estimate the normal stress increase on the pipe surface for MDPE pipes to calculate pipe wall strains observed in their experiments. Reza et al. (2023) also successfully applied the cavity expansion theory to calculate the experimentally observed pipe wall strains, developing simplified equations. Thus, higher normal stress than the mean geostatic stress for the pipes in dense sand has been recognized. While

it is assumed that the higher normal stress is associated with shear-induced dilation, the mechanism could not be validated experimentally. However, O'Rourke et al. (1990) observed no volume change or dilatancy at the interface of smooth HDPE geomembrane and dense sand in direct shear tests. Dove and Jarrett (2002) also reported a nondilative interface for sand grains contacting a smooth polymer, while a dilative interface could be expected for a rough polymer surface. Schlosser (1982) suggested earlier that the dilation behaviour of the soil essentially governs the interface frictional resistance only for rough surfaces of inclusions. For rough surfaces, shear stresses on the interface cause soil particles to slide and roll around the inclusion, resulting in the dilation of the soils in the vicinity of the inclusion. Since the surface of MDPE pipes is relatively smooth, the shear-induced dilation of the interface soil could be less. This mechanism is investigated in the current study, using three-dimensional (3D) finite-element (FE) analysis through simulation of the test conditions reported in Reza et al. (2023).

Reza et al. (2023) reported full-scale pipe tests conducted with 42.2- and 60.3-mm diameter MDPE pipe samples in a soil box 4.0 m long, 2.0 m wide, and 1.5 m deep. Table 6.1 provides a summary of the test program undertaken. Details of the test cell and pipe installation methods are available elsewhere (Reza and Dhar 2021ab; Reza et al. 2023). During the tests, the pipe samples were backfilled in the soil box using locally available manufactured sand compacted to the densities of 18.0 to 19.2 kN/m^3. These densities corresponded to 100% of the standard Proctor maximum dry density (i.e., 18.8 kN/m^3, after Saha et al. 2019). Pipe burial depths were selected to provide a depth ratio (ratio of soil cover measured from pipe springline to pipe diameter) of 8. The pipe samples were axially pulled to a displacement of 120 mm at the pulling rates of 0.5, 1, and 2 mm/min, respectively.

Continuum-based 3D FE modelling was first employed to simulate the test conditions described above (Reza et al. 2023). The stress fields calculated from the continuum-based FE analysis were examined. Based on the results, a modified equation is proposed to calculate the maximum spring force for pipeline evaluation using the beam-on-spring type FE modelling techniques recommended in the design guidelines. Finally, the beam-on-spring analysis technique with modified spring force was evaluated through comparison with the test results.

6.3 Continuum-Based FE Modelling

6.3.1 *Model Development*

FE analysis was performed using Abaqus (Dassault System 2019). Figure 6.1 shows a typical continuum-based FE model used in the analysis. The model dimensions are the same as those in the tests (Tests 1–5). The pipe and soil domains were modelled using C3D8R (eight-node linear brick element with reduced integration) solid elements available in Abaqus. A finer mesh was used in the pipe's close vicinity over a radial distance of 2.5 times the pipe diameter (2.5D) based on a mesh sensitivity analysis. A zero-displacement boundary condition was used for the bottom and each side of the test box, assuming rigid walls, except for the pipe's axial movement. Murugathasan et al. (2021) demonstrated that the test cell's boundary walls could reasonably be assumed as rigid under axial pullout loading. A quasi-static analysis was performed using the dynamic implicit modelling technique with the full Newton solution algorithm. A similar approach was used for the analysis of pipes in loose to medium-dense sands (Reza and Dhar 2021ab).

6.3.2 *Material Models*

Soil exhibits complex elasto-plastic behaviours during loading that depend on various factors,

including density, stress history, existing stress level, and the load path. Various constitutive models were developed for sand to capture the complex elasto-plastic behaviours (Duncan and Chang 1970; Jeffries 1993; Wan and Guo 1998; Desai 1996; Yao et al. 2008; Yang et al. 2022). The suitability of the models in any analysis depends on the purpose of the simulation, which varies widely from problems to problems. Some of the models are too complex for implementation in FE analysis and are often not understood by practicing engineers, while have insignificant effects on the results of analysis for certain problems. In such cases, the complex models are not employed during the analysis. For soil–pipe interaction analysis, the simple Mohr-Coulomb (MC) model was widely and successfully used (e.g., Yimsiri et al. 2004; Ni et al. 2018; Almahakeri et al. 2019; Katebi et al. 2021; Chen et al. 2023). According to the conventional MC model, plastic deformation occurs when the stress state reaches a constant yield surface and the soil dilates at a constant dilation angle, ψ. Although the soil in the field may experience a more complex yield surface and deformations, their effects on the pipe responses were not significant. As a result, the pipe responses were successfully simulated in various studies using equivalent constant values of ϕ' and ψ for the MC model. For pipe–soil interaction problems experiencing excessive plastic shear strains (plastic shear strain >10%) over large regions, a modified Mohr-Coulomb (MMC) was required where the friction angle and the dilation angle were varied with the plastic shear strains (Guo and Stolle 2005; Daiyan et al. 2011; Robert and Thusyanthan 2015; Roy et al. 2016, 2018). However, for the axial pipe–soil interaction problem presented in the current study, the plastic deformation of the soil is expected only within the vicinity of the pipe surface (shown later in this study). Therefore, the conventional MC model was suitably used.

Elastic soil modulus, E_s, was estimated based on the nonlinear model of Janbu (1963) as a

power function of the confining pressure, p', as expressed in Eq. (6.1).

$$E_s = Kp'_a \left(\frac{p'}{p'_a}\right)^n \tag{6.1}$$

where p' is the initial mean effective stress at the springline of the pipe; p'_a is the atmospheric pressure (= 101.3 kPa); K is a material constant that determines the scale of E_s, and n is an exponent. In the present study, K = 150 and n = 0.5 were used (after Fellenius 2009; Roy et al. 2016). Thus, E_s = 5 MPa was calculated at geostatic stresses corresponding to the pipe burial depth. Poisson's ratio (v) of the soil was assumed as 0.33, which is within the typical values for dense sand (Budhu 2011).

The parameters of the MC model used in this numerical study were selected based on laboratory tests performed on the sand for a wide range of stress conditions (Saha et al. 2019, 2020). As the soil stresses were low around the pipes during the tests, the equivalent soil friction angle of ϕ'=45° at the low-stress level was selected for the analysis. The critical state friction angle (ϕ_{cv}) for the sand is 35° (Saha et al. 2019, 2020). The peak dilation angle, ψ_{max}, could be estimated for high confining stress (p') based on the relationship proposed by Bolton (1986). However, for pipes buried at shallow depth, the confining pressure is low. At low p', soil dilation could be higher depending on the initial soil density (Lee and Seed 1967; Chakraborty and Salgado 2010; Ansari et al. 2018). Based on the triaxial compression test data for Toyoura sand, Chakraborty and Salgado (2010) proposed relationships for calculating the dilation angle under very low confining pressure (Eqs. 2–4).

$$\psi_{max} = \phi'_{max} - \phi'_{cv} = 3.8 I_R \tag{6.2}$$

$$I_R = I_D \left(Q - \ln \frac{100\sigma'_{mp}}{p_A} \right) - R \tag{6.3}$$

$$Q = 7.4 + 0.60 \ln\sigma'_c \tag{6.4}$$

where I_R = relative dilatancy index; $I_D = \frac{D_r(\%)}{100}$ = relative density (ranging from 0 to 1); σ'_{mp} = mean effective stress in kPa; σ'_c = confining pressure in kPa; Q , R (=1) = fitting parameters that depend on the intrinsic sand characteristics; and p_A = reference pressure = 100 kPa.

Based on the relationships, a maximum ψ = 18° was calculated for the stress-levels expected in this study. Note that even though the dilation can be high, the pressure increase on the pipe due to dilation can be low due low confining pressure of the shallow buried pipes. A sensitivity study was conducted with varying ψ from 8° to 18° (while keeping E_s = 5 MPa, ϕ' = 45°, δ = 38° as constants) that showed no significant effect on the peak pullout resistance. The cohesion (c) for sand is zero; however, a minimum value of 0.1 kPa was assigned to avoid numerical instability.

The stress–strain responses of MDPE pipe material are nonlinear and strain rate–dependent. Das and Dhar (2021) developed a strain rate–dependent hyperbolic model for the pipe material. Based on the model of Das and Dhar (2021), the stress–strain responses of MDPE pipe material were obtained at the strain rates observed during the tests that were used as input in the FE analysis (Figure 6.2). The maximum strain rates during the tests ranged from 1×10^{-5}/s to 4×10^{-5}/s with pulling rates of 0.5 to 2 mm/min. The isotropic elastic-plastic model was employed with the yield stress and strain shown in Figure 6.2. The Poisson's ratio and density of MDPE were assumed as 0.46 and 940 kg/m^3, respectively, at the laboratory temperature (23 °C), after Bilgin et al. (2007).

The contact between the pipeline and the surrounding soil was modelled using the general contact algorithm. Normal and tangential behaviours between contacting surfaces were defined to prevent penetration and allow surface slippage, respectively. Normal behaviour was considered as "hard" (i.e., non-penetrating) contact, while tangential behaviour was defined by the Coulomb friction criterion. Reza and Dhar (2021a) reported that the interface friction angle for MDPE pipe materials in sand depends on the pulling rates. They found the interface friction angles as $0.75\phi'$, $0.86\phi'$, and $0.90\phi'$, corresponding to the pulling rates of 0.5, 1, and 2 mm/min, respectively. These interface friction angles are considered applicable to the current study.

This finite-element modelling technique successfully simulated the pipe responses during axial pullout tests in loose to medium-dense sands (Reza and Dhar 2021ab). However, as discussed later in this paper, the modelling technique underestimated the pullout forces and the pipe responses for the pipes in dense sand. Pipes in dense sand experience compaction-induced stress in the soil. The effect of the compacted-induced stress on the behaviour of buried pipe was observed earlier in Wang et al. (2017), Saleh et al. (2021), and others. However, the compaction-induced stress cannot be predicted using the conventional approach of finite-element modelling. A review of previous studies on compaction-induced stress and a method employed to account for the stress in the current study are discussed in the following section.

6.3.3 *Modelling Compaction-induced Stresses*

Katona (1978) explained the mechanism of developing compaction-induced stress in the soil. Firstly, both vertical and horizontal earth pressures within the soil increase during compaction due to the forces exerted by the compactor. Then, when the compactor is removed, the vertical

pressures decrease to the overburden values, whereas the horizontal stress also decreases but remains above the pre-compaction values (often referred to as residual stress). He suggested a squeeze layer method to account for the compaction effects during analysis, where vertical pressure is applied on the surface of the backfill. The applied vertical pressure induces additional horizontal stress due to Poisson's effect. Duncan and Seed (1986) suggested applying 80 kPa of vertical stress to simulate the compaction pressure on retaining wall backfill. Duncan et al. (1991) used the theory proposed by Duncan and Seed (1986) and developed earth pressure charts and tables to estimate the compaction-induced horizontal pressures. According to the charts and tables, the lateral earth pressure is greater than the at-rest earth pressure at shallow depths. At greater depths, below the compaction-influenced zone, the horizontal earth pressure converged with the earth pressure at rest. Chen and Fang (2008) confirmed the variation of horizontal earth pressure with depths, measuring the lateral earth pressure at various depths against a retaining wall during vibratory compaction of backfill.

Researchers employed different approaches to account for the effect of compaction-induced earth pressure in the FE analysis of buried pipes. McGrath (1998) applied horizontal nodal forces directly on the pipe during analysis using the FE software CANDE. Taleb and Moore (1999) applied additional horizontal stresses equal to the passive earth pressure during FE analysis of buried culverts. Elshimi and Moore (2013) introduced an empirical kneading factor, K_n (up to 2), to the passive earth pressure to account for the effect of soil kneading during compaction on the horizontal earth pressure.

Wang et al. (2015) measured the earth pressure around steel-reinforced high-density

polyethylene (SRHDPE) pipes during backfilling. The measured vertical earth pressures at the top of the pipe were 10% to 47% greater than the overburden stresses (explained as the negative soil arching effect). They found that the lateral earth pressure coefficient at the pipe springline decreased with the increase of the soil cover thickness. The lateral earth pressure coefficients were higher than the earth pressure coefficients at rest but lower than the passive earth pressure coefficients. Wang et al. (2017) conducted a numerical analysis, applying a uniformly distributed pressure of 80 kPa (after Duncan and Seed 1986) on the surface of each lift of the backfill to simulate the compaction effects. The hardening soil model was used, employing FE software PLAXIS 2D to capture the elastic-plastic behaviour of the backfill material and the residual horizontal stress after the removal of compaction loads. Dezfooli et al. (2014a) simulated compaction-induced horizontal stresses to analyze a pipe test in a soil box by applying an equivalent temperature loading to the soil layers between the fixed boundaries of the test cell. The temperature loading was applied only in the direction perpendicular to the pipe axis and was zero in the other directions. Dezfooli et al. (2014b) considered springs between the thermal soil and the trench boundaries to simulate pipes buried in different trench configurations. Saleh et al. (2021) utilized a simple model shown in Figure 6.3 to obtain the fictitious temperature for simulating the compaction-induced stress at any soil layer under fix-fix boundary conditions. Eq. (6.5) can be used to calculate the temperature to be applied for a given coefficient of thermal expansion if the stress increase at the layer is known.

$$\Delta\sigma_{soil} = (E\alpha\Delta T)_{soil} \tag{6.5}$$

where $\Delta\sigma_{soil}$ = compaction-induced lateral stress in the soil; E = modulus of elasticity of soil; α = coefficient of expansion for soil; ΔT = temperature applied to the soil layer.

The compaction-induced stresses with depths for the test conditions were calculated using the procedure proposed in Duncan and Seed (1986). Figure 6.4 shows the distribution of the calculated peak and residual lateral earth pressure increases acting against a rigid wall. The compaction-inducted stresses for the FE analysis were estimated by subtracting the at-rest values from the peak stresses in Figure 6.4. The peak values corresponding to x = 0.15 m were used. Then, the corresponding temperature loads were calculated using Eq. (6.5). For example, using Figure 6.4, the increase in horizontal pressure due to compaction is calculated as 24.7 kPa and 16.2 kPa at the pipe springline for Tests 1–3 and Tests 4–5, respectively. The temperature loading is calculated as 100 °F and 65 °F for Tests 1–3 and Tests 4–5, respectively, using Eq. (6.5) for E = 5 MPa and α = 0.00005 1/°F. The thermal load was applied only as a predefined field in the horizontal direction during the analysis. Figure 6.5 shows the applied temperature for each layer in the FE model for Tests 1–5.

6.3.4 *Simulation Procedures*

The FE models were developed with several layers of material, as shown in Figure 6.5, to assign different temperature loads in the layers. The layer thicknesses were similar to those used during backfilling in the test box. Mechanical and thermal material parameters were assigned for each of the layers. Then, analysis was performed first by applying the gravity load and then the thermal load. As discussed earlier, a uniform thermal load was applied in each of the layers, calculated using the method in Duncan and Seed (1986). Analyses were also performed by simultaneously applying the gravity and thermal load and simulating staged construction (after Saleh et al. 2021). However, no significant difference in the results was observed. Finally, an axial displacement was applied on one end of the pipe (herein termed the “leading end”) up to the displacement of 120 mm.

6.4 FE Results

6.4.1 *Force–Displacement Responses and Pipe Wall Strains*

Figure 6.6 compares the measured axial pullout forces from Tests 1–5 with the FE calculations. It clearly demonstrates the importance of including compaction-induced stress in the FE simulation. Pullout resistances calculated using conventional FE analysis without considering compaction-induced stress are significantly less than those calculated simulating the compaction effects. Calculations considering compaction-induced stress are close to the measurements. There are some differences between the FE calculations and the test results before the peak values in Figure 6.6, which might be due to the use of a linear elastic perfectly plastic MC model for the soil material where a nonlinear stress–strain relation was expected. The classical MC model for the pipe–soil interaction successfully simulated the peak soil resistance during the axial pullout (Figure 6.6), similar to those reported earlier in others' research (e.g., Yimsiri et al. 2004; Katebi et al. 2021). It is likely due to the plastic deformation of the soil not extending too far from the pipe surface, as seen in Figure 6.7. Figure 6.7 plots sample distributions of plastic strain in the soil over the elements located at the distances of $L/4$, $L/2$, and $3L/4$ from the pulling end. It reveals that the plastic strains developed within a thin zone of soil around the pipe surface that is higher near the pulling end (i.e., at $L/4$) and decreases with distances from the pulling end (i.e., $3L/4$). For changing the dilation angle from 8° to 18°, the volumetric strain was increased by about 0.3% within the pipe vicinity. The volumetric strain (dilation) was concentrated near the pipe crown above which the soil was not restrained. As a result, the dilation of soil did not cause significant increase of stresses on the pipe surface.

The comparisons in Figure 6.6 also reveal that the rate–dependent interface friction angles of

$0.75\phi'$, $0.86\phi'$, and $0.90\phi'$, corresponding to the pulling rates of 0.5, 1, and 2 mm/min, respectively, for pipes in loose to medium-dense sands (Reza and Dhar 2021a), are applicable for the MDPE pipes buried in dense sand. The method of applying temperature load appears to successfully simulate the compaction-induced effects, reasonably simulating the pullout forces observed during the tests.

Note that the burial depths of the pipes were less during the tests in Reza et al. (2023), at 340 mm and 480 mm. As seen in Figure 6.4, the compaction-induced horizontal stress is significant for shallow buried pipes with depths less than ~1.0 m. To evaluate this further, pipe tests with a shallow burial depth (0.57 m) and a greater burial depth (0.98 m) available in Wijewickreme and Weerasekara (2015) were analyzed. Wijewickreme and Weerasekara (2015) conducted an axial pullout test with a 60-mm diameter MDPE pipe at the burial depths of 0.57 m and 0.98 m. The information of the test with 0.98 m burial depth included sample length, L = 8.5 m, unit weight of soil, γ = 15.8 kN/m^3, and pulling rate = 2.185 mm/min. The soil parameters for these conditions were estimated as E_s = 6 MPa [Eq. (6.1)], ϕ' = 45°, ψ = 12°, and $\delta = 0.9\phi$. As the burial depth was close to 1.0 m, no effect of compaction-induced stress was anticipated. Therefore, no temperature load was applied during the analysis. The test conditions with 0.57 m burial depth were L = 8.5 m, γ = 16.1 kN/m^3, and pulling rate = 2.145 mm/min) (Wijewickreme and Weerasekara, 2015). Based on the information, the soil parameters were estimated as E_s = 5 MPa [Eq. (6.1)], ϕ' = 45°, ψ = 12°, and $\delta = 0.9\phi$. For the pipe burial depth of 0.57 m, the compaction-induced additional horizontal pressure at the pipe springline was calculated as 14.15 kPa [equivalent to the temperature loading of 57 °F, according to Eq. (6.5)]. Figure 6.8 shows the results of FE calculations that match well with the data extracted from Wijewickreme and Weerasekara (2015). Thus, the compaction-

induced horizontal stress proposed in Duncan and Seed (1986) was applicable for the test conditions.

In Figure 6.6 (also in Figure 6.8), the pullout forces increase nonlinearly with the pulling displacements, both from the experiments and the FE analysis. Nonlinearity is associated with the progressive mobilization of interface shearing resistance, starting from the leading end towards the trailing end. This mechanism was observed earlier in Weerasekara and Wijewickreme (2008), Reza and Dhar (2021ab), and Reza et al. (2023). The pullout force increased until the shear strength at the pipe–soil interface was fully mobilized over the entire pipe sample length. Beyond the point of full mobilization, the experimental pulling forces are slightly reduced due to the release of the trailing end, demonstrating the release of the load from the pipe to the surrounding soil. The FE calculations were intended to model up to the peak pullout force, as the mechanism beyond the peak is influenced by the test cell length and, therefore, not expected in the field.

A parallel set of tests corresponding to Tests 1–5 was also conducted in Reza et al. (2023), where the pipe wall strains were measured at three locations at distances of one-fourth ($L/4$), half ($L/2$), and three-fourths ($3L/4$) from the leading end. Although the strain gauges were reported to affect the surface roughness and pullout resistance, the measurements provided a general understanding of the load transfer mechanism along the pipe length. The strain measurements demonstrated gradual load transfer from the leading end toward the trailing end for flexible MDPE pipes. As a result, the strain gauge located toward the leading end showed a reading first, and then the following gauges read subsequently. The measured strains are compared with the FE calculations in Figure 6.9, showing general agreements of the load transfer mechanism. During the

application of an axial displacement, the flexible MDPE pipes start elongating from the leading end, propagating gradually towards the trailing end. The axial deformation can be observed from the FE calculation, as seen in Figure 6.10. For example, the leading end of the pipe section is elongated by an amount equal to the applied displacement (30 mm), while the deformation at the trailing end is zero (Figure 6.10).

6.4.2 *Interface Stresses*

Ground load is transferred to the pipe through the pipe–soil interface when subjected to ground movements. However, the interface stresses could not be measured during the tests (Reza et al. 2023). Since the FE model reasonably simulated the test results, the interface stresses from the FE analysis were examined. Figure 6.11 shows the normal interface stresses around the pipe circumferences due to the installation loads (gravity and compaction-induced loads). As seen in the figure, the stresses are higher on the sides (around the springline) and less at the top (crown) and bottom (invert). The side stresses are higher for the 42-mm diameter pipes than for the 60-mm diameter pipes, due to higher compaction-induced load for the smaller pipe buried at relatively shallow depths. During axial pullout, the normal interface stresses (or contact stress) offer frictional resistance to pipe movements. However, the normal stress can increase due to shear-induced dilation and decrease due to the pipe diameter reduction that can affect the pullout resistance.

The variation of normal stresses at three different points along the pipe length (i.e., at the distances of $L/4$, $L/2$, and $3L/4$ from the pulling end) at the springline are plotted in Figure 6.12 against the pulling displacements (leading end displacements). The stress was the maximum at the

springline. Figure 6.12 shows that the normal stresses are higher for the 42-mm diameter pipe than for the 60-mm diameter pipes. As a result, normalized pullout resistance was higher from the tests for the 42-mm diameter pipes than for the 60-mm diameter pipe (Reza et al. 2023). The higher normal stress for the 42-mm diameter pipe is due to the higher compaction-induced stress associated with shallower burial depth. As seen in Figure 6.12, the normal stresses initially increase with the leading end displacement due to the dilation effects for the 42-mm diameter pipes but not for the 60-mm diameter pipes. Thus, the dilation-induced stress increase was also higher for the pipe at the shallow burial depth, where the contact pressure was higher. The effect of shear-induced dilation is insignificant for the 60-mm diameter pipe, due to lower contact pressure on the pipe. After certain leading end displacements, the normal stresses decreased with the displacements for both pipes (Figure 6.12). The normal stress reduction is attributed to the pipe diameter decrease during axial pulling that was observed in the FE calculations. Beyond the points of trailing end movement, the contact stresses are constant when the shear strength is mobilized over the entire pipe sample.

Figure 6.12 also reveals that the normal stresses at different points start changing from the initial values (before pullout) at different leading end displacements due to the gradual mobilization of the axial forces. The interface shear strength mobilization was also consistent with the changes in the normal stresses (Figure 6.12). Figure 6.12 plots the circumferential averaged shear stresses at particular locations of the pipes (i.e., $L/4$, $L/2$, $3L/4$) against the pipe displacements at those locations. The shear stress at any point increased once the elongation (or relative displacement between pipe element and soil element) was initiated and reached the peak shear strength (Figure 6.13). Beyond the peak values, the mobilized shear strengths were less due to the reduction of the

normal stresses. The peak shear strengths were reached at around 1.0 mm and 0.7 mm elongations for the 42- and 60-mm diameter pipes, respectively. Note that the elongation corresponding to the peak shear strength is not constant but depends on the normal stress and pipe diameter. Thus, the pipe–soil interface behaviour is very complex and might be difficult to incorporate into the spring model recommended in the design guidelines. However, the pipelines in service possess high internal pressure. As a result, the pipe diameter decrease and normal stress change may be less under axial force. However, a normal stress adjustment factor, ζ, can be used to account for the interface stress change during axial pullout, as discussed below.

6.4.3 *Maximum Spring Force*

As discussed above, the employed 3D FE modelling technique can reasonably simulate the soil–pipe interaction for the pipes subjected to axial ground movements. However, the 3D continuum-based modelling technique is often not preferred in the conventional assessment and design of buried pipelines. Existing design guidelines recommend using the beam-on spring analysis. Eq. (6.6) was recommended to calculate the maximum spring force per unit length based on the maximum interface shear resistance for pipes in cohesionless soils.

$$p_u = \pi D \left(\frac{\gamma H + K_0 \gamma H}{2}\right) \tan(\delta) \qquad (6.6)$$

In Eq. (6.6), the normal stress on the pipe surface is assumed as the average of the vertical overburden stress (γH) and at-rest lateral earth pressure ($K_0 \gamma H$) at the pipe springline. The equation does not account for compaction-induced lateral stress and the changes in contact pressure due to shear-induced dilation or pipe diameter change. It is proposed to increase the lateral earth pressure by the compaction-induced lateral earth pressure ($\Delta\sigma_{com}$) and include the normal stress adjustment factor (ζ) to account for the contact pressure change [Eq. (6.7)].

$$p = \zeta \pi D \left(\frac{\gamma H + K_0 \gamma H + \Delta\sigma_{com}}{2} \right) \tan(\delta) \quad (6.7)$$

where $\Delta\sigma_{com}$ can be obtained using the procedure described in Duncan and Seed (1986). The factor, ζ, depends on a number of factors, including interface stress level, internal pressure, stiffness of the soil and pipe materials, and interface friction angle. It can be determined from laboratory pipe pullout tests under specific conditions expected in the field using Eq. (6.8).

$$\zeta = \frac{Pullout\ resistance\ from\ tests}{\pi D L \left(\frac{\gamma H + K_0 \gamma H + \Delta\sigma_{com}}{2} \right) \tan(\delta)} \quad (6.8)$$

Detailed 3D FE analysis can also be performed, and the factor can be calculated as the ratio of circumferential averaged normal contact stress to the average of the geostatic stress (vertical and horizontal earth pressure after backfilling) [Eq. (6.9)].

$$\zeta = \frac{\sigma'_{avg}\ \text{from FE analysis}}{\frac{\gamma H + K_0 \gamma H + \Delta\sigma_{com}}{2}} \quad (6.9)$$

For the tests analyzed in the current study, the factor ζ varied along the pipe length due to the pipe diameter change. Variation of ζ along the pipe length, calculated from FE analysis using Eq. (6.9), is shown in Figure 6.14 at the maximum pulling force. It shows a very low value (e.g., 0.21) at the leading end and close to unity at the trailing end of the pipes. The average value of the factor was estimated as 0.48 to 0.50. A similar value (i.e., 0.50) was calculated from the experiment using Eq. (6.8).

6.5 Beam-on-Spring Analysis

Since the 3D continuum-based pipe–soil interaction analysis is computationally demanding, the beam-on-spring analysis is generally used for pipeline analysis. The performance of beam-on-spring analysis has been evaluated through comparison with the test results in Reza et al. (2023). The analysis was performed using Abaqus. The pipeline was modelled as a Timoshenko beam

using PIPE21 elements, and the soil–pipeline interaction (PSI) was modelled using the pipe–soil interaction element (PSI24) in Abaqus. The pipe was discretized with a uniform element size of 1 mm. The width of the PSI elements is the same as the length of the pipe element, as the PSI elements share the same nodes with the pipe elements (as discussed later). A mesh sensitivity analysis was conducted by varying the element sizes, and no noticeable change in pullout resistance was observed for element sizes smaller than 1 mm.

6.5.1 *PSI Elements*

The PSI element defines the soil as a Winkler media. The element interacts with the structural beam element, as illustrated in Figure 6.15. One edge of the element shares nodes with the beam-type elements that model the pipeline. The nodes on the other edge represent a far-field surface, such as the ground surface. Thus, the element's depth is equal to the height of the ground surface from the pipe springline, H. It has only the displacement degrees of freedom at its nodes. The relative displacements between two edges of the PSI elements transmit force to the pipeline through their stiffness. The interaction between pipe and soil can be modelled in four different directions: axial (longitudinal), transverse horizontal, vertical upward, and vertical downward. A suitable constitutive model can define the force–displacement relation of the PSI elements in each direction. The force–displacement relation of PSI elements can be defined using tabular input as force per unit length at each point along the pipeline caused by relative displacement between that point and the point on the far-field surface. The degrees of freedom on the far-field nodes are fully fixed in this study.

6.5.2 *Model Parameters*

The PSI element requires spring parameters in axial, vertical, and lateral directions. The existing design guidelines (e.g., ALA 2005) recommend bilinear elastic-perfectly plastic spring models. The spring models are defined using the ultimate forces and the corresponding relative displacements. As the current study focuses on axial pullout behaviour, only the parameters for axial spring were relevant and discussed here. According to the current guidelines, the ultimate axial spring force (p_u) per unit length for dense sand is given by Eq. (6.6). The corresponding relative displacement (x_u) is 3 mm. However, based on the study discussed in this paper, Eq. (6.7) is proposed to estimate the maximum spring force for the MDPE pipes in dense sand. The spring parameters calculated based on Eq. (6.6) and Eq. (6.7) for each of the tests (Reza et al. 2023) are compared in Table 6.2. The relative displacement recommended in ALA (2005) is considered applicable. The loading rate–dependent interface friction angle was used to calculate the maximum spring force (after Reza and Dhar 2021a). Analyses were performed using both sets of spring parameters (Table 6.2) to investigate the effects.

6.5.3 *Comparison of Results*

Figure 6.16 compares the load–displacement responses from the FE analysis with those from the experiments for 42.2 mm (Test 1–3) and 60.3 mm (Test 4–5) diameter pipes. The FE calculations with the maximum spring force proposed by Eq. (6.7) reasonably simulate the load–displacement responses. Although the spring force for the test condition varied along the pipe length, a constant value of the spring force successfully simulated the responses. Thus, the effect of the variation of the spring force is less significant for the length of the pipe sample considered. However, the FE analyses with the spring force from Eq. (6.6) underestimated the responses. The difference

between FE calculations based on Eq. (6.6) and test results is large for the shallow buried pipes (42-mm diameter pipes) due to higher compaction-induced stresses in the test conditions. Note that the difference between the maximum spring forces obtained from Eq. (6.6) and Eq. (6.7) is due to the effects of the compaction-induced lateral earth pressure, $\Delta\sigma_{com}$. As the compaction-induced lateral earth pressure is less for deeper burial depths (Figure 6.4), the difference between the FE calculations based on two sets of spring parameters is less. Thus, the spring parameters recommended in the design guidelines might apply to deeply buried pipes. However, the effect of shear-induced dilation and pipe diameter decrease might contribute to the pipe responses that could be accounted for using the normal stress adjustment factor (ζ).

6.6 Conclusions

In this paper, a 3D continuum-based FE modelling technique was employed to understand the load transfer mechanism of buried MDPE pipes subjected to axial ground movement, simulating five test results conducted earlier by the authors. The compaction-induced effect on the lateral earth pressure was implemented in the analysis. Based on the findings from the analyses, a modification is proposed to the equation in the current design guidelines for calculating the maximum axial spring force for the analysis of pipes using beam-on-spring idealization. The major findings from the study are as follows.

- Compaction-induced horizontal stress can significantly influence the axial pullout resistance of shallow buried pipes. The compaction effect on earth pressure is significant at shallow depths and is negligible at greater depths.
- The lateral pressures due to compaction effects proposed by Duncan and Seed (1986) reasonably represent the test conditions investigated.

- The equivalent thermal load method successfully simulated the compaction effects on the earth pressure during FE analysis. The developed FE model successfully simulated the force–displacement responses and pipe wall strains observed in the tests. The FE simulations showed that increased contact stresses due to compaction effects increase the axial pullout resistances of the pipes.
- The rate–dependent interface friction angles of $0.75\phi'$, $0.86\phi'$, and $0.90\phi'$, corresponding to the pulling rates of 0.5, 1, and 2 mm/min, respectively, are applicable for the MDPE pipes buried in loose and dense sand.
- The normal contact pressure at the pipe–soil interface changes during the axial pullout of pipes, depending on the confining stresses around the pipe's cross-section. The shear-induced dilation increases the contact pressure, while pipe diameter reduction decreases the pressure. The normal contact pressure was increased due to shear-induced dilation for the shallow buried pipe, attributable to higher confining pressure. The dilation-inducted stress increase was negligible for deeply buried pipes.
- A normal stress adjustment factor ζ is proposed to account for the normal stress change on the pipe during the axial pullout. The factor can be determined from full-scale tests or 3D FE analyses simulating field conditions. For the pipes without internal pressure, the value of ζ is lowest at the leading end and highest at the trailing end. Based on the test results and the FE analysis, the average value of ζ over the entire pipe length was calculated as between 0.48 and 0.50 at the maximum pullout resistance. However, ζ can be higher over the pipe length for pipes subjected to internal pressure.
- The current design guidelines (i.e., ALA 2005) recommend beam-on-spring analysis for the pipes subjected to ground movements. However, the analyses with the maximum spring

force recommended in the design guidelines may not simulate the pipe responses correctly. A modification to the current design equation to calculate the maximum spring force is proposed, incorporating the compaction-induced lateral earth pressure ($\Delta\sigma_{com}$) and the normal stress adjustment factor (ζ). The modified spring force could successfully be used to estimate the pipe responses observed during the tests.

6.7 Acknowledgments

The authors acknowledge the financial and/or in-kind support for this research provided by the Natural Science and Engineering Research Council of Canada, Innovate NL program of the Government of Newfoundland and Labrador, FortisBC Energy Inc. and WSP Canada Inc.

6.8 References

ALA (American Lifelines Alliance) (2005). *Guidelines for the design of buried steel pipe*. Washington, DC and Reston, VA, USA: Federal Emergency Management Agency (FEMA) and American Society of Civil Engineers (ASCE).

Almahakeri, M., Moore, I. D. & Fam, A. (2019). Numerical techniques for design calculations of longitudinal bending in buried steel pipes subjected to lateral Earth movements. *Royal Society Open Science*, **6**, No. 7, 181550.

Ansari, Y., Kouretzis, G. & Sloan, S. W. (2018). Development of a prototype for modelling soil–pipe interaction and its application for predicting uplift resistance to buried pipe movements in sand. *Canadian Geotechnical Journal*, **55**, No. 10, 1451–1474.

Bilgin, Ö., Stewart, H. E. & O'Rourke, T. D. (2007). Thermal and mechanical properties of polyethylene pipes. *Journal of Materials in Civil Engineering*, **19**, No. 12, 1043–1052.

Bolton, M. D. (1986). The strength and dilatancy of sands. *Géotechnique*, **36**, No. 1, 65–78.

Budhu, M. (2011). *Soil mechanics and foundations*. 3rd edition. John Wiley & Sons, Inc., United States of America.

CGA (Canadian Gas Association) (2021). *When Was Canada's Natural Gas Distribution System Built, and What Is It Made Of*? Energy Magazine, Issue 1.

Chakraborty, T. & Salgado, R. (2010). Dilatancy and shear strength of sand at low confining pressures. *Journal of Geotechnical and Geoenvironmental Engineering*, **136**, No. 3, 527–532.

Chen, T. J. & Fang, Y. S. (2008). Earth pressure due to vibratory compaction. *Journal of Geotechnical and Geoenvironmental Engineering*, **134**, No. 4, 437–444.

Chen, Q., Ni, P. & Qin, X. (2023). Numerical investigation on failure modes of bell-spigot jointed ductile iron pipelines subjected to dip-slip faults with different dip angles. *Tunnelling and Underground Space Technology*, **133**, 104982.

Daiyan, N., Kenny, S., Phillips, R. & Popescu, R. (2011). Investigating pipeline–soil interaction under axial–lateral relative movements in sand. *Canadian Geotechnical Journal*, **48**, No. 11, 1683–1695.

Das, S. & Dhar, A. S. (2021). Nonlinear Time-Dependent Mechanical behavior of a Medium Density Polyethylene Pipe Material. *Journal of Materials in Civil Engineering*, **33**, No. 5, 04021068.

Dassault Systems. (2019). ABAQUS/CAE user's guide, Providence, RI: Dassault Systemes Simulia.

Desai, C. S. (2016). Disturbed state concept as unified constitutive modeling approach. *Journal of Rock Mechanics and Geotechnical Engineering*, **8**, No. 3, 277–293.

Dezfooli, M. S., Abolmaali, A. & Razavi, M. (2014a). Coupled nonlinear finite-element analysis of soil–steel pipe structure interaction. *International Journal of Geomechanics*, **15**, No. 1,

04014032.

Dezfooli, M. S., Abolmaali, A., Park, Y., Razavi, M. & Bellaver, F. (2014b). Staged Construction Modeling of Steel Pipes Buried in Controlled Low-Strength Material Using 3D Nonlinear Finite-Element Analysis. *International Journal of Geomechanics*, **15**, No. 6, 04014088.

Dove, J. E. & Jarrett, J. B. (2002). Behavior of dilative sand interface in a geotribology framework. *Journal of Geotechnical and Geoenvironmental Engineering*, **128**, No. 1, 25–37.

Duncan, J. M. & Chang, C. Y. (1970). Nonlinear analysis of stress and strain in soils. *Journal of the Soil Mechanics and Foundations Division*, **96**, No. 5, 1629–1653.

Duncan, J. M. & Seed, R. B. (1986). Compaction induced earth pressures under K_0 conditions. *Journal of Geotechnical Enginnering*, **112**, No. 1, 1–22.

Duncan, J. M., Williams, G. W., Sehn, A. L. & Seed, R. B. (1991). Estimation earth pressures due to compaction. *Journal of Geotechnical Engineering*, **117**, No. 12, 1833–1847.

Elshimi, T. M. & Moore, I. D. (2013). Modeling the effects of backfilling and soil compaction beside shallow buried pipes. *Journal of Pipeline Systems Engineering and Practice*, **4**, No. 4, 04013004.

Fellenius, B. H. (2009). *Basics of Foundation Design*. Electronic: Calgary, AB, Canada. Available online: www.fellenius.net (accessed on 2 August 2022).

Guo, P. & Stolle, D. (2005). Lateral pipe-soil interaction in sand with reference to scale effect. *Journal of Geotechnical and Geoenvironmental Engineering*, **131**, No. 3, 338–349.

Janbu, N. (1963). Soil compressibility as determined by oedometer and triaxial tests. *Proceedings of the European Conference on Soil Mechanics and Foundation Engineering*, vol. 1, pp. 19–25. Essen, Germany: German Society for Earthworks and Foundations.

Jefferies, M. G. (1993). Nor-Sand: a simple critical state model for sand. *Géotechnique*, **43**, No. 1,

91–103.

Katona, M. G. (1978). Analysis of long-span culverts by the finite element method. *Transportation Research Record*, 678, Transportation Research Board, Washington, DC, 59–66.

Katebi, M., Wijewickreme, D., Maghoul, P. & Roy, K. (2021). Lateral force–displacement response of buried pipes in slopes. *Géotechnique*, 1–13.

Lee, L. L. & Seed, H. B. (1967). Drained Strength Characteristics of Sands. *Journal of the Soil Mechanics and Foundations Division*, **93**, No. 6, 117–141.

McGrath, T. J. (1998). *Pipe–soil interactions during backfill placement*, PhD dissertation, University of Massachusetts, Amherst, MA.

Murugathasan, P., Dhar, A. S. & Hawlader, B. C. (2021). An experimental and numerical investigation of pullout behaviour of ductile iron water pipes buried in sand. *Canadian Journal of Civil Engineering*, **48**, No. 2, 134–143.

Ni, P., Moore, I. D. & Take, W. A. (2018). Numerical modeling of normal fault-pipeline interaction and comparison with centrifuge tests. *Soil Dynamics and Earthquake Engineering*, **105**, 127–138.

O'Rourke, T. D., Druschel, S. J. & Netravali, A. N. (1990). Shear strength characteristics of sand-polymer interfaces. *Journal of Geotechnical Engineering*, **116**, No. 3, 451–469.

Paulin, M. J., Phillips, R., Clark, J. I., Hurley, S. & Trigg, A. (1997). Establishment of a full-scale pipeline/soil interaction test facility and results from lateral and axial investigations in sand. *Proceedings of the 16th International Conference of Offshore Mechanics and Arctic Engineering*. Yokohama, Japan: Ocean, Offshore and Arctic Engineering (OOAE) Division, American Society of Mechanical Engineers, vol. 5, pp. 139–146.

PHMSA (Pipeline & Hazardous Materials Safety Administration) (2015). *Fact Sheet: Pipeline*

Materials, U.S. Department of Transportation, New Jersey Avenue, Washington, DC 20590. https://primis.phmsa.dot.gov/comm/FactSheets/FSPipelineMaterials.htm (accessed on Nov. 4, 2022).

PRCI (Pipeline Research Council International) (2017). *Pipeline seismic design and assessment guideline*, Catalogue No: PR-268-134501-R01. Chantilly, VA, USA: PRCI.

Reza, A. & Dhar, A. S. (2021a). Axial Pullout behavior of Buried Medium Density Polyethylene Gas Distribution Pipes. *International Journal of Geomechanics*, **21**, No. 7, 04021120.

Reza, A. & Dhar, A. S. (2021b). Effects of Axial Relative Ground Movement on Small Diameter Polyethylene Piping in Loose Sand. *Infrastructures*, **6**, No. 12, 168.

Reza, A., Dhar, A. S. & Rahman, M. (2023). Strain assessment of polyethylene pipes in dense sand subjected to axial displacements. *Geosynthetics International*. (Accepted, in press)

Robert, D.J. & Thusyanthan, N. I. (2015). Numerical and experimental study of uplift mobilization of buried pipelines in sands. *Journal of Pipeline Systems Engineering and Practice*, **6**, No. 1, 04014009.

Roy, K., Hawlader, B., Kenny, S. & Moore, I. (2016). Finite element modeling of lateral pipeline–soil interactions in dense sand. *Canadian Geotechnical Journal*, **53**, No. 3, 490–504.

Roy, K., Hawlader, B., Kenny, S. & Moore, I. (2018). Upward pipe–soil interaction for shallowly buried pipelines in dense sand. *Journal of Geotechnical and Geoenvironmental Engineering*, **144,** No. 11, 04018078.

Saha, R. C., Dhar, A. S. & Hawlader, B. C. (2019). Shear strength assessment of a well-graded clean sand. *Proceedings of the 72nd Canadian Geotechnical Conf., GeoSt.John's 2019*, St. John's, Newfoundland and Labrador, Canada: Canadian Geotechnical Society.

Saha, R. C., Dhar, A. S. & Hawlader, B. C. (2020). Assessment of shear strength parameters of

moist sands using conventional triaxial tests. *Proceedings of the 73rd Canadian Geotechnical Conf., GeoVirtual 2020*, Virtual (Online), Canada: Canadian Geotechnical Society.

Saleh, A. E., Jalali, H. H., Pokharel, A. & Abolmaali, A. (2021). Deformation of buried large diameter steel pipes during staged construction and compaction-case study and finite element analysis. *Transportation Geotechnics*, **31**, 100649.

Sarvanis, G. C., Karamanos, S. A., Vazouras, P., Mecozzi, E., Lucci, A. & Dakoulas, P. (2017). Permanent earthquake-induced actions in buried pipelines: Numerical modeling and experimental verification. *Earthquake Engineering Structural Dynamics*, **47**, No. 4, 966–987.

Schlosser, F. (1982). Behaviour and design of soil nailing. *Proceedings of the symposium, Held at Asia Institute of Technology*, pp. 399–419.

Sheil, B. B., Martin, C. M., Byrne, B. W., Plant, M., Williams, K. & Coyne, D. (2018). Full-scale laboratory testing of a buried pipeline in sand subjected to cyclic axial displacements. *Géotechnique*, **68**, No. 8, 684–698.

Sheil, B. B., Martin, C. M. & Byrne, B. W. (2021). Simulation of overburden pressure during laboratory investigations of axial pipe–soil interaction. *Géotechnique*, **71**, No. 3, 272–278.

Taleb, B. & Moore, I. D. (1999). Metal culvert response to earth loading performance of two-dimensional analysis. *Transportation Research Record*, **1656**, No. 1, 25–36.

Wan, R. G. & Guo, P. J. (1998). A simple constitutive model for granular soils: Modified stress-dilatancy approach. *Computers and Geotechnics*, **22**, No. 2, 109–133.

Wang, F., Han, J., Khatri, D. K., Parsons, R. L., Brennan, J. J. & Guo, J. (2015). Field installation effect on buried steel-reinforced high density polyethylene pipes. *Journal of Pipeline Systems Engineering and Practice*, **7**, No. 1, 0401503.

Wang, F., Han, J., Corey, R., Parsons, R. L. & Sun, X. (2017). Numerical modeling of installation

of steel-reinforced high-density polyethylene pipes in soil. *Journal of Geotechnical and Geoenvironmental Engineering*, **143**, No. 11, 04017084.

Weerasekara, L. & Wijewickreme, D. (2008). Mobilization of soil loads on buried polyethylene natural gas pipelines subject to relative axial displacements. *Canadian Geotechnical Journal*, **45**, No. 9, 1237–1249.

Wijewickreme, D., Karimian, H. & Honegger, D. (2009). Response of buried steel pipelines subjected to relative axial soil movement. *Canadian Geotechnical Journal*, **46**, No. 7, 735–752.

Wijewickreme, D. & Weerasekara, L. (2015). Analytical modelling of field axial pullout tests performed on buried extensible pipes. *International Journal of Geomechanics*, **15**, No. 2, 04014044.

Yang, M., Taiebat, M. & Dafalias, Y. F. (2022). SANISAND-MSf: a sand plasticity model with memory surface and semifluidised state. *Géotechnique*, **72**, No. 3, 227–246.

Yao, Y. P., Sun, D. A. & Matsuoka, H. (2008). A unified constitutive model for both clay and sand with hardening parameter independent on stress path. *Computers and Geotechnics*, **35**, No. 2, 210–222.

Yimsiri, S., Soga, K., Yoshizaki, K., Dasari, G. & O'Rourke, T. D. (2004). Lateral and upward soil–pipeline interactions in sand for deep embedment conditions. *Journal of Geotechnical and Geoenvironmental Engineering*, **130**, No. 8, 830–842.

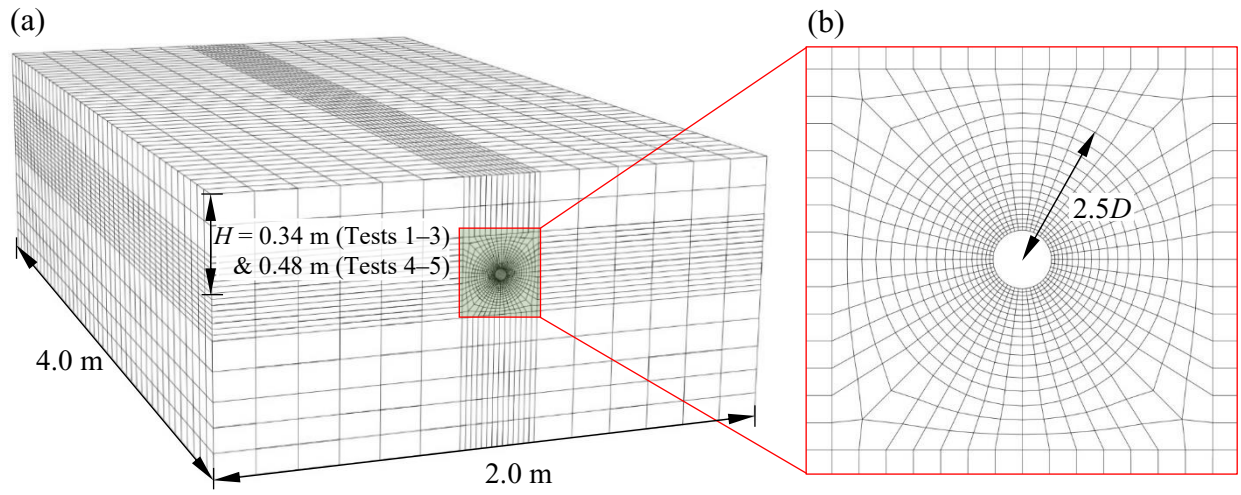

Figure 6.1: A typical FE model of the pipe–soil system: (a) 3D FE mesh; and (b) cross-section near the pipe

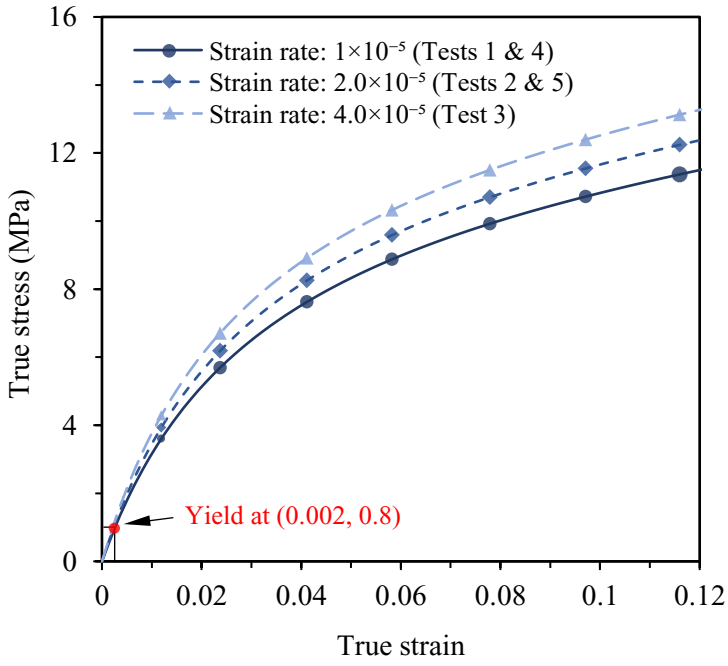

Figure 6.2: True stress–strain responses for MDPE pipes (after Das and Dhar 2021)

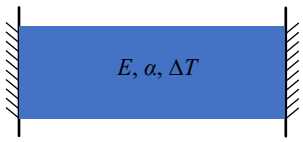

Figure 6.3: Model for thermal load calculation (after Saleh et al. 2021)

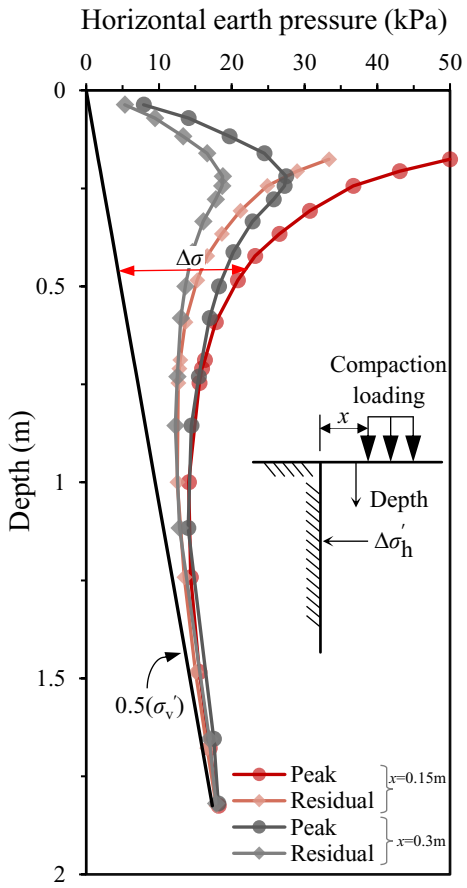

Figure 6.4: Calculated compaction-induced lateral earth pressure, after Duncan and Seed (1986)

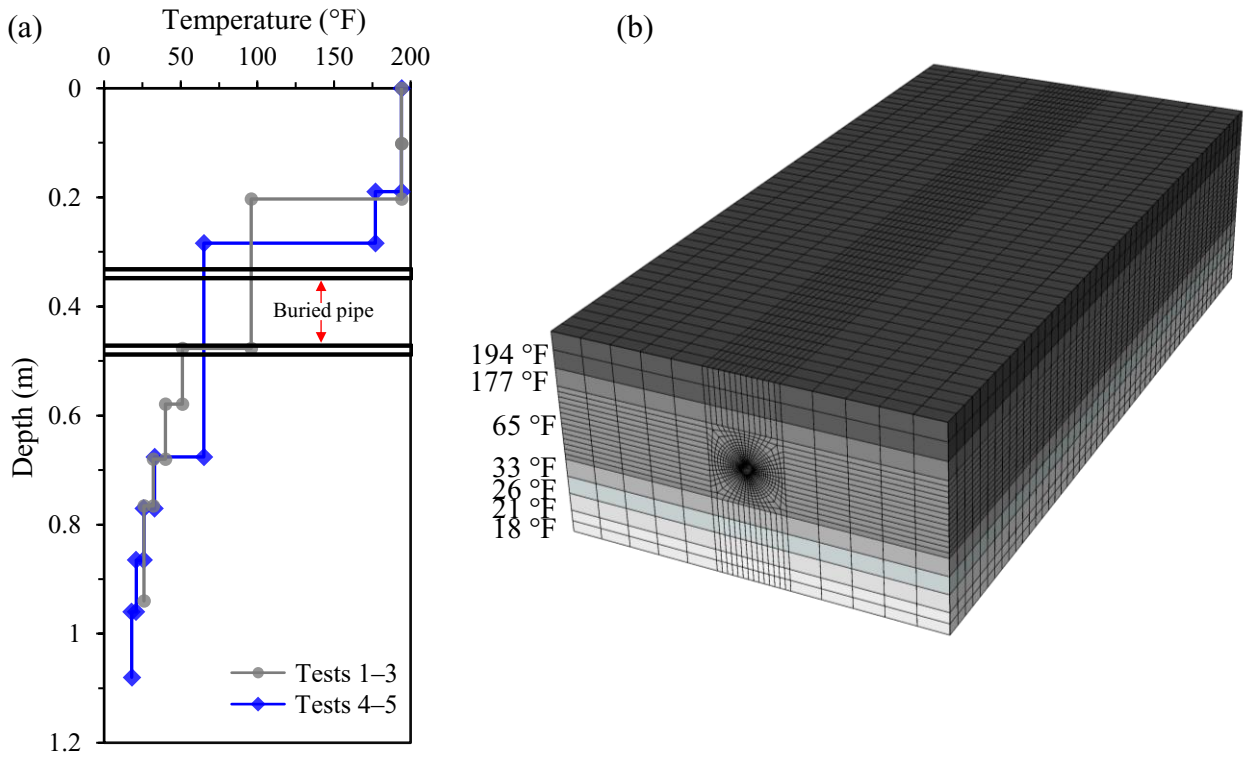

Figure 6.5: Compaction modelling: (a) Applied temperature to the backfill soil layers; and (b) FE model (Tests 4–5)

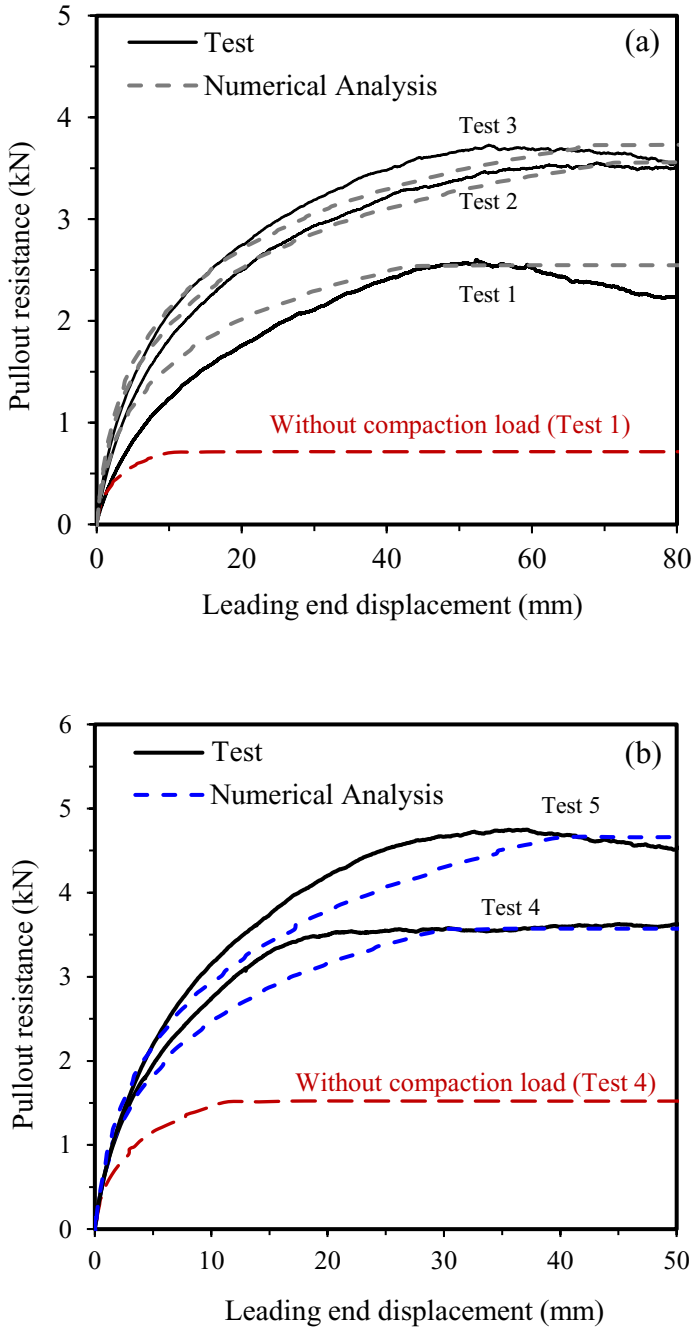

Figure 6.6: Comparison of pullout resistances with measurements: (a) D = 42.2-mm; (b) D = 60.3-mm

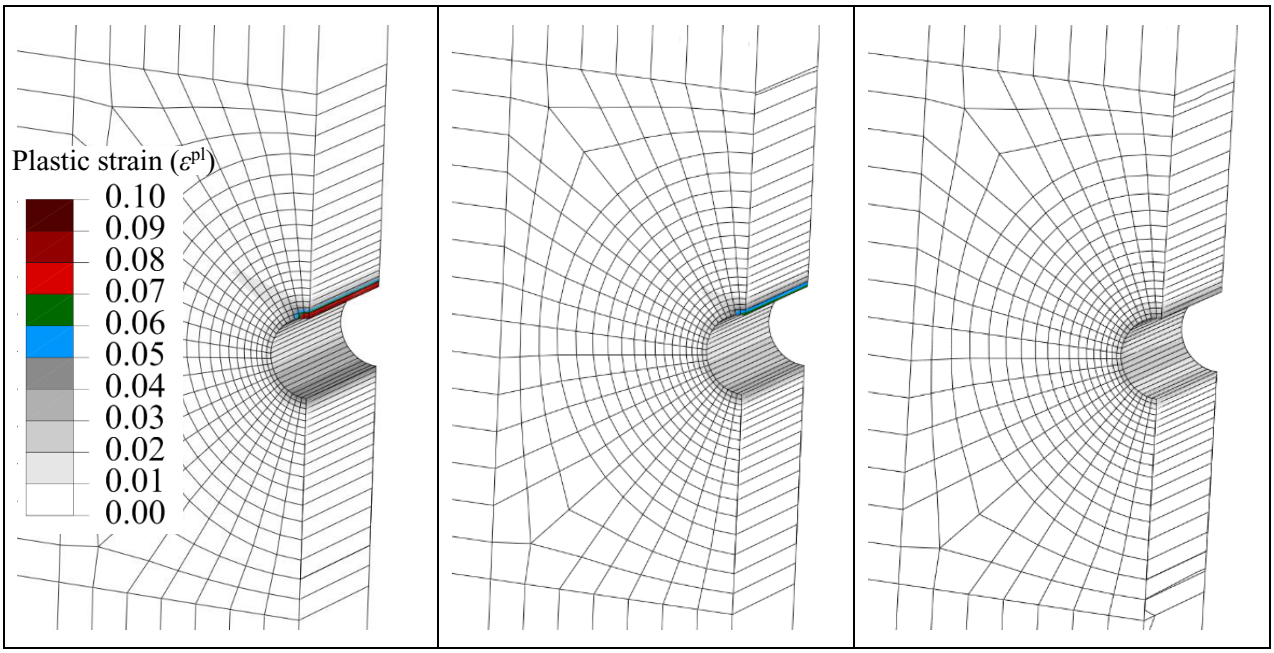

Figure 6.7: Plastic strain distributions at peak pullout load in Test 2 (FE): (a) $L/4$; (b) $L/2$; and (c) $3L/4$

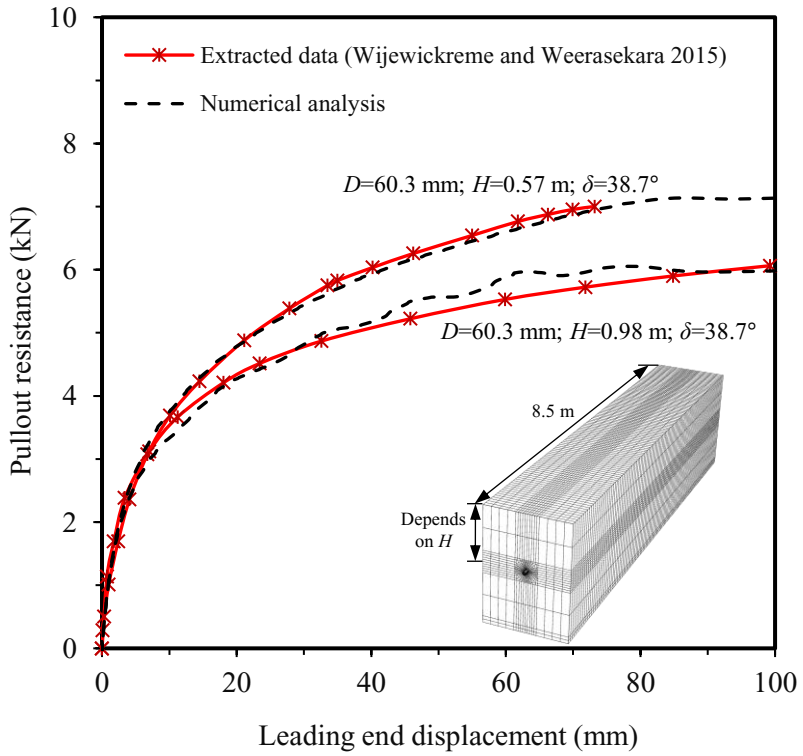

Figure 6.8: Comparison of pullout resistances with measurements in Wijewickreme and Weerasekara (2015)

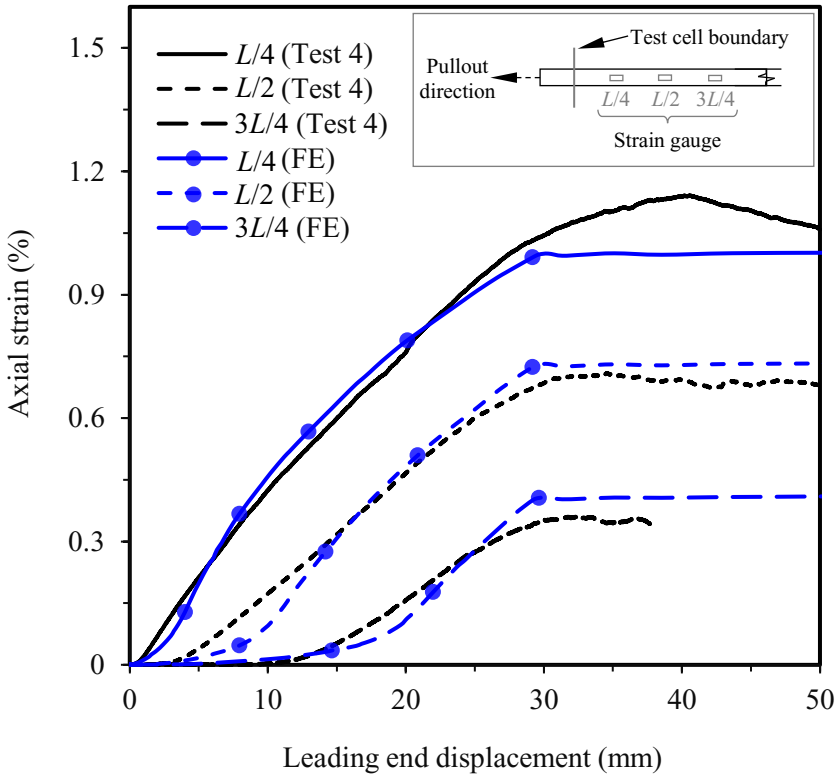

Figure 6.9: Comparison of axial strains at various locations in Test 4 (parallel test)

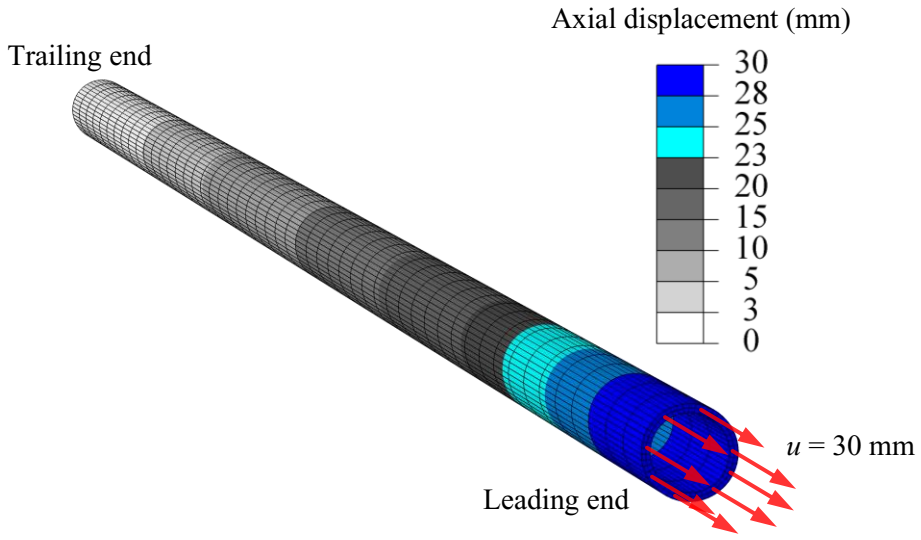

Figure 6.10: Axial displacement along the pipe length in Test 4 (FE calculation)

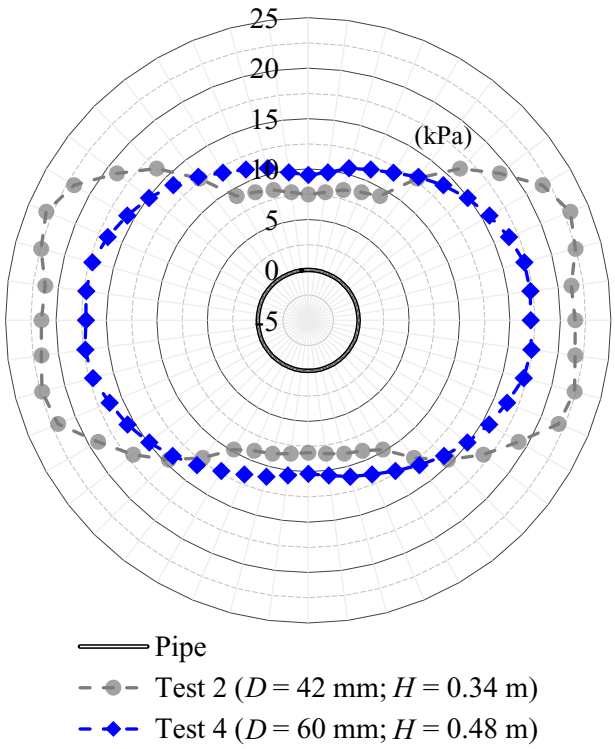

Figure 6.11: Interface normal stresses around the pipe circumference after installation in Test 2 and Test 4

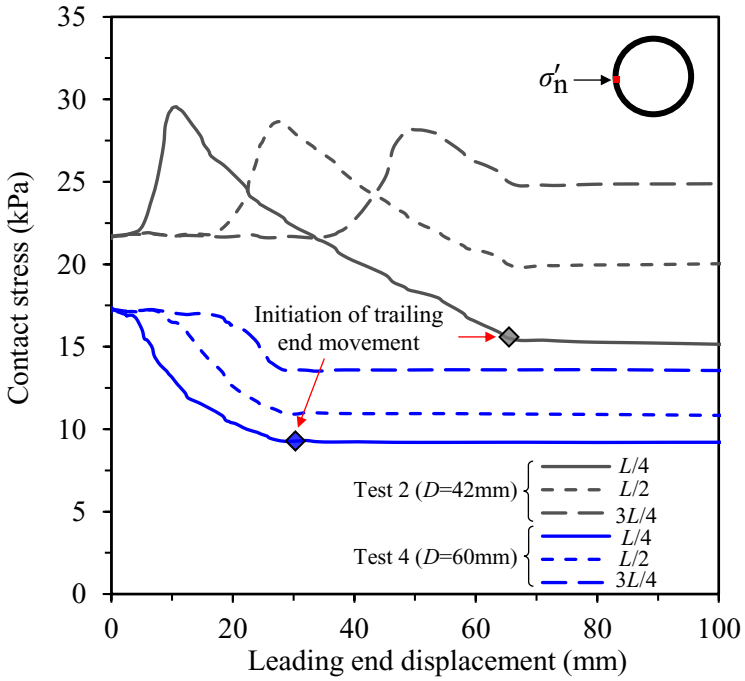

Figure 6.12: Changes in contact normal stresses at pipe springline in Test 2 and Test 4 (FE)

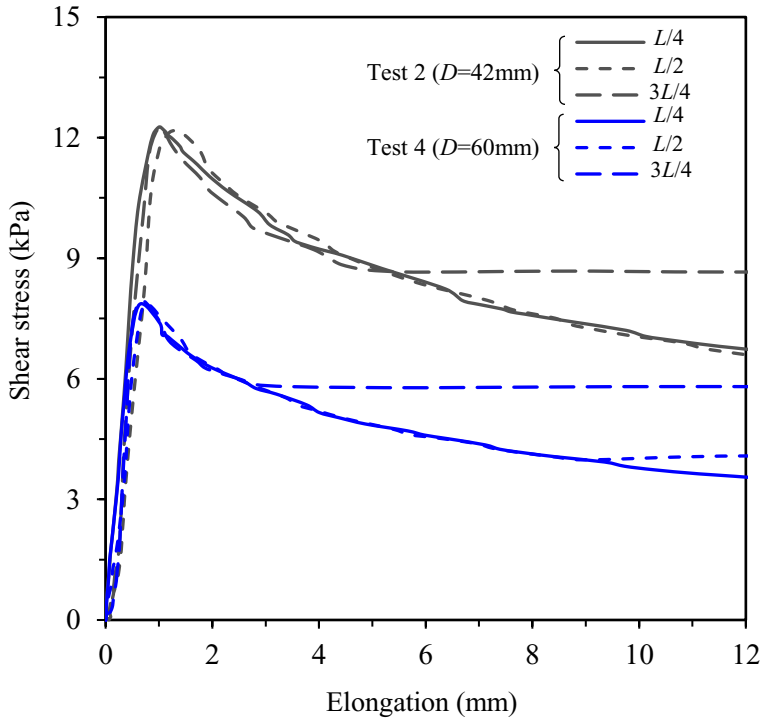

Figure 6.13: Variation of shear stresses with displacements of pipe points

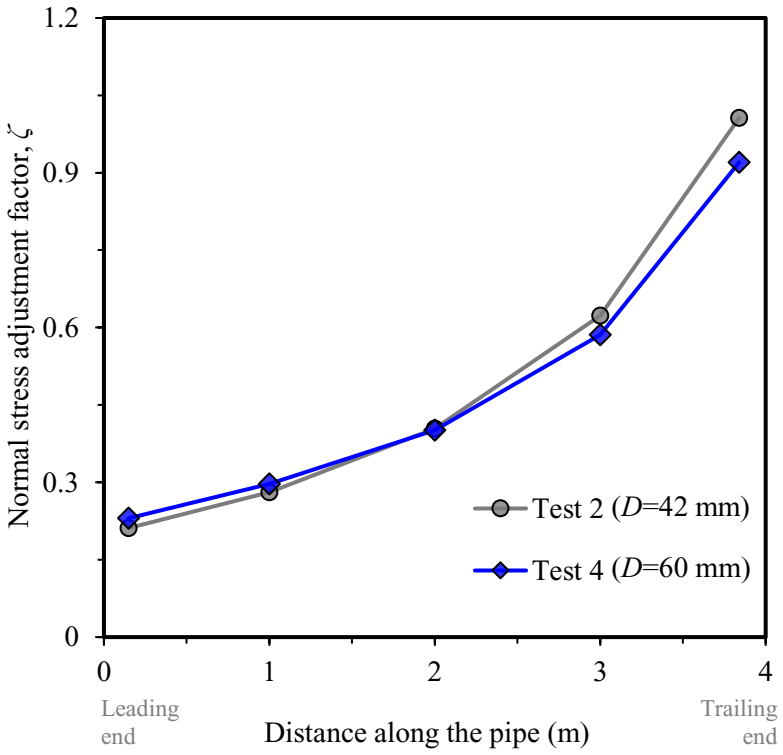

Figure 6.14: Variation of normal stress adjustment factor

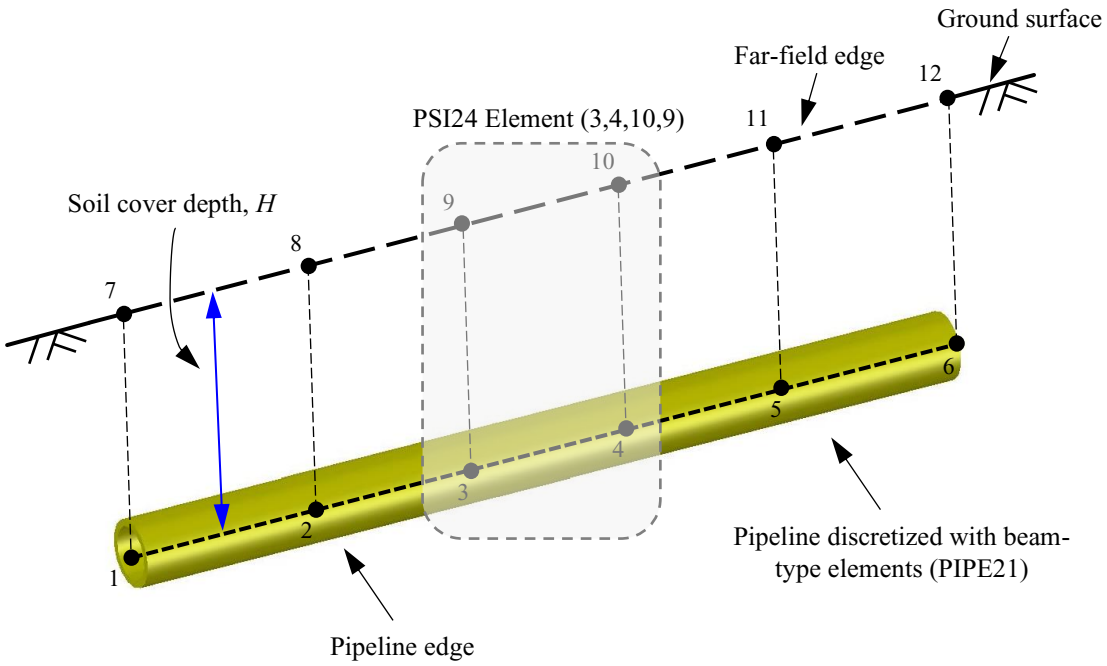

Figure 6.15: Pipe–soil interaction (PSI) model

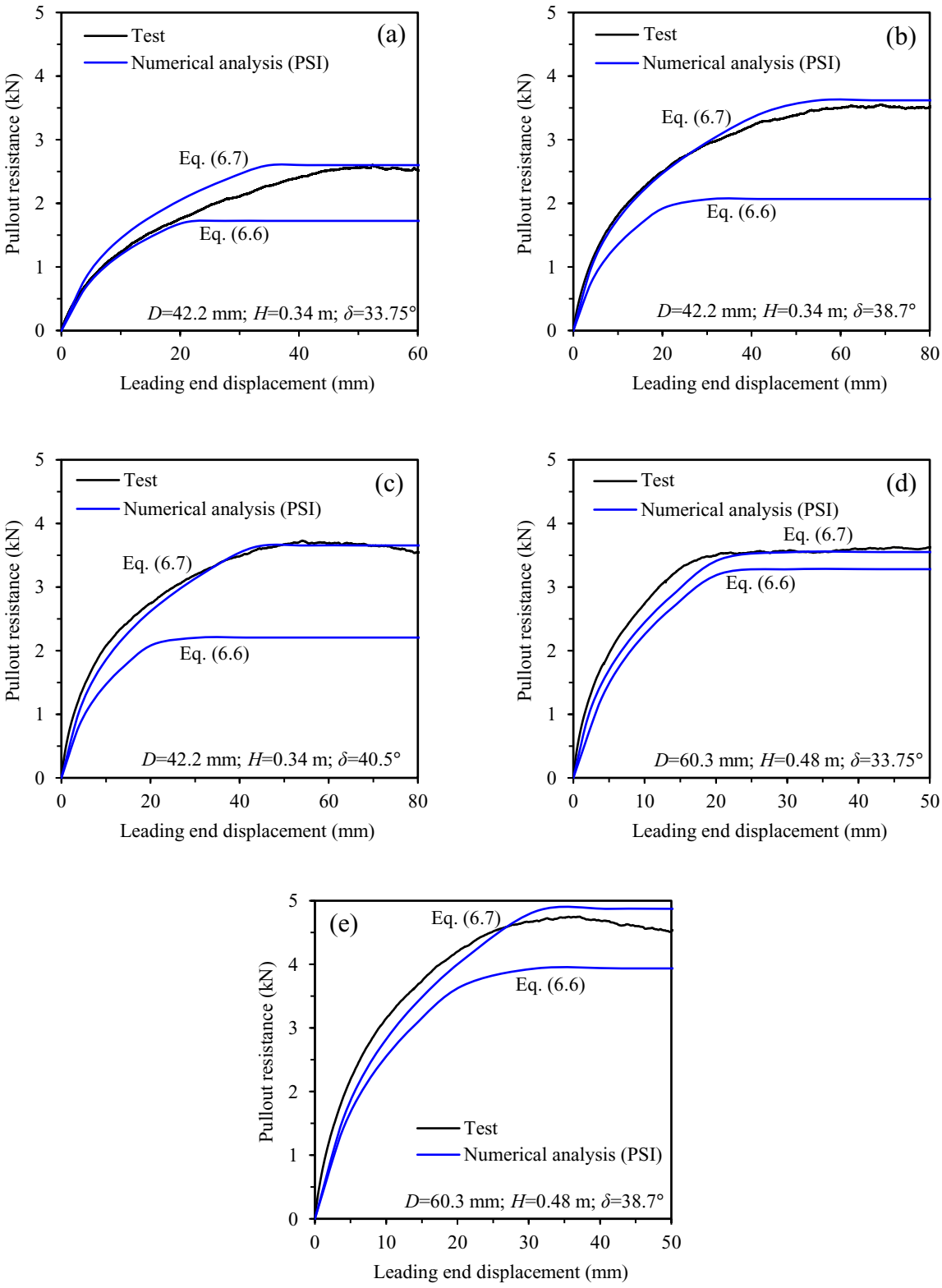

Figure 6.16: Comparison of results for: (a) Test 1; (b) Test 2; (c) Test 3; (d) Test 4; and (e) Test 5

Table 6.1. Summary of the test program (After Reza et al. 2023)

Test No	Avg. unit weight, $\overline{\gamma}$ (kN/m^3)	Burial depth, H (m)	Pulling rate (mm/min)	Pipe diameter, D (mm)	Wall thickness, t (mm)
1–3	19	0.34	0.5, 1, 2	42.2	4.22
4–5	18	0.48	0.5, 1	60.3	5.48

Table 6.2. Spring parameters

Test no.	Axial resistance (N/m)		Axial elastic displacement (mm)
	Eq. (6)	Eq. (7)	
Test 1	429.2	640.4	3
Test 2	514.6	894.5	
Test 3	548.6	904.1	
Test 4	816.2	882.9	
Test 5	978.6	1209.5	

CHAPTER 7

Conclusions and Recommendations for Future Research

7.1 Conclusions

Buried pipelines often require passing through unstable ground where permanent ground deformations can occur. Due to the ground movements, the pipeline can undergo displacements and experience wall stresses/strains, which may eventually lead to the failure of the pipeline. The ability of the pipelines to respond safely to ground movements is an important consideration for safe and economical pipeline design. Therefore, the maintenance and operational decisions of the pipelines exposed to ground movements require evaluation of pipeline distress (i.e., wall strains) due to the forces from the moving ground. Studies on the responses of buried polyethylene (PE) pipe subjected to ground movement is very limited. With this background, the research work presented in this thesis involved full-scale testing of buried medium-density polyethylene (MDPE) pipes to develop a database of pipe responses under various ground conditions and finite-element (FE) modelling simulating the test conditions to explore the mechanics of soil–pipe interaction. Through exploring the mechanics of soil–pipe interaction, simplified methods are developed for pipe wall strain calculation.

The following general conclusions are drawn from the study presented in this thesis. The problem-specific conclusions are presented at the end of each chapter (Chapters 3–6) and in the appendices (Appendices A–E).

7.1.1 *Development of Simplified Methods for Strain Calculation for MDPE Pipes Buried in Loose to Medium-Dense Sand*

Six axial pullout test results of 60.3-mm diameter MDPE pipes in loose to medium-dense sands under three different pulling rates are presented in Chapter 3. FE analysis of the tests is also performed to interpret the observed behaviour and determine the soil–pipe interaction parameters. The pullout force on MDPE pipe is found to be influenced by the rates of pulling. The peak pullout force is higher for the tests with higher displacement rates, implying that the soil resistance on PE pipes depends on the rates of the relative ground movement. However, current design guidelines, ALA (2005) and PRCI (2009), do not take into consideration the rate of ground movements. The conventional Mohr–Coulomb (MC) model successfully simulated the peak soil resistance during the axial pullout. One of the key findings of the present study is that the loading rate effect is found to be more significant on the pipe–soil interface behaviour, demonstrating that a rate–dependent interface friction angle could be used to account for the loading rate–dependent effect.

The strain distribution is almost linear over the lengths of the interface friction mobilization, implying that the unit shear resistance at the pipe–soil interface can be assumed to be constant over the pipe length. Based on the findings from the test and FE analysis, the existing equation for maximum pullout force is modified by incorporating a pulling rate–dependent friction factor to calculate the axial pullout force. Finally, based on the assumption of the linear distribution of axial strain (i.e., axial force), a method is developed for calculating pipe wall strains based on relative ground movement.

7.1.2 *Evaluation of Pipe Strain Calculation Method for Small-Diameter Pipes*

Ground movement-related problems with small-diameter (i.e., 42.2-mm diameter) MDPE pipes are more complex due to their smaller sizes, intricate configurations, and components. The axial pullout tests on 42.2-mm diameter pipes in loose sand are presented in Chapter 4 under various rates of relative axial displacement. Similar to 60-mm diameter pipes, as discussed in Chapter 3, the pullout force of the 42-mm diameter pipe also increases with the rate of relative ground movement. It is seen that the maximum pullout force (non-dimensional) in loose/medium sand follows a general trend of increasing nonlinearly with the increase of pulling rate, regardless of pipe diameter. The FE analysis method applied in Chapter 3 is found to simulate the test results, confirming that the proposed analysis method is suitable for small-diameter pipes. The force–displacement curves obtained from FE analysis revealed that the pulling rate–dependent friction reduction factors for 42-mm diameter pipes reasonably match those for 60-mm diameter pipes (Figure 4.6).

Both for 42- and 60-mm diameter pipes, the effect of pipe diameter decrease on normal stress is less pronounced for the pipes in loose to medium-dense sands. The normal stress adjustment factor (ζ) is calculated as between 0.9 to 1. Linear distributions of the axial strains are also observed for the 42-mm diameter pipes presented in this chapter. Finally, it is found that the strain calculation method proposed in the previous chapter for a 60-mm diameter pipe can be used for 42-mm diameter pipes.

7.1.3 *Pipe Strain Calculation for MDPE Pipes in Dense Sand*

Chapter 5 presents full-scale laboratory tests performed to investigate the responses of 42.2- and 60.3-mm diameter MDPE gas distribution pipes in dense sand when subjected to axial ground movements. This chapter presents the results of a total of 11 tests: six with strain gauges and five without strain gauges.

The test results reveal that the effects of strain gauges for pipes in dense sand are significantly higher (up to 35%) than those for pipes in loose to medium-dense sand (around 10%). The load–displacement responses of the pipes are pulling-rate dependent. The pullout resistances are higher for higher pulling rates. Similar observations are previously reported for the same pipes buried in loose to medium-dense sand in Chapters 3 and 4. However, the non-dimensional pullout forces are significantly higher for pipes in dense sand than those in loose sand. The maximum axial pullout forces measured during the tests in dense sand are much higher than the forces calculated using the current guidelines. It is assumed that shear-induced dilation can increase the normal stress on the pipe wall during the axial pullout, resulting in a higher axial soil resistance. A normal stress adjustment factor based on a sawtooth-type model for cavity expansion theory is used to account for the dilation-induced increase of normal stress on the pipes for calculating the pullout resistance.

Strain distributions along the pipe length for different leading end displacements during the tests show a nonlinear distribution over the mobilized friction length (Figure 5.14). The nonlinearity is attributed to the nonlinear stress–strain relations of pipe material, particularly at high strains experienced by the pipes in dense sand. However, the strain distribution is linear for pipes in loose to medium-dense sand, where the pipe strains are relatively less (Figures 3.14 and 4.9). Assuming a parabolic distribution of the strains, a simplified method for calculating pipe

strains is proposed in Chapter 5. Using the proposed simplified method, a strain and strain rate–dependent constant modulus is used to analyze test results with time–dependent PE pipes.

7.1.4 *Developing FE Modelling Techniques for Dense Sand*

Note that, as discussed in Chapter 5, current design guidelines have been reported to underpredict the axial pullout resistance measured in laboratory tests for pipes buried in dense sand. Assuming that the shearing-induced dilation at the pipe–soil interface increases the normal stresses, which leads to a higher axial soil resistance, researchers applied the cavity expansion theory to estimate the normal stress increase on the MDPE pipe surface. However, it is known that the amount of dilation would depend on the roughness of the interacting surface, with a lesser amount of dilation on a smooth PE surface. On the other hand, pipes in dense sand can experience compaction-induced stress in the soil during backfilling, which can increase the interface frictional resistance, resulting in a higher pullout resistance of the pipe.

Chapter 6 numerically investigates the pipe–soil interaction for MDPE pipes in dense sand when subjected to axial loading, simulating five test results (without strain gauges on the pipe) reported in Chapter 5. The numerical study shows that FE modelling of pipes in dense sand is more complex than pipes in loose sand. Three-dimensional FE analysis revealed that the effect of shearing-induced dilation could be insignificant for MDPE pipes, depending on the magnitude of the earth pressures. It is found that compaction-induced horizontal stress can significantly influence the axial pullout resistance of shallow buried pipes. For deeply buried pipelines, the compaction effect on earth pressure is negligible. The compaction-induced lateral earth pressure increase is modelled using equivalent temperature loads. A temperature loading is applied only in

the direction perpendicular to the pipe axis for simulating the compaction-induced stress at any soil layer under fix-fix boundary conditions.

It is shown that the normal contact pressure is increased due to shear-induced dilation for the shallow buried pipe, attributable to higher contact pressure. The dilation-induced stress increase is negligible for deeply buried pipes due to lower contact pressure on the pipe. FE results also show that the calculated normal contact stresses at the interface can significantly decrease due to the pipe diameter reduction during axial pullout. As the pipe diameter reduces, the contact stress at the interface decreases, causing a reduction in the interface shearing stress at any section of the pipeline.

Finally, based on the findings, a modification to the current design equation to calculate the maximum axial spring force for pipes in dense sand is proposed in Chapter 6, incorporating the compaction-induced lateral earth pressure and a normal stress adjustment factor. The conventional beam-on-spring analysis with the modified spring force is performed using the pipe–soil interaction (PSI) element in Abaqus. Although the axial spring force (i.e., frictional shear force) for the test condition varied along the pipe length, as shown in Figure 6.12, a constant value of the spring force (as proposed in Eq. 6.6) successfully simulates the pipe responses observed during the tests.

7.2 Future Work and Recommendations

The following are some areas which could be studied further.

i. A very limited number of full-scale laboratory axial pullout tests for PE pipes with deeper burial depths (greater than 600 mm) is available in the literature. Additional tests for these conditions could be very useful for further validation of the present numerical simulations and simplified approaches.

ii. Direct measurement of soil stresses on the pipe, and their variation during pullout for PE pipes could be examined using tactile pressure sensors wrapped around a pipe. However, wrapping the pressure sensors along the pipe length could affect the interface property (i.e., pullout resistance of pipes). Further research is needed to address the issue and validate the current understanding of contact pressure.

iii. The present study investigates pipe responses to longitudinal tensile force using axial pullout tests. However, the longitudinal force can be tension or compression depending upon the locations of the pipe with respect to the moving ground. For example, a pipe segment toward the downstream boundary of the moving ground experiences axial compression. Buried pipeline response under axial compression loading could be considered as a future scope of work.

iv. Loading-reloading cycle is expected when the pipeline is subjected to intermittent ground movements. In addition, buried pipelines can experience cyclic axial displacement due to the changes in temperature of the transporting liquid, diurnal temperature fluctuations, and/or periodic pipeline start-ups and shutdowns. This cyclic nature of the axial loading can result in fatigue damage to the pipeline. Experimental studies could be performed to

investigate the influence of cyclic axial pipe displacements on the overall axial soil resistance of the pipeline.

v. Pipelines in service possess high internal pressure. Moreover, the reduction in PE pipe diameter due to pipe elongation during the axial pullout tests is expected to decrease with increased pressure inside the pipe. However, to the author's knowledge, no experimental study has explicitly considered pipes with internal pressure during pullout tests.

vi. In the current study and those in published literature, a buried pipe is pulled through a static soil mass to simulate the relative movement of the soil with respect to the pipe. Further studies, such as pulling the soil box with the buried pipe in it, would simulate real ground movement scenarios in the field.

vii. In the present study, soil behaviour is modelled using the built-in elastic-perfectly plastic MC model to capture the peak axial resistance. However, a more advanced and sophisticated constitutive model for the sand could better capture the complex pipe–soil interaction behaviour.

REFERENCES

ALA (American Lifelines Alliance) (2005). *Guidelines for the design of buried steel pipe*. Washington, DC and Reston, VA, USA: Federal Emergency Management Agency (FEMA) and American Society of Civil Engineers (ASCE).

Alam, S., Allouche, E. N., Bartlett, C., Sherpa, A. & Keil, B. (2013). Experimental evaluation of soil–pipe friction coefficients for coated steel pipes. *Proceedings of the Pipelines 2013: Pipelines and Trenchless Construction and Renewals—A Global Perspective*, Fort Worth, TX, USA, 23–26 June 2013, pp. 360–371.

Al-Khazaali, M. & Vanapalli, S. K. (2019a). A novel experimental technique to investigate soil–pipeline interaction under axial loading in saturated and unsaturated sands. *Geotechnical Testing Journal*, **43**, No. 1, 70–93.

Al-Khazaali, M. & Vanapalli, S. K. (2019b). Axial force–displacement behaviour of a buried pipeline in saturated and unsaturated sand. *Géotechnique*, **69**, No. 11, 986–1003.

Anderson, C. (2004). Soil–pipeline interaction of polyethylene natural gas pipelines in sand. *M.Sc. thesis*, Department of Civil Engineering, The University of British Columbia, Vancouver, BC, Canada.

Ansari, Y., Kouretzis, G. & Sloan, S. W. (2018). Development of a prototype for modeling soil–pipe interaction and its application for predicting uplift resistance to buried pipe movements in sand. *Canadian Geotechnical Journal*, **55**, No. 10, 1451–1474.

Bilgin, Ö. & Stewart, H. E. (2009a). Pullout Resistance Characteristics of Cast Iron Pipe. *Journal of Transportation Engineering*, **135**, No. 10, 730–735.

Bilgin, Ö. & Stewart, H. E. (2009b). Design Guidelines for Polyethylene Pipe Interface Shear Resistance. *Journal of Geotechnical and Geoenvironmental Engineering*, **135**, No. 6, 809–818.

The Canadian Broadcasting Corporation (CBC) news. (2014). Published online on Dec. 03, 2014.

CEPA (Canadian Energy Pipeline Association). (2016). Pipeline industry performance report. Accessed January 14, 2020. www.aboutpipelines.com/en/pipeline-101/pipeline-history/.

Chan, P. D. & Wong, R. C. (2004). Performance evaluation of a buried steel pipe in a moving slope: a case study. *Canadian Geotechnical Journal*, **41**, No. 5, 894–907.

CGA (Canadian Gas Association) (2021). When Was Canada's Natural Gas Distribution System Built, and 448 What Is It Made Of? *Energy Magazine*, Issue 1.

Cruden, D. M. & Varnes, D. J. (1996). *Landslide types and processes. Landslides—Investigations and mitigation*, pp. 36–75, edited by Turner, A. K. and Schuster, R. L. Special Report, 247. Washington, DC: Transportation Research Board.

Cugnetto, P., Robert, D. & Kajtaz, M. (2021). Improved Design Guidelines for Pipelines Subjected to Vertical Fault Movement in Dry Sand. *Journal of Pipeline Systems Engineering and Practice*, **12**, No. 4, 04021056.

DeJong, J. T. & Westgate, Z. J. (2005). Role of overconsolidation on sand-geomembrane interface response and material damage evolution. *Geotextiles and Geomembranes*, **23**, 486–512.

Dezfooli, M. S., Abolmaali, A. & Razavi, M. (2014a). Coupled nonlinear finite-element analysis of soil–steel pipe structure interaction. *International Journal of Geomechanics*, ASCE, **15**, No. 1, 04014032.

Dezfooli, M. S., Abolmaali, A., Park, Y., Razavi, M. & Bellaver, F. (2014b). Staged Construction Modeling of Steel Pipes Buried in Controlled Low-Strength Material Using 3D Nonlinear Finite-Element Analysis. *International Journal of Geomechanics*, ASCE, **15**, No. 6, 04014088.

Dove, J. E. & Frost, J. D. (1999). Peak friction behavior of smooth geomembrane–Particle interfaces. *Journal of Geotechnical Engineering*, **125**, No. 7, 544–555.

Dove, J. E. & Jarrett, J. B. (2002). Behavior of dilative sand interface in a geotribology framework. *Journal of Geotechnical and Geoenvironmental Engineering*, **128**, No. 1, 25–37.

Duncan, J. M. & Chang, C. Y. (1970). Nonlinear analysis of stress and strain in soils. *Journal of the Soil Mechanics and Foundations Division*, ASCE, **96**, No. 5, 1629–1653.

Esmaeilzadeh, M. (2019). Experimental and numerical modeling of lateral pipeline-trench interaction backfilled with sand. *M.Sc. thesis*, Department of Civil Engineering, Memorial University of Newfoundland, St. john's, NL, Canada.

EGIG (European Gas Pipeline Incident Data Group) (2020). *Gas Pipeline Incidents*: 11th Report of the European Gas Pipeline Incident Data Group (period 1970–2019), The Netherlands.

Elshimi, T. M. & Moore, I. D. (2013). Modeling the effects of backfilling and soil compaction beside shallow buried pipes. *Journal of Pipeline Systems Engineering and Practice*, ASCE, **4**, No. 4, 04013004.

Guo, P. J. & Stolle, D. F. E. (2005). Lateral Pipe–Soil Interaction in Sand with Reference to Scale Effect. *Journal of Geotechnical and Geoenvironmental Engineering*, **131**, No. 3, 338–349.

Jaky, J. (1944). The coefficient of earth pressure at rest. *Journal of the Society of Hungarian Architects and Engineers*, 355–358.

Kalaugher, P. G., Hodgson, R. L. P. & Grainger, P. (2000). Pre-failure strains as precursors of sliding in a coastal mudslide. Quarterly *Journal of Engineering Geology and Hydrogeology*, **33**, No. 4, 325–334.

Karimian, S. A. (2006). Response of buried steel pipelines subjected to longitudinal and transverse ground movement. *Ph.D. thesis*, University of British Columbia, Canada.

Keefer, D. K. & Johnson, A. M. (1983). Earth flows-Morphology, mobilization, and movement. *U.S. Geological Survey Professional Paper*, **1264**, 56.

Marino, G. & Osouli, A. (2020). Slip Resistance Behaviour of Coal Tar–Coated Steel Pipelines Buried in Clayey and Sandy Backfills from Ground Movement. *Journal of Pipeline Systems Engineering and Practice*, **11**, No. 3, 05020001.

Meidani, M., Meguid, M. A. & Chouinard, L. E. (2017). Evaluation of Soil–Pipe Interaction under Relative Axial Ground Movement. *Journal of Pipeline Systems Engineering and Practice*, **8**, No. 4, 1–10.

Meidani, M., Meguid, M. A. & Chouinard, L. E. (2018). A finite-discrete element approach for modeling polyethylene pipes subjected to axial ground movement. *International Journal of Geotechnical Engineering*, **14**, No. 7, 717–729.

Morshed, A. (2019). Numerical modeling of oblique pipeline–soil interaction in dense sand. M.Eng. thesis, Department of Civil Engineering, Memorial University of Newfoundland, St. john's, NL, Canada.

Muntakim, A. H. & Dhar, A. S. (2021). Assessment of Axial Pullout Force for Buried Medium-Density Polyethylene Pipelines. *Journal of Pipeline Systems Engineering and Practice*, **12**, No. 2, 04020074.

Murugathasan, P., Dhar, A. S. & Hawlader, B. C. (2021). An experimental and numerical investigation of pullout behaviour of ductile iron water pipes buried in sand. *Canadian Journal of Civil Engineering*, **48**, No. 2, 134–143.

Nakamura, T., Mitachi, T. & Ikeura, I. (1999). Direct shear testing method as a means for estimating geogrid–sand interface shear–displacement behaviour. *Soils and Foundations*, **39**, No. 4, 1–8.

O'Rourke, T. D., Druschel, S. J. & Netravali, A. N. (1990). Shear strength characteristics of sand-polymer interfaces. *Journal of Geotechnical Engineering*, **116**, No. 3, 451–469.

O'Rourke, M. J. & Nordberg, C. (1992). Longitudinal permanent ground deformation effects on buried continuous pipelines. Taipei, Taiwan: National Center for Earthquake Engineering Research, Project Number 90-3003.

O'Rourke, M. J., Liu, X. & Flores-Berrones, R. (1995). Steel pipe wrinkling due to longitudinal permanent ground deformation. *Journal of Transportation Engineering*, ASCE, **121**, No. 5, 443–451.

Paulin, M. J., Phillips, R., Clark, J. I., Trigg, A. & Konuk, I. (1998). A full-scale investigation into pipeline–soil interaction. *Proceedings of the International Pipeline Conference, IPC1998, ASME,* Calgary, Alberta, June 7–11, pp. 779–788.

Petley, D. N. (2004). The evolution of slope failures–Mechanisms of rupture propagation. *Natural Hazards and Earth System Sciences*, **4**, No. 1, 147–152.

Picarelli, L. & Russo, C. (2004). Remarks on the mechanics of slow active landslides and the interaction with man-made works, in Lacerda, W. A. *Proceedings of the 9th International Symposium on Landslides*, London, A.A. Balkema Publishers, **2**, 1141–1176.

PRCI (Pipeline Research Council International) (2017). *Pipeline seismic design and assessment guideline*. Catalogue No: PR-268-134501-R01. Chantilly, VA, USA: PRCI.

Reddy, E. S., Chapman, D. N. & Sastry, V. V. R. N. (2000). Direct shear interface test for shaft capacity of piles in sand. *Geotechnical Testing Journal*, **23**, No. 2, 199–205.

Robert, D. J. & Thusyanthan, N. I. (2015). Numerical and experimental study of uplift mobilization of buried pipelines in sands. *Journal of Pipeline Systems Engineering and Practice*, **6**, No. 1, 04014009.

Roy, K., Hawlader, B., Kenny, S. & Moore, I. D. (2016). Finite element modeling of lateral pipeline–soil interactions in dense sand. *Canadian Geotechnical Journal*, **53**, No. 3, 490–504.

Saberi, M., Annan, C. D., Konrad, J. M. & Lashkari, A. (2016). A critical state two-surface plasticity model for gravelly soil-structure interfaces under monotonic and cyclic loading. *Computers and Geotechnics*, **80**, 71–82.

Saberi, M., Annan, C. D. & Konrad, J. M. (2017). Constitutive Modeling of Gravelly Soil-Structure Interface Considering Particle Breakage. *Journal of Engineering Mechanics*, **143**, No. 8, 04017044.

Saberi, M., Annan, C. D. & Sheil, B. B. (2022). An efficient numerical approach for simulating soil-pipe interaction behaviour under cyclic loading. *Computers and Geotechnics*, **146**, 104666.

Sarvanis, G. C., Karamanos, S. A., Vazouras, P., Mecozzi, E., Lucci, A. & Dakoulas, P. (2017). Permanent earthquake-induced actions in buried pipelines: Numerical modeling and experimental verification. *Earthquake Engineering Structural Dynamics*, **47**, No. 4, 966–987.

Schlosser, F. (1982). Behaviour and design of soil nailing. *Proceedings of the symposium*, Held at Asia Institute of Technology, pp. 399–419.

Scarpelli, G., Sakellariadi, E. & Furlani, G. (2003). Evaluation of soil–pipeline longitudinal interaction forces. *Rivista Italiana di Geotecnica*, **4**, No. 3, 24–41.

Sherif, M. A., Fang, Y. S. & Sherif, R. I. (1984). K_A and K_0 Behind Rotating and Non-Yielding Walls. *Journal of Geotechnical Engineering*, **110**, No. 1, 41–56.

Sheil, B. B. Ã., Martin, C. M. Ã., Byrne, B. W. Ã., Plant, M., Williams, K. & Coyne, D. (2018). Full-scale laboratory testing of a buried pipeline in sand subjected to cyclic axial displacements. *Géotechnique*, **68**, No. 8, 684–694.

Sheil, B. B., Martin, C. M. & Byrne, B. W. (2021). Simulation of overburden pressure during laboratory investigations of axial pipe–soil interaction. *Géotechnique*, **71**, No. 3, 272–278.

Trautmann, C. H. & O'Rourke, T. D. (1983). Load–Displacement Characteristics of a Buried Pipe

Affected by Permanent Earthquake Ground Movements. Earthquake Behaviour and Safety of Oil and Gas Storage Facilities, Buried Pipe. and Equip., PVP-77, ASME, New York, June.

Vanapalli, S. K., Fredlund, D. G., Pufahl, D. E. & Clifton, A. W. (1996). Model for the Prediction of Shear Strength with Respect to Soil Suction. *Canadian Geotechnical Journal*, **33**, No. 3, 379–392.

Vanapalli, S. K. & Oh, W. T. (2013). A Model for Predicting the Modulus of Elasticity of Unsaturated Soils Using the Soil-Water Characteristic Curve. *International Journal of Geotechnical Engineering*, **4**, No. 4, 425–433.

Vanden Berghe, J. F., Cathie, D. & Ballard, J. C. (2005). Pipeline uplift mechanisms using finite element analysis. *Proceedings of the 16th International Conference on Soil Mechanics and Geotechnical Engineering*, Amsterdam, Netherlands: IOS Press, pp. 1801–1804.

Wang, F., Han, J., Corey, R., Parsons, R. L. & Sun, X. (2017). Numerical modeling of installation of steel-reinforced high-density polyethylene pipes in soil. *Journal of Geotechnical and Geoenvironmental Engineering*, ASCE. **143**, No. 11, 04017084.

Weerasekara, L. & Wijewickreme, D. (2008). Mobilization of soil loads on buried polyethylene natural gas pipelines subject to relative axial displacements. *Canadian Geotechnical Journal*, **45**, No. 9, 1237–1249.

Weerasekara, L. & M. Rahman. (2019). Framework for assessing the integrity of natural gas distribution pipes in landslide areas. *Proceedings of the 72nd Canadian Geotechnical Conf., GeoSt.John's 2019*, St. John's, Newfoundland and Labrador, Canada: Canadian Geotechnical Society.

Weidlich, I. & Achmus, M. (2008). Measurement of normal pressures and friction forces acting on buried pipes subjected to cyclic axial displacements in laboratory experiments. *Geotechnical*

Testing Journal, **31**, No. 4, 334–343.

Wijewickreme, D. & Weerasekara, L. (2015). Analytical Modeling of Field Axial Pullout Tests Performed on Buried Extensible Pipes. *International Journal of Geomechanics*, **15**, No. 2, 04014441-12.

Wijewickreme, D., Karimian, H. & Honegger, D. (2009). Response of buried steel pipelines subjected to relative axial soil movement. *Canadian Geotechnical Journal*, **46**, No. 7, 735–752.

Williams, N. D. & Houlihan, M. F. (1987). Evaluation of interface friction properties between geosynthetics and soils. *Proceedings of the Geosynthetics*, 616–627.

Yimsiri, S., Soga, K., Yoshizaki, K., Dasari, G. R. & O'Rourke, T. D. (2004). Lateral and upward soil–pipeline interactions in sand for deep embedment conditions. *Journal of Geotechnical and Geoenvironmental Engineering*, **130**, No. 8, 830–842.

Zhang, G., Wang, L. P. & Zhang, J. M. (2011). Dilatancy of the interface between a structure and gravelly soil. *Géotechnique*, **61**, No. 1, 75–84.

APPENDIX A

Full-Scale Laboratory Pullout Testing of 60-mm Diameter Buried MDPE Pipes

This paper has been published and presented in 7th International Conference on Engineering Mechanics and Materials, CSCE 2019, Laval (Greater Montreal), QC, Canada, June 12–15, 2019. Most of the research work presented in this paper was conducted by the first author. He also prepared the draft manuscript. The other authors supervised the research and reviewed the manuscript.

CSCE Annual Conference
Growing with youth – Croître avec les jeunes

Laval (Greater Montreal)
June 12 - 15, 2019

Full-Scale Laboratory Pullout Testing of 60-mm Diameter Buried MDPE Pipes

Auchib Reza [1], Ashutosh Sutra Dhar [1] and Abu Hena Muntakim [1]
[1] Department of Civil Engineering – Memorial University of Newfoundland, St. John's, NL, Canada

Abstract: Buried pipelines are extensively used for transporting oil, gas and water in Canada and worldwide, since pipelines are considered as the most convenient and economical means of transporting liquid and gas. The pipelines often cross active landslide areas, which are subjected to additional loads due to ground movements. Assessment of the effects of ground movements on the performance of the pipeline is, therefore, an important consideration for pipeline integrity assessment. The existing pipe design methods for the assessment of the performance of pipelines crossing active landslide area recommend using a simplified method to calculate maximum pullout force due to axial landslide without proper consideration of soil–pipe interaction. Researchers employed analytical and numerical modelling approaches to explain the soil–pipe interaction during relative ground movements. However, the assumptions used in the analytical and numerical models require validation with experimental evidence. In this research, a new full-scale pipe test facility has been developed to investigate the behaviour of flexible medium-density polyethylene (MDPE) pipes subjected to movements relative to the backfill soil. Pullout tests of 60-mm diameter MDPE pipes are performed using the test facility. The study reveals that the pullout behaviour of the pipe significantly depends on the viscoelastic response of the pipe material. Pipe strains developed almost linearly from the leading end to the tailing end when the shear strength is fully mobilized over the entire pipe length. Research findings demonstrate the need for considering the time–dependent effects of pipe materials in describing the soil–pipeline interaction during the axial pullout.

1 INTRODUCTION

Pipelines are the most efficient and common means of transporting fluids from one point to another. Pipes of different materials such as cast iron, ductile iron, steel and polymers are used for liquid and gas transportation and distribution systems. Polyethylene (PE) pipes have become popular owing to their corrosion resistant, fatigue resistant, leak-free joints, adaptability and other advantageous properties. Two types of polyethylene pipes, medium-density polyethylene and high-density polyethylene are widely used for new pipeline installation as well as for replacing the existing aged old pipeline systems. Due to the higher flexibility and long-term strength of medium-density polyethylene (MDPE) compared to high-density polyethylene (HDPE), more than 60% of pipes used in the natural gas distribution industry are MDPE materials (Stewart et al. 1999). Though polyethylene pipes can accommodate larger displacement than steel pipes, the ground movements have the potential to induce significant strain on the polyethylene piping system.

Ground deformation may occur from hazards that include a lateral spread of sloped surfaces, liquefaction, and differential soil movement at the fault lines. Ideally, the routing of a buried pipe is selected to avoid these natural hazards. Where this is not possible, the effects of postulated ground motions are considered

in the design. However, among the most threats associated with pipeline failure, ground movement/weather-related threat to onshore pipeline operation is reported to be 16% in North America and 15% in Europe (Mohitpour et al. 2010). Over the years, numerous studies have been conducted to understand the soil–pipe interaction mechanisms of the pipes subjected to ground movement (Wijewickreme et al. 2009; Bilgin et al. 2009; Liu et al. 2011; Sheil et al. 2016). Most of the earlier studies focused on understanding the behavior of steel pipe. The design methods developed based on steel pipes are often used in the design of PE pipes. However, the difference between the behaviors of PE and steel pipes subjected to ground loads are now well recognized. PE pipe materials are flexible compared to steel and show nonlinear time–dependent stress–strain responses. As a result, stress or strain developing in the pipe due to ground movement is influenced by the rate of loading and its flexibility. Weerasekara et al. (2008) performed full-scale laboratory axial pullout tests on MDPE pipes buried in dense Fraser River Sand and demonstrated the effects of the time–dependent response of the pipe on the pullout forces. However, the effects of strain rate–dependent response of the axial pullout were not extensively investigated in that study. In the current research, pullout tests of 60-mm diameter MDPE pipes are conducted under different rates of loading to investigate the strain rate effect. Tests are conducted in a newly developed laboratory test facility. The test pipes are buried in local sand available in Newfoundland and Labrador.

2 REVIEW OF SOIL RESISTANCE AGAINST AXIAL PIPE MOVEMENT

ASCE (1984) guidelines were the standard reference for pipeline design against seismically induced ground movement, which later was adopted by the ALA (2001). ASCE (1984) and ALA (2001) are the existing guidelines for the assessment of the performance of pipelines subjected to ground movements. These guidelines recommend using a simplified method to calculate the maximum pullout force due to axial landslide without proper consideration of soil–pipe interaction. As the general form of the equations was not varied significantly over the past 20 years, it is a common practice to determine the axial loads for the onshore buried pipeline in cohesionless sand using the following expression as in Eq. 1:

[1] $F_A = \gamma' \times H \times (\pi D L) \times (\frac{1+K_0}{2}) \times \tan\delta$

where D = pipe outside diameter, H = depth to pipe centerline (springline), γ' = effective unit weight of soil, K_0 = effective co-efficient of horizontal earth pressure, δ = interface angle of friction between the pipe and the surrounding soil. The term '$\gamma' H$ $(\frac{1+K_0}{2})$' is used as the average normal stress, σ_n, acting on the pipe surface. The average normal stress is then multiplied by the friction co-efficient 'tanδ' to obtain the maximum unit shearing resistance along the soil–pipeline interface. The peak pullout force F_A is calculated multiplying the unit shearing resistance by the surface area of the pipe (πDL). Thus, the interface friction, which depends on the normal stress acting on the pipe, is the primary source of axial soil resistance on the pipe. However, the simplified approach of calculating normal stress and hence the maximum pullout force was found to be unsuccessful in predicting the axial resistance measured in the laboratory tests (Paulin et al., 1998, Weerasekara et al. 2008). Moreover, Eq. (1) does not account for the relative stiffness of the pipe with respect to the surrounding soil. Based of FE analysis, Muntakim et al. (2017) revealed that the pullout force also depends on the relative stiffness of the pipe. However, no experimental validation of the FE finding is currently available. To this end, a new full-scale pipe testing facility developed at Memorial University of Newfoundland (Murugathasan et al. 2018) has been used in this study to investigate the behaviour of flexible MDPE pipes subjected to axial ground movement.

3 GROUND MOVEMENT RATES

Polyethylene pipe material shows viscoelastic/ viscoplastic behavior when subjected to load. Thus, the loads on the pipelines due to landslides may depend on the rate of ground movement. Various rates of landslide movement have been reported in the literature ranging from imperceptibly slow (millimeters per year) to extremely rapid (many meters per second). Varnes (1978) and Cruden and Varnes (1996) proposed a landslide velocity scale as shown in Table 1.

Table 1: Landslide velocity scale (Cruden and Varnes, 1996)

Velocity class	Description	Velocity (mm/s)	Typical velocity
7	Extremely rapid	5×10^{3}	5 m/s
6	Very rapid	5×10^{1}	3 m/min
5	Rapid	5×10^{-1}	1.8 m/hr
4	Moderate	5×10^{-3}	13 m/month
3	Slow	5×10^{-5}	1.6 m/year
2	Very Slow	5×10^{-7}	16 mm/year
1	Extremely Slow		

Even though the movement of many slow landslides appears to be relatively steady, detailed monitoring has shown that movement may be episodic or that movement rates may vary greatly over timescales ranging from hours to years (Keefer et al., 1983; Kalaugher et al. 2000; Coe et al. 2003; Petley 2004; Picarelli et al., 2004). The effects of different rates of landslide on pipeline integrity have not been investigated extensively. In the current research, MDPE pipes are tested under different rates of loading to investigate the effect of landslide rates.

4 EXPERIMENTAL ASPECTS

4.1 Test Equipment, Instrumentation, and Data Collection

The pipe test facility is a steel box with inside dimensions of 2 m in width, 4 m in length, and 1.5 m in depth. The test pipe is buried in local sand in the box. The pipe is protruded out of the test box from two ends through two circular openings. The circular openings are adjustable to accommodate pipes of different diameters. The openings are somewhat larger than the pipe diameter, which is filled using a rubber gasket with lubrication to minimize friction between the pipe and the cell wall at the openings. One protruded end of the pipe is connected using a specially designed pulling mechanism to a hydraulic actuator for axial pulling. This end of the pipe called herein as the leading end. Movement of the leading end is measured from the movement of the head of the actuator. At the other end of the pipe, called herein as tailing end, a LVDT (linear variable differential transformer) is connected to measure the axial movement. The difference between the leading end movement and tailing end movement is the total elongation of the pipe due to axial pulling. Pipe wall strains are also monitored using electronic strain gauges. Four uniaxial strain gauges are installed: one near the leading end and the others at one-fourth, half and three-fourths of the pipe length within the box. The uniaxial strain gauges are placed at the pipe crown. One biaxial strain gauge is attached at the $1/2^{th}$ length of pipe within the test box at the springline to monitor longitudinal and circumferential strains. The plan view of the test box along with pipe instrument locations and pulling mechanism is shown in Figure 1. The actuator is fitted with a reaction frame made of steel I-sections. A load cell is connected to the actuator that has 22.5 kN capacity with an accuracy of ±4.45 N. The LVDT has a total travel capacity of 110 mm with an accuracy of about 0.025 mm.

The data from the load cell, LVDT and strain gauges are monitored using a computer-controlled data acquisition system. The pipes are pulled at varying rates such as 0.5, 1, and 2 mm/min during the tests (termed herein as Test 1, 2, and 3, respectively).

4.2 Pipe Installation

Three tests are conducted using the MDPE pipes of 60.3 mm nominal diameter at various loading rates. Standard Dimension Ratio (SDR) (ratio of the pipe outside diameter to wall thickness) of the pipes is 11. These pipes are commonly used for the gas distribution system in Canada (Anderson et al. 2005). The pipes are buried at a depth of 0.48 m, which is 8 times the pipe diameter. The soil width on each side of pipes in the 2 m wide test cell is about 16 times the pipe diameter, which is sufficiently far to minimize the

boundary effects during axial pullout tests.

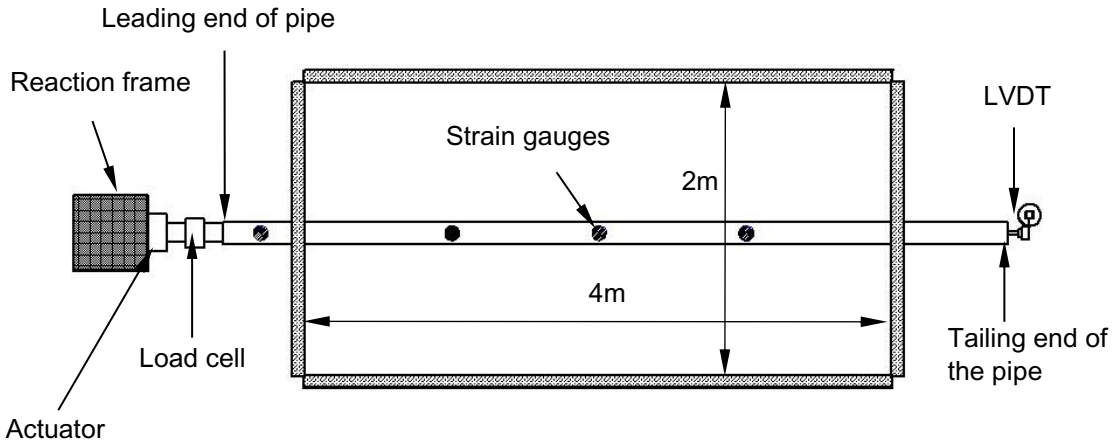

Figure 1: Plan of the MDPE pullout test setup (top view)

The pipe in the test cell has to be straight and horizontal during the axial pullout tests. Phillips et al. (2004) reported that slight axial misalignment can cause a significant increase in the mobilized axial resistance. During installation in the test box, a large spirit level of 1000 mm basic length is used to ensure straightness of the pipe during backfilling.

4.3 Backfill Sand

A locally available well-graded sand (USCS classification = SW) is used as the backfill material for the pipe. The material contains approximately 1.30% of fines and 98.70% of sand. The maximum dry density is obtained as 18.9 kN/m^3 with a corresponding optimum moisture content of 0% from Standard Proctor Compaction tests (ASTM D698 2003) (Saha et al. 2019).

About 8.65 m^3 of sand is required to achieve the desired depth of soil cover from the bottom of the tank for each test. The sand is compacted in layers by kneading at every 2 m^3 (approximately) of placement. After the completion of axial pullout, density measurements are taken at three different locations inside the testing tank, which yielded an average unit weight of 14.5±0.5 kN/m^3 from the top surface to the pipe springline level. Thus, the average relative compaction of the backfill material is roughly 75% of the Standard Proctor Maximum dry density and relative density is 60-65% which confirms the medium-dense conditions of the test sand. Moisture content of the soil is also measured and found to be less than 2%.

5 TEST RESULTS

5.1 Load–Displacement Responses

During axial pullout of pipes in the tests, surrounding soil offers resistance to the pipe movements. The resisting force of the soil is equal to the pullout forces applied to the pipe. The flexible MDPE pipe elongates with the application of pullout forces. The pullout forces (soil resistance) and elongation of the pipes obtained during the tests are presented in Figure 2. As seen in Figure 2(a), the soil resistance increases non-linearly with the pulling displacement at the leading end of the pipes. The soil resistances reach peak values and then decrease with further application of leading end displacements. The peak soil resistance is higher for the tests with higher displacement rates that occur at higher leading end displacements. In Test 1, 2, and 3 performed at a displacement rates of 0.5, 1, and 2 mm/min, the peak resistances are approximately 1.35, 1.70, and 2.36 kN that occurred at the pipe leading end displacements of 5, 8.55, and 9 mm, respectively. The peak axial force is also calculated using the current design guidelines (ASCE 1984, ALA 2001) that provided the maximum pullout resistance of 1.55 kN (shown in Figure 2a). In calculating

the pullout resistance using the current design guidelines, the coefficient of lateral earth pressures is calculated using Jaky's formula (i.e., K_0 = 1-sinϕ) using ϕ = 40°, corresponding to the peak friction angle of the local sand at the test density. The interface friction angle (δ) between the MDPE pipe surface and sand is assumed to be 24°. From the comparison of peak pullout resistances, it reveals that the maximum pullout resistance for the MDPE pipes depends on the pulling rate of the pipes, which is not accounted for in the current design guidelines. As a result, the equation in the design guidelines underpredicted the axial force for pipe subjected to 1 mm/min and 2 mm/min of displacement rates and overpredicted the axial force for the pipe subjected 0.5 mm/min of displacement rate. It is to be noted that the current design guidelines developed for steel pipes are the only resource available for assessing the pipelines subjected to ground movement. However, the test results presented in this study demonstrate that the existing design guidelines are not applicable for calculation of pullout force for MDPE pipes.

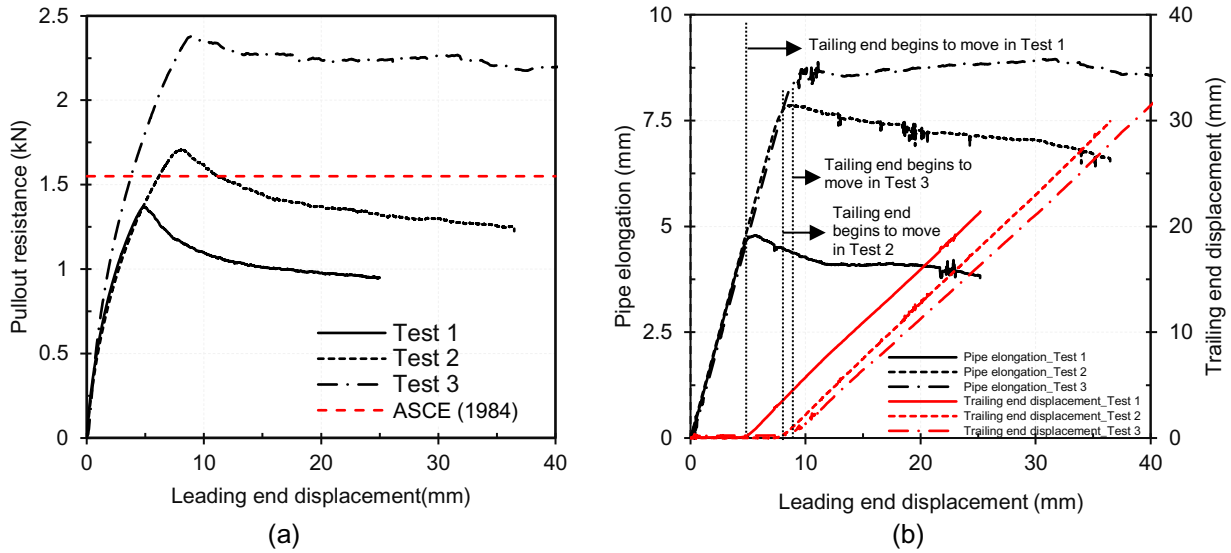

Figure 2: A relationship between (a) pullout resistance (b) pipe elongation-trailing end displacement with leading end displacement of the pipe

Figure 2(b) explains the deformation mechanism of the pipelines during the pullout tests. The figure plots pipe elongations, calculated from the difference between the loading end displacements and tailing end displacements, against the leading end displacements. In the figure, the pipe elongation increases linearly with the leading end displacement up to a peak value, after which the pipe elongation is stabilized or decreases. It also shows that the tailing end starts to move at the leading end displacements of 5 mm, 8.55 mm and 9.0 mm in Tests 1, 2, and 3, respectively. Thus, the leading end displacement is initially due to the elongation of the pipes only. Therefore, the interface shear strength is not mobilized over the entire length of the pipes at these displacements. This is confirmed by the maximum pullout forces (Figure 2a) and the maximum pipe elongations (Figure 2b) at these leading end displacements. The pullout resistance reaches to the maximum value at the point of full mobilization of shear strength over the entire length of the pipe. Beyond the maximum value, the pullout resistance reduces likely due to shear strength degradation.

It is to be noted that the flexible pipe elongates with the application of pullout forces. As a result, the mobilized shear strength is expected to be non-uniform along the length of the pipe. The mobilized shear stress at a point would depend on the relative movement of this point of the pipe with respect to the surrounding soil. However, the current design guidelines employ a simplified equation for calculating the maximum pullout force assuming uniform shearing stress over the entire length of the pipe. This assumption may not be applicable for flexible MDPE pipelines.

5.2 Pipe Wall Strains

During the tests, pipe wall strains are measured at four locations along the length of the pipes. Electronics

strain gauges are placed near the pulling end and at the distances of a quarter (*L*/4), half (*L*/2) and a three-quarter (3*L*/4) of the pipe length within the test cell measured from the pulling end. The measured pipe wall strains are examined here to understand the progression of the mobilized soil loads along the pipe.

Figure 3 plots the measured axial strains against the leading end displacements in two of the tests (Test 1 and Test 3). Axial strain data at various points is not available from Test 2. As expected, the axial strains are different at different locations along the pipe length (Figure 3). The strain near the leading end starts increasing immediately at the application of the leading end displacement. However, the points within the segment of the pipe buried in the sand experience axial strains at different magnitudes of leading end displacements. For example, in Tests 3, the point at *L*/4 experiences axial strain almost immediately after application of leading end displacement, while the points at the distances of *L*/2 and 3*L*/4 experience axial strains at around 2 mm and 4 mm of leading end displacements, respectively. Thus, for the leading end displacements of up to 2 mm and 4 mm, the axial force is not mobilized beyond the distances of one-half and three-quarter of the pipe length from the leading end of the test cell, respectively. Figure 3 shows that the axial strains increase with the further increase of the leading end displacement and reach the peak values at the point where the interface shear strength is fully mobilized, and the peak pullout resistance is reached. Beyond the leading end displacement of about 9 mm, the pipe elongation as well as the axial strains stabilize. Thus, although the axial strains along the lengths of the pipe are non-uniform (i.e., different at different locations), the shear strength of the soil at the soil–pipe interface appears to be mobilized over the entire pipe length at the maximum pullout force.

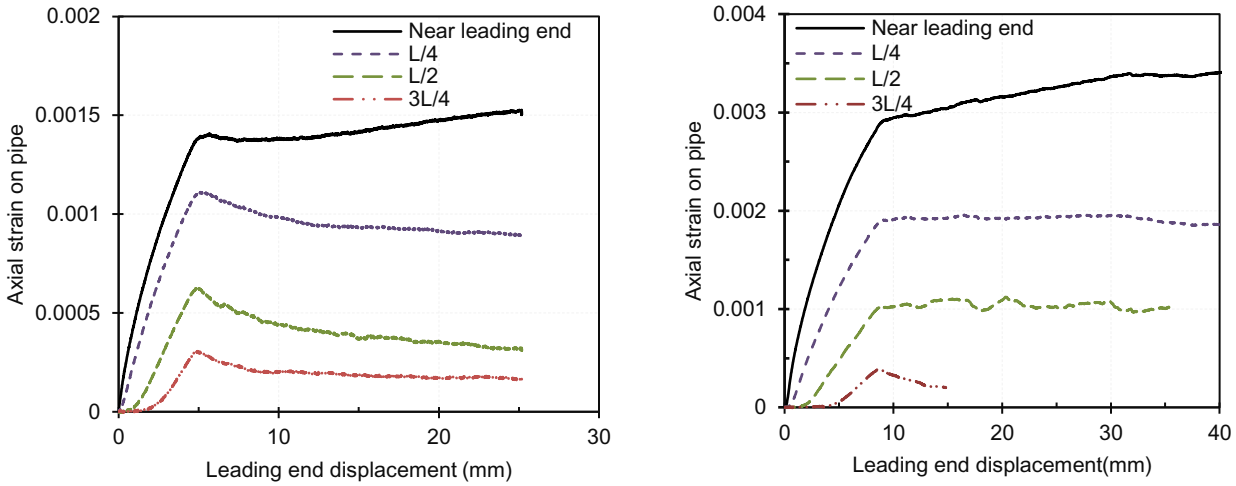

Figure 3: Axial strains at different locations of the pipes

The mobilization of axial force along the length of the pipe can be examined from the axial strains along the pipe length. The distributions of axial strain along the pipe length at different leading end displacements are plotted in Figure 4. It shows again that the axial strain is higher toward the leading end and less toward the tailing end. The tailing end strain is zero at the point where the axial force is not mobilized during the pullout. As discussed above, the axial force is mobilized over the entire length of the pipe when the pullout force is the maximum. The distribution of axial strain along the pipe length is almost linear after full mobilization of the interface shear strength at the peak pullout resistance (or pullout force). Thus, the distribution of the axial force can be assumed to be linear along the pipe length. This implies that unit shear resistance at the pipe–soil interface is constant along the pipe length after full mobilization of the shear strength. Therefore, the maximum pullout resistance can be calculated through prediction of the unit interface shear resistance.

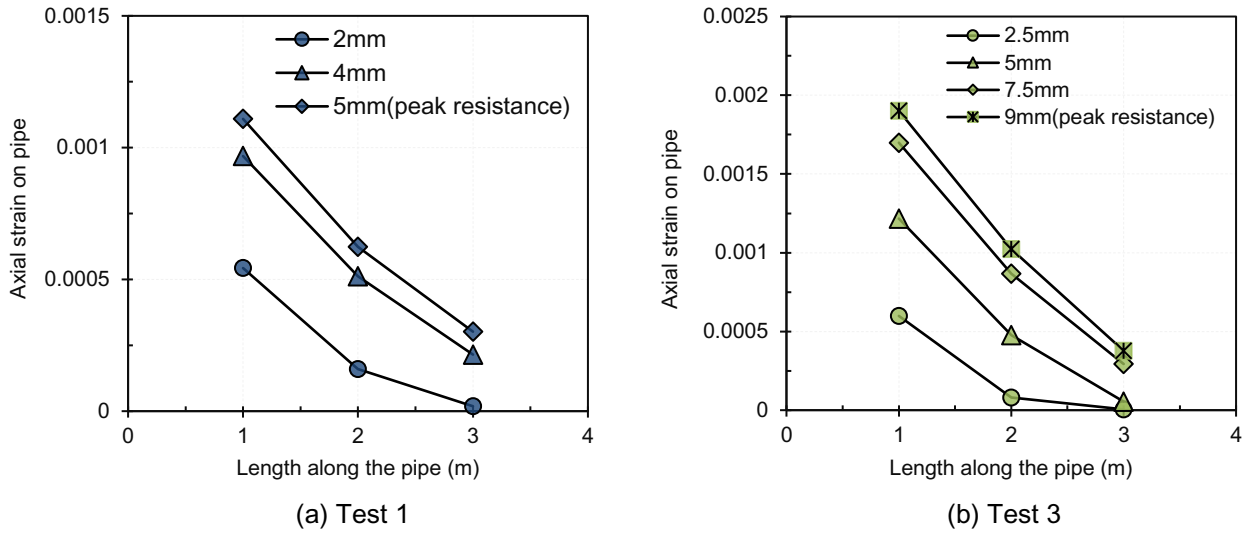

Figure 4: Distribution of axial strains along the pipe length.

A biaxial strain gauge is attached in Test 1 and Test 2 at the mid-length (*L*/2) of pipe at the springline to monitor longitudinal and circumferential strains, as shown in Figure 5. Figure 5 shows circumferential compressive strain at the springline which is likely associated with the changing diameter of the pipeline during the test. Bilgin et al. (2009) showed that the diameter change of the pipe can influence the pullout resistance of flexible pipes. They only investigated the diameter change due to temperature change. However, the study presented here reveals that pipe diameter can also change during the pullout of pipe at a constant temperature which might be due to the Poisson's effect. This diameter change is also not accounted in the current design method for calculation of the maximum pullout force.

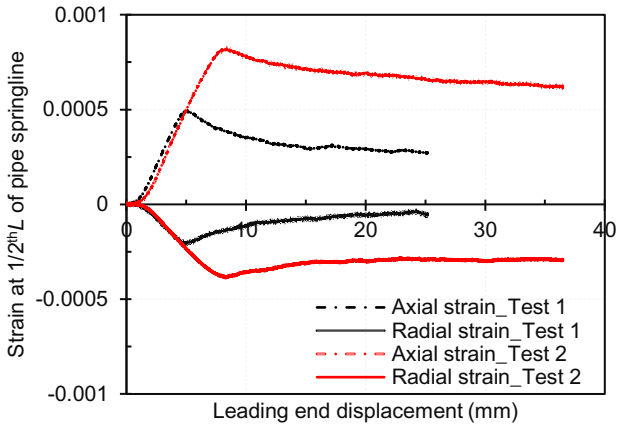

Figure 5: Longitudinal and circumferential strains at pipe springline

5.3 Interface Shearing Zone

As pullout force on the pipe depends on the shearing of the soil at the pipe–soil interface, an understanding of the shearing mechanism of the interface soil has been of great interest. Dove et al. (1999) revealed for geomembrane that sliding and plowing between sand–PE geomembrane are the principal mechanisms at their interfaces, which governs peak interface shear behaviour. During axial displacement, shear-induced volumetric strains are expected to occur within an annular shear zone around the pipe. The interface shearing was reported to occur within a narrow shear zone around the smooth sand-geomembrane interface (DeJong et al. 2005). Dove et al. (2006) monitored the thickness of active shear zone for Fraser

River sand using micro-scale particle image velocimetry (PIV) and found the thickness in the order of 1 to 2.3 mm, which is 5-7 times particle diameters of D_{50}. Karimian (2006) observed based on the movement of 15 mm coloured sand strips placed in the vicinity of the steel pipes as well as polyethylene (PE) pipes during axial loading and found that nearly 2 mm thickness of a zone is being shared during the axial pullout.

To investigate the shearing zone during the pullout test presented here, a 25 mm wide layer of paint is spread on the pipe and the sand during backfilling. The shear mechanism observed at the end of the test is shown in Figure 6. It is found that the shear occurs over a narrow zone of about 2 to 2.5 mm thickness, which is 3 to 3.5 times of particle diameters adjacent to the interface of the MDPE pipe. The mean particle size (D_{50}) of the backfill soil is 0.70 mm. This finding is consistent with the observation in Karimian (2006) for buried pipes.

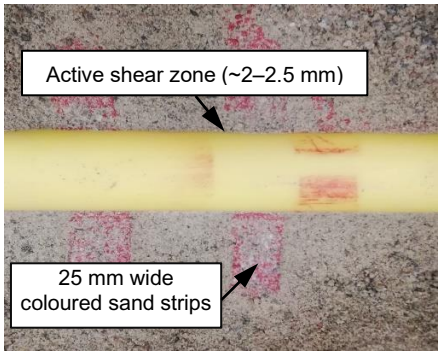

Figure 6: Movement of the coloured sand particles in the shear zone (Test 3)

6 CONCLUSION

Laboratory pullout test of 60-mm diameter MDPE pipes is conducted using a new test facility to develop an understanding of the behavior of the flexible pipeline subjected to axial ground movement. The test results reveal that the existing design guidelines (ASCE 1984, ALA 2001) may not be applicable for predicting the maximum axial force on MDPE pipelines due to ground movement. The following presents some specific finding from the research:

- The maximum pullout force on MDPE pipes depends on the rate of relative ground movement. The peak pullout force is higher in the tests with higher displacement rates. ASCE (1984) and ALA (2001) design guidelines do not account for the rate of ground movement. As a result, the equation in the design guidelines underpredicted the axial for pipe subjected to 1 mm/min and 2 mm/min of displacement rates and overpredicted for the pipe subjected 0.5 mm/min of displacement rate.

- MDPE pipes elongate during application of pullout force and axial force is not mobilized over the entire length of the pipe at the same time. Pipe–soil interface shear strength is also not mobilized at the same time. The mobilized shear stress at a particular point depends on the relative movement of the point of the pipe with respect to the surrounding soil. However, the current design guidelines employ a simplified equation for calculating the maximum pullout force assuming constant shearing stress over the entire length of the pipe.

- The distribution of axial strain along the pipe length is almost linear after full mobilization of the interface shear strength at the peak pullout resistance (or pullout force). Thus, the distribution of the axial force can be assumed to be linear along the pipe length. This implies that unit shear resistance at the pipe–soil interface can be assumed to be constant along the pipe length after full mobilization of the shear strength.

- Pipe diameter can change during pullout of MDPE pipe. The effect of diameter change should be considered for calculating the maximum shear resistance of the soil.

- During axial pullout, shearing occurred within a narrow zone of about 2 to 2.5 mm thickness, which is 3 to 3.5 times of particle diameters adjacent to the interface of the MDPE pipe.

This paper presents the preliminary results of axial pullout tests conducted for MDPE pipes. Research is currently underway on investigating the pullout behavior under more controlled laboratory conditions considering loose and dense conditions of the backfill soil.

7 ACKNOWLEDGEMENTS

The financial and/or in-kind support for this research is provided by the Collaborative Research and Development Grant program of Natural Science and Engineering Research Council of Canada, InnovateNL program of the Government of Newfoundland and Labrador, FortisBC Energy Inc. and WSP Canada Inc., which are gratefully acknowledged. The authors are thankful for the technical assistance by Jason Murphy, Shawn Organ and Matt Curtis in the Faculty of Engineering and Applied Science at Memorial University of Newfoundland. Undergraduate students Alex David McNeil and Shadi Soliman helped with instrumentation and pipe installation and deinstallation during the tests.

8 REFERENCES

ALA. 2001. *Guidelines for the design of buried steel pipe*. American Lifeline Alliance (ALA), available from www.americanlifelinesalliance.org/Products_new3.htm.

Anderson, C., Wijewickreme, D., Ventura, C. and Mitchell, A. 2005. Full-Scale Laboratory Testing of Soil-Pipe Interaction in Branched Polyethylene Pipelines. *Experimental Techniques*, March, 33-37.

ASCE. 1984. *Guidelines for the seismic design of oil and gas pipeline systems*. Committee on Gas and Liquid Fuel Lifelines, Technical Council on Lifeline Earthquake Engineering, American Society of Civil Engineers, ASCE, New York, pp. 573.

ASTM D698. 2003. *Standard test method for laboratory compaction characteristics of soil using standard effort (12,400 ft-lbf/ft^3 (600kN-m/m^3)*. 2003 annual book standards, West Conshohocken, Pa, **4**(8).

Bilgin, Ö. and Stewart, H. E. 2009. Design Guidelines for Polyethylene Pipe Interface Shear Resistance. *Journal of Geotechnical and Geoenvironment Engineering*, **135**(6): 809–818.

Bilgin, Ö. and Stewart, H. E. 2009. Pullout Resistance Characteristics of Cast Iron Pipe. *Journal of Transportation Engineering, ASCE,* October **135**: 730–735.

Coe, J.A., Ellis, W.L., Godt, J.W., savage, W.Z., Savage, J.E., Michael, J.A., Kibler, J.D., Powers, P.S., Lidke D.J. and Debray, S. 2003. Seasonal movement of the Slumgullion landslide determined from Global Positioning System surveys and field instrumentation. July 1998-march 2002, *Engineering Geology*, **68**(1-2): 67-101.

Cruden, D.M. and Varnes, D.J. 1996. Landslide types and processes. *Landslides – Investigations and mitigation*. Turner, A.K., and Schuster, R.L. eds., Transportation Research Board, Special Report 247, 36-75.

DeJong, J. T. and Westgate, Z. J. 2005. Role of overconsolidation on sand-geomembrane interface response and material damage evolution. *Geotextile Geomembrane*, **23**: 486–512.

Dove, J. E., Bents, D. D., Wang, J. and Gao, B. 2006. Particle-scale surface interactions of non-dilative interface systems. *Geotextile Geomembrane*, 24: 156–168.

Dove, J. E. and Frost, J. D. 1999. Peak friction behavior of smooth geomembrane-particle interfaces. *Journal of Geotechnical and Geoenvironmental Engineering,* **125**(7): 544–555.

Kalaugher, P.G., Hodgson, R.L.P. and Grainger, P. 2000. Pre-failure strains as precursors of sliding in a coastal mudslide. *Quarterly Journal of Engineering Geology and Hydrogeology*, **33**: 325-334.

Karimian, A.H. 2006. Response of buried steel pipelines subjected to longitudinal and transverse ground movement. PhD thesis, Department of Civil Engineering, University of British Columbia, Vancouver, B.C.

Keefer, D.K., and Johnson, A.M. 1983. Earth flows-Morphology, mobilization and movement. *U.S. Geological Survey Professional Paper*, **1264**: 56.

Liu, R., Guo, L., Yan, S. and Xu, Y. 2011. Studies on Soil Resistance to Pipelines Buried in Sand, May, doi:org/10.4028.

Mohitpour, M., Murray, A., McManus, M. and Colquhoun, I. 2010. *Pipeline Integrity Assurance – A Practical Approach*. 2nd ed., ASME Press, Three Park Avenue, New York, NY 10016, USA.

Muntakim, A.H., Dhar, A. S. and Rahman, M. 2017. Pipeline behaviour subjected to large ground

movement. *70th Canadian Geotechnical Conference*, GEOOTTAWA 2017, Oct. 1-4, Ottawa, ON.
Murugathasan, P., Dhar, A. S. and Hawlader, B. C. 2018. A laboratory facility for studying pullout behaviour of buried pipelines. *71st Canadian Geotechnical Conference,* GeoEdmonton2018, September 23-26, Edmonton, Alberta.
Paulin, M. J., Phillips, R. and Clark. J. I. 1998. A full-scale investigation into pipeline/soil interaction. *International Pipeline Conference*, ASME, Volume II.
Petley, D.N. 2004. The evolution of slope failures – Mechanisms of rupture propagation. *Natural Hazards and Earth System Sciences*, **4**: 147-152.
Phillips, P., Nobahar, A. and Zhou, J. 2004. Combined Axial and Lateral Pipe–Soil Interaction Relationship. *Proceedings IPC2004*, *International Pipeline Conference,* Alberta, Canada.
Picarelli, L. and Russo, C. 2004. Remarks on the mechanics of slow active landslides and the interaction with man-made works, in Lacerda, W.A. *Proceedings of the 9th International Symposium on Landslides*, London, A.A. Balkema Publishers, **2**: 1141-1176.
Saha, R. C., Dhar, A. S., Muntakim., A. H. and Hawlader, B. C. 2019. Strength and deformation behaviour of a local sand. *General Conference, CSCE,* June 12-15 , Laval (Greater Montreal), QC, Canada.
Sheil, B. B. Ã., Martin, C. M. Ã., Byrne, B. W. Ã., Plant, M., Williams, K. and Coyne, D. 2016. Full-scale laboratory testing of a buried pipeline in sand subjected to cyclic axial displacements. *Geotechnique*, https://doi.org/10.1680/jgeot.16.P.275.
Stewart, H. E., Bilgin, O., O'Rourke, T.D. and Keeney, T. M. 1999. *Technical reference for improved design and construction to account for thermal loads in plastic gas pipelines*. Technical report, Cornell University, Ithaca, NY.
Varnes, D.J. 1978. Slope movement types and processes, Landslides Analysis and Control. *Special Report 176, Transportation Research Board*, National Academy of Sciences, p. 11-33.
Weerasekara, L. and Wijewickreme, D. 2008. Mobilization of soil loads on buried polyethylene natural gas pipelines subject to relative axial displacements. *Canadian Geotechnical Journal*, **45**: 1237–1249, doi:org/10.1139/T08-043.
Wijewickreme, D., Karimian, H. and Honegger, D. 2009. Response of buried steel pipelines subjected to relative axial soil movement. *Canadian Geotechnical Journal*, **46**: 735– 752, doi:org/10.1139/T09-019.

APPENDIX B

Numerical Evaluation of Buried Medium Density Polyethylene Pipelines Subjected to Axial Ground Movement

This paper has been published and presented in 100th Transportation Research Board Meeting, TRB 2021, Washington D.C., USA, January 25–29, 2021. Most of the research work presented in this paper was conducted by the first author. He also prepared the draft manuscript. The other author supervised the research and reviewed the manuscript.

Numerical Evaluation of Buried Medium Density Polyethylene Pipelines Subjected to Axial Ground Movement

Auchib Reza[1] and *Ashutosh Sutra Dhar*[1]
[1]Department of Civil Engineering, Memorial University of Newfoundland
St. John's, Newfoundland and Labrador, Canada

ABSTRACT
Buried pipeline network forms an indispensable infrastructure that is extensively used for transporting and distributing natural gas and liquid. One of the major problems associated with the performance of this network is related to the deformation of pipelines in areas prone to ground movement. The maximum axial force on the pipeline subjected to axial ground movement is commonly calculated using a design equation developed without proper consideration of soil–pipe interaction. The authors' recent work revealed that soil–pipe interaction significantly contributes to the axial pullout load, particularly for flexible pipes. This paper presents the results of numerical study conducted to explore the mechanics of soil–pipe interaction that could not be measured during tests. Particularly, the effect of rate–dependent interface behaviour of the polyethylene pipe material on pulling resistance could not be measured during the tests. The FE model is developed through validation with full-scale laboratory test results performed at Memorial University of Newfoundland. The study reveals that FE analysis with interface friction angles of 75% to 90% of the peak friction angle of surrounding soil can successfully simulate ground movements of various rates. Based on the results obtained, a simplified equation is proposed to estimate the mobilized frictional lengths for pipeline performance assessment.

Keywords: Pipelines, Axial pullout, Finite-element analysis, Interface friction angle, Mobilized frictional length.

INTRODUCTION
Pipelines are widely used for transporting water and hydrocarbons. These pipelines travel large distances through a wide variety of ground conditions, which affect the performance of buried pipelines. Pipelines are also exposed to ground movement due to landslide or earthquake. A proper understanding of pipeline response to ground movements (such as axial, lateral and vertical) is essential in pipeline design. Pipelines are subjected to axial force when the direction of ground movement is parallel to the pipe axis. Current design codes (i.e., *1-2*) adopted a design equation to calculate the maximum axial force in cohesionless soil, as expressed in **Eqution 1**:

$$F_{\mathrm{A}} = \gamma \times H \times (\pi\, D\, L) \times \left(\frac{1+K_0}{2}\right) \times \tan\delta \qquad (1)$$

where F_{A} = the maximum axial force, which is equal to the maximum soil resistance to pipe movement; γ = unit weight of soil; H = depth from the ground surface to pipe springline; L = pipe length; D = pipe outer diameter; K_0 = coefficient of lateral earth pressure at rest, and δ = interface friction angle between the pipe and the surrounding soil.

Over the years, numerous studies were conducted to validate the equation through proper understanding of the soil–pipe interaction mechanisms for pipes subjected to axial ground movements (*3-9*). Most of these studies have focused on steel pipe; the pipes are assumed to be rigid. Flexible polyethylene pipes are also extensively used for oil and gas transportation, particularly in the gas distribution system. Studies on the performance of flexible polyethylene pipe subjected to ground movement are very limited. Polyethylene pipe material shows viscoelastic/ viscoplastic behavior when subjected to load. Reza et al. (*8*) showed that the pullout behaviour of the MDPE pipe significantly depends on the viscoelastic response of the pipe material. Thus, the forces on polyethylene pipes may depend on the rate of ground movements. The forces experienced by the polyethylene pipes subjected to these various rates of ground movements are not well understood.

Wijewickreme and Weerasekara (*10*) conducted full-scale field tests of 60-mm diameter MDPE

pipes at various pulling rates and found that the pulling rate has significant effects on the pullout resistance. In an attempt to account for the pulling rate effects, they considered a rate–dependent modulus of elasticity of the pipe material to determine the pipe response under axial soil loading. However, interaction of the pipe surface with the surrounding soil is also expected to be rate–dependent, which was not considered. One of the challenges in identifying the rate–dependent interaction is the difficulty in measuring the effect during the tests. This challenge could be overcome through finite-element modelling, with validation of the model using the responses that could be measured during the tests. This paper presents the results of three-dimensional (3D) finite-element modelling performed by the authors to identify the contribution of the soil, pipe and interface parameters on the pipes behaviour. More details of the investigation has been discussed in Reza and Dhar (*11*). Some results of the investigation are also presented here.

FE MODELLING OF AXIAL MOBILIZATION IN BURIED PIPELINES

Finite-Element Modelling

Reza and Dhar (*11*) conducted a full-scale test of MDPE pipe buried in local sand in a test cell of 4 m (length) × 2 m (width) × 1.5 m (height) in dimensions. The pipe was buried at a depth (*H*) of 0.48 m. The diameter (*D*) of the pipe was 60.3 mm and the thickness were 6 mm. The tests *H/D* ratio was 8. Three-dimensional (3*D*) analyses are performed to simulate the test conditions, to explore the mechanics of soil–pipe interaction and the parameters contributing to the axial pullout forces under various rates of pullout displacement. The modelling is performed using the commercially available FE software, Abaqus (*12*). Dynamic analysis is performed using the Abaqus/Standard module that uses implicit time integration to calculate the response of a system. Geometric nonlinearity and large strain formulation in the elements are considered during numerical simulation. The nonlinear geometry option, NLGEOM, in Abaqus ensures the equilibrium of the current configuration of the model considering the changes in geometry during the analysis. The pipe and soil domain are modelled using C3D8R solid elements, available in Abaqus. A finer mesh is used in the close vicinity of the pipe over a radial distance of 2.0 times the pipe diameter (2*D*). A mesh sensitivity study was conducted which showed that a minimum element size of 3.5 mm was suitable, which was selected for the analysis. Coarser mesh is used beyond 2*D* to reduce the computational time. **Figure 1** shows a typical FE mesh used in the analysis.

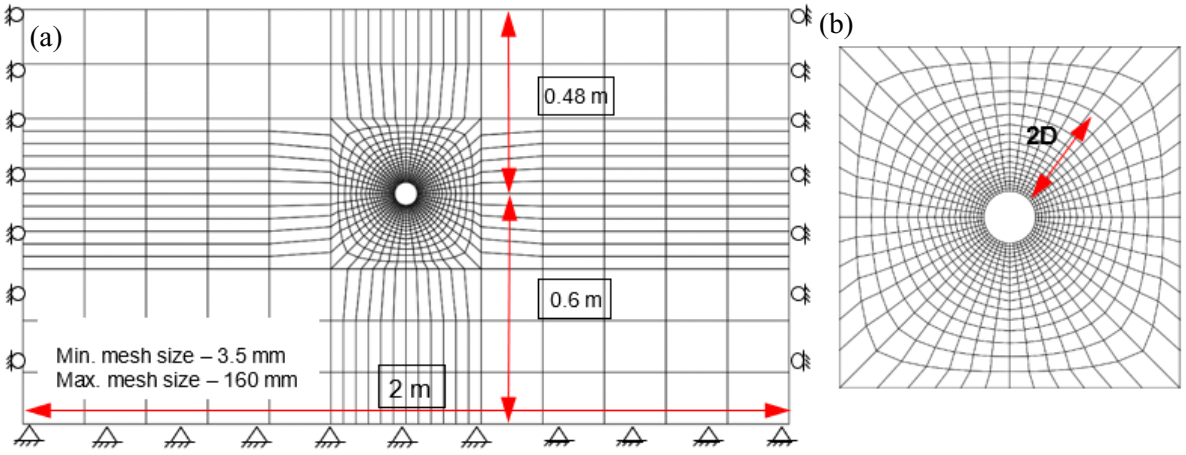

Figure 1 Finite-element model (a) FE mesh (b) Cross-section near the pipe (after Reza and Dhar [*11*])

Contact Formulation between Soil and Pipeline

The contact between soil and pipeline is modelled using the general contact algorithm that can model all possible contacts between the bodies. A penalty algorithm is used to model tangential contact behaviour with a friction coefficient. For the general contact interaction, the pipes surface is modelled as a pure master

and the soil surface is modelled as slave. It is common practice to model the stiffer surface as pure master and the relatively low stiff surface as a slave (*12*). This technique allows slip and/or separation between different elements in the contact. The pipe is extended beyond the test cell boundary at the front and rear ends so that the total length of contact of the soil with the pipe remains unchanged during axial pullout (like the laboratory tests).

Boundary Conditions

Murugathasan et al. (*13*) demonstrated that the boundary walls of the test cell could reasonably be considered as rigid under axial pullout loading. A zero horizontal displacement boundary condition is therefore used for each side of the test box, except for the axial movement in the pipe. Axial movement of the pipe is allowed to apply pullout force. The load is applied using the following steps: (i) application of a gravitational load in layers to simulate the initial condition, (ii) application of axial displacements from one end of the pipe (herein termed the "leading end"); the other end (termed as the "tailing end") is free to move.

Material Parameters

Pipe Model

The MDPE pipe is idealized as a linear elastic material. However, the stress–strain relation for polymer material is non-linear and known to be strain rate and temperature-dependent. Suleiman and Coree (*14*) proposed a modified hyperbolic model to account for the strain rate–dependent modulus of elasticity of polyethylene pipe material, as expressed in **Equation 2**:

$$E_{ini} = a\,(\dot{\varepsilon})^{b} \qquad (2)$$

where E_{ini} = initial Young's modulus of the material, $\dot{\varepsilon}$ = strain rate; and a and b = constants obtained from uniaxial tension or compression tests. Wijewickreme and Weerasekara (*10*) reported the constant a and b as 2020 and 0.109, respectively. Using this hyperbolic stress–strain relation with a = 2020 and b = 0.109, Young's modulus corresponding to the average strain rate experienced by the pipe during the tests, i.e., ranging from 2.85×10^{-6} to 5.85×10^{-6}, is estimated to be 500–550 MPa. Thus, the modulus of elasticity pipe material, E_p, is expected to vary between 500 MPa to 550 MPa during the test with the pulling rates of 0.5 mm/min to 2 mm/min. The modulus of elasticity of pipe, E_p = 550 MPa, is assumed to calculate the maximum pullout load of the MDPE pipe in finite element analysis.

However, a dynamic analysis would be required to simulate the rate–dependent effect of the soil structure interaction. While time domain analysis could be used in this case, but may be complex, time consuming, and expensive. In engineering practice, designers and researchers often prefer using simple models with sufficient accuracy to capture the main feature of soil–pipe interaction behaviour relevant to the particular problem of interest. Hence, a simplified method using equivalent static analysis of pipelines subjected to ground movement is developed, which is the key feature of the current study.Similarly, Luo et al. (*15*) interpreted the velocity of typical high-speed landslides during earthquakes and suggested the use of the constitutive model of Suleiman and Coree (*14*) based on a strain rate of 3×10^{-3} s^{-1} to eliminate the influence of the rate–dependence of the HDPE material. Therefore, it should be clarified that the measured true stress versus true strain curves for the CSA B137.4 certified MDPE pipe can be used to reproduce the material's behaviour adequately for use in designs or assessments, particularly when the pipe is subjected to heavy ground loads (e.g., deep buried depth, highly compacted backfill).

Soil Constitutive Models

Soil behaviour is modeled using the built-in elastic-perfectly plastic Mohr–Coulomb (MC) constitutive model, available in Abaqus, to simulate the stress–strain behaviour and shear failure of the sand. Since MC model only demands a few soil properties (such as friction angle and dilation angle of soils), it is widely popular for modelling the behaviour of soils. In this model, the soil is assumed to deform elastically until the stress state reaches the MC failure criteria (yield surface). When the stress state reaches the yield surface,

plastic deformation occurs, and the soil dilates at a constant dilation angle. Although the soil in the field may experience plastic strains before it reaches the yield surface and may have a non-constant dilation angle, the conventional MC model is found to successfully simulate the ultimate soil resistance during the axial pullout (*16-17*).

The Young's modulus for the soil is mostly determined from the unload-reload parts of the drained triaxial compression tests for saturated soils. However, the modulus of elasticity of unsaturated soils might be different from modulus of elasticity of saturated soils due to the influence of matric suction, $(u_a - u_w)$ (u_a, pore-air pressure and u_w, pore-water pressure) and degree of saturation, *S*. Janbu (*18*) showed that the initial tangent modulus of elasticity, E_{ini}, is varied using the power function of the confining pressure, p', as expressed in **Equation 3**:

$$E_{ini} = Kp_a \left(\frac{p'}{p_a}\right)^n \quad (3)$$

where K is a material constant; p_a is the atmospheric pressure (i.e., 101.3 kPa); p' is mean effective confining pressure, and n is an exponent determining the rate of variation of E_{ini} with p'. This power function is widely used in the numerical modelling of pipe–soil interaction problems (*17, 19-21*). The value of E_{ini} is estimated based on the mean effective stress (p') at the springline level of the pipe with K = 150 and n = 0.5 (*22*) as E_{ini} = 5 MPa for the sand used in the tests. A constant Poisson's ratio of 0.3 is assumed for the sand. The angle of internal friction is selected based on the test results of Saha et al. (*23*). Saha et al. (*23*) determined that the angle of internal friction of the sand is high at a low stress level, decreases with the increase of stress level, and eventually reaches a constant value. The dilation angle was found to be negligible for the moist condition of the sand. Therefore, a constant angle of internal friction of 40° is used, which corresponds to the average stress level (~10 kPa) expected in the tests. A small dilation angle of 0.1° and a small cohesion of 0.1 kPa is applied for numerical stability during analysis. The minimum values of dilation angle and cohesion are required to avoid ill-conditioning during numerical calculations.

In the field, the sand around a pipeline is often in the state of medium to dense conditions. Hence, the soil–pipe interaction in medium-dense sand state (unit weight of 14.5 kN/m^3), corresponds to the relative compaction of the backfill material is roughly 75% of the Standard Proctor dry density, are investigated in this study.

Interface Parameter

The interface between the pipeline and surrounding soil is simulated using general contact algorithm available in Abaqus/ Standard. The Coulomb friction model is used for the frictional interaction between the pipe and soil. In this method, the slipping along the interface between the buried pipe and surrounding soil occurs when the shear stress, τ, at the contact interface reaches the critical shear stress, τ_{crit}, (i.e., interface shear strength), which is the friction coefficient (i.e., $\mu = \tan\delta$) times the normal stress, σ_n'. The interface shear strength is limited to the shear strength of the surrounding soil. The value of angle of interface shearing resistance, δ, depends on the interface characteristics between the soil and the pipe, including the roughness and hardness of the pipe surface. The lower values of δ represent the characteristics of smoothly coated pipes, while the larger values would correspond to rough uncoated pipes with rusty or corroded surfaces. ALA (*2*) code suggests that δ can be estimated as $\delta = f\phi$, where 'ϕ' is the internal friction angle of the backfill material, and 'f' is the interface friction reduction factor, relating the internal friction angle of the soil to the friction angle at the soil–pipe interface. Generally, the value of δ lies between $\phi_{max}/2$ and ϕ_{max} (*17*). Furthermore, Scarpelli et al. (*24*) conducted measurements of the friction coefficient, tanδ, for various materials, and showed that soil grains can penetrate some materials (**Figure 2**), increasing the friction coefficient. Grain penetration can also occur on MDPE pipe surface, causing a higher value of the interface friction angle. Also, interface behaviour for the MDPE pipe is expected to be pulling rate–dependent, due to the time–dependent behaviour of the material. A pulling rate–dependent angle of interface friction can be used to account for the time–dependent effects. Thus, FE analysis is performed with various angles of interface friction to simulate the test results for various rates of pulling. **Table 1** summarizes the parameters for the interface friction for various test conditions.

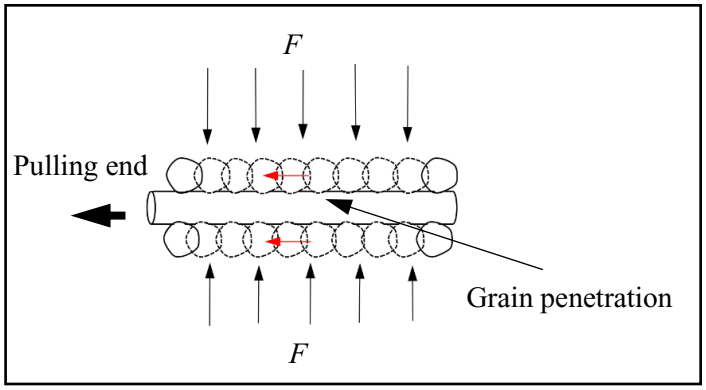

Figure 2 Grain penetration on MDPE pipe surface (after Reza and Dhar [*11*])

Table 1 Friction coefficients corresponding to the test conditions

Loading rate	Interface friction reduction factor, f	Friction angle, ϕ	Interface angle of shear resistance, $\delta = f\phi$	Tangential friction coefficient, tanδ
0.5 mm/min	0.75	40°	30°	0.577
1 mm/min	0.86		34.4°	0.684
2 mm/min	0.90		36°	0.726

RESULTS AND DISCUSSIONS

Investigation of Force–Displacement Responses

Figure 3 shows the load–displacement responses during axial pulling of pipe. FE analysis was conducted to simulate the results of experiments performed at three different pulling rates: 0.5 mm/min (Test 1), 1 mm/min (Test 2) and 2 mm/min (Test 3) at the leading end. It is to be noted here that these pulling rates fall within the range of moderate landslide velocity scale (*25*). FE analysis with various interface friction coefficients is conducted to simulate the measured load–displacement responses. As seen in the figure, the maximum pullout forces are successfully simulated using the FE analysis with the 'f' (interface friction reduction factor) of 0.75, 0.86, and 0.90 for Test 1 (0.5 mm/min), Test 2 (1 mm/min) and Test 3 (2 mm/min), respectively. Thus, interface friction reduction factors of 0.75, 0.86, and 0.9 correspond to the loading rates of 0.5, 1, and 2 mm/min, respectively. However, the initial responses of the pipe were not successfully simulated for Test 2 and Test 3 in **Figure 3**. This might be due to the use of a linear elastoplastic model for the soil and a linear elastic model for the pipe material. An investigation of the maximum pullout force is the interest of the current study, as it is the concern for pipeline design.

Based on the results of FE analysis, the friction reduction factors (f) are obtained for various rates of relative ground movement, as shown in **Figure 4**. **Figure 4** illustrates that the factor can be less at the slower ground movement and increases nonlinearly with the increase of the rate of relative ground movement. It stabilizes to a value close to 0.9 (i.e., $\delta = 0.9\phi$) at highest rate of ground movement. This rate–dependant friction factor can be considered for calculating the pullout force using existing design equation.

Distributions of Pullout Forces and Pipe Axial Strain

For the flexible MDPE pipe, the axial force is not mobilized over the entire pipe length immediately. With application of the pulling force, the axial force is mobilized over the pipe length gradually. The mobilization of the axial force is captured using the measurement of axial strains. The axial force can be assumed to have mobilized up to the location of a strain gauge when the strain reading starts to increase. The strain gauges were placed at distances of $L/4$, $L/2$ and $3L/4$ from the leading end. Therefore, the pulling forces required

to mobilize axial forces over these distances are plotted in the figure. The pulling force required to mobilize axial forces at various distances along the pipe length are plotted in **Figure 5**. The pulling force is normalized by the overburden pressure at the springline level and the contact surface area of the pipe with the surrounding soil (i.e., $P_u/\pi DL\gamma H$). **Figure 5** shows that the pullout force increase is high initially, with the increase of pulling rate, and then is stabilized. Thus, the pullout force is expected to be less when the rate of ground movement is less. The corresponding strains on the pipe are also expected to be less if the relative ground movement is slow. Note that the non-dimensional peak pullout forces at $L/2$, $3L/4$ and L are almost in the same magnitude for all the pulling rates except at $L/4$, which is located very close to the leading end. This mean that pullout resistance is uniform over the mobilized length. Therefore, the distribution of axial force/ shearing resistance can be assumed to be linearly distributed over the length of the pipe. Further discussion on the axial force distribution can be found in the following section.

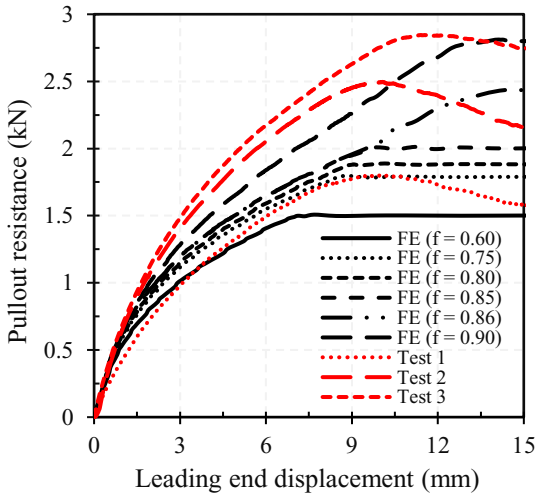

Figure 3 Comparison of FE calculation of pullout resistance with measurements (after Reza and Dhar [*11*])

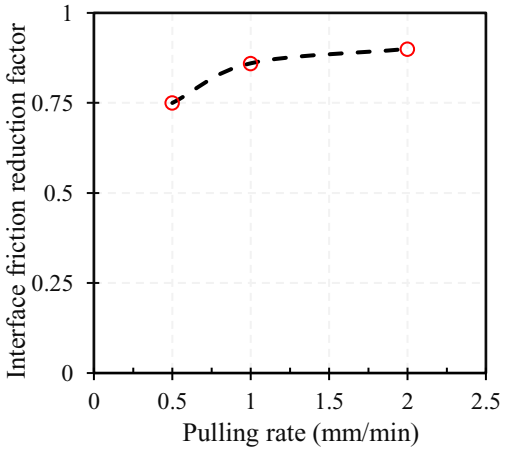

Figure 4 Interface friction reduction factor with pulling rates (after Reza and Dhar [*11*])

The strain distributions along the pipe length in Test 1 and FE ($f = 0.75$) model is plotted in **Figure 6** at various leading end displacements. The strain at the distances of $L/4$ starts increasing with a very small leading end displacement that increases with the increase of the leading end displacement. The strains at $L/2$ and $3L/4$ do not start immediately but begin at certain levels of leading end displacements. For example, the strains at $L/4$, $L/2$ and $3L/4$ started at the leading end displacements of $u_1 = 0.65$ mm, $u_2 = 2.3$ mm and $u_3 = 4.47$ mm, respectively. This observation confirms again that the axial force of flexible MDPE pipe is not mobilized over the entire pipe length at the same time (unlike for steel pipe, based on which the existing design guidelines were developed). The distributions of strain are linear over the length of axial force mobilization indicating that the axial force is also linearly distributed. Measurements and FE calculations reasonably match each other in the figure.

Pipe wall deformation at these leading end displacements is plotted in **Figure 7** from FE analysis. The displacements could not be measured during the tests. It is found that pipe wall deformation has developed nonlinearly along the full length of pipe when the interface shear strength is fully mobilized. Since these deformations on the pipe develop nonlinearly (second degree of polynomial), the distribution of the axial force can be assumed to be linear along the pipe length at full mobilization. As a result, assuming a linear distribution of the axial force, p, over the full length of the pipe, mobilized frictional length, l, can be assumed for the assessment of the pipeline.

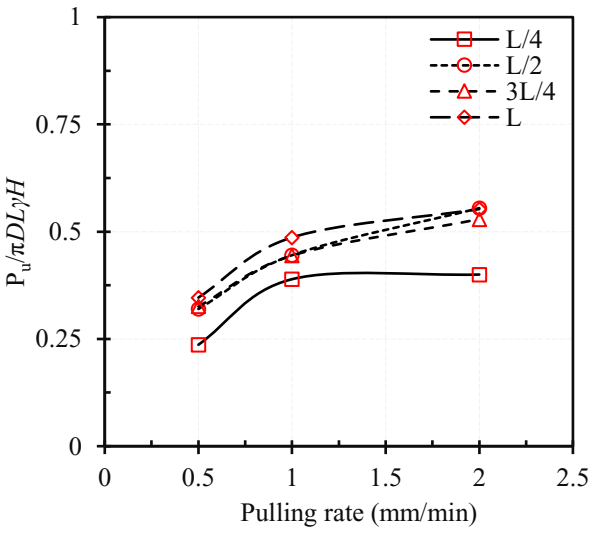

Figure 5 Normalized peak pullout force at different distances along the pipe

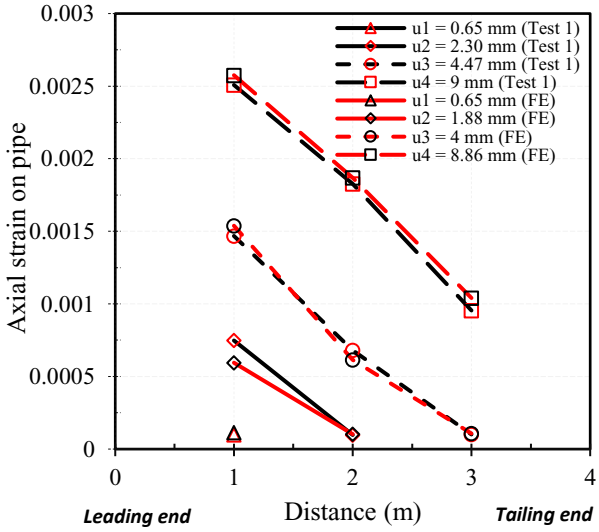

Figure 6 Strain distribution along the length of pipe at various leading end displacements (after Reza and Dhar [*11*])

Mobilized Frictional Length

Assuming a linear distribution of the axial force (p) over the length of the mobilized friction length (l), l can be related to the leading end displacement (u), as below:

$$\frac{1}{2}\frac{pl}{AE} = u \qquad (4)$$

$$l = \frac{2AE}{p}u \qquad (5)$$

where A is the cross-sectional area of the pipe and E is the modulus of elasticity of the pipe material. The length of axial force mobilization is experimentally examined during the tests based on the initiation of axial strains at various points along the length of the pipe, as shown in **Figure 8**. The axial force is mobilized to a point when the strain gauge located at this point starts to give a reading. Mobilized lengths of axial force from the experiment are compared with those calculated using **Equation 5** and FE analysis in **Figure 9**.

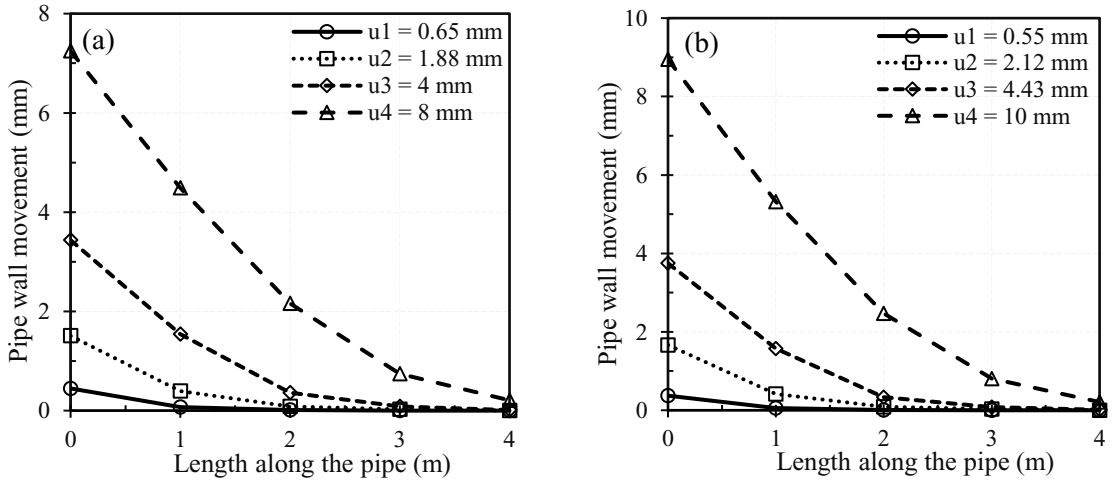

Figure 7 Pipe wall movement along the length of pipe from FE calculation: (a) $f = 0.75$ (b) $f = 0.90$

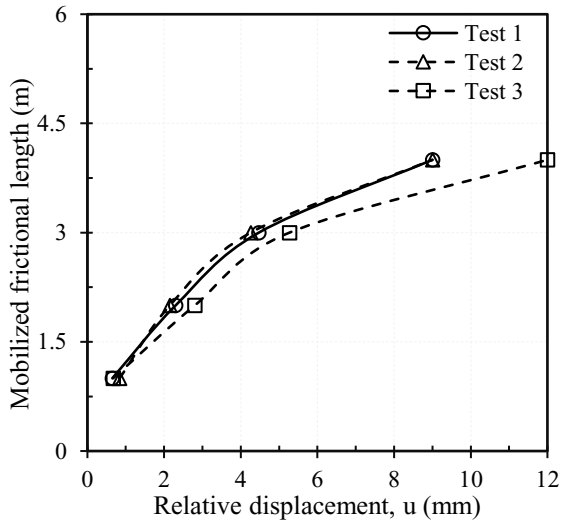

Figure 8 Experimental mobilized length

The figure shows that the FE calculation matches well with the measurements, while **Equation 5** provides reasonable estimations of the mobilized friction lengths. Thus, if the axial force (p) and relative ground movement (u) are known, the mobilized friction length can be estimated using **Equation 5**.

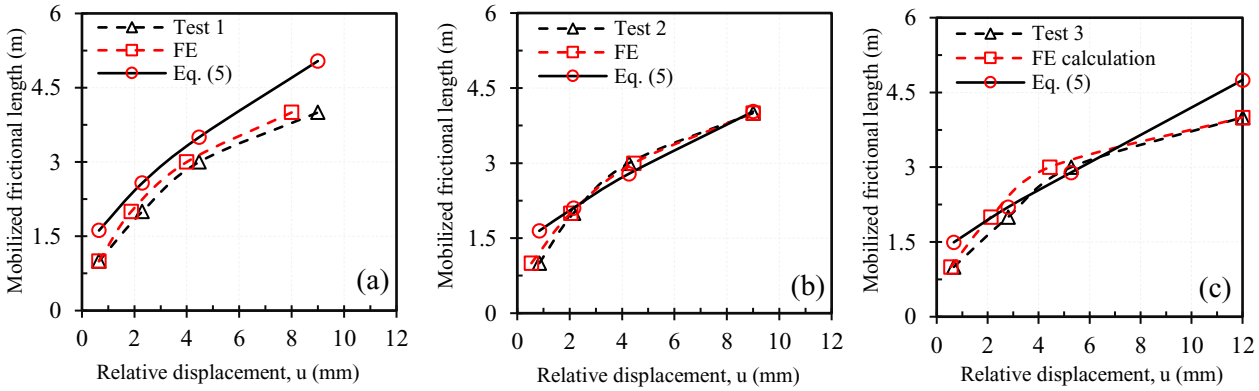

Figure 9 Comparison of mobilized friction lengths versus relative displacement: (a) Test 1 (b) Test 2 (c) Test 3 (after Reza and Dhar [11])

CONCLUSIONS

The following conclusions are drawn from this study.

- Three-dimensional FE analysis successfully simulated the responses observed during full-scale laboratory tests. Analysis with various angles of interface friction was conducted, which demonstrates that friction angles of 0.75ϕ, 0.86ϕ, and 0.9ϕ reasonably correspond to the test conditions with pulling rates of 0.5, 1, and 2 mm/min, respectively.
- The distribution of axial strain of the pipe is almost linear over the length of mobilized axial force (hence, friction). Thus, the distribution of the axial force can be assumed to be linear.
- Based on the assumption of the linear distribution of axial strain, a simplified equation is proposed to estimate the mobilized frictional lengths from known pulling force (p) and leading end displacement (u). The equation is found to reasonably estimate the mobilized frictional length observed during the tests and calculations using the FE analysis.

ACKNOWLEDGEMENTS

The work presented in this paper has been supported by the Collaborative Research and Development Grant program of the Natural Science and Engineering Research Council of Canada (NSERC), Innovate NL program of the Government of Newfoundland and Labrador, FortisBC Energy Inc. and WSP Canada Inc.

AUTHOR CONTRIBUTIONS

Dr. Ashutosh Sutra Dhar conceptualized the project and wrote the proposal for funding. Auchib Reza and Dr. Dhar designed the experiment, analyzed the data, and wrote the paper. All authors reviewed the results and approved the final version of the manuscript.

REFERENCES

1. American Society of Civil Engineers. Committee on Gas, Liquid Fuel Lifelines. Guidelines for the seismic design of oil and gas pipeline systems. Amer Society of Civil Engineers; 1984.

2. Alliance AL. Guidelines for the design of buried steel pipe. InAmerican Society of Civil Engineers 2001. Available from https://www.americanlifelinesalliance.com/pdf/Update061305.pdf [accessed 28 May 2020].

3. Wijewickreme D, Karimian H, Honegger D. Response of buried steel pipelines subjected to relative axial soil movement. Canadian Geotechnical Journal. 2009 Jul;46(7):735-52. doi: org/10.1139/T09-019

4. Meidani M, Meguid MA, Chouinard LE. Evaluation of soil–pipe interaction under relative axial ground movement. Journal of Pipeline Systems Engineering and Practice. 2017 Nov 1;8(4):04017009. doi: org/10.1061/(ASCE)PS.1949-1204.0000269

5. Liu R, Guo LP, Yan SW, Xu Y. Studies on Soil Resistance to Pipelines Buried in Sand. InAdvanced Materials Research 2011 (Vol. 243, pp. 3151-3156). Trans Tech Publications Ltd.

6. Gerlach T, Achmus M, Terceros M. Numerical Investigations on District Heating Pipelines Under Combined Axial And Lateral Loading. Energy Procedia. 2018 Sep 1;149:435-44.

7. Sheil BB, Martin CM, Byrne BW, Plant M, Williams K, Coyne D. Full-scale laboratory testing of a buried pipeline in sand subjected to cyclic axial displacements. Géotechnique. 2018 Aug;68(8):684-98.

8. Reza A, Dhar AS, Muntakim AH. Full-Scale Laboratory Pullout Testing of 60-mm Diameter Buried MDPE Pipes. 7th International Conference on Engineering Mechanics and Materials, CSCE. Laval (Greater Montreal), QC, Canada. 2019a Jun 12-15.

9. Reza A, Dhar AS, Rahman M. Weerasekara L. Pulling rate effects on the pullout force of buried small diameter MDPE pipe in loose sand. 72th Canadian Geotechnical Conference, GeoSt.John's. St.John's, NL. 2019b Sep 29- Oct. 2.

10. Wijewickreme D, Weerasekara L. Analytical modeling of field axial pullout tests performed on buried extensible pipes. International Journal of Geomechanics. 2015 Apr 1;15(2):04014044. doi: 10.1061/(ASCE)GM.1943-5622.0000388.

11. Reza A. Dhar AS. Axial Pullout Behaviour of Buried Medium Density Polyethylene Gas Distribution Pipes. International Journal of Geomechanics, ASCE. 2020. (under review).

12. Dassault Systems. ABAQUS/CAE user's guide. Dassault Systemes Simulia Corporation, Providence, RI, USA. 2014.

13. Murugathasan P, Dhar AS, Hawlader BC. An Experimental and Numerical Investigation of Pullout Behavior of Ductile Iron Water Pipes Buried in sand. Canadian Journal of Civil Engineering. 2020 Jan 13(ja). doi: org/10.1139/cjce-2019-0366

14. Suleiman MT, Coree BJ. Constitutive model for high density polyethylene material: systematic approach. Journal of materials in civil engineering. 2004 Dec;16(6):511-5. doi: 10.1061/(ASCE)0899-1561(2004)16:6(511)

15. Luo X, Ma J, Zheng J, Shi J. Finite element analysis of buried polyethylene pipe subjected to seismic landslide. Journal of Pressure Vessel Technology. 2014 Jun 1;136(3).

16. Muntakim AH, Dhar AS, Rahman M. Pipeline behavior subjected to large ground movement. *70th* Canadian Geotechnical Conference, GEOOTTAWA. Ottawa, ON. 2017 Oct. 1-4.
17. Yimsiri S, Soga K, Yoshizaki K, Dasari GR, O'Rourke TD. Lateral and upward soil–pipeline interactions in sand for deep embedment conditions. Journal of geotechnical and geoenvironmental engineering. 2004 Aug;130(8):830-42.

18. Janbu N. Soil compressibility as determined by odometer and triaxial tests. InProc. Europ. Conf. SMFE 1963 (Vol. 1, pp. 19-25).
19. Guo PJ, Stolle DF. Closure to "Lateral Pipe–Soil Interaction in Sand with Reference to Scale Effect" by PJ Guo and DFE Stolle. Journal of Geotechnical and Geoenvironmental Engineering. 2006 Oct;132(10):1372-. doi:10.1061/(ASCE)1090-0241(2005)131:3(338)

20. Daiyan N, Kenny S, Phillips R, Popescu R. Investigating pipeline–soil interaction under axial–lateral relative movements in sand. Canadian Geotechnical Journal. 2011 Nov;48(11):1683-95.

21. Jung JK, O'Rourke TD, Olson NA. Uplift soil–pipe interaction in granular soil. Canadian Geotechnical Journal. 2013;50(7):744-53.

22. Roy K, Hawlader B, Kenny S, Moore I. Finite element modeling of lateral pipeline–soil interactions in dense sand. Canadian Geotechnical Journal. 2015;53(3):490-504.

23. Saha RC, Dhar A, Hawlader B. Shear strength assessment of a well-graded clean sand. InAnnual conference of Canadian Geotechnical Society, GeoSt. John's 2019.

24. Scarpelli G, Sakellariadi E, Furlani G. Evaluation of soil–pipeline longitudinal interaction forces. Rivista Italiana di Geotecnica. 2003;37(4):24-41.

25. Cruden DM, Varnes DJ. Landslides: investigation and mitigation. Chapter 3-Landslide types and processes. Transportation research board special report. 1996(247).

APPENDIX C

Pulling Rate Effects on the Pullout Force of Buried Small Diameter MDPE Pipe in Loose Sand

This paper has been published and presented in 72nd Canadian Geotechnical Conference, GeoSt.John's 2019, St. John's, NL, Canada, Sept. 29–Oct. 2, 2019. Most of the research work presented in this paper was conducted by the first author. He also prepared the draft manuscript. The other authors supervised the research and reviewed the manuscript.

Pulling rate effects on the pullout force of buried small diameter MDPE pipe in loose sand

Auchib Reza[1], Ashutosh Sutra Dhar[1], Mujib Rahman[2] & Lalinda Weerasekara[3]
[1]*Department of Civil Engineering – Memorial University of Newfoundland, St. John's, NL, Canada*
[2]*FortisBC Energy Inc., Surrey, BC, Canada*
[3]*WSP Canada Inc., Vancouver, BC, Canada*

ABSTRACT
Buried pipelines have been operated worldwide for decades as the most convenient means of transporting natural gas and liquid. Polyethylene pipes came into extensive use during the latter half of the twentieth century. These pipelines are sometimes impacted by ground movements triggered by landslides, earthquake fault rupture as well as other natural hazard and human-induced sources. Owing to the lack of alternative approaches, soil–pipe interaction models developed for steel pipes are often used for assessing the PE pipe subjected to ground movement. However, the difference between the behaviours of PE and steel pipes subjected to ground loads are well recognized. PE pipe materials are flexible compared to steel and show nonlinear time and temperature dependent stress–strain responses. As a result, stress or strain developing in the pipe due to ground movement is influenced by the rate of loading and the temperature. However, limited studies have been performed to examine the impact of temperature and ground movement rates. In the current research, a series of full-scale laboratory tests were performed at Memorial University of Newfoundland to investigate the effects of loading rates on buried medium-density polyethylene (MDPE) pipes subjected to axial movements relative to the soil. Although pipes with different diameters buried in dense and loose sand are being investigated as a part of the research project, tests completed for small diameter MDPE pipes in loose sand are discussed in this paper. The study reveals that a relatively higher loading rate offered a higher axial pullout resistance from the soil and induced higher axial strains on the pipe.

RÉSUMÉ
Les conduites enterrées sont exploitées dans le monde entier depuis des décennies et constituent le moyen de transport le plus pratique pour le gaz naturel et les liquides. Les tuyaux en polyéthylène ont été largement utilisés au cours de la seconde moitié du vingtième siècle. Les mouvements de terrain provoqués par des glissements de terrain, la rupture d'une faille sismique, ainsi que par d'autres dangers naturels ou d'origine anthropique, sont parfois à l'origine de ces pipelines. Faute d'approches alternatives, les modèles d'interaction sol-tuyau développés pour les tubes en acier sont souvent utilisés pour évaluer le tube en PE soumis au mouvement du sol. Cependant, la différence entre les comportements des tubes en PE et des tubes en acier soumis à des charges au sol est bien reconnue. Les matériaux des tuyaux en PE sont flexibles par rapport à l'acier et présentent des réponses contrainte-déformation non linéaires en fonction du temps et de la température. En conséquence, les contraintes ou les déformations dans la conduite dues au mouvement du sol sont influencées par la vitesse de chargement et la température. Cependant, des études limitées ont été réalisées pour examiner l'impact de la température et des taux de mouvement du sol. Dans les recherches actuelles, une série d'essais en laboratoire à grande échelle a été réalisée à l'Université Memorial de Newfoundland pour étudier les effets des taux de charge sur les canalisations enterrées en polyéthylène à moyenne densité (MDPE) soumises à des mouvements axiaux par rapport au sol. Bien que des recherches sur des tuyaux de différents diamètres enfouis dans du sable dense et en vrac fassent partie du projet de recherche, les essais réalisés pour les tuyaux en MDPE de petit diamètre dans du sable en vrac sont discutés dans le présent document. L'étude révèle qu'un taux de charge relativement élevé offre une résistance à l'arrachement axial plus élevée du sol et induit des contraintes axiales plus élevées sur le tuyau.

1. INTRODUCTION

Buried pipelines are extensively used as a dependable mode of transportation of oil and gas. About 2 million km of transmission pipelines are operated worldwide (CIA 2009). About half a million km of local distribution pipelines are operated in Canada (NRC 2016). Failure of transmission and/or distribution pipes can have adverse effects on the associated utility, economy, and public health. Among the various causes of pipeline failure, ground deformation has been responsible for 15% of the total incidents of onshore pipelines over the last ten years, as reported in the 10th report of European Gas Pipeline Incident Data Group (EGIG, 2018).

Ground deformation may occur from hazards including landslide, mining, erosion, liquefaction, and differential soil movement at the fault lines. Landslides are by far the most typical types of ground movements encountered by the pipelines. Ideally, the routing of a buried pipe is selected to avoid these natural hazards. Where this is not possible, the effects of postulated ground motions are considered.

Pipelines crossing active landslide areas are subjected to additional loads due to ground movements. Longitudinal load on the pipeline is expected when the direction of the

ground movement is parallel to the pipe axis. The regions where ground movement can occur, have the potential to cause significant strain on the pipelines in a network. With the development of modern technologies (e.g., Global Positioning System (GPS) surveys, in-place slope inclinometer (IPSI) string) ground movements and its variations over time can be detected reasonably precisely in the field. However, estimating the strains in a buried pipe is difficult, even with available ground deformation data. It is essential to understand the response of the pipe to those induced strains to define a safe operating window.

Over the years, numerous studies have been conducted to understand the soil–pipe interaction mechanisms of pipes subjected to ground movements (Wijewickreme et al. 2009; Meidani et al. 2017; Bilgin and Stewart, 2009ab; Liu et al. 2011; Gerlach and Achmus, 2018; Sheil et al., 2016). However, most of these studies focused on understanding the behaviour of steel pipe. PE pipe materials are flexible compared to steel and show nonlinear time and temperature dependent stress–strain responses. As a result, stresses or strains developing in the pipe due to ground movement are influenced by the rate of loading and the temperature. However, limited studies have been performed on evaluating the temperature and rate–dependent responses of the soil–pipe interaction. Weerasekara and Wijewickreme (2008) and Wijewickreme and Weerasekara (2015) experimentally observed the effects of loading rate on the axial strain development on a buried MDPE pipe. They proposed an analytical method to calculate the pipe strain observed in their experiments. Bilgin and Stewart (2009b) revealed that the diameter of polyethylene pipe changes with temperature that affects the pullout force. As mentioned earlier, the loads on the pipelines due to landslides may depend on the rate of ground movement, the effects of different rates of landslide on the pipeline integrity have not been investigated extensively. Thus, the objective of the current research is to develop an improved understanding of the rate–dependent effect of buried MDPE pipes using full-scale tests. While pipes buried in dense and loose sand are investigated in this research, the results of pipe tests in loose sand are presented in this paper.

2. AXIAL PULLOUT FORCE

The maximum axial soil load on a pipe subjected to axial ground movements can be calculated using the formula recommended in ASCE (1984) and ALA (2001) guidelines. These guidelines use a simplified method to calculate the maximum pullout force due to axial landslide without proper consideration of soil–pipe interaction. As the general form of the equations was not varied significantly over the past 30 years, it is a common practice to determine the axial loads for the onshore buried pipeline in cohesionless soil using the following expression as in Eq. 1:

$$F_A = \gamma \times H \times (\pi\, D\, L) \times \left(\frac{1+K_0}{2}\right) \times \tan\delta \qquad [1]$$

where, F_A = the maximum axial soil resistance; γ = average effective unit weight of the soil; H = depth from the ground surface to pipe springline; L = pipe length; D = pipe outer diameter; K_0 = coefficient of lateral earth pressure at rest and δ = interface friction angle between the pipe and the surrounding soil. This equation employs the average of the estimated vertical and lateral stresses at the springline of the pipe as the normal stress on pipe wall. It is assumed that the normal stresses on the pipe remain the same even after shear displacements occur at the soil–pipe interface, and the pipe is rigid so that an uniform shearing stress occurs over the entire length of the pipe. However, (Muntakim and Dhar 2018) revealed through finite element analysis that the axial pullout force on pipeline depends on relative rigidity of pipe with respect to surrounding soil. It is reported that the interface normal stresses during axial pullout was higher for the pipe with higher rigidity (i.e., the steel pipe). Thus, the recommended equation in current guidelines may not be applicable for flexible MDPE pipelines. To validate these findings experimentally, full-scale tests are conducted using a new laboratory testing facility developed at Memorial University of Newfoundland. Tests conducted with a 42.2-mm diameter MDPE pipe in loose sand subjected to relative axial movements are discussed in the current paper.

3. TEST MATERIAL, EQUIPMENT, AND METHODS

A new full-scale pipe test facility has been designed and constructed at Memorial University of Newfoundland at St. John's, NL, to investigate the behaviour of flexible pipes subjected to axial pullout. The pipe test facility is a steel box with inside dimensions of 2 m in width, 4 m in length, and 1.5 m in depth. The test pipe is backfilled with sand found locally. The pipe is protruded out of the test box from two ends through two circular openings which are adjustable to accommodate pipes of different diameters. The openings are somewhat larger than the pipe diameter, which is filled using a rubber gasket with lubrication to minimize friction between the pipe and the tank wall at the openings. The profile view of the test box is given in Figure 1. The test sand is directly in contact with the inside walls of the steel box. No step has been taken to reduce the sidewall friction. Weerasekara and Wijewickreme (2008) revealed that the effect of sidewall friction on axial pullout test is insignificant during the axial pullout. Researchers commonly employ sidewall treatment to reduce the effects of arching under vertical loads (Dhar and Moore 2006).

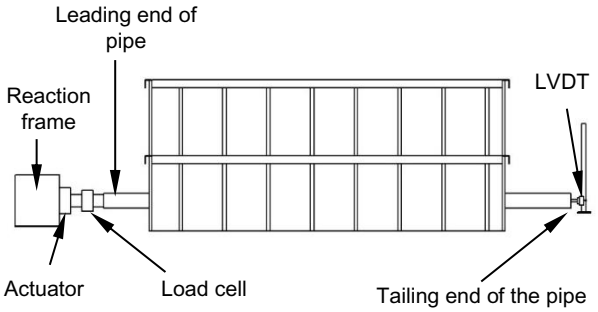

Figure 1. Profile view of the test box along with pipe instrumentations

3.1 Test Pipe

Four 4.6 m long 42.2-mm nominal diameter, with a standard dimension ratio (SDR, a ratio of the pipe outside diameter to wall thickness) of 10, MDPE pipe segments are used for the tests. These gas distribution pipes are CSA B137.4 certified and mostly used for the gas utilities across Canada. The pipe once used for pullout test is never used in subsequent tests to avoid the effects of residual stresses.

3.2 Sand Backfill

A locally available well-graded sand (USCS classification = SW) is used as the backfill material for the pipe. The soil contains, by weight, approximately 1.30% of fines and 98.70% of sand. The coefficient of uniformity (C_u) and the coefficient of curvature (C_c) were 6.5 and 0.75 respectively. The particle size distribution is given in Figure 2. The maximum dry density is obtained as 18.9 kN/m^3 from Standard Proctor Compaction tests (ASTM D698 2003) (Saha et al. 2019).

The strength parameters of the sand have been determined using direct shear tests at normal stress ranging from 25 kPa to 50 kPa representing the typical field soil stress conditions of oil and gas distribution network using polyethylene (PE) pipelines. An internal friction angle of 33° is obtained from the direct shear test of this sand at the loosest state at a unit weight of 12 kN/m^3 (nearly 2% of moisture content) at these stress levels (Saha et al. 2019).

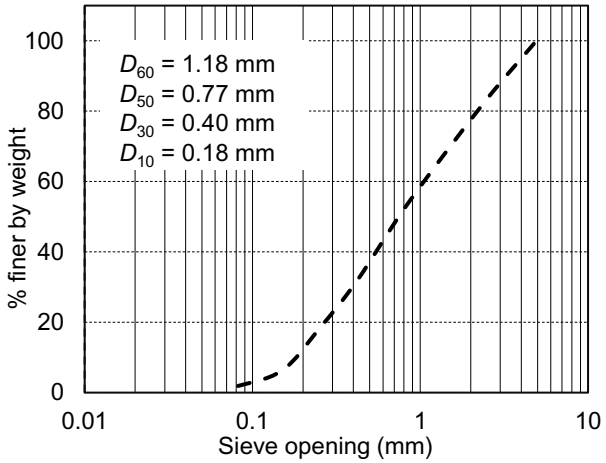

Figure 2. Particle size distribution of test sand (After Saha et al. 2019)

3.3 Pipe Installation

Test cell is first backfilled up to a depth of five times the pipe diameter below the pipe center to represent native soil. Soil is then placed at 100 mm thick lifts which are spread over the test box using a wooden spreader. Extra precautions have been taken while spreading the sand to prepare the backfill in loose conditions. When the pipe invert level is reached, the soil surface is uniformly levelled to minimize stress concentrations at potential localized hard spots. Then the pipe is placed straight on the levelled soil surface. Placing of soil is then continued consistently until the desired burial depth for the pipe is achieved. Density measurements are taken at three different locations inside the testing tank. Note that the flexible MDPE pipe may not always be straight, particularly in uneven ground, which may affect the pullout force. The effect of out-of-straightness on the pullout force has not been investigated here.

Density of the backfill sand plays a vital role in the pullout resistance because interface friction angle between the pipe and sand increases with increasing density of sand. More importantly, the densities of soil influence the normal stresses on the pipe during the axial pullout. After the completion of axial pullout test, density measurements are taken at different locations, which yielded an average unit weight of 12 kN/m^3 from the top surface to the pipe springline level. Thus, the average relative compaction of the backfill material is roughly 60% of the Standard Proctor Maximum dry density. Air-dry condition of sand with the water content of around 1.5% for Test 1 and less than 1% for Tests 2–4 is confirmed during the tests through measurements of water content.

Figure 3. Bedding for MDPE pipe in loose sand inside the testing cell

The tested MDPE pipe and sand are removed from the tank after each test, and the pipe installation procedure is repeated in a consistent manner for the next tests (Figure 3).

There different pipe pullout tests were conducted with pulling rates of 0.5, 1, and 2 mm/min (termed herein as Test 1, 2, and 3, respectively)

3.4 Instrumentation

Four different types of instrumentation were used including piezoresistive tactile pressure sensor (Tekscan 2009), linear variable differential transducer (LVDT), load cell and strain gauges. Pressure sensors are used to measure the changes of vertical and lateral soil pressures near to the pipe during axial pullout (not discussed in this paper). LVDTs are needed to measure the axial movement during

the pullout tests. Load cell is used to measure the resisting force of the soil to the pipe movements, which is equal to the pullout forces applied to the pipe. Also, pipe wall strains are monitored using an array of electrical resistivity strain gauges. A pipe without strain gauge is also tested to examine if the surface roughness caused by the strain gauge placement may affect the pullout force. However, no significant effect on the pullout force due to strain gauge placement was found. The data from the load cell, LVDT and strain gauges are monitored using a computer-controlled data acquisition system. There was a total of seven channels for reading measurements in the data acquisition system: one for the load cell, five for the strain gauges and one for the LVDT. For the selected range of displacement rates, all measurements were recorded at two samples per second.

(a) (b)

Figure 4. Strain gauge installation techniques (a) before wrapping (b) after wrapping using duct tape and electrical tape.

The capacity of the load cell used is 22.25 kN with a system accuracy of ±4.45 N. The stroke and piston area of the load cell are 150 mm and 32,390 mm^2 respectively. A LVDT was attached to the opposite end of the load cell, called herein as the tailing end. The LVDT has a total travel capacity of 110 mm with an accuracy of about 0.50 mm. Three uniaxial strain gauges were installed: at one-fourth, half and three-fourths of the pipe length within the box. The uniaxial strain gauges were placed at the pipe crown. One biaxial strain gauge was attached to the pipe invert at the mid-length of pipe within the test box to monitor longitudinal and circumferential strains. Strain gauge installation techniques are shown in Figure 4. A further detailed description of the testing facility with instrumentation is available in Reza et al. (2019).

4. EXPERIMENTAL RESULTS

4.1 Axial Load Versus Displacement Response

The pullout forces measured during the tests are presented in Figure 5. As seen in Figure 5, the pullout resistance increases nonlinearly with the displacement of the leading end of the pipes. The soil resistances reach its first peak and then slightly decrease with displacement. Afterwards, the axial soil force starts to increase again that continues up to the end of the experiment. The experiments were terminated when the leading end displacement reached 120 mm. The initial part of the load–displacement response is associated with the elongation of the pipe under the axial pullout force. No movement of the tailing end of the pipe is observed during this period. The axial force in the pipe increases with the increase of pullout displacement at the leading end and reaches the peak value when the tailing end starts to move. The tailing end of the pipe starts to move when the shear strength at the soil–pipe interface is mobilized over the entire length of the pipe. Immediately after mobilization of the shear strength over the entire pipe, the pullout force slightly reduces. Then, the pullout force increases again at a much slower rate, which is potentially due to the densification of the loose soil with rigid body movement of the pipes. The increase of the pullout force due this effect is significant, particularly at large displacement. However, the magnitudes of axial force for the pipes are less (<1.5 kN). The effect of the post-peak increase of pullout force may not be observed in the field since the soil is not confined within a boundary as in the case of the laboratory test box.

Figure 5 reveals that the rate of loading significantly affects the maximum pullout forces of the pipes. The pullout force is the highest for the test conducted at the loading rate of 2 mm/min (Test 3). However, the maximum pullout force in Test 2 conducted at 1 mm/min of loading rate is less than the pullout force in Test 1 conducted at a loading rate of 0.5 mm/min in Figure 5. To confirm the results of Test 2, an additional test with a loading rate of 1 mm/min (Test 4) was conducted, and almost identical results were observed (Figure 5). An additional test for Test 1 has not been conducted. The higher pullout force in Test 1 is likely due to a different level of compaction of the backfill soil, which was challenging to maintain at the loose condition. Besides, the water content of the backfill in Test 1 was higher than the water content of the backfill in other tests.

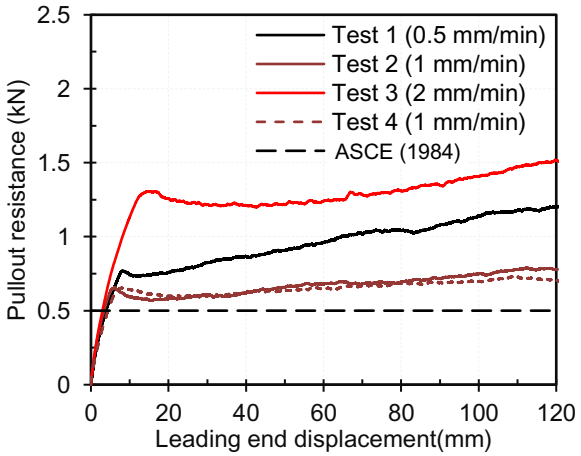

Figure 5. Pullout resistance with leading end displacement of the pipe

The peak axial force is also calculated using the current design guidelines (ASCE 1984, ALA 2001) that provided the maximum pullout resistance of 0.5 kN (shown in Figure 5). Here the k_0 value (from Jaky's formula, $K_0 = 1\text{-}\sin\phi$) is calculated using ϕ of 33°, corresponding to the peak friction angle of the local sand at the test density, the interface friction angle (δ) between the MDPE pipe surface and sand

is assumed to be 18°and effective unit weight of sand used (γ) of 12 kN/m^3 which is in loose condition. The calculated pullout force from the design equation is less than the maximum pullout force observed during the tests. From the comparison of peak pullout resistances, it reveals that the maximum pullout resistance for the MDPE pipes depends on the pulling rate of the pipes, which is not considered in the current design guidelines. As a result, the equation in the design guidelines underestimated the axial force for the pipes. As may be noted, the current design guidelines developed for steel pipes are the only resource available for assessing the pipelines subjected to ground movement. The study reveals that the existing design guidelines are not applicable for calculation of pullout force for MDPE pipes.

4.2 Pipe Deformation

The elongation of the pipes obtained during the tests is presented in Figure 6. The figure plots pipe elongations, calculated from the difference between the leading end displacements and tailing end displacements, against the leading end displacements. In the figure, the pipe elongation increases linearly up to leading end displacement of 8 mm, 6 mm and 12 mm in Tests 1, 2 and 3, respectively where mobilization of interface shear stress occurs over the entire pipe length. After that, the pipe elongation is stabilized or increased at a slower rate. The increase in pipe elongation beyond the first peak load is associated with the increase of soil resistance to the axial pipe movement. It also shows that the tailing end begins to move at the leading end displacement of 8, 6, and 12 mm in Tests 1, 2, and 3, respectively. Thus, the leading end displacement is initially due to the elongation of the pipes only. Therefore, the interface shear strength is not mobilized over the entire length of the pipes up to these displacements.

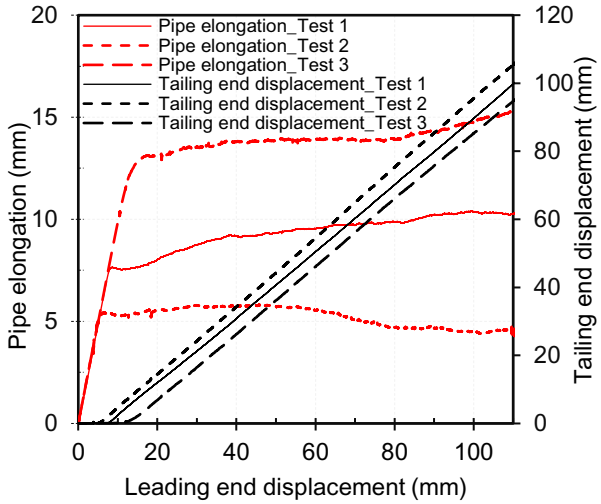

Figure 6. Pipe elongation and tailing end displacement with leading end displacement of the pipe

4.3 Axial Strain

During the tests, pipe wall strains are measured at three locations along the length of the pipes. Strain gauges are placed on the pipe crown at the distances of a quarter (L/4), half (L/2) and a three-quarter (3L/4) of the pipe length within the test cell measured from the pulling end. Figure 7 shows that the axial strains increase linearly with the increase of the leading end displacement and reach its first peak values at the point where the interface shear strength is fully mobilized, and the first peak pullout resistance is reached. Beyond this point, the tailing end of the pipe moves, and the axial strain continues to increase at a very slow rate. The rate of increase of axial strain is higher in Test 3 up to its first peak, which is consistent with higher pullout resistance discussed earlier.

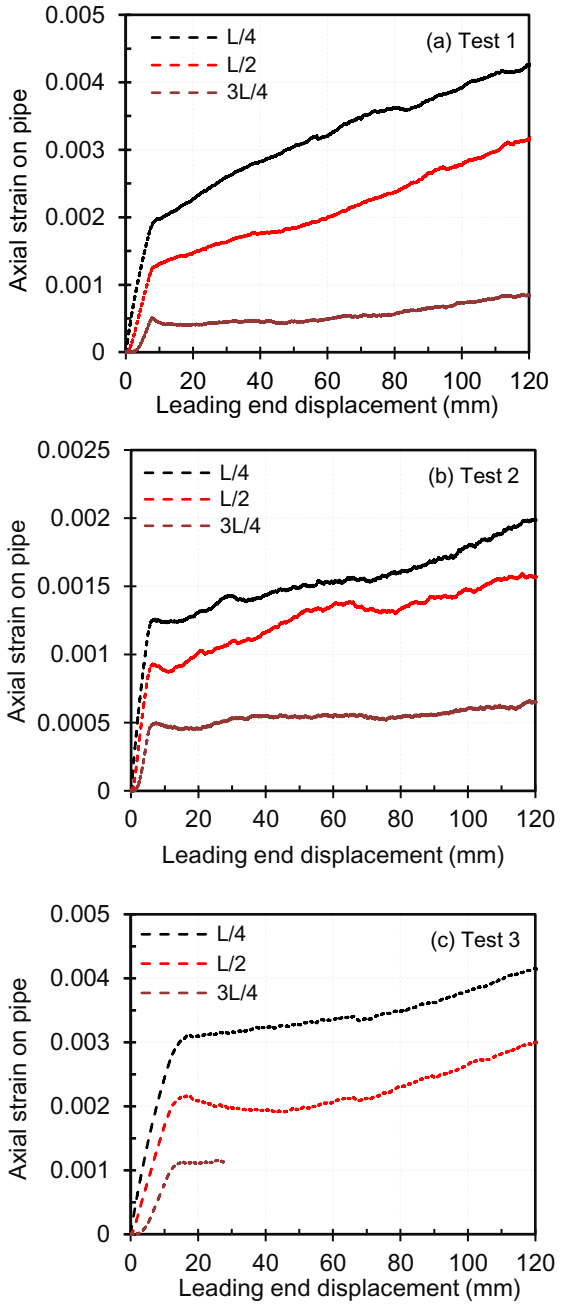

Figure 7. Axial strains at different locations of the pipes

The mobilization of axial force along the length of the pipe can be examined from the axial strains along the pipe length. The strain distribution along the MDPE pipe length for different leading end displacement of the pipe in Test 1 is shown in Figure 8. It shows that with leading end displacement, axial strain propagates progressively from the leading end towards the tailing end of the pipe (such as higher toward the leading end and less toward the tailing end). For example, in Test 1, the point at *L*/4 (i.e., at 1 m from the leading end within the test box) experiences axial strain almost immediately after application of leading end displacement, while the points at the distances of *L*/2 (i.e., at 2 m length) and 3*L*/4 (i.e., at 3 m length) experience axial strains at around 2.5 mm and 5 mm of leading end displacements, respectively. Therefore, soil resistance is developed over 50% of pipe length at ~2.5 mm leading end displacement and over 75% of pipe length at ~5 mm leading end displacement. Initially, the soil resistance increases almost linearly that reach the peak below when the interface shear strength is fully mobilized. After mobilization of shear strength over the entire pipe length unit shearing resistance is expected to be constant, which can be examined from the distribution of axial strains along the pipe length. The distributions of the axial strain are almost linear along the pipe length until higher leading end displacement is reached (Figure 8). This implies that unit shear resistance at the pipe–soil interface is constant along the pipe length, after full mobilization of the shear strength. Thus, the maximum pullout resistance may be calculated through prediction of the unit interface shear resistance. The maximum axial strains experienced by the pipe is 0.5% at the leading end displacement of 100 mm of the pipe, which is not significant for the MDPE pipe.

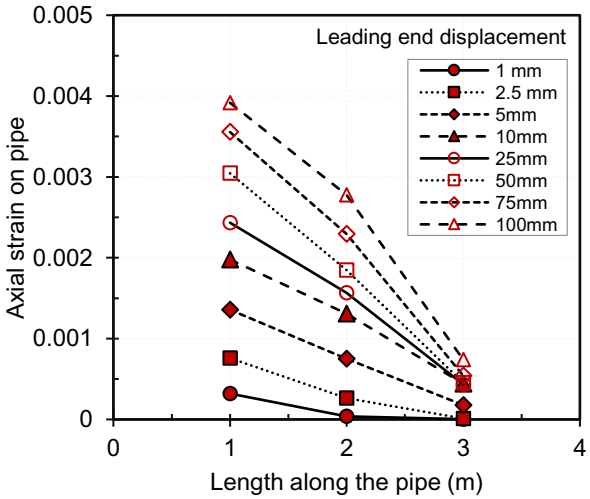

Figure 8. Axial strain distribution along pipe length (Test 1)

A biaxial strain gauge is attached in Test 1 and Test 3 at the 1/2 length of pipe at the invert level to monitor axial and circumferential strains, as shown in Figure 9. Figure 9 shows circumferential compressive strain develops at the invert, which is associated with the change in the pipe diameter during the test. This diameter change is also not accounted in the current design method for calculation of the maximum pullout force. However, the effect of the change in diameter may be insignificant for pipes with high internal pressures. The circumferential compression and the change in pipe diameter are likely due to the Poisson's effect under the axial load. The ratio of the circumferential strain to the longitudinal strain is 0.45, which is the Poisson's ratio of the pipe material.

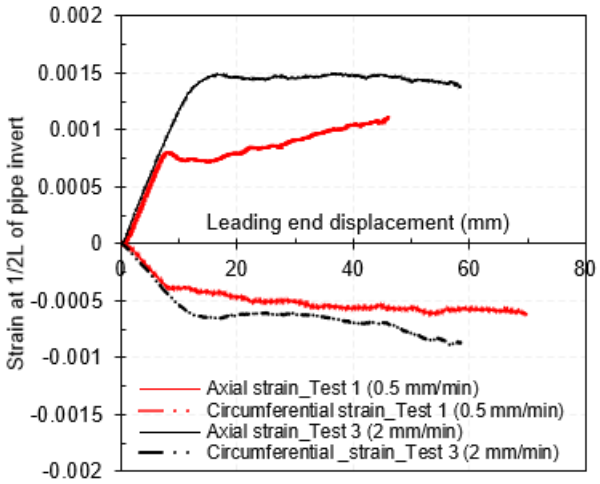

Figure 9. Axial and circumferential strains at pipe invert level

4.4 Strain Rate on Pipe during Pullout

Since MDPE pipes are viscoelastic, it responds to induced strain in a time–dependent manner. The response to the pullout forces applied to the pipe not only depends upon the resistance offered by the surrounding soil but also on the strain rate of the pipe, since stress is not only a function of strain but also a function of strain rate for MDPE.

The strain rates during the tests are examined from the measured axial strains as shown in Figure 10. Figure 10 shows that initial high strain rates reduce with the leading end displacement. The strain rates significantly drop beyond the full mobilization of shear strength over the entire pipe length (i.e., peak pullout force). After full mobilization of shear strength pipe movements as rigid body contributes, and therefore the strain rate is decreased and reaches close to zero. The computed strain rate at the distances of *L*/4 starts to decrease immediately after application of leading end displacement, while the strain rates at the distances of *L*/2 and 3*L*/4 increase up to 6 to 8 mm leading end displacements, and then begins to decrease. Beyond the leading end displacement of about 20 mm, the rate of strains stabilizes (reaches to a constant value) at different points (e.g., *L*/4, *L*/2, 3*L*/4 distances along the pipe length) on the pipe wall.

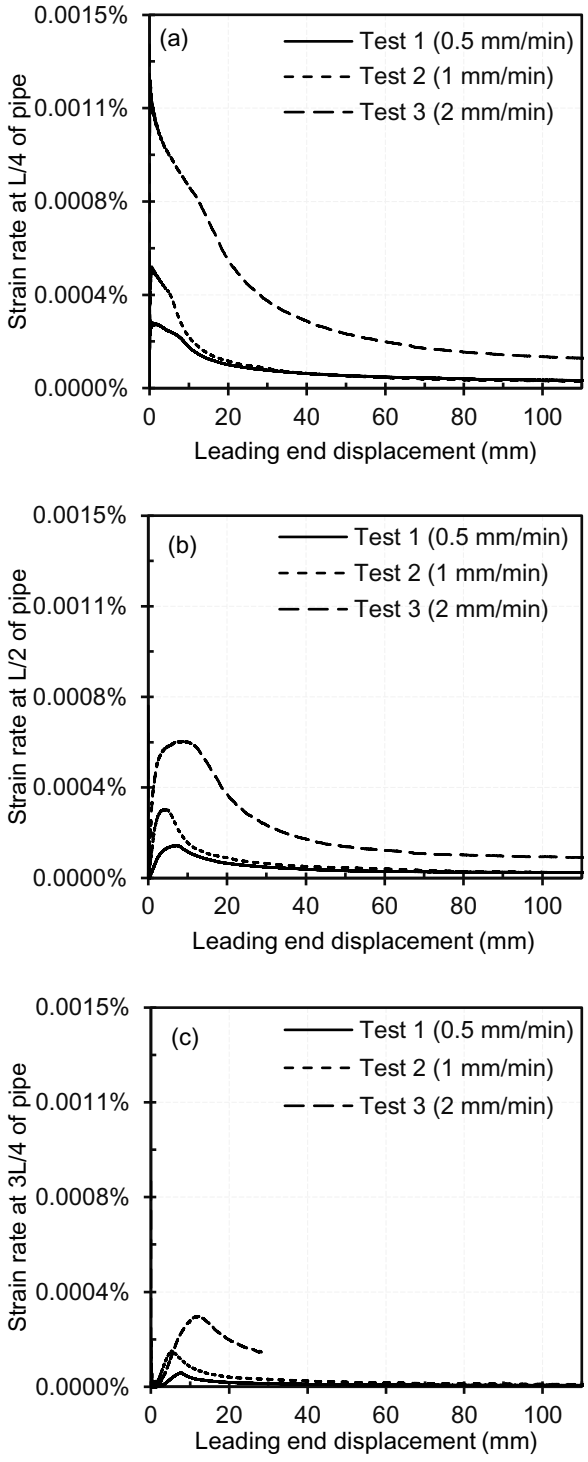

Figure 10. Strain rate responses to pipe movements at (a) *L*/4 (b) *L*/2 (c) 3*L*/4 distances along the pipe length

5. CONCLUSION

A full-scale testing facility at Memorial University of Newfoundland is used to investigate the behaviour of the flexible 42.2-mm diameter MDPE pipes buried in loose sand subjected to axial ground movements. The measurements of axial pullout resistance, pipe movements and axial pipe strains mounted at different circumferential locations on the pipe wall were monitored during the tests. The test results reveal that the existing design guidelines (ASCE 1984, ALA 2001) may not be applicable for predicting the maximum axial force on MDPE pipelines due to ground movement. The main conclusions are:

- The maximum pullout force on MDPE pipes depends on the rate of relative ground movement. The peak pullout force is higher in the tests with higher displacement rates. ASCE (1984) and ALA (2001) design guidelines do not account for the effect of the rate of ground movement.
- MDPE pipes elongate during application of pullout force, and axial force is not mobilized over the entire length of the pipe at the same time. Pipe–soil interface shear strength is also not mobilized at the same time.
- The distribution of axial strain along the pipe length is almost linear after full mobilization of the interface shear strength at leading end displacement beyond 10 mm. Thus, the distribution of the axial force can be assumed to be linear along the pipe length. A maximum of 0.5% axial strain is attained after the leading end of the pipe has reached over 100 mm of relative movements (in Test 1), which is not significant.
- The strain rate is not the same along the pipe length during axial pullout. The variation of strain rates may affect the soil–pipe interaction for buried MDPE pipe.

6. ACKNOWLEDGEMENTS

The financial and/or in-kind support for this research is provided by the Collaborative Research and Development Grant program of Natural Science and Engineering Research Council of Canada, InnovateNL program of the Government of Newfoundland and Labrador, FortisBC Energy Inc. and WSP Canada Inc., which are gratefully acknowledged. The authors are thankful for the technical assistance by Jason Murphy, Shawn Organ and Matt Curtis in the Faculty of Engineering and Applied Science at Memorial University of Newfoundland. Undergraduate students Alex David McNeil and Shadi Soliman helped with instrumentation and pipe installation and deinstallation during the tests.

7. REFERENCES

ALA. 2001. *Guidelines for the design of buried steel pipe*, American Lifeline Alliance (ALA), available from www.americanlifelinesalliance.org/Products_new3.htm.

ASCE. 1984. *Guidelines for the seismic design of oil and gas pipeline systems*, ASCE, New York.

ASTM. 2003a. *Standard test method for coefficient of linear thermal expansion of plastics between −30°C and 30°C with a vitreous silica dilatometer*, D696, 2003 annual book of standards, Vol. 08.01, West Conshohocken, Pa.

ASTM. 2003d. *Standard test method for rubber property—Durometer hardness*, D2240, 2003 annual book of standards, Vol. 09.01, West Conshohocken, Pa.

ASTM. 2003e. *Standard test method for tensile properties of plastics*, D638, 2003 Annual book of standards, Vol. 08.01, ASTM, West Conshohocken, Pa.

ASTM D698. 2003. *Standard test method for laboratory compaction characteristics of soil using standard effort (12,400 ft-lbf/ft^3 (600kN-m/m^3)*. 2003 annual book standards, West Conshohocken, Pa, 4(8).

Bilgin, Ö. and Stewart, H. E. 2009a. Pullout Resistance Characteristics of Cast Iron Pipe, *Journal of Transportation Engineering*, ASCE, 135(10): 730–735.

Bilgin, Ö., & Stewart, H. E. 2009b. Design Guidelines for Polyethylene Pipe Interface Shear Resistance, *Journal of Geotechnical and Geoenvironmental Engineering*, ASCE, 135(6): 809-818.

CIA. 2009. *Central Intelligence Agency,* The World Factbook.Availablefromhttps://www.cia.gov/library/publications/download/download-2009/index.html

Dhar, A.S. and Moore, I.D. 2006. Evaluation of Local Bending in Profile-Wall Polyethylene Pipes, *Journal of Transportation Engineering*, ASCE, 132(11): 898-906.

European Gas Pipeline Incident Data Group, 2018. Gas pipeline incidents. *European Gas pipeline Incident Data Group (EGIG)*, Groningen, Netherlands. 10th EGIG Report 1970–2016, No. VA 17.R.0395.

Gerlach, T. and Achmus, M. 2018. Numerical Investigations on District Heating Pipelines Under Combined Axial and Lateral Loading, *16th International Symposium on District Heating and Cooling, DHC2018*, 9-12 September 2018, Hamburg, Germany.

Liu, R., Guo, L., Yan, S. and Xu, Y. 2011. Studies on Soil Resistance to Pipelines Buried in Sand, May, doi:org/10.4028.

Muntakim, A.H. and Dhar, A.S. 2018. Investigating axial pullout behavior of buried polyethylene pipelines, Newsletter, *International Association For Computer Methods And Advances In Geomechanics*, Volume 23, January- December 2018.

Meidani, M., Meguid, M. A. and Chouinard, L. E. 2017. Evaluation of Soil–Pipe Interaction under Relative Axial Ground Movement, *Journal of Pipeline Systems Engineering and Practice*, ASCE, 8(4): 1–10, doi:org/10.1061/(ASCE)PS.1949-1204.0000269.

NRC. 2016. Pipelines Across Canada, Natural Resources Canada, www.nrcan.gc.ca/energy/infrastructure/18856 accessed on May 10, 2019.

Reza, A., Dhar, A. S. and Muntakim., A. H. 2019. Full-Scale Laboratory Pullout Testing of a 60-mm Diameter Buried MDPE Pipes. *7th International Conference on Engineering Mechanics and Materials, CSCE,* June 12-15, Laval (Greater Montreal), QC, Canada.

Sheil, B. B. Ã., Martin, C. M. Ã., Byrne, B. W. Ã., Plant, M., Williams, K. and Coyne, D. 2016. Full-scale laboratory testing of a buried pipeline in sand subjected to cyclic axial displacements, *Geotechnique*, doi.org/10.1680/jgeot.16.P.275.

Saha, R. C., Dhar, A. S., Muntakim., A. H. and Hawlader, B. C. 2019. Strength and deformation behaviour of a local sand. *General Conference, CSCE,* June 12-15, Laval (Greater Montreal), QC, Canada.

Weerasekara, L. and Wijewickreme, D. 2008. Mobilization of soil loads on buried, polyethylene natural gas pipelines subject to relative axial displacements, *Canadian Geotechnical Journal*, 45: 1237–1249, doi: org/10.1139/T08-043.

Tekscan .2009. I-scan and High Speed I-scan User Manual (v. 6.0x), Tekscan Inc., Boston, MA.

Wijewickreme, D., Karimian, H. and Honegger, D. 2009. Response of buried steel pipelines subjected to relative axial soil movement, *Canadian Geotechnical Journal,* 46(7): 735–752, doi:org/10.1139/T09-019.

Wijewickreme, D. and Weerasekara, L. 2015. Analytical Modeling of Field Axial Pullout Tests Performed on Buried Extensible Pipes, *International Journal of Geomechanics*, 15(2): 0401444-1-11, doi:10.1061/(ASCE)GM.1943-5622.0000388.

APPENDIX D

Finite Element Modeling of Pipe–soil Interaction under Axial Loading in Dense Sand

This paper has been published and presented in 74th Canadian Geotechnical Conference, GeoNiagara 2021, Niagara Falls, ON, Canada, Sept. 26–29, 2021. Most of the research work presented in this paper was conducted by the first author. He also prepared the draft manuscript. The other author supervised the research and reviewed the manuscript.

Finite element modeling of pipe–soil interaction under axial loading in dense sand

Auchib Reza[1] & Ashutosh Sutra Dhar[1]
[1]*Department of Civil Engineering – Memorial University of Newfoundland, St. John's, NL, Canada*

ABSTRACT
Ground movement is one of the challenges to the structural integrity of buried pipelines, which are the primary ways of transporting oil and gas. In the current study, the axial ground force is investigated for a medium-density polyethylene pipe buried in dense sand. A full-scale laboratory test is conducted, and numerical modeling using the finite-element (FE) method is then performed to explore the pipe–soil interaction mechanics for the pipe in dense sand under axial loading conditions. Three-dimensional (3D) FE analysis is performed using Mohr-Coulomb model available in Abaqus/Standard for the backfill material. The laboratory study demonstrated significant influence of soil compaction that increased the contact stress on the pipe surface. The compaction induced contact stresses are simulated applying a uniform thermal load to a thin layer of soil surrounding the pipe. The results of FE analysis are shown to successfully simulate the test results. Finally, the normal stress distribution along the pipe length is investigated using the FE analysis.

RÉSUMÉ
Le mouvement du sol est l'un des défis pour l'intégrité structurelle des pipelines enterrés, qui sont les principaux moyens de transport du pétrole et du gaz. Dans la présente étude, la force axiale au sol est étudiée pour un tuyau en polyéthylène de densité moyenne enfoui dans du sable dense. Un essai en laboratoire à grande échelle est effectué et une modélisation numérique utilisant la méthode des éléments finis (FE) est ensuite effectuée pour explorer la mécanique de l'interaction tuyau-sol pour le tuyau dans le sable dense dans des conditions de chargement axial. L'analyse FE tridimensionnelle (3D) est réalisée à l'aide du modèle Mohr-Coulomb disponible dans Abaqus/Standard pour le matériau de remblai. L'étude en laboratoire a démontré une influence significative du compactage du sol qui a augmenté la contrainte de contact sur la surface du tuyau. Les contraintes de contact induites par le compactage sont simulées en appliquant une charge thermique uniforme à une fine couche de sol entourant le tuyau. Les résultats de l'analyse FE sont montrés pour simuler avec succès les résultats du test. Enfin, la distribution normale des contraintes le long de la longueur du tuyau est étudiée à l'aide de l'analyse FE.

1 INTRODUCTION

Pipelines are one of the safest ways of transporting liquids and gases from source to the users. However, ground movements resulting from various causes, including landslides, subsidence, and settlement, can pose severe threats to the performance and integrity of pipelines. Local distribution pipelines (e.g., small diameter pipes) are highly susceptible to ground movement impacts due to their operations inside the local community. Therefore, the performance of small diameter pipelines buried in areas prone to ground movement needs considerable attention.

Over the past few decades, many experimental and numerical studies were carried out to develop simplified design methods for assessing the pipeline subjected to ground movements (Trautman and O'Rourke 1983; Guo and Stolle 2005; Weerasekara and Wijewickrame 2008; Sheil et al. 2016). Pipelines are subjected to longitudinal force, inducing potentially unacceptable strains, when the direction of ground movement is parallel to the pipe axis. The current understanding of the longitudinal frictional force along the pipeline, due to relative axial displacement between soil and pipe, is based on the normal stresses acting on the pipe and the frictional characteristics of the soil–pipe interface. Thus, the maximum axial loads on pipes buried in cohesionless soils can be calculated using a simple formula as follows:

$$F_A = \gamma H\left(\frac{1+K_0}{2}\right)\pi DL\tan\delta \quad [1]$$

where F_A = the maximum axial force on the pipe (i.e., soil resistance); γ = unit weight of soil; H = burial depth measured from the ground surface to pipe springline; L = pipe length; D = pipe outer diameter; K_0 = at-rest lateral earth pressure coefficient; and δ = interface friction angle between the pipe and the surrounding soil. Eq. 1 has been recommended for the calculation of axial soil resistances in most design guidelines, such as ASCE (1984), ALA (2005), PRCI (2009). However, discrepancies between the calculated soil resistances and the pipe pullout forces from laboratory tests have been well recognized, particularly for flexible pipes [e.g., polyethylene (PE) pipe] and pipes buried in dense sand (Anderson 2004; Weerasekara 2011).

Flexible polyethylene pipes have been widely used in the natural gas distribution system by utility companies (Bilgin and Stewart 2009; Bilgin 2014). Since PE material exhibits time–dependent material behavior, the pipe–soil interaction is also expected to be time–dependent. Reza and Dhar (2021) experimentally examined the ratedependent axial pullout behavior of medium-density polyethylene (MDPE) pipes in medium sand. A loading rate–dependent interaction factor was found to reasonably simulate the experimental responses for the pipes in medium sand. For pipes in dense sand, the volumetric

expansion (i.e., dilation) of soil during shearing often plays an important role in interface shearing behavior (Robert and Thusyanthan 2015; Wijewickreme and Weerasekara 2015). Besides, the stresses due to compaction of the soil during backfilling can increase the interface frictional resistance, resulting in a higher pullout resistance of the pipe. However, no method is currently available to properly account for the effect of dilation and compaction.

This paper focuses on investigating the effect of dilation and compaction on the pullout behavior of pipelines buried in compacted dense sand. A three-dimensional (3D) FE modeling technique was developed through evaluation with laboratory pullout behavior of MDPE pipes. Compaction-induced stress increases at the interface were simulated through the application of thermal load within a thin soil zone surounding the pipe circumference. The loading rate–dependent interface behavior was modeled based on a previous study of the authors (Reza and Dhar 2021). The results of FE analyses were then used to investigate the normal stresses on the pipe.

2 STUDIES ON THE SOIL COMPACTION EFFECTS

Several studies are available on the effects of soil compaction on buried structures. Katona (1978) noted that, during compaction, both vertical and horizontal pressures in the soil increase due to the dynamic force generated by the compactor. Duncan and Seed (1986) proposed the hysteretic K_0 method to evaluate the compaction-induced stresses on the retaining wall and buried culverts. In this method, the increase of lateral stress could be calculated using the increase of vertical pressure caused by the compaction load times K_0. Taleb and Moore (1999) proposed a technique to model soil compaction, which involves applying additional horizontal stresses within a newly placed soil layer (like those remains in the soil after compaction). The horizontal earth pressure was set equal to the passive earth pressure. The passive earth pressure was associated with the fully mobilized shear strength of the soil and represented the largest values of horizontal stress that could be induced during backfill compaction. Later, Elshimi and Moore (2013) introduced an empirical kneading coefficient, K_n (up to 2), with the passive earth pressure imposed on the soil layer to account for the soil kneading during compaction.

Wang et al. (2017) conducted a numerical study to investigate the effects of the magnitude of compaction pressure on steel-reinforced high-density polyethylene (SRHDPE) pipes during installation. A uniformly distributed pressure of 80 kPa (corresponding to 90-95% degree of compaction) was applied on the surface of each backfill layer to simulate the compaction. However, the compaction pressure was removed when a new lift of backfill was placed, and uniform pressure of 80 kPa was applied on the top of the newly placed soil layer. The residual horizontal stresses were reported 10 kPa, consistent with the compaction-induced residual horizontal stresses reported by Duncan and Seed (1986).

Dezfooli et al. (2014a) applied 20 to 70 kPa horizontal compaction stresses (simulating 85%-95% Standard Proctor Maximum Dry Density) to the soil layer using an equivalent temperature loading. They found that stress values of 20 kPa and 30-50 kPa at the haunch and above springline area of the pipeline, respectively, could successfully simulate the observed behavior of compaction loading. Furthermore, Dezfooli et al. (2014b) derived a formula using the mechanics of material formulations to calculate the temperature required for the simulation of the compaction-induced stresses. The induced lateral stress in the soil due to compaction for different soil types and trench configurations was applied to the FE model using uniform thermal loading.

Soil compaction can also cause stress redistribution around the inclusion, such as buried pipes. Chakraborty et al. (2020) measured the soil pressures around a flexible 60.3 mm MDPE pipe. They found the vertical stresses at the pipe's invert 50% higher than the corresponding geostatic stresses. Wang et al. (2015) measured the earth pressure around SRHDPE pipes during backfilling. The measured vertical earth pressures at the top of the pipe were 10 to 47% greater than the overburden stresses (explained as the negative soil arching effect). The study demonstrated that the lateral earth pressure caused by the compaction of the backfill is constant around the pipe (as suggested in Masada and Sargand 2007).

3 EXPERIMENTAL SOIL BOX TEST

A full-scale pipe testing facility developed at Memorial University of Newfoundland, St. John's, NL, is used to investigate MDPE pipes subjected to axial ground movements. The details of the testing cell, pulling mechanisms, and data acquisition system are described in Murugathasan et al. (2020) and Reza and Dhar (2021).

Table 1 summarises the tests used for the investigation conducted in this paper. These are a subset of a larger test program performed to investigate the axial pullout response of buried MDPE pipes under various pulling rates. More details of the test results will appear elsewhere as a journal article. The results of three pullout tests on 42.2-mm diameter MDPE pipe segments were employed in the current study. The pipe segments were 4.6 m long (4 m inside the cell). The pipe outside diameter to wall thickness, known as Standard Dimension Ratio (SDR), is 10. These gas distribution pipes are CSA B137.4 certified and primarily used for gas distribution across Canada. In each test, the pipe is axially pulled to a displacement of 120 mm. The pipes are buried at a depth of 340 mm (resulting H/D = 8), which falls within the range of standard practice of installation of gas distribution pipes at shallow depth from 0.3 m to 1.5 m (Groves and Wijewickreme 2013). The soil width on each side of the pipes is 1 m, about 24 times the pipe diameter, which is sufficiently far to minimize the boundary effects during axial pullout tests. The tests (Tests 1–3) are performed in compacted sand backfills at three different pulling rates: 0.5 mm/min (Test 1), 1 mm/min (Test 2), and 2 mm/min (Test 3) at the leading end. The pulling rates were selected based on feasibility under the laboratory condition. Note that the pulling rates fall in the velocity Class 5 (>0.3 and <30 mm/min), corresponding to moderate landslide velocity, according to Cruden and Varnes (1996).

Since maintaining consistency in the soil condition (e.g., in situ density) of the test cell is an important consideration for the quality control of the constructions, the same construction method during soil placement and compaction was adopted. Soil density was also measured using the sand cone method for quality control. The backfill material used in each test was in air-dry condition (moisture content less than 1%). Therefore, no increase in soil–pipe interaction forces due to soil suction was expected.

A locally available manufactured sand (Newfoundland and Labrador, Canada) was used as the backfill material for the pipe. This material has been frequently used for geotechnical research purposes at Memorial University of Newfoundland (Chakraborty et al. 2020; Murugathasan et al. 2020; Reza et al. 2019; Reza and Dhar 2021; Saha et al. 2020). The properties of the soil are documented in Saha et al. (2019, 2020).

Table 1. Axial pullout of pipes (D = 42 mm) buried in dense sand

Test No	Avg. unit weight, $\bar{\gamma}$ (kN/m^3)	Burial depth, H (m)	Pulling rate (mm/min)	Pipe thickness, t (mm)	H/D
1-3	19	0.34	0.5, 1, 2	4.22	8

4 FE MODEL DEVELOPMENT

The FE model was developed using the technique employed in Reza and Dhar (2021) for 60.3-mm diameter MDPE pipes. However, as soil dilation and compaction-induced stresses may contribute significantly for the pipes in dense sand, these are considered in the current study, as discussed below.

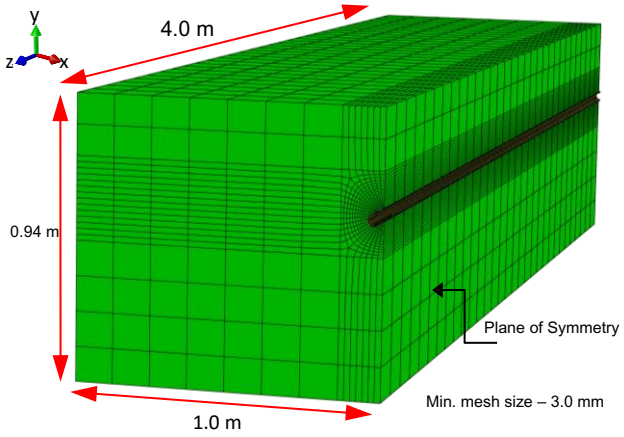

Figure 1. Typical mesh used in FE model

Figure 1 shows a 3D FE model developed to simulate the laboratory pipe pullout tests. The model dimensions are the same as those in the physical model: 4.0 m in length, 2.0 m in width, and 0.94 m in height, where the pipe is buried at a depth of 0.34 m. A commercially available FE software, Abaqus (version 2019), was used (Dassault Systems 2019). Dynamic analysis was performed using the Abaqus/ Standard module that uses implicit time integration to calculate the response of a system. The geometric nonlinearity and large strain formulation in the elements were considered. The nonlinear geometry option, NLGEOM, in Abaqus ensures the equilibrium of the current configuration of the model, considering the changes in geometry during the analysis. The pipe and soil domains were modeled using reduced integration eight-noded linear (lower order) hexahedral elements (C3D8R), available in Abaqus. Because “lower order” elements might be overly stiff, extremely fine meshes are often required to obtain accurate results. Therefore, a finer mesh is used in the close vicinity of the pipe over a radial distance of 2.0 times the pipe diameter (2D) using biased mode seeding. A mesh sensitivity study was conducted, which showed that a minimum element size of 3.0 mm was suitable, which was selected for the analysis. Coarser mesh is used beyond 2D to reduce the computational time. The sides of the soil block are constrained in the horizontal direction. The bottom is constrained in all translational directions. Symmetrical boundary conditions are applied to the pipe and soil on the symmetrical plane (Figure 1).

4.1 Constitutive Models and Materials Parameters

Soil behavior is modeled using the built-in elastic-perfectly plastic non-associated Mohr-Coulomb (MC) model, available in Abaqus, to simulate the sand's stress-strain behavior and shear failure. Since the MC model only demands a few constant soil properties (such as friction angle and dilation angle of soils), it is widely popular for modeling the behavior of soils. Although the soil in the field may experience mobilizations in friction angle and dilation angle with plastic shear strain, the conventional MC model is found to successfully simulate the ultimate soil resistance during the axial pullout (Muntakim and Dhar 2020).

Poisson’s ratio (ν) of the soil was considered as 0.3, which is within the typical values for dense sand (Budhu 2011). The Young’s modulus for the soil was estimated based on the nonlinear model of Janbu (1963). Janbu (1963) showed that the initial tangent modulus of elasticity, E_{s_ini}, varies as a power function of the confining pressure, p', as expressed in Eq. 2.

$$E_{s\_ini} = Kp_a\left(\frac{p'}{p_a}\right)^n \quad [2]$$

where K is a material constant; p_a is the atmospheric pressure (i.e., 101.3 kPa); p' is the mean effective confining pressure, and n is an exponent determining the rate of variation of E_{s_ini} with p'. The value of E_{s_ini} is estimated based on p' at the springline level of the pipe with K = 150 and n = 0.5 (Roy et al. 2015) as E_{s_ini} = 5 MPa for the sand used in the tests. The stress-dependent Young’s modulus of the soil (i.e., depth-dependent soil modulus distribution) was implemented based on the Janbu model by developing a user-defined subroutine called USDFLD (written in FORTRAN) in Abaqus. The USDFLD allows field variables at a material point to be defined as a function of time or any of the available material point quantities available in the Abaqus analysis output file.

For sand, the cohesion is zero; however, a minimum value of 0.1 kPa is assigned to avoid numerical instability. For the sand used in the laboratory test, a friction angle of 45° is selected based on the test results of Saha et al. (2019). The maximum dilation angle (i.e., to simulate volume change behavior of sand during interface shear) is estimated based on the relationship proposed in Bolton (1986) [Eq. 3].

$$\psi_{max} = \frac{\phi_p' - \phi_{cv}'}{k_\psi} \quad [3]$$

where ϕ_p' is the peak friction angle and ϕ_{cv}' is the critical state friction angle and k_ψ = 0.8 for plane strain (PS) and 0.5 for triaxial (TX) loading conditions. With a critical state friction angle of 34° for the sand (Saha et al. 2019), the dilation angle of 22° is calculated for triaxial stress condition. A constant dilation angle ranging from 5 to 22° was, therefore, used to examine the effects.

For MDPE pipe material, the elastic-plastic isotropic model is implemented in the FE model. Das and Dhar (2021) reported that the stress-strain responses of MDPE pipe material are highly nonlinear and strain rate–dependent. It was also reported that the initial value of the modulus of elasticity significantly depends on the strain rates. A strain rate–dependent constitutive model was developed for the pipe material based on the test results of Das and Dhar (2021) and the hyperbolic constitutive model proposed in Suleiman and Coore (2004).

Suleiman and Coree (2004) proposed a modified hyperbolic model to account for the strain ratevdependent behavior of polyethylene pipe material, as expressed in Eq. 4:

$$\sigma = E_{ini}\left(\frac{\varepsilon}{1+\eta\varepsilon}\right) \quad [4]$$

where E_{ini} is the initial modulus, and η is a hyperbolic constant. These strain rate–dependent parameters could be obtained using the following equations proposed by Suleiman and Coree (2004):

$$E_{ini} = a(\dot{\varepsilon})^b \quad [5]$$

$$\eta = \frac{a(\dot{\varepsilon})^b}{c + d\ln(\dot{\varepsilon})} \quad [6]$$

where $\dot{\varepsilon}$ = strain rate; and a, b, c, and d = constants that could be determined by curve-fitting the stress-strain responses obtained from the uniaxial extension or compression tests. In the present study, these model parameters are calculated based on the uniaxial tensile test results conducted at various strain rates (Das and Dhar 2021). The average strain rate experienced by the pipe during the tests ranged from 2.4×10^{-6}/s to 8.8×10^{-6}/s. The true stress-strain curves of pipe material under these strain rates were input into the FE model. Thus, the modulus of elasticity pipe material, E_p, is expected to vary between 340 to 410 MPa during the test with the pulling rates of 0.5 to 2 mm/min. However, Das and Dhar (2021) found no significant influence of the strain rate between 5.5×10^{-6} /s and 10^{-6} /s on the stress-strain response of MDPE pipe material. It was reported that the stress-strain responses of MDPE pipe material could be approximated to be independent of the strain rate at a strain rate at or below 10^{-6}/s. The Poisson's ratio and density of MDPE were 0.46 and 940 kg/m^3, respectively.

4.2 Pipe–soil Interface Modeling

The contact between the pipeline and the surrounding soil was modeled using the general contact algorithm available in Abaqus/ Standard. Tangential and normal behavior was defined between the contact surfaces. For the tangential contact behavior, the friction coefficient, μ, between the soil and the pipe was introduced using a penalty friction formulation, while for the normal interaction behavior, a non-penetrating condition was defined (referred to as "hard" contact in Abaqus). The Coulomb friction model was used for the frictional interaction between the pipe and soil. In this method, the maximum allowable frictional (shear) stress across the interface is related to the contact pressure between the contacting bodies. Sliding along the interface between the buried pipe and surrounding soil occurs when the shear stress, τ, at the contact interface reaches the critical shear stress, τ_{crit} (i.e., interface shear strength). The critical shear stress, τ_{crit}, is a fraction of the contact pressure, p, between the surfaces ($\tau_{crit} = \mu p$). The fraction, μ, is known as the coefficient of friction. The friction coefficient, μ, is calculated as the tangent of the interface friction angle, δ, between the pipe and the test sand.

The value of δ depends on the interface characteristics, hardness and roughness of the pipe surface, and relative movement between the pipe and soil. According to ALA (2005), δ is related by a factor, f, (termed as interface friction reduction factor) to the internal friction angle of the soil (ϕ) as $\delta = f\phi$, where f = 0.6 is recommended for the polyethylene pipe coating. However, the pipe surface interaction with the surrounding soil could be pulling rate–dependent due to the time–dependent behavior of the polymer (Reza and Dhar 2021). It was reported that interface friction angles of 75% to 90% of the peak friction angle of the surrounding soil could successfully simulate ground movements of various rates. The values of f were calculated as 0.75, 0.86, and 0.9, correspondings to the pulling rates of 0.5, 1, and 2 mm/min, respectively (Reza and Dhar 2021). Table 2 summarizes the parameters used for the interface friction for various test conditions.

Table 2. Friction coefficients corresponding to the test conditions

Loading rate (mm/min)	Interface friction reduction factor, f	Friction angle, ϕ	Interface angle of shear resistance, $\delta = f\phi$
0.5	0.75	45°	33.75°
1	0.86		38.7°
2	0.90		40.5°

4.3 Simulation Procedures

Analysis was performed to simulate the gravity load, soil compaction load, and pipe pullout behavior. Thus, the FE simulation was performed in three steps: applying

gravitational loads in pipe and soil, the soil compaction load, and the pullout.

First, the gravitational load was introduced to the model by gradually increasing the gravitational constant from zero to 9.81 m/s^2 to simulate the initial condition. Secondly, a uniform thermal loading was applied over a thin zone (2.75 mm thickness) around the pipe circumference, as shown in Figure 2, to apply a compaction load equivalent to the passive earth pressure recommended in Taleb and Moore (1999). Finally, an axial displacement was applied on one end of the pipe (herein termed the "leading end") up to 120 mm.

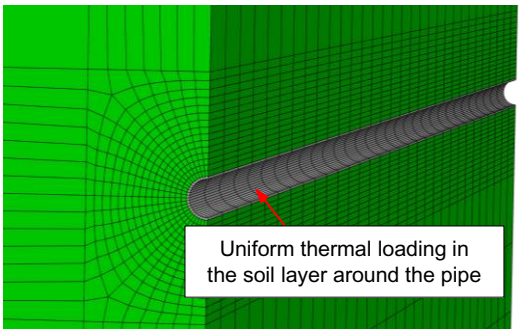

Figure 2. Simulation of compaction load

5 RESULTS

5.1 Force–Displacement Response

Figure 3 compares the measured axial pullout forces from Tests 1–3 with the numerical calculations using FE analysis. The pullout forces increase nonlinearly with the pulling displacements both from the experiments and the FE models. The nonlinearity is associated with the progressive mobilization of interface shearing resistance nonlinearly. The increase of pullout force continued until the shear strength at the pipe–soil interface was fully mobilized over the entire pipe length. Beyond the point of full mobilization, the experimental pulling forces are reduced due to the release of the trailing end, while the FE calculations show constant pulling forces. The FE analysis could not capture the complex mechanism of soil–pipe interaction beyond the peak pullout force. An investigation of the maximum pullout force is the interest of the current study, as it is a concern for pipeline design. The FE analysis was performed with various dilation angles (ψ), as shown in Figure 3. The maximum pullout forces are successfully simulated using the FE analysis with ψ = 15°.

Figure 3 shows that the maximum pullout resistance from the experiment was at the pulling end displacement (x_{max}) of 50 to 60 mm. Note that these displacements are not the relative movement required for mobilization of the shearing resistance at the soil–pipe interface but include the elongation of the flexible MDPE pipe.

5.2 Effect of Change in Dilation Angle

The effect of soil dilatancy on the peak pullout forces was investigated by using the FE analysis for different dilation angles. The analyses were performed for four values of ψ (= 5°, 8°, 15° and 22°), with constant ϕ' (= 45°) for the test conditions in Tests 1–3 (Figure 4). Figure 4 illustrates that the peak pullout force increases as ψ increases, which is primarily due to the volumetric expansion of dense sand during shearing. At higher ψ, volume expansion of the interface soil is higher, which leads to an increase of the normal soil stresses on the pipe's surface, resulting in the higher pullout resistance.

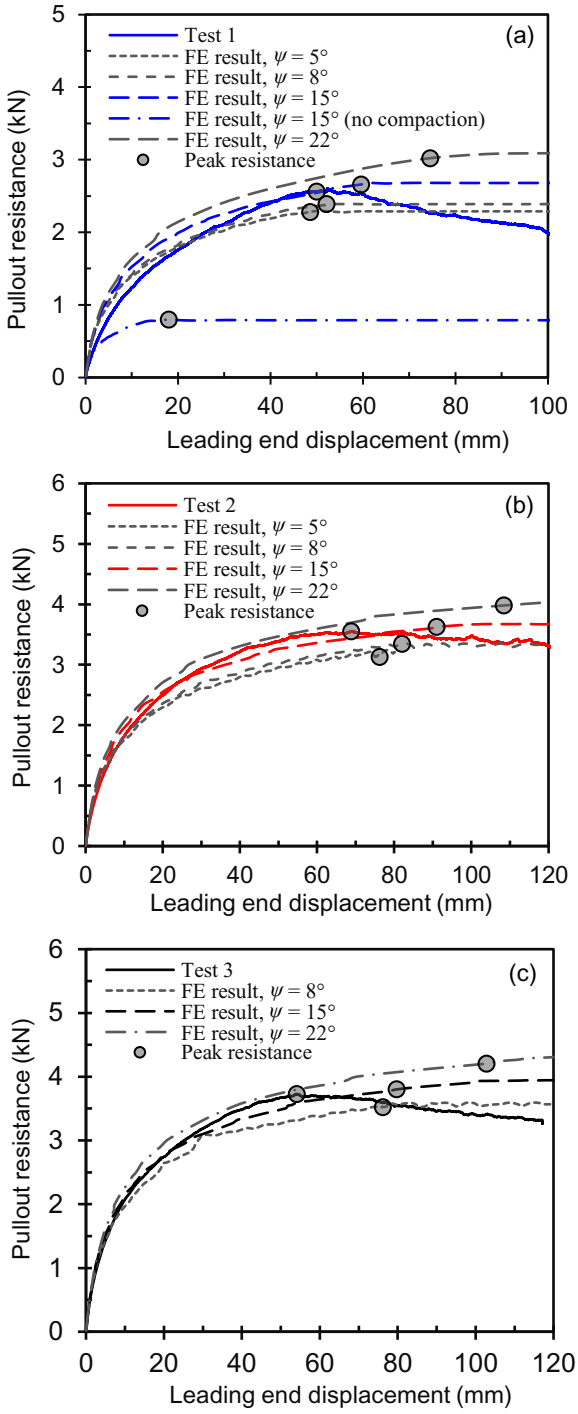

Figure 3. Comparison of FE calculation of pullout resistance with measurements

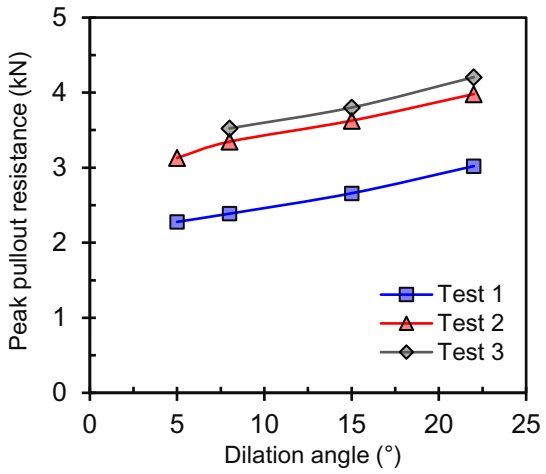

Figure 4. Peak pullout forces with dilation angle

5.3 Effect of Variation of Soil Modulus with Depth

Figure 5 shows the changes of modulus of elasticity of soil (soil modulus) with depth based on the Janbu (1963) model implemented in Abaqus. Due to the variation of confining pressure, the soil modulus varies from a very low value up to 5 MPa. However, the effects of increasing soil modulus with depth were not significant, as shown in Figure 6. Figure 6 plots the pullout force against leading end displacement based on analyses performed assuming soil modulus varying with depth and a uniform soil modulus (E_s = 5 MPa). The experimental results are also included in the figure. The comparison shows that the peak pullout force is not significantly affected (difference <1.5%) for the two approaches of analysis. However, analysis with variation soil modulus with depth simulates the initial force–displacement response better.

5.4 Normal Stress Distribution Around the Pipe

The distributions of normal stresses around the pipe circumference at different locations along the pipe length were obtained from FE analysis, as plotted in Figure 7. The normal stresses were normalized by the average normal stresses at the relevant depth recommended in existing design guidelines (i.e., ALA 2005). Figure 7 indicates that the normal stress distribution around the pipe circumference is not symmetrical about the horizontal axis during the axial pullout. Then normal stresses are much greater than the average normal stress calculated using the ALA (2005) design equation, $0.5(1+K_0)\,\gamma H$. As a result, the axial pullout resistance calculated using the ALA design equation would be less. Figure 7 also reveals that the normal stress along the pipe length is not uniform. The normal stress is the lowest at the leading end and increases toward the trailing end. The reduction of the normal stress at the leading end is associated with the diameter decrease of the MDPE pipe (Reza and Dhar 2021).

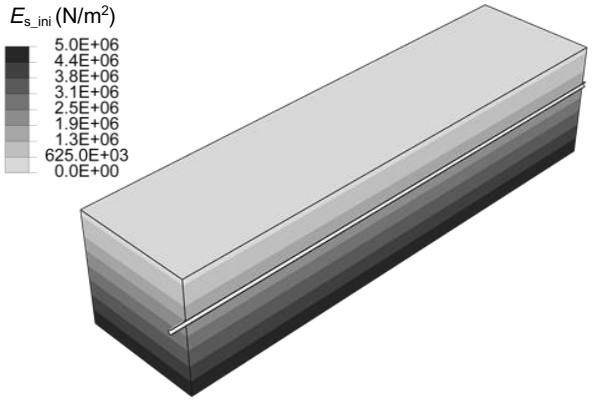

Figure 5. Varying soil modulus using Janbu model

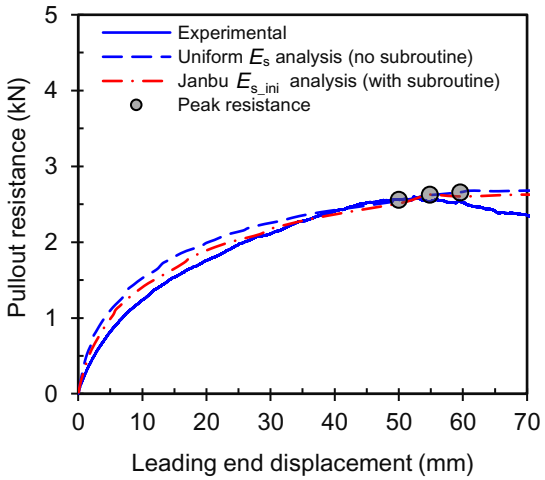

Figure 6. Effect of varying soil modulus on the load–displacement curve in Test 1

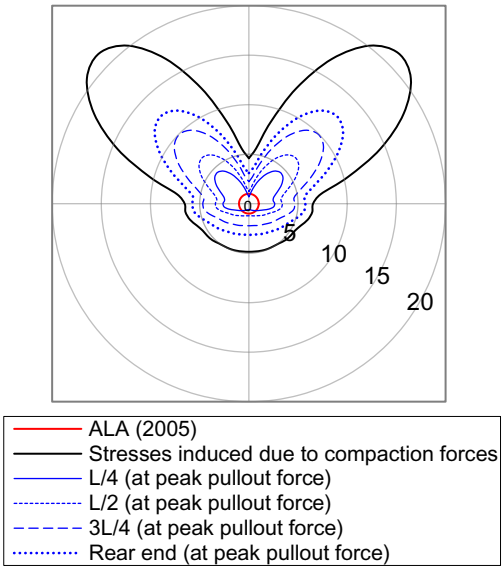

Figure 7. Distribution of dimensionless normal stresses around the pipe circumference in Test 1

The normal stresses averaged over the pipe circumference are examined, as shown in Figure 8. The average normal stress after the gravity load step (prior to the application of compaction force) is close to the normal stress calculated ALA (2005) equation. However, additional stress in a range of 30-50 kPa was applied during the analysis to simulate the stresses induced due to compaction. The compaction-induced stresses of 40-45 kPa satisfactorily simulated the pullout behaviors observed during the tests. The compaction stresses are also consistent with the passive earth pressure applied in Taleb and Moore (1999). The compaction-induced stresses are not accounted for in the ALA (2005) design guidelines.

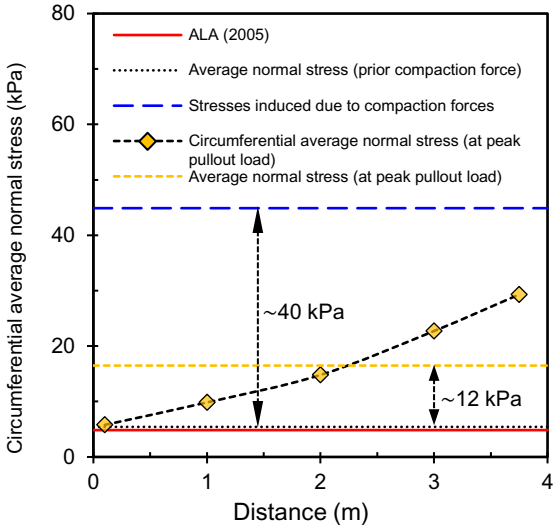

Figure 8. Normal stress distribution along the pipe length from the FE calculation in Test 1

Figure 8 shows again that the average normal stress on the pipe circumference is not uniform along the length of the pipe. The stress is the lowest at the leading end and highest at the tailing end due to a non-uniform reduction of pipe diameter (as discussed earlier). The average normal stress over the entire pipe length was calculated at peak pullout force (shown using yellow dash line in Figure 8). The average stress is more than 2 times the stresses obtained using the ALA (2005) design equation. Thus, the current design equation will significantly underpredict the pullout load for pipes buried in dense sand.

6 CONCLUSIONS

This paper presents a 3D FE modeling technique for simulation of the axial pullout behavior of MDPE pipes buried in dense sand. In this method, the compaction-induced load was simulated using an equivalent temperature load, and the soil dilation effect was simulated using the non-associated flow rule in the Mohr-Coulomb model. Three laboratory pullout tests were simulated using the FE analyses. The comparison of the results indicates that the developed FE modeling technique can reasonably simulate the pullout load observed during the tests.

The compaction-induced stresses and the dilation of interface soil were found to increase the axial pullout resistance of the pipes. The increase of pullout resistance due to compaction-induced stresses and dilation are not accounted for in the current design guidelines. The average normal stress at peak pullout load calculated from FE analysis was more than 2 times the average normal stress calculated using the equation in existing design guidelines.

7 ACKNOWLEDGEMENTS

The Collaborative Research and Development Grant program of the Natural Science and Engineering Research Council of Canada, Innovate NL program of the Government of Newfoundland and Labrador, FortisBC Energy Inc., and WSP Canada Inc., are gratefully acknowledged for providing the financial and/or in-kind support for this research.

8 REFERENCES

ALA (American Lifelines Alliance). 2005. Guidelines for the design of buried steel pipe, Reston, VA, USA: ASCE.

Anderson, C. 2004. Soil–pipeline interaction of polyethylene natural gas pipelines in sand, *M.Sc. thesis*, Dept. of Civil Engineering, Univ. of British Columbia, Vancouver, BC, Canada.

ASCE (American Society of Civil Engineers). 1984. Guidelines for the seismic design of oil and gas pipeline systems, Committee on Gas and Liquid Fuel Lifelines, Technical Council on Lifeline Earthquake Engineering, New York, pp. 573.

Bilgin, Ö. and Stewart, H.E. 2009. Design Guidelines for Polyethylene Pipe Interface Shear Resistance, *Journal of Geotechnical and Geoenvironmental Engineering*, ASCE, 135(6): 809-818.

Bilgin, Ö. 2014. Modeling viscoelastic behavior of polyethylene pipe stresses, *Journal of Materials in Civil Engineering*, ASCE, 26: 676-683.

Bolton, M.D. 1986. The strength and dilatancy of sands, *Géotechnique*, 36 (1): 65–78.

Budhu, M. 2011. *Soil mechanics and foundations*, 3rd edition. John Wiley & Sons. United States of Arizona.

Chakraborty, S., Dhar, A.S., Talesnick, M. and Muntakim, A.H. 2020. Behavior of a branched buried MDPE gas distribution pipe under axial ground movement, In Proc., *GeoVirtual 2020*, 73rd Canadian Geotechnical Conf. (virtual), Canada: Canadian Geotechnical Society.

Cruden, D.M. and Varnes, D.J. 1996. Landslide types and processes. Landslides – Investigations and mitigation, *Transportation Research Board*, Special Report 247, pp: 36-75.

Dassault Systems. 2019. ABAQUS/CAE user's guide, Providence, RI: Dassault Systemes Simulia.

Das, S. and Dhar, A.S. 2021. Nonlinear Time-Dependent Mechanical Behavior of a Medium Density Polyethylene Pipe Material, *Journal of Materials in Civil Engineering*, ASCE, 33(5): 04021068.

Dezfooli, M.S., Abolmaali, A. and Razavi, M. 2014a. Coupled nonlinear finite-element analysis of soil–steel pipe structure interaction, *International Journal of Geomechanics*, ASCE, 15(1): 04014032.

Dezfooli, M.S., Abolmaali, A., Park, Y., Razavi, M. and Bellaver, F. 2014b. Staged Construction Modeling of Steel Pipes Buried in Controlled Low-Strength Material Using 3D Nonlinear Finite-Element Analysis, *International Journal of Geomechanics*, ASCE, 15(6): 04014088.

Duncan, J. M. and Seed, R.B. 1986. Compaction induced earth pressures under K_0 conditions, *Journal of Geotechnical Enginnering*, ASCE, 112(1): 1-22.

Elshimi, T. M. and Moore, I.D. 2013. Modeling the effects of backfilling and soil compaction beside shallow buried pipes, *Journal of Pipeline Systems Engineering and Practice*, ASCE, 4(4): 04013004.

Groves, A. and Wijewickreme, D. 2013. Field monitoring of buried polyethylene natural gas pipelines subjected to ground movement, In Proc., *66th Canad. Geotech. Conference, GeoMontreal 2013*, Sept. 29- Oct. 3, Montreal, Quebec, Canada.

Guo, P.J. and Stolle, D.F.E. 2005. Lateral pipe–soil Interaction in Sand with Reference to Scale Effect, *Journal of Geotechnical and Geoenvironmental Engineering*, ASCE, 131 (3):338-349.

Janbu, N. 1963. Soil compressibility as determined by oedometer and triaxial tests, In Vol. 1 of Proc., *European Conf. on Soil Mechanics and Foundation Engineering* (ECSMFE), 19–25. Essen, Germany: German Society for Earthworks and Foundations.

Katona, M.G. 1978. Analysis of long-span culverts by the finite element method, *Transportation Research Record*, 678, 59–66.

Masada, T. and Sargand, S.M. (2007). Peaking deflections of flexible pipe during initial backfilling process, *Journal of Transportation Engineering*, ASCE, 133(2):105-111.

Muntakim, A.H. and Dhar, A.S. 2020. Assessment of Axial Pullout Force for Buried Medium-Density Polyethylene Pipelines, *Journal of Pipeline Systems Engineering and Practice*, ASCE, 12(2): 04020074.

Murugathasan, P., Dhar, A.S. and Hawlader, B.C. 2020. An experimental and numerical investigation of pullout behavior of ductile iron water pipes buried in sand, *Canadian Journal of Civil Engineering*. 48 (2): 134-143.

PRCI (Pipeline Research Council International). 2009. Guidelines for constructing natural gas and liquid hydrocarbon pipelines through areas prone to landslide and subsidence hazards, Report prepared for the Design, Material, and Construction committee, Chantilly, VA, USA: Pipeline Research Council International, Inc.

Reza, A., Dhar, A.S., Rahman, M. and Weerasekara, L. 2019. Pulling rate effects on the pullout force of buried small diameter MDPE pipe in loose sand, *72nd Canadian Geotechnical Conference*, *GeoSt.John's 2019*, Sept. 29- Oct. 2, St. John's, NL.

Reza, A., and Dhar, A.S. 2021. Axial Pullout Behavior of Buried Medium Density Polyethylene Gas Distribution Pipes, *International Journal of Geomechanics*, ASCE, 21(7):04021120.

Robert, D.J. and Thusyanthan, N.I. 2015. Numerical and experimental study of uplift mobilization of buried pipelines in sands, *Journal of Pipeline Systems Engineering and Practice*, ASCE, 6 (1): 04014009.

Roy, K., Hawlader, B., Kenny, S. and Moore, I.D. 2015. Finite element modeling of lateral pipeline–soil interactions in dense sand, *Canadian Geotechnical Journal*, 53(3): 490-504.

Saha, R. C., Dhar, A.S. and Hawlader, B.C. 2019. Shear strength assessment of a well-graded clean sand, In Proc., *GeoSt.John's 2019, 72nd Canadian Geotechnical Conference.* St. John's, Newfoundland and Labrador, Canada: Canadian Geotechnical Society.

Saha, R. C., Dhar, A.S. and Hawlader, B.C. 2020. Assessment of shear strength parameters of moist sands using conventional triaxial tests, In Proc., GeoVirtual 2020, *73rd Canadian Geotechnical Conf*erence (virtual), Canada: Canadian Geotechnical Society.

Sheil, B. B. Ã., Martin, C.M.Ã., Byrne, B.W.Ã., Plant, M., Williams, K. and Coyne, D. 2016. Full-scale laboratory testing of a buried pipeline in sand subjected to cyclic axial displacements, *Géotechnique*, 68(8): 684-694.

Suleiman, M.T. and Coree, B.J. 2004. Constitutive model for high density polyethylene material: Systematic approach, *Journal of Materials in Civil Engineering*, ASCE, 16(6): 511-515.

Taleb, B. and Moore, I.D. 1999. Metal culvert response to earth loading performance of two-dimensional analysis, *Transportation Research Record*. 1656, 25–36.

Trautmann, C.H. and O'Rourke, T.D. 1983. Behavior of pipe in dry sand under lateral and uplift loading, *Geotechnical Engineering Report*, 83-7, Cornell Univ., Ithaca, NY.

Wang, F., Han, J., Khatri, D.K., Parsons, R.L., Brennan, J.J. and Guo, J. 2015. Field installation effect on buried steel-reinforced high density polyethylene pipes, *Journal of Pipeline Systems Engineering and Practice*, ASCE, 7(1):0401503.

Wang, F., Han, J., Corey, R., Parsons, R.L. and Sun, X. 2017. Numerical modeling of installation of steel-reinforced high-density polyethylene pipes in soil, *Journal of Geotechnical and Geoenvironmental Engineering*, ASCE. 143(11):04017084.

Weerasekara, L., and Wijewickreme, D. 2008. Mobilization of soil loads on buried polyethylene natural gas pipelines subject to relative axial displacements, *Canadian Geotechnical Journal*, 45(9): 1237–1249.

Weerasekara, L. 2011. Pipe–soil interaction aspects in buried extensible pipes, *Ph.D. thesis*, Department of Civil Engineering, University of British Columbia, Vancouver, B.C., Canada.

Wijewickreme, D. and Weerasekara, L. 2015. Analytical Modeling of Field Axial Pullout Tests Performed on Buried Extensible Pipes, *International Journal of Geomechanics*, ASCE, 15(2): 04014441-12.

APPENDIX E

Axial Ground Movement Analysis for Buried Polyethylene Pipelines using Nonlinear Pipe–soil Interaction Model

This paper has been published and presented in 75th Canadian Geotechnical Conference, GeoCalgary 2022, Calgary, AB, Canada, Oct. 2–5, 2022. Most of the research work presented in this paper was conducted by the first author. He also prepared the draft manuscript. The other author supervised the research and reviewed the manuscript.

Axial ground movement analysis for buried polyethylene pipelines using nonlinear pipe–soil interaction model

Auchib Reza[1] & *Ashutosh Sutra Dhar*[1]
[1]*Department of Civil Engineering – Memorial University of Newfoundland, St. John's, NL, Canada*

GeoCalgary 2022 October 2-5 Reflection on Resources

ABSTRACT
Pipelines crossing the areas exposed to permanent ground deformation are often at risk. The pipe strains due to the ground movements depend on soil–pipe interaction. Current design guidelines recommend using nonlinear springs to model soil-pipe interaction during the assessment of pipelines. However, no spring parameters accounting for the soil-pipe interaction for flexible polyethylene pipe are available in the design guidelines. This study develops a two-dimensional Winkler-based numerical model using finite-element analysis to investigate polyethylene pipes subjected to axial relative ground movement. The results of FE analysis show that calculations based on parameters recommended in the current guidelines underestimate the maximum axial soil resistance measured during the test. The pipe–soil interaction parameters recommended in the guidelines were modified to simulate the measured responses for the MDPE pipes in dense sand. The analysis was extended for various burial depths to examine the safe strain limits for MDPE pipes.

RÉSUMÉ
Les canalisations traversant les zones exposées à des déformations permanentes du sol sont souvent à risque. Les déformations du tuyau dues aux mouvements du sol dépendent de l'interaction sol-tuyau. Les directives de conception actuelles recommandent l'utilisation de ressorts non linéaires pour modéliser l'interaction sol-tuyau lors de l'évaluation des pipelines. Cependant, aucun paramètre de ressort tenant compte de l'interaction sol-conduite pour les conduites flexibles en polyéthylène n'est disponible dans les directives de conception. Cette étude développe un modèle numérique bidimensionnel basé sur Winkler utilisant une analyse par éléments finis pour étudier les tuyaux en polyéthylène soumis à un mouvement axial relatif du sol. Les résultats de l'analyse FE montrent que les calculs basés sur les paramètres recommandés dans les directives actuelles sous-estiment la résistance axiale maximale du sol mesurée lors de l'essai. Les paramètres d'interaction tuyau-sol recommandés dans les lignes directrices ont été modifiés pour simuler les réponses mesurées pour les tuyaux en MDPE dans le sable dense. L'analyse a été étendue à différentes profondeurs d'enfouissement afin d'examiner les limites de déformation sûres pour les tuyaux en MDPE.

1. INTRODUCTION

Most onshore pipelines are buried underground to avoid damage caused by human activities. However, ground movement resulting from natural disasters (e.g., landslides, earthquakes, ground subsidence) can still jeopardize the pipeline network's structural integrity. Therefore, the performance of pipes buried in unfavourable ground conditions requires special attention.

Pipelines can be subjected to longitudinal, transverse, or combined ground loading depending on their orientation with respect to the direction of ground movement. The longitudinal movement is parallel to the pipeline axis, whereas the transverse movement is perpendicular to the pipeline axis. As the ground moves, the pipeline can undergo displacements and excessive strains due to the loads from the moving ground. Thus, buried pipes crossing areas susceptible to ground movements are designed to withstand the displacements and strains. The pipe wall strains due to the ground movements are estimated using design guidelines. The current design guidelines are developed based on the assumption that the soil reactions to the pipelines behave like a series of independent bilinear elastoplastic Winkler springs (ALA 2005; PRCI 2017). The springs are defined in the axial, lateral, upward, and downward directions to account for the corresponding direction of ground movement. This paper focuses on the pipes subjected to relative ground movement in the axial direction.

Practitioners commonly follow simplified formulas and methods recommended in pipe design guidelines (e.g., ALA 2005; NEN3650-1 2003; PRCI 2017) to determine the parameters of the axial spring. The guidelines were developed based on laboratory and field observations of rigid buried pipe responses. In these methods, the soil force is assumed to be constant at its maximum value. The maximum values of the axial spring force are obtained as the longitudinal frictional force per unit length along the pipe length, calculated based on the estimation of the normal stresses acting on the pipe and the frictional characteristics of the soil–pipe interface. The normal stresses are estimated as the mean value of the overburden stress and the at-rest lateral earth pressure at the pipe springline. However, soil compaction can significantly increase lateral earth pressures on buried pipes during installation (Elshimi and Moore 2013; Dezfooli et al. 2014ab; Wang et al. 2017). As a result, the stresses due to compaction of the soil during backfilling can increase the interface frictional resistance, resulting in a higher pullout resistance of the pipe. However, no method is currently available to properly account for the effect of compaction during backfilling. Furthermore, these methods

and guidelines do not consider the dilation effect of interface soil surrounding the buried pipes in dense sand (Wijewickreme and Weerasekara 2015; Meidani et al. 2017; Sarvanis et al. 2017).

In addition, in calculating the earth pressure, the effects of pipe material are not considered in the existing model. Muntakim and Dhar (2021) demonstrated, based on three-dimensional (3D) finite-element modeling, that the relative rigidity of the pipe with respect to the surrounding soil can influence the normal stress on the pipe. The finding is consistent with Meidani et al. (2018), where soil resistance was affected by the reduction of pipe cross-sectional area due to the axial elongation of medium-density polyethylene (MDPE) pipes when exposed to axial relative ground movements. The behavior of polyethylene (PE) pipes is more complex due to their time–dependent material behavior. Reza and Dhar (2021a) experimentally examined the rate-dependent axial pullout behavior of MDPE pipes in medium-dense sand. They proposed pulling-rate-dependent interface friction reduction factors to account for the rate-dependent effects. Thus, the spring parameters recommended for rigid pipes in the design guidelines require further improvement with a proper understanding of various contributing factors for assessing PE pipes during a ground movement episode.

The authors previously conducted full-scale axial pullout tests on MDPE pipes in dense sand to address some of these limitations in current methods. The details are described in Reza and Dhar (2022). In the current study, a 3D continuum-based finite-element (FE) modeling technique and 2D Winkler spring-based FE analysis were performed to evaluate the results of the laboratory pullout tests. Based on the results of the analyses, axial soil spring parameters recommended in the guidelines were modified for the analysis of pipes using the 2D method. Finally, the analysis was extended to higher burial depth ratios to examine the safe strain limit for MDPE pipes using the validated spring parameters.

2. FULL-SCALE PULLOUT TESTS

Table 1 shows a list of laboratory tests reported in Reza and Dhar (2022) used for the numerical investigation conducted in this paper. The tests were conducted with 42.2-mm and 60.3-mm diameter MDPE pipes in a test box of 4 m in length. In each test, the pipe was axially pulled to a displacement of 120 mm with the pulling rates of 0.5, 1, and 2 mm/min to simulate the axial relative ground movement events. Pipes were buried in a compacted sand backfill. Backfill soil density was 18 kN/m^3 to 19 kN/m^3.

Table 1. Summary of the test program (After Reza and Dhar 2022)

Test No	Avg. unit weight, $\overline{\gamma}$ (kN/m^3)	Burial depth, H (m)	Pulling rate (mm/min)	Pipe diameter, D (mm)	Wall thickness, t (mm)
1–3	19	0.34	0.5, 1, 2	42.2	4.22
4–5	18	0.48	0.5, 1	60.3	5.48

3. CONTINUUM-BASED FE MODEL

Three-dimensional (3D) FE analysis was performed using Abaqus (Dassault System 2019) to understand the load transfer mechanism during the tests. A similar approach as in Reza and Dhar (2021a) was employed, except that a modelling technique for the compaction-induced earth pressure was implemented. The compaction-induced stresses contribute significantly to the pipes in dense sand. Figure 1 shows the FE model used in the analysis. The model dimensions are the same as those in the tests.

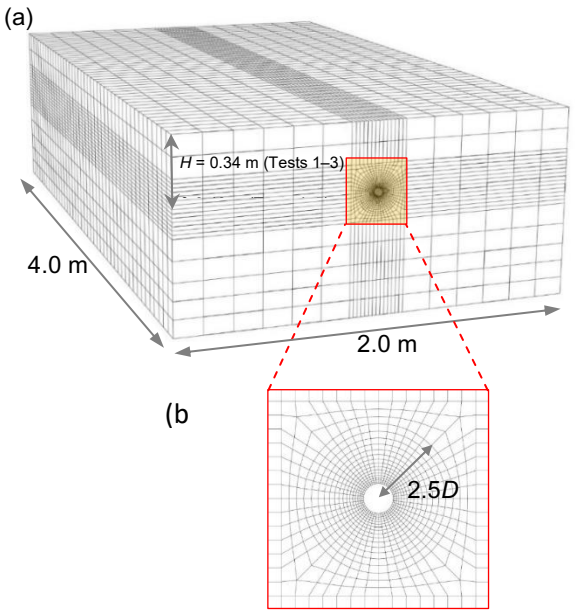

Figure 1. FE mesh of the pipe–soil system: (a) 3D FE mesh; and (b) cross-section near the pipe

The pipe and soil domains were modeled using C3D8R solid elements, available in Abaqus. A finer mesh is used in the pipe's close vicinity over a radial distance of 2.5 times the pipe diameter (2.5D). The contact between the pipeline and the surrounding soil was modeled using the general contact algorithm. Normal and tangential behaviors between contacting surfaces were defined to prevent penetration and allow surface slippage. The normal behavior was considered as "hard" (i.e., non-penetrating) contact; while the tangential behavior was defined by the Coulomb friction criterion with interface friction angles of 0.75ϕ, 0.86ϕ, and 0.90ϕ, correspondings to the pulling rates of 0.5, 1, and 2 mm/min, respectively, after Reza and Dhar (2021a).

An elastic-perfectly plastic Mohr–Coulomb (MC) model with a nonassociated flow rule was used to simulate the sand behavior. The parameters of the MC model used in this numerical study were selected based on the laboratory tests performed on the sand material for a wide range of stress conditions (Saha et al. 2019, 2020). Table 2 shows the modulus of elasticity (E_s), cohesion (c), friction angle (ϕ), and dilation angle (ψ) for the backfill sand material used in the FE analyses. Poisson's ratio (ν) of the soil was

considered 0.33, which is within the typical values for dense sand (Budhu 2011). More detail on the selection of these parameters can be found in Reza and Dhar (2021b).

Table 2. Sand parameters used for FE analysis

γ (kN/m^3)	E_s (MPa)	ν	ϕ (°)	ψ (°)	c (kPa)
18–19	5	0.33	45	22	0.1

The stress–strain responses of MDPE pipe material are highly nonlinear and strain rate-dependent (Das and Dhar 2021). A strain rate-dependent hyperbolic constitutive model was developed for the material using the test results in Das and Dhar (2021). The maximum strain rates during the tests ranged from 1×10^{-5}/s to 4×10^{-5}/s with pulling rates of 0.5 to 2 mm/min. The true stress–strain responses of MDPE pipe material at these strain rates were used as input in the FE analysis, as shown in Figure 2. The inset of the figure shows the hyperbolic equation of Suleiman and Coore (2004) to represent the stress–strain relations. The isotropic elastic-plastic model was implemented with the yield stress and strain shown in Figure 2. The Poisson's ratio and density of MDPE were assumed as 0.46 and 940 kg/m^3, respectively, at the laboratory temperature (23°C), after Bilgin et al. (2007).

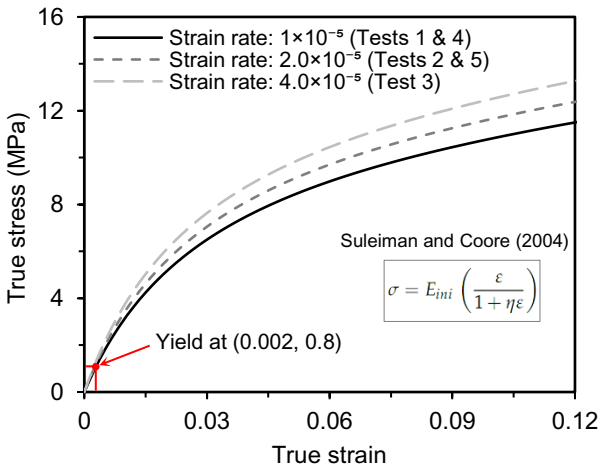

Figure 2. True stress-strain responses for MDPE pipes (after Das and Dhar 2021)

3.1 Compaction Modeling

Modeling the compaction-induced earth pressure is very challenging owing to the complicated nature of compaction and the limitations of the modeling techniques. Duncan and Seed (1986) developed an incremental analytical model to calculate the maximum and residual compaction-induced lateral earth pressures on vertical, nondefecting soil-structure interfaces. They also presented a simplified hand calculation procedure for cases where all soil layers are identically compacted. It was found that the horizontal earth pressure near surfaces may be many times greater than the theoretical at-rest values and may approach passive earth pressure magnitude. At greater depths, the horizontal earth pressure is converged to the state of stresses at rest (i.e., simply equal to K_0 times σ_v'). The horizontal earth pressures were calculated using the method in Duncan and Seed (1986), as shown in Figure 3. Figure 3(a) illustrates the distribution of the calculated peak and residual lateral earth pressure increases acting against a rigid wall (due to a roller operating at a distance of 0.15 m from the wall). The contribution of compaction-induced coefficient of lateral earth pressure (K_1) was then determined, dividing calculated lateral earth pressures by K_0-based lateral earth pressures, as shown in Figure 3(b).

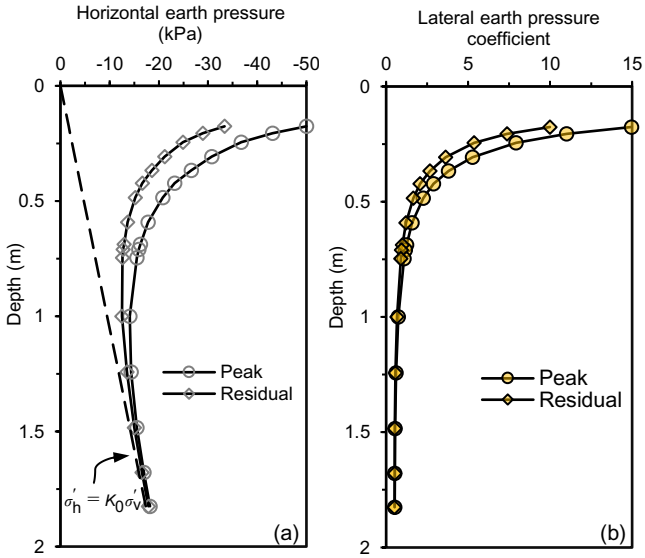

Figure 3. Compaction-induced earth pressure after Duncan and Seed (1986): (a) lateral earth pressure; and (b) lateral earth pressure coefficient.

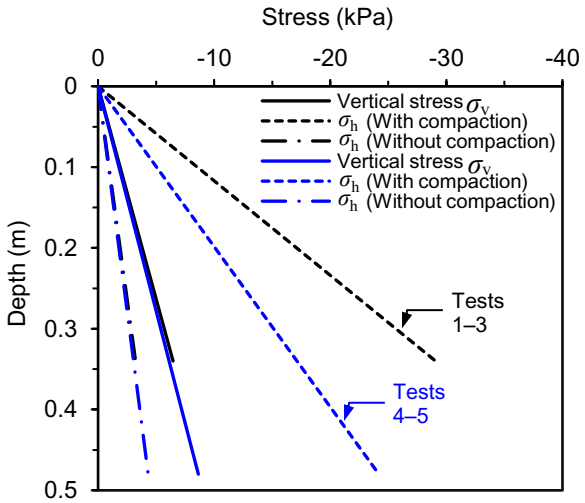

Figure 4. Earth pressures with and without compaction effects

Peak K_1 values corresponding to the pipe springline depth were used to calculate the earth pressures due to compaction (Figure 4). Figure 4 shows that while the vertical earth pressures are the same with and without compaction, the lateral earth pressures were significantly higher when the compaction effect was incorporated. These earth pressures were applied in the FE as the initial stress condition. The gravity was then applied. In analysis, initial stress conditions enforce equilibrium and ensure zero displacements after applying geostatic stresses, simulating the test condition before the pullout operation was performed.

3.2 FE Results

Figure 5 compares the measured axial pullout forces from Tests 1–5 with the calculations using FE analysis. The pullout forces increase nonlinearly with the pulling displacements both from the experiments and the FE models. The nonlinearity is associated with the progressive mobilization of interface shearing resistance, starting from the leading end towards the trailing end. This mechanism was observed earlier in Weerasekara and Wijewickreme (2008) and Reza and Dhar (2021a). The pullout force increased until the shear strength at the pipe–soil interface was fully mobilized over the entire pipe length. Beyond the point of full mobilization, the experimental pulling forces are slightly reduced due to the release of the trailing end, while the FE calculations show constant pulling forces. Figure 5 illustrates that the pullout resistances calculated without modeling the compaction effects are significantly lower than the resistances calculated while simulating the compaction effects. The proposed method of accounting for the compaction effects reasonably simulated the pullout forces observed during the tests. However, there are some differences between the numerical results and the physical tests before reaching the peak values, which might be due to the use of a linear elastoplastic MC model for the soil material. The classical MC model can successfully capture the peak soil resistance during pullout (Yimsiri et al. 2004; Guo and Stolle 2005). As an investigation of the peak pullout force is the primary focus here, the MC model is used in the present study.

To understand the load transfer mechanism, the results of FE analysis were used to examine the normal stresses on the pipe surface and the pipe diameter changes that could not be measured during the tests. Calculations showed that the circumferential average of the normal stresses varied along the pipe length, with the lowest value toward the leading end and the highest value toward the trailing end. The diameter decrease due to axial pullout was higher toward the leading end than the trailing end. Figure 6 shows the calculated diameter decreases along the pipe length at the maximum pullout force, indicating the highest diameter decrease at the leading end. The higher pipe diameter reduction toward the leading end caused a lower pipe surface stress due to the arching effect. As a result, the normal stresses to the pipe surface could be less than the average geostatic stress for the flexible MDPE pipes. However, the current design guidelines (e.g., ALA 2005) recommend using the average geostatic stress at the springline level of the pipe to calculate the axial pullout resistance. The ratio of circumferential averaged normal stress and the average of the geostatic stress (vertical and horizontal earth pressure) can be used to define a normal stress reduction factor, ζ, due to pipe diameter decrease (Eq. 1).

$$\zeta = \frac{\sigma'_{avg} \text{ from FE analysis}}{\frac{(1+K_1)}{2}\gamma H} \quad [1]$$

Note that the coefficient lateral earth pressure K_1 is used in the equation that accounts for the compaction effects. The variation of the normal stress reduction factor along the pipe length at the maximum pullout resistance is shown in Figure 7. It reveals that the factor ζ is very low (e.g., 0.15) toward the leading end and close to unity at the trailing end of the pipes. From these values, the average normal stress factor can be calculated over the friction force mobilization length of the pipe (the entire buried pipe length for the maximum pullout resistance) for comparison with test results.

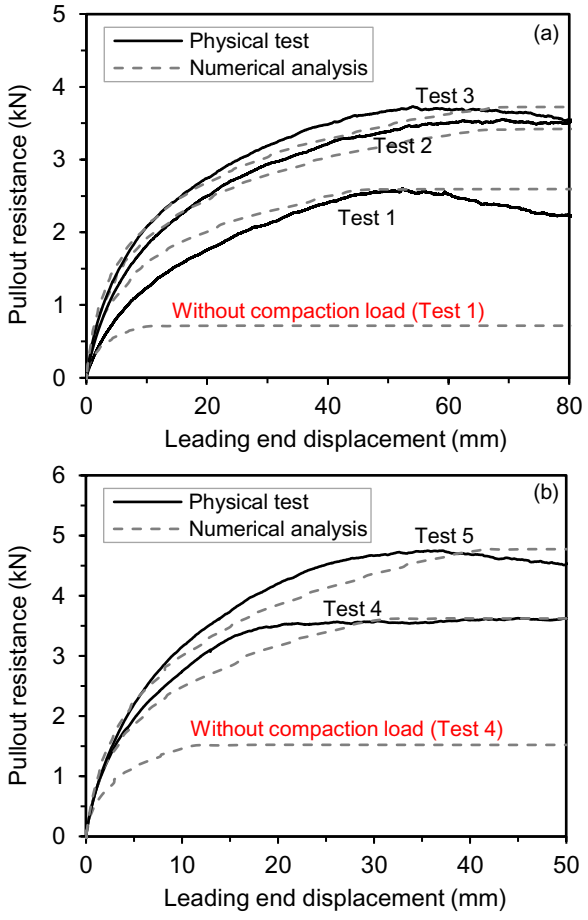

Figure 5. Comparison of pullout resistances with measurements: (a) D = 42.2 mm; (b) D = 60.3 mm

The normal stress reduction factor could not be measured during the tests. However, the average value could be back-calculated using the pullout force and friction force mobilization length, L (Eq. 2).

$$\zeta = \frac{\textit{Pullout resistance from tests}}{\pi DL\frac{(1+K_1)}{2}\gamma H\tan\delta} \quad [2]$$

The friction force mobilization lengths and the pullout forces (or resistances) were measured during the tests using strain gauges and load cells, respectively. At the maximum pullout resistance, the frictional resistance is mobilized over the entire length of the buried pipe. The average factors (ζ) from the experiments (Eq. 2) and FE analysis (Eq. 1) calculated for the maximum pullout resistance are compared in Table 3. The factors from FE analysis match well with those obtained from experiments in the table. Thus, the 3D FE models reasonably represent the test conditions. It also indicates that the average normal stress on the pipe can be calculated from the average geostatic stress considering K_1 and using a normal stress reduction factor. However, the normal stress reduction factor ζ depends on the stiffness and friction angle of the surrounding soil (Muntakim and Dhar 2021). Detailed investigation of the variation of ζ for various magnitudes of soil parameters has not been investigated here.

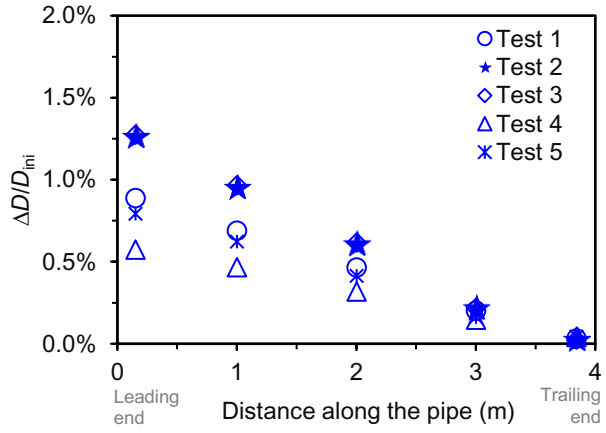

Figure 6. Variation of pipe diameter decrease

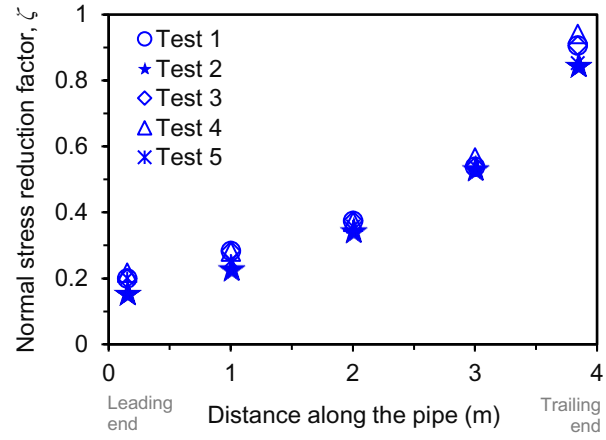

Figure 7. Variation of normal stress reduction factor

Table 3. Comparison of average normal stress reduction factors (ζ)

Test no.	Back-calculated from test results	3D FE calculations
Test 1	0.41	0.46
Test 2	0.41	0.42
Test 3	0.42	0.45
Test 4	0.42	0.45
Test 5	0.42	0.44

4. BEAM-ON-SPRING ANALYSIS

The 3D continuum-based pipe–soil interaction analysis is computationally demanding, which may take days or weeks to get one set of pipe responses for a given combination of input parameters. Thus, the beam-on-spring type of analysis is generally recommended during design. The suitability of the beam-on-analysis was evaluated through comparison with the test results. The pipeline was modeled as a Timoshenko beam (good for dealing with large axial strain) using PIPE21 elements, and the soil–pipeline interaction was modeled using the pipe–soil interaction element (PSI24) in Abaqus. The pipe was discretized with a uniform element size of 1 mm. The width of the PSI elements is the same as the length of the pipe element, as the PSI elements share the same nodes with the pipe elements (as discussed later). A mesh sensitivity analysis was conducted by varying the element sizes, and no noticeable change in pullout resistance was observed for element sizes smaller than 1 mm.

4.1 Pipe–Soil Interaction Element

The pipe–soil interaction (PSI) element in Abaqus was used to define the soil as a Winkler media. The PSI element interacts with the structural beam element, as illustrated in Figure 8. One edge of the element shares nodes with the beam-type elements that model the pipeline. The nodes on the other edge represent a far-field surface, such as the ground surface. Thus, the element's depth is equal to the height of the ground surface from the pipe springline, H. It has only the displacement degrees of freedom at its nodes. The relative displacements between two edges of the PSI elements transmit force to the pipeline through their stiffness. The interaction between pipe and soil can be modeled in four different directions: axial (longitudinal), transverse horizontal, vertical upward, and vertical downward. A suitable constitutive model can define the stiffness of the PSI elements in each direction. The constitutive behavior of PSI elements is defined by force per unit length at each point along the pipeline, caused by relative displacement between that point and the point on the far-field surface. The degrees of freedom on the far-field nodes are fully fixed in this study. A linear (elastic) or nonlinear (elastic-plastic) constitutive model can be defined using tabular input in Abaqus.

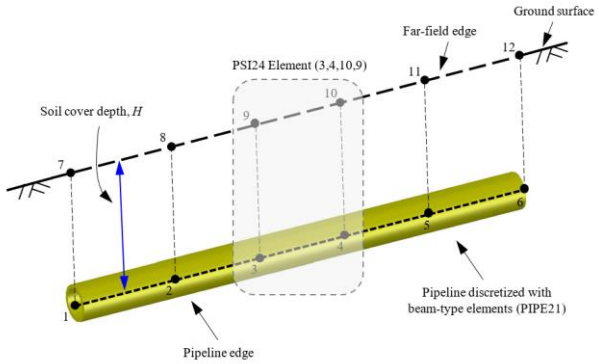

Figure 8. Pipe–soil interaction (PSI) model

4.2 PSI Model Parameters

The PSI element requires spring parameters in axial, vertical, and lateral directions. The existing design guidelines (e.g., ALA 2005) recommend bilinear elastic-perfectly plastic spring models. The spring models are defined using the ultimate forces and the corresponding relative displacements. As the current study focuses on axial pullout behaviour, parameters for axial spring were only relevant and discussed here. According to ALA (2005) guidelines, the ultimate axial spring force (t_u) per unit length for dense sand is given by Eq. (3). The corresponding relative displacement (x_u) is 3 mm.

$$t_u = \pi D \gamma H \left(\frac{1+K_0}{2}\right) \tan(f\phi) \quad [3]$$

In Eq. (3), the normal stress on the pipe was assumed as the average geostatic stress based on the coefficient of lateral earth pressure at rest (K_0). However, as discussed in the 3D FE analysis above, the coefficient of the lateral earth pressure in dense sand can be significantly higher due to the compaction-induced effects. The normal stress reduction due to the diameter decrease of the pipeline is also not considered in Eq. (3). It is therefore proposed to modify Eq. (3), including the compaction-induced coefficient of lateral earth pressure (K_1) and the normal stress reduction factor (ζ) to calculate the ultimate axial spring force (Eq. 4). The relative displacement recommended in ALA (2005) is considered applicable.

$$t_u = \zeta \pi D \gamma H \left(\frac{1+K_1}{2}\right) \tan(f\phi) \quad [4]$$

Table 4 presents the spring parameters obtained based on ALA (2005) recommendations and Eq. (4). The loading rate-dependent friction reduction factors (f) were used (after Reza and Dhar 2021a) to get the interface friction angle. Analyses were performed with both sets of spring parameters to investigate the effects.

Table 4. Spring parameters

Test no.	Axial resistance (N/m)		Axial elastic displacement (mm)
	ALA (2005)	Proposed in this study	
Test 1	429.2	645.2	3
Test 2	514.6	855.2	3
Test 3	548.6	921.7	
Test 4	816.2	930.4	
Test 5	978.6	1164.5	

4.3 Results

Figure 9 compares the load–displacement responses from the Winkler-based FE analysis and the experiments for 42.2-mm diameter pipes. The figure shows that the FE method with the proposed parameters (Eq. 4) reasonably simulates the load–displacement responses for Tests 1–3. However, the analyses based on ALA (2005) recommended parameters underestimated the pullout resistances. Again, it should be noted that the nonlinearity in Figure 9 is due to the nonuniform elongation of MDPE pipes associated with the progressive failure response of the interface soil. Similar results were observed for the 60.3-mm diameter pipes but not included here for brevity. Thus, the proposed modification of the ALA (2005) equation successfully simulates the behavior of MDPE pipe using beam-on-spring type analysis.

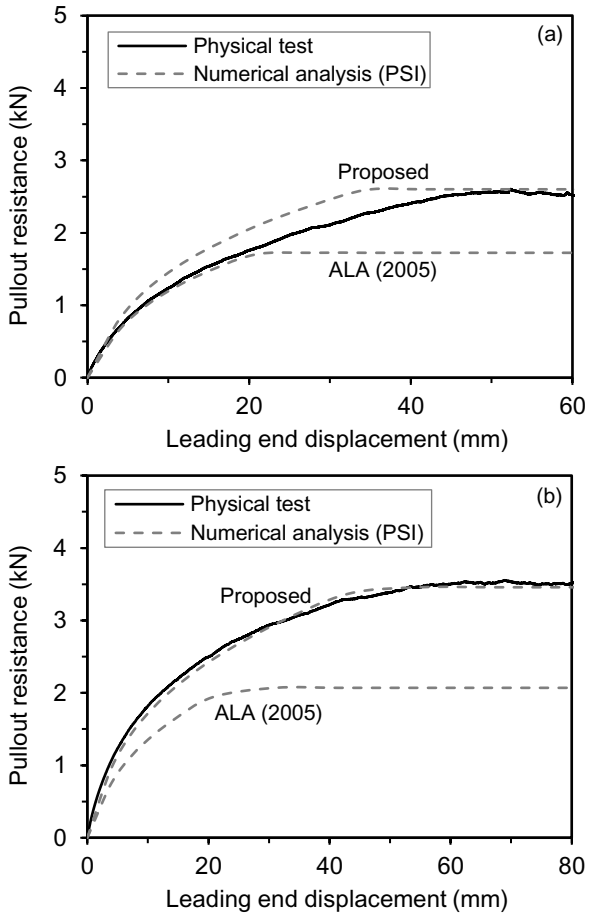

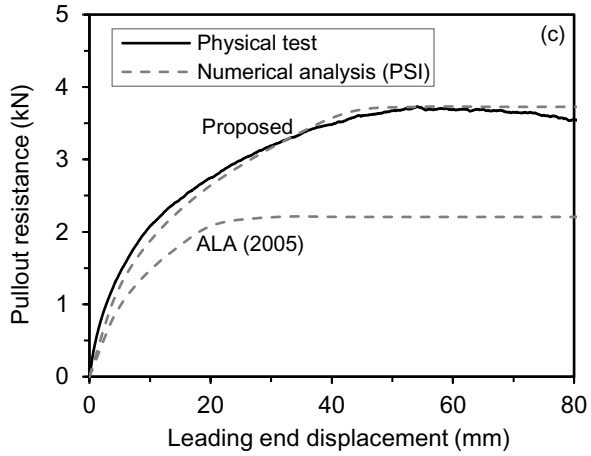

Figure 9. Comparison of results for 42.2-mm diameter pipes: (a) Test 1; (b) Test 2; and (c) Test 3

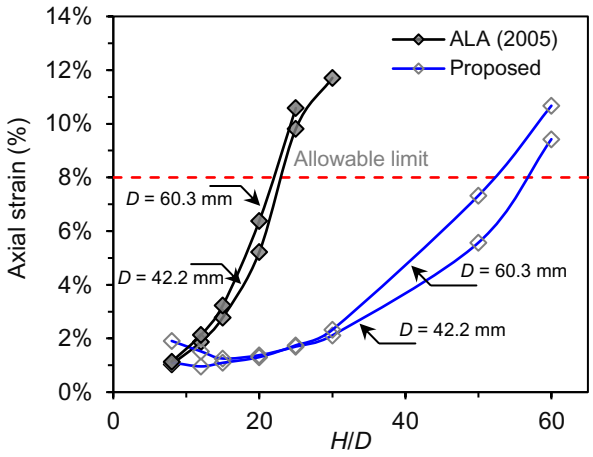

Figure 10. Maximum pipe wall strains with burial depth

Note that the difference between the maximum spring forces obtained from Eq. (3) and Eq. (4) is due to different lateral earth pressure coefficients. However, as shown earlier in Figure 3, the compaction-induced lateral earth pressure coefficient is higher at shallow depths. As the depth increases, the compaction effect is reduced on the lateral earth pressure. Thus, K_0 (recommended in ALA 2005) can be used to calculate the maximum spring force for the deeply buried pipes. Then, the maximum spring force from Eq. (4) can be less than the force from Eq. (3) since the normal stress reduction factor in Eq. (4) is less than 1 for flexible pipes. Thus, a higher pullout force will be predicted using the ALA (2005) method for the deeply buried pipes.

To examine the effect of burial depth on the pipe distress (i.e., wall strain) using the two assumptions (Eq. 3 and Eq. 4), analyses were performed with various burial depths of the pipes. Pipes with 42.2- and 60.3-mm diameters with a 4 m of length were considered. The backfill soil was dense sand with a unit weight (γ) of 19 kN/m^3 and an internal friction angle (ϕ) of 45°. The depth-dependent compaction-induced lateral earth pressure coefficient was selected from Figure 3. The pipe–soil interface friction angle was defined as 0.75ϕ, correspondings to the pulling rate of 0.5 mm/min. A nonlinear hyperbolic stress–strain relation corresponding to the strain rate of 1×10^{-5}/s was used to model MDPE pipe behavior (Figure 2).

Figure 10 shows the results of the analysis with various burial depths of the pipe. The maximum axial strain at the leading end (landslides with tension cracks or ground separation point) is plotted in the figure. Note that the maximum strain is reached when the peak reaction of axial springs is fully mobilized along the length of the pipe. It can be seen in the figure that ALA recommended method provides significantly higher axial strains for pipes with higher burial depth ratios (when H/D>12). Thus, the ALA method can provide a conservative estimate of pipe responses for the deeply buried pipes.

5. CONCLUSIONS

In this paper, a 3D continuum-based FE modeling technique was employed to understand the load transfer mechanism of buried MDPE pipes subjected to axial ground movement simulating five test results conducted earlier by the authors. The compaction-induced effect on the lateral earth pressure was implemented in the analysis. Based on the results of the analyses, a modified equation is proposed to calculate the maximum axial spring force for the analysis of pipe using beam-on-spring idealization. The major findings from the study are as follows.

- The compaction-induced coefficient of at-rest lateral earth pressure (K_1) recommended in Duncan and Seed (1986) can successfully simulate the responses observed during the tests.
- A modification to the ALA (2005) equation for maximum axial spring force through the incorporation of K_1 and a normal stress reduction factor, ζ, is proposed. The proposed method could simulate the observed pipe responses reasonably using beam-on-spring idealization.
- The compaction effect on earth pressure is significant at shallow depths and negligible at greater depths.
- The ALA (2005) method can underestimate the responses for shallow buried pipes and overestimate the responses for deeply buried pipes.

6. ACKNOWLEDGEMENTS

The authors gratefully acknowledge the financial and/or in-kind support provided by the Natural Science and Engineering Research Council of Canada through its Discovery and Collaborative Research and Development Grant programs, Innovate NL program of the Government of Newfoundland and Labrador, FortisBC Energy Inc., and WSP Canada Inc.

8. REFERENCES

ALA (American Lifelines Alliance). 2005. Guidelines for the design of buried steel pipe, Reston, VA, USA: ASCE.

Bilgin, Ö., Stewart, H.E. and O'Rourke, T.D. 2007. Thermal and mechanical properties of polyethylene pipes. *Journal of Materials in Civil Engineering,* ASCE, 19(12): 1043–1052.

Budhu, M. 2011. *Soil mechanics and foundations*, 3rd edition. John Wiley & Sons. United States of Arizona.

Dassault Systems. 2019. ABAQUS/CAE user's guide, Providence, RI: Dassault Systemes Simulia.

Das, S. and Dhar, A.S. 2021. Nonlinear Time-Dependent Mechanical Behavior of a Medium Density Polyethylene Pipe Material, *Journal of Materials in Civil Engineering*, ASCE, 33(5): 04021068.

Dezfooli, M.S., Abolmaali, A. and Razavi, M. 2014a. Coupled nonlinear finite-element analysis of soil–steel pipe structure interaction, *International Journal of Geomechanics*, ASCE, 15(1): 04014032.

Dezfooli, M.S., Abolmaali, A., Park, Y., Razavi, M. and Bellaver, F. 2014b. Staged Construction Modeling of Steel Pipes Buried in Controlled Low-Strength Material Using 3D Nonlinear Finite-Element Analysis, *International Journal of Geomechanics*, ASCE, 15(6): 04014088.

Duncan, J. M. and Seed, R.B. 1986. Compaction-induced earth pressures under K_0-conditions, *Journal of Geotechnical Enginnering*, ASCE, 112(1): 1-22.

Elshimi, T. M. and Moore, I.D. 2013. Modeling the effects of backfilling and soil compaction beside shallow buried pipes, *Journal of Pipeline Systems Engineering and Practice*, ASCE, 4(4): 04013004.

Guo, P. J. and Stolle, D. F. E. 2005. Lateral pipe–soil interaction in sand with reference to scale effect. *Journal of Geotechnical and Geoenvironmental Engineering*, ASCE, 131(3): 338–349.

Meidani, M., Meguid, M.A. and Chouinard, L.E. 2017. Evaluation of soil–pipe interaction under relative axial ground movement. *Journal of Pipeline Systems Engineering and Practice*, ASCE, 8(4): 04017009.

Meidani, M., Meguid, M.A. and Chouinard, L.E. 2018. A finite-discrete element approach for modelling polyethylene pipes subjected to axial ground movement. *International Journal of Geotechnical Engineering*, 14(7): 717–729.

Muntakim, A.H. and Dhar, A.S. 2021. Assessment of Axial Pullout Force for Buried Medium-Density Polyethylene Pipelines, *Journal of Pipeline Systems Engineering and Practice*, ASCE, 12(2): 04020074.

NEN3650-1. 2003. Requirements for pipeline systems - Part 1: General - Quire 1 to 6. Nederlands Normalisatie Instituut.

PRCI (Pipeline Research Council International). 2017. Pipeline seismic design and assessment guideline, Catalogue No: PR-268-134501-R01. Chantilly, VA, USA: PRCI.

Reza, A. and Dhar, A.S. 2021a. Axial Pullout Behavior of Buried Medium Density Polyethylene Gas Distribution Pipes, *International Journal of Geomechanics*, ASCE, 21(7):04021120.

Reza, A. and Dhar, A.S. 2021b. Finite element modeling of pipe–soil interaction under axial loading in dense sand, *74th Canadian Geotechnical Conference*, *GeoNiagara 2022*, Sept. 26-29, Niagara, ON.

Reza, A. and Dhar, A.S. 2022. Developing a simplified method for assessing polyethylene pipings in dense sand subjected to axial displacements, *Geosynthetics International* (under review).

Sarvanis, G.C., Karamanos, S.A., Vazouras, P., Mecozzi, E., Lucci, A. and Dakoulas, P. 2017. Permanent earthquake-induced actions in buried pipelines: Numerical modeling and experimental verification. *Earthquake Engineering Structural Dynamics*, 47(4): 966–987.

Saha, R. C., Dhar, A.S. and Hawlader, B.C. 2019. Shear strength assessment of a well-graded clean sand, In Proc., *GeoSt.John's 2019, 72nd Canadian Geotechnical Conference.* St. John's, Newfoundland and Labrador, Canada: Canadian Geotechnical Society.

Saha, R. C., Dhar, A.S. and Hawlader, B.C. 2020. Assessment of shear strength parameters of moist sands using conventional triaxial tests, In Proc., GeoVirtual 2020, *73rd Canadian Geotechnical Conf*erence (virtual), Canada: Canadian Geotechnical Society.

Suleiman, M.T. and Coree, B.J. 2004. Constitutive model for high density polyethylene material: Systematic approach, *Journal of Materials in Civil Engineering*, ASCE, 16(6): 511-515.

Wang, F., Han, J., Corey, R., Parsons, R.L. and Sun, X. 2017. Numerical modeling of installation of steel-reinforced high-density polyethylene pipes in soil, *Journal of Geotechnical and Geoenvironmental Engineering*, ASCE. 143(11):04017084.

Weerasekara, L. and Wijewickreme, D. 2008. Mobilization of soil loads on buried polyethylene natural gas pipelines subject to relative axial displacements, *Canadian Geotechnical Journal*, 45(9): 1237–1249.

Wijewickreme, D. and Weerasekara, L. 2015. Analytical Modeling of Field Axial Pullout Tests Performed on Buried Extensible Pipes, *International Journal of Geomechanics*, ASCE, 15(2): 04014441-12.

Yimsiri, S., Soga, K., Yoshizaki, K., Dasari, G. R. and O'Rourke, T. D. 2004. Lateral and upward soil–pipeline interactions in sand for deep embedment conditions. *Journal of Geotechnical and Geoenvironmental Engineering*, ASCE, 130(8): 830–842

APPENDIX F

Effects of Internal Pressure on Pulling Resistance

F.1 Introduction

In this thesis, the effect of internal pressure on the performance of the pipe was not investigated during axial pullout tests. However, polyethylene (PE) pipelines in service possess a high internal gas pressure (maximum operating pressure of around 700 kPa). It is apparent that the pipe response under axial loading will be affected by increased pressure inside the pipe. The purpose of this appendix is to numerically examine the impact of internal pressure on axial pipe–soil interaction behaviour using the three-dimensional (3D) finite-element (FE) model developed in Chapter 6.

F.2 FE Modelling with Internal Pressure

The performance of a PE pipe for a range of internal pressures ($p_{\text{int.}}$ = 0–700 kPa) subjected to an axial displacement at the leading end was investigated. The numerical methodology for Test 2 (D = 42.2 mm, H = 340 mm, and $\delta = 0.86\phi$) presented in Section 6.3, Chapter 6, was used for the analysis, while pressure was applied inside the pipe before the pullout.

F.3 FE Results and Discussion

F.3.1 *Interface Normal Stresses and Force–Displacement Responses*

Figure F-1 shows the interface normal stresses around the pipe circumferences due to various internal pressures inside the pipe before the axial pullout. As seen in the figure, the stresses are greater for the pipes with higher internal pressure. The pressure inside the pipe may expand its diameter, resulting in higher contact forces from the surrounding soil on its outer surface (a similar mechanism to cavity expansion). The contact stresses are also greater on the sides (around the springline) due to compaction-induced horizontal earth pressure on the pipes.

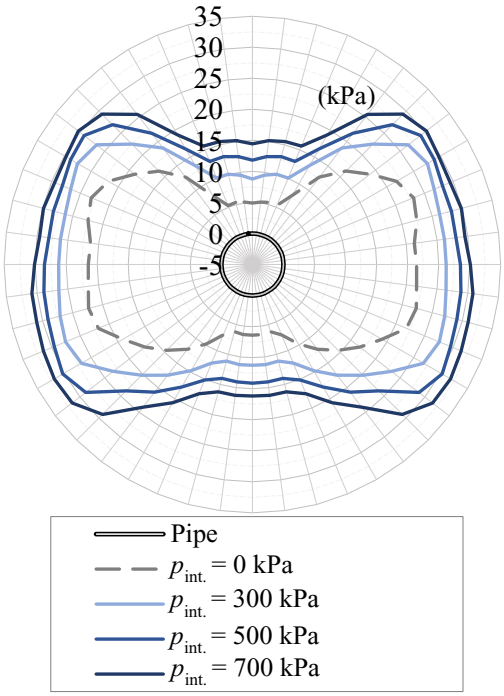

Figure F-1: Variation of interface normal stresses around the pipe circumference with and without internal pressure after installation in Test 2 (D = 42.2 mm; H = 340 mm)

Figure F-2 presents the calculated axial pullout forces for pressurized and non-pressurized pipes against pullout resistance. For the case of $p_{int.}$ = 0 kPa, the force–displacement response calculated from FE calculation matched well with the pullout force observed during Test 2. For the same pipes with internal pressure, the peak pullout resistances were found to increase by about 38% by increasing the pressure from 0 to 700 kPa. This increase in pullout resistance is mainly attributed to the higher interface normal stresses (as shown in Figure F-1). The higher interface normal stresses (or contact stress) offer higher frictional resistance to pipe movements during axial pullout. The FE results show that the leading end displacement (or pipe elongation) required to mobilize the frictional resistance over the full length of the pipe (i.e., initiation of the trailing end movement) increases as the internal pressure increases (shown using the yellow circle in Figure F-2).

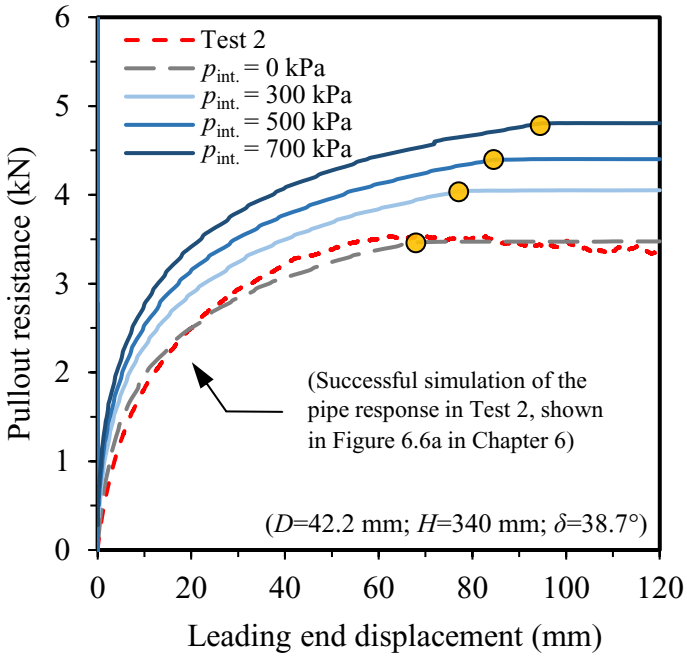

Figure F-2: Axial pullout resistance with leading end displacement for pressurized and non-pressurized pipe from the FE calculation

F.3.2 *Contact Stresses*

The variation of normal stresses at three different points along the pipe length (i.e., at the distances of $L/4$, $L/2$, and $3L/4$ from the pulling end) are plotted in Figure F-3 against the leading end displacements. Figure F-3a plots the contact stresses at the springline, and Figure F-3b plots the circumferential averaged contact stresses at those locations (i.e., $L/4$, $L/2$, $3L/4$). The contact stresses at the springline increase at $L/4$, $L/2$, and $3L/4$ at various displacements due to shear-induced dilation, beyond which the contact stress reduces due to diameter decrease. The increase in stress from the initial value to the peak value is higher for the non-pressurized pipe. The circumferential averaged contact stresses show that the effect of shear-induced dilation is insignificant for the pressurized pipe.

Figure F-4 plots the pipe diameter changes and the variation of the circumferential average of the normal stresses along the pipe length at the peak pullout force. For the pipes with internal pressure, the value of ζ (normal stress adjustment factor, proposed in Chapter 6) was calculated from FE analysis using Eq. (6.9). Variation of ζ along the pipe length for $p_{int.}$ = 0–700 kPa is shown in Figure F-5 at the maximum pulling force. The factor is higher for the pipe with internal pressure than for non-pressurized pipe. The average value of the factor is increased to 0.72 from 0.50 by increasing the internal pressure from 0 to 700 kPa. Therefore, the proposed Eq. (6.7) ignoring the operating pressure would underestimate the pressurized pipe response. However, the factor, ζ, for pressured pipe may also depend on the pipe diameter, interface stress level, stiffness of the soil and pipe, and interface friction angle, which are not investigated in this thesis.

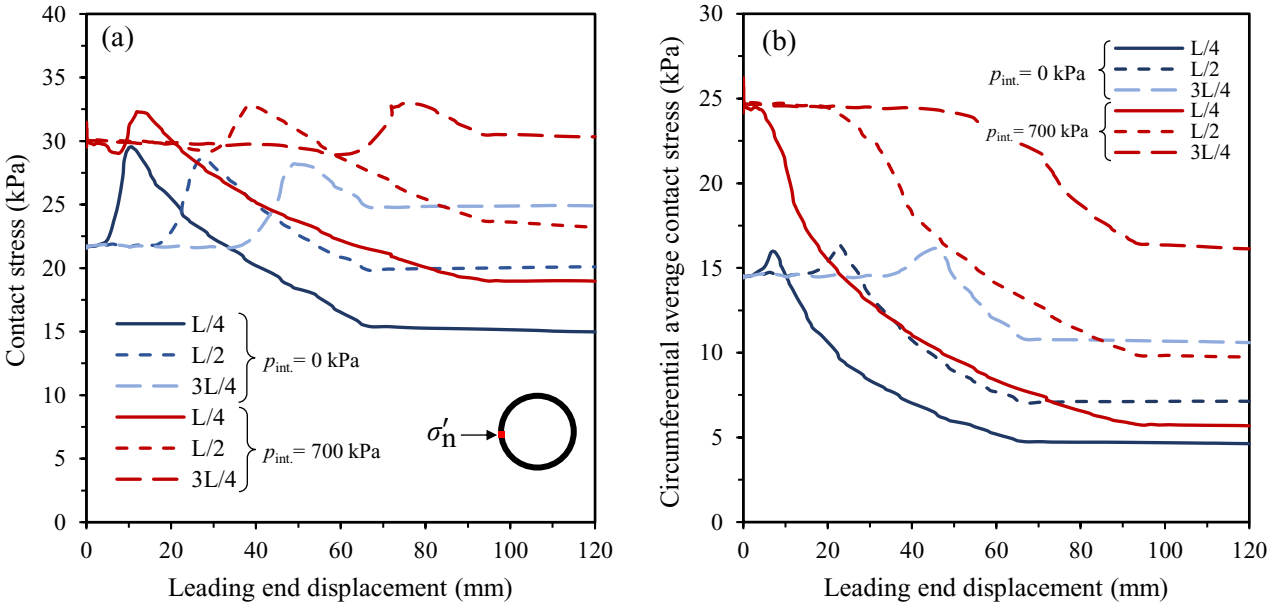

Figure F-3: Changes in (a) Contact normal stresses at pipe springline; and (b) Circumferential average contact stresses

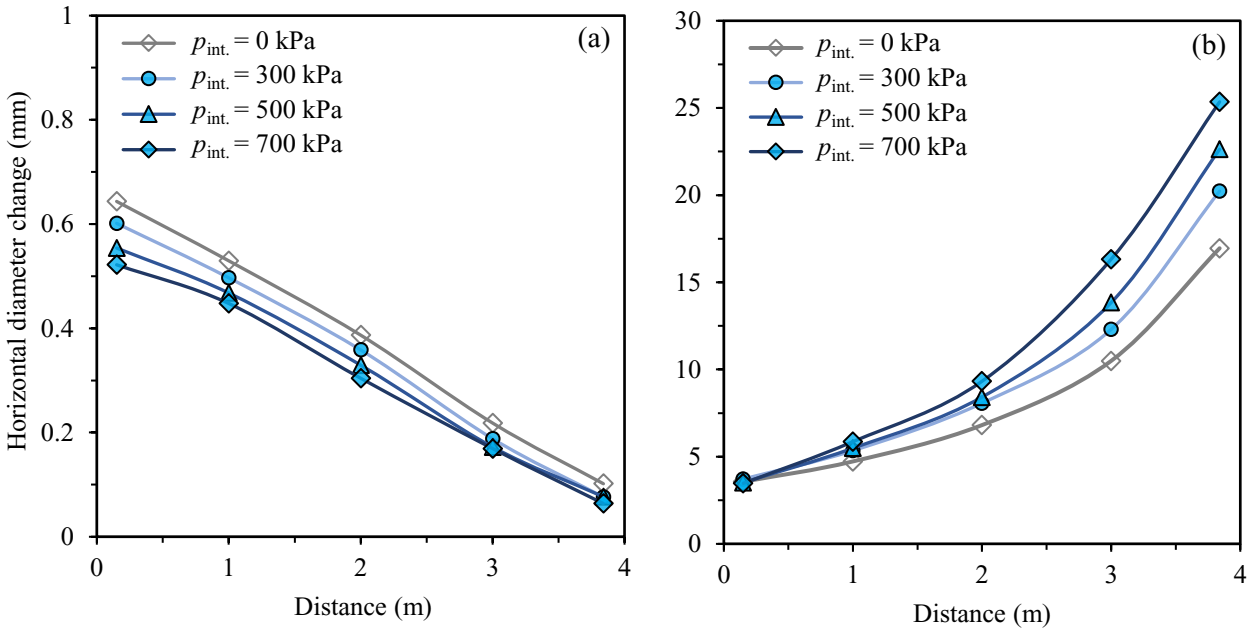

Figure F-4: Variation of (a) Horizontal diameter decrease; and (b) Normal stress distribution along the pipe length

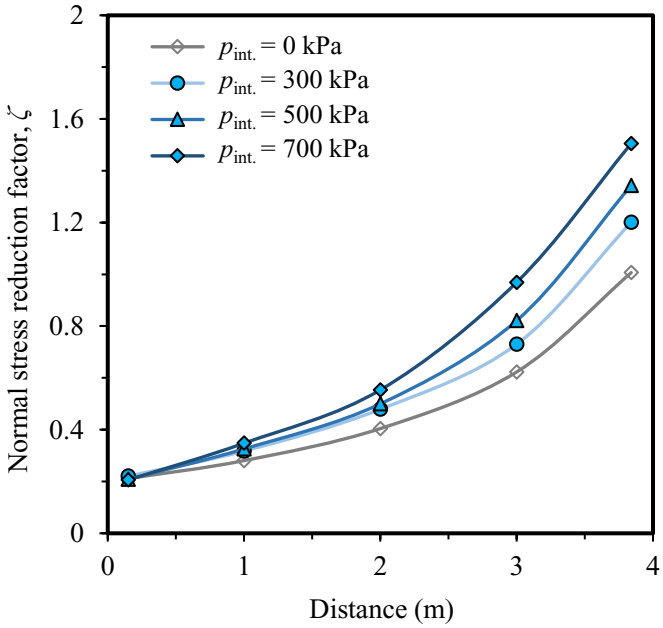

Figure F-5: Variation of normal stress adjustment factor

APPENDIX G

Relaxation Effect of MDPE Pipe during Axial Pullout

G.1 Introduction

Ground movements experienced by buried pipes in real life can be intermittent. In such situations, the time–dependent effects in the form of material creep and/or relaxation are expected in the polyethylene (PE) pipe response under the ground loads. However, due to time constraints in the laboratory, investigations of the time–dependent behaviour of PE pipes have rarely been undertaken. This appendix provides details on the investigation of the impact of stress relaxation in PE pipes during axial pullout, which is not discussed in Chapters 3–6 and Appendices A–E.

G.2 Test Program

An additional axial pullout test was performed under similar conditions to Test 1, reported in Chapter 5, but at a higher burial depth of 600 mm. During the test, after 25 minutes of pulling the pipe's leading end at 0.5 mm/min, the pulling was paused (i.e., allowing the pipe to relax) for nine (9) days before resuming at the same rate. Table G.1 summarises the test program undertaken. Two uniaxial strain gauges were installed at the leading end of the pipe (outside the test box) and one-half of the pipe length within the box from the leading end. Both gauges were placed at the pipe crown. The schematic test configuration for the relaxation test is illustrated in Figure G-1. The pipe installation method and sand density measurement were similar to those discussed in Chapter 5.

Table G.1. Relaxation test of pipes (D = 42.2 mm) buried in dense sand

Test No	Avg. unit weight, $\overline{\gamma}$ (kN/m^3)	Burial depth, H (m)	Pulling rate (mm/min)	Pipe thickness, t (mm)	H/D
1	19.9	0.60	0.5	4.22	14.2

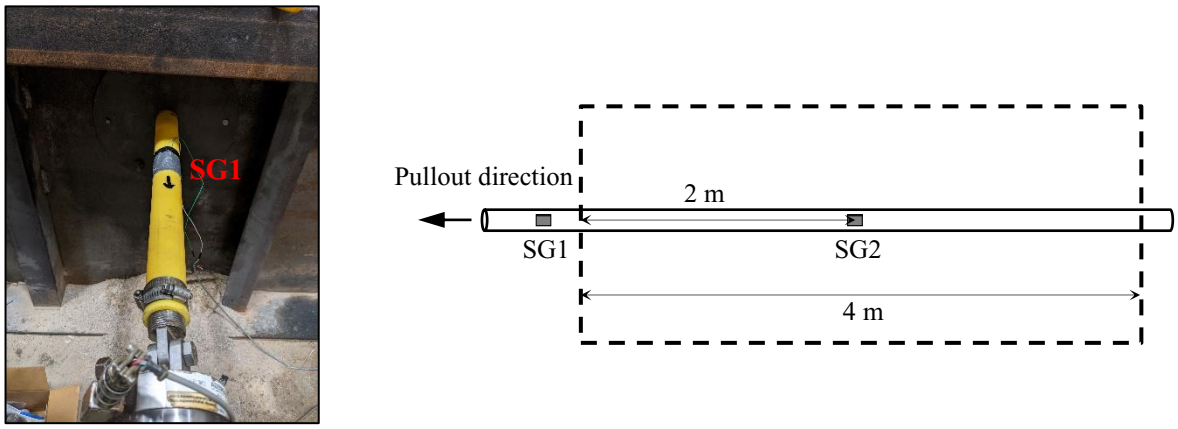

Figure G-1: Schematic test configuration for the relaxation test

G.3 Test Results and Discussion

Figure G-2a plots the variation of displacement at the leading end of the pipe for the entire time span of testing. As seen in the figure, the leading end of the pipe was pulled to a displacement of 12.5 mm, and then the pulling was stopped for 9 days. After 9 days (i.e., after the relaxation phase), the pipe's leading end was further pulled to a displacement of 102 mm. The variation of pullout resistance with time, presented in Figure G-2b, reveals that the measured pullout resistance dropped by about 20% over the period of 9 days during which the loading was paused. This drop in measured pullout load might be caused by the stress-relaxation behaviour observed in PE pipes. Therefore, the stress-relaxation behaviour of PE pipes is advantageous when considering the pipes' response to external loading. The mechanism is further discussed with an evaluation of the pipe's axial strain below.

The force–displacement and axial strain–displacement relationships for the test are shown in Figures G-3 and G-4. The monotonic axial pullout load–displacement behaviour of a 42.2-mm diameter MDPE pipe, from Chapter 5 (Test 1), (with γ = 19.2 kN/m^3, H = 0.34 m, and pulling rate 0.5 mm/min) is included in Figure G-3. Figure G-3 shows that the load–displacement response was

stiffer initially for the pipe with the higher burial depth. The pulling force increased with the displacement until the pulling was stopped at the displacement of 12.5 mm. At this displacement, the interface frictional resistance was not mobilized over the full pipe length (trailing end of the pipe did not move). Thus, the leading end displacement corresponds to the elongation of the pipe over the length of interface shear stress mobilization. During the relaxation, the pullout force was reduced. The pullout force was increased again during reloading. Note that the load–displacement is stiffer during the reloading phase, indicating interface soil was stabilized during the relaxation phase. As a result, the maximum pullout resistance was relatively higher.

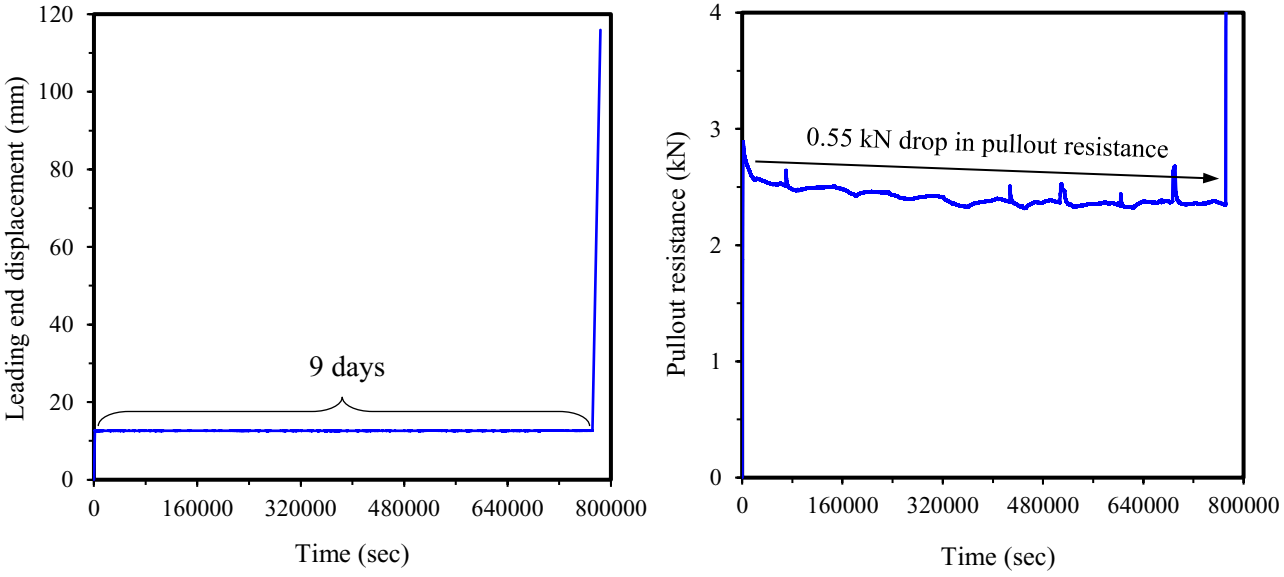

Figure G-2: Variation of (a) leading end displacement with time; and (b) pullout resistance with time

The pipe wall strain outside the test box (leading end) was also reduced during the relaxation phase (Figure G-4a). The strain reduction was not evident at *L*/2 distance from the leading end (Figure G-4b). It is apparent that the strain and stress were redistributed along the pipe length during the relaxation period (over 9 days). The redistribution of axial strain demonstrated that the frictional

stresses were released from the pipe to the surrounding soil gradually, allowing the drop in pullout resistance at the pulling end, and finally, stabilization of interface soil. Note that when the pipe was pulled again after the relaxation phase, the axial strain at $L/2$ did not increase immediately but began to increase after some leading end displacements (6 mm). The strain at this location also increased at the similar leading end displacement (i.e., 6 mm) during initial loading. Thus, when the pipe was subsequently reloaded, the interface friction started to mobilize again, starting from the leading end of the pipe. This is consistent with the stiffer load–displacement response and higher pulling force during reloading, which can induce higher strain in the pipe wall. This mechanism should be further investigated in future research.

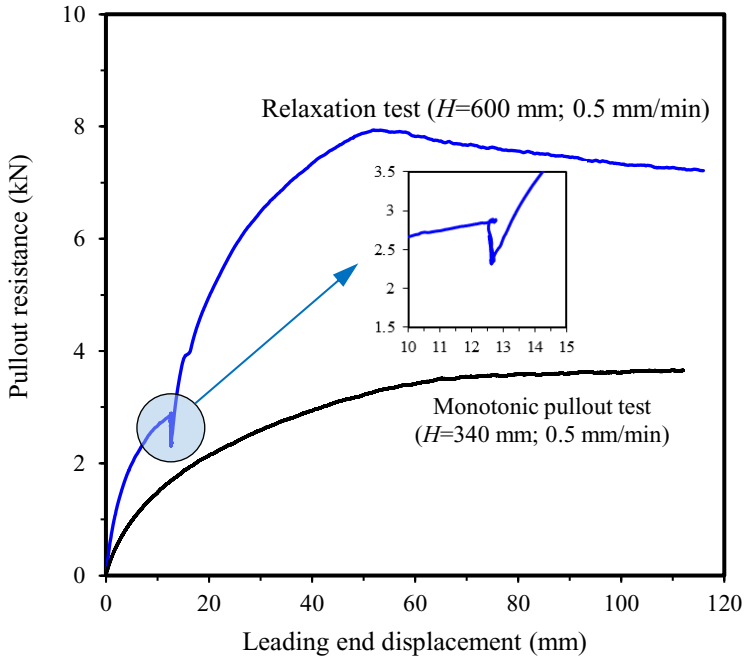

Figure G-3: Variation of pullout resistance with leading end displacement

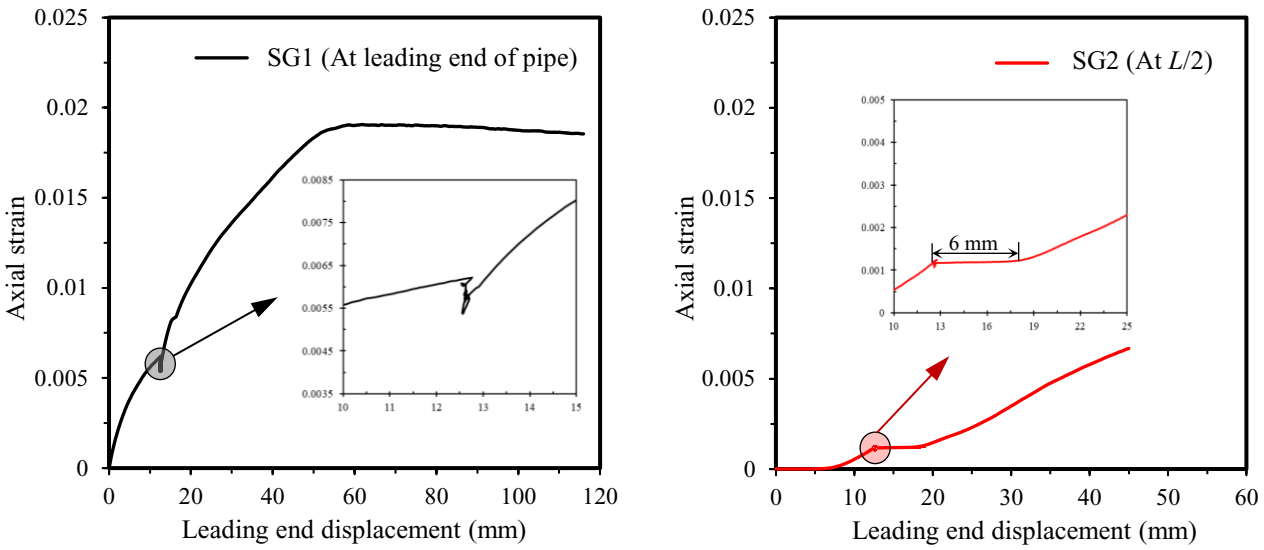

Figure G-4: Variation of axial strain with leading end displacement: (a) At leading end of pipe; and (b) At *L*/2 (2 m)

Additional studies were conducted to assess pipe loading scenarios expected in the field and identify some of the research gaps to be addressed through future research. The preliminary results from these studies are included in Appendices F and G.